



Fakultät für Medizin

Deutsches Herzzentrum München an der TU München
Fachgebiet für Experimentelle und Molekulare Kinderkardiologie

Hypoxia and reactive oxygen species signaling in cardiovascular and cancer disease models

Damir Kračun

Vollständiger Abdruck der von der Fakultät für Medizin der Technischen Universität München zur Erlangung des akademischen Grades eines

Doktors der Naturwissenschaften (Dr. rer. nat.)

genehmigte Dissertation.

Vorsitzender: Prof. Dr. Dr. Stefan Engelhardt.

Prüfer der Dissertation:

1. Prof. Dr. Agnes Görlach

2. Prof. Dr. Michael Groll

Die Dissertation wurde am 08.05.2018 bei der Technischen Universität München eingereicht und durch die Fakultät für Medizin am 11.10.2018 angenommen.

Anhang I

Eidesstattliche Erklärung

Ich erkläre an Eides statt, dass ich die bei der promotionsführenden Einrichtung Fakultät für Medizin der TUM zur Promotionsprüfung vorgelegte Arbeit mit dem Titel: Hypoxia and reactive oxygene species signaling in cardiovascular and cancer disease models im Fachgebiet Experimentelle und Molekulare Kinderkardiologie, Deutsches Herzzentrum München an der TU München unter der Anleitung und Betreuung durch Univ.-Prof. Dr. med. Agnes Görlach ohne sonstige Hilfe erstellt und bei der Abfassung nur die gemäß § 6 Ab. 6 und 7 Satz 2 angebotenen Hilfsmittel benutzt habe.

Ich habe keine Organisation eingeschaltet, die gegen Entgelt Betreuer für die Anfertigung von Dissertationen sucht oder die mir obliegenden Pflichten hinsichtlich der Prüfungsleistungen für mich ganz oder teilweise erledigt.

Ich habe die Dissertation in dieser oder ähnlicher Form in keinem anderen Prüfungsverfahren als Prüfungsleistung vorgelegt.

Die vollständige Dissertation wurde in der Universitätsbibliothek der TUM veröffentlicht. Die promotionsführende Einrichtung Fakultät für Medizin hat der Veröffentlichung zugestimmt.

Ich habe den angestrebten Doktorgrad noch nicht erworben und bin nicht in einem früheren Promotionsverfahren für den angestrebten Doktorgrad endgültig gescheitert.

Die öffentlich zugängliche Promotionsordnung der TUM ist mir bekannt, insbesondere habe ich die Bedeutung von § 28 (Nichtigkeit der Promotion) und § 29 (Entzug des Doktorgrades) zur Kenntnis genommen. Ich bin mir der Konsequenzen einer falschen Eidesstattlichen Erklärung bewusst.

Mit der Aufnahme meiner personenbezogenen Daten in die Alumni Datei bei der TUM bin ich einverstanden.

München, 23.04.2018



Dedicated to my parents, Marija and Milan
Posvećeno mojim roditeljima, Mariji i Milanu

Table of Contents

1	Summary	1
2	Zusammenfassung	3
3	List of abbreviations and symbols	6
4	Introduction	12
4.1.	Oxygen homeostasis	12
4.2.	Adaptation to hypoxia: hypoxia-inducible transcription factors	13
4.3.	Oxygen toxicity: reactive oxygen species	15
4.3.1.	Chemical properties of oxygen	15
4.3.2.	Chemical properties of ROS	16
4.3.3.	Antioxidant systems	16
4.4.	DNA damage response	18
4.5.	ROS signaling	19
4.6.	Sources of reactive oxygen species	20
4.6.1.	Mitochondrial electron transfer chain	20
4.6.2.	NADPH oxidases	21
4.6.3.	Nitric oxide synthases	24
4.7.	Oxygen homeostasis and disease	26
4.7.1.	Angiogenesis, integrins and vascular homeostasis	26
4.7.2.	Pulmonary hypertension	27
4.7.3.	Cancer	28
4.7.4.	Glucocorticoid-dependent stress response	30
5	Aims	31
6	Materials and methods	32
6.1.	Materials	32
6.1.1.	Equipment	32
6.1.2.	Chemicals	34
6.1.3.	Plastic ware	35

6.1.4.Primary antibodies	36
6.1.5.Secondary antibodies horse radish peroxidase conjugated	36
6.1.6.Secondary antibodies fluorescently conjugated	37
6.1.7.Cell culture media and additives	37
6.1.8.Kits	37
6.2.Methods	38
6.2.1.Cell lines	38
6.2.1.1.Human pulmonary artery endothelial cells	38
6.2.1.2.Human microvascular endothelial cells	38
6.2.1.3.Human pulmonary artery smooth muscle cells	38
6.2.1.4.Human malignant melanoma cells	39
6.2.1.5.Cell culture under hypoxia	39
6.2.1.6.Storage of cells	39
6.2.2.Animals	39
6.2.3.Transfections, luciferase assays and viral transduction	40
6.2.3.1.Transfections	40
6.2.3.2.Luciferase assays	40
6.2.3.3.Plasmids	40
6.2.3.4.Gene silencing by RNAi	41
6.2.3.5. Gene silencing by lentiviral transduction	41
6.2.4.Biochemical and molecular biology techniques	42
6.2.4.1.Protein isolation	42
6.2.4.2.Electrophoretic protein separation and immunoblotting	42
6.2.4.3.Gene expression analysis	43
6.2.4.4.Chromatin immunoprecipitation	44
6.2.4.5.Immunofluorescence	44
6.2.4.6.Immunohistochemistry	45
6.2.5.Physico-chemical techniques	46
6.2.5.1.Detection of reactive oxygen species	46

6.2.5.1.1.Detection of superoxide anion radical by electron paramagnetic resonance	46
6.2.5.1.2.Detection of reactive oxygen species by high pressure liquid chromatography	47
6.2.5.2.Detection of nitric oxide	47
6.2.5.2.1.Detection of nitric oxide radical by EPR	47
6.2.5.2.2.Detection of nitrates by HPLC	47
6.2.5.3.Detection of pterins by HPLC	48
6.2.6. <i>In vitro</i> assays	48
6.2.6.1.BrdU incorporation assay	48
6.2.6.2.Tube formation assay	49
6.2.7. <i>Ex vivo</i> assays	49
6.2.7.1.Wire myography	49
6.2.7.2. <i>Ex vivo</i> hypoxia experiments	50
6.2.8. <i>In vivo</i> animal experiments	50
6.2.8.1.Chronic hypoxia and treatment regimens	50
6.2.8.2.Gross morphology analysis	50
6.2.8.3.Wheat germ agglutinin assay	51
6.2.8.4.Right ventricular hypertrophy	51
6.2.8.5.Hemodynamic measurements	51
6.2.8.6.Echocardiography	52
6.2.8.7. <i>In vivo</i> angiogenesis	52
6.2.9.Statistics	52
7 Results	53
7.1.Folic acid protects against hypoxia-induced pulmonary hypertension	53
7.1.1.Nitric oxide and 5',6',7',8' tetrahydrobiopterin bioavailability are decreased under hypoxia	53
7.1.2.Folic acid increases dihydrofolate reductase levels and BH ₄ bioavailability under hypoxia	54
7.1.3.Folic acid increases hypoxic NO bioavailability	56
7.1.4.Folic acid improves vasoconstriction in pulmonary arteries	58

7.1.5.Hypoxia uncouples eNOS	59
7.1.6.Superoxide production is decreased under hypoxia	60
7.1.7.Folic acid improves hypoxic NO bioavailability <i>in vivo</i>	62
7.1.8.Folic acid decreases hypoxic ROS levels <i>in vivo</i>	63
7.1.9.Folic acid protects against hypoxia-induced right ventricular hypertrophy, right ventricular pressure increase and pulmonary vascular remodeling	64
7.2.Dexamethasone promotes cardiac and pulmonary vascular remodeling <i>via</i> reactive oxygen species and hypoxia inducible factor 1	67
7.2.1.Dexamethasone induces superoxide production in vascular cells and vessels	67
7.2.2.Dexamethasone-induced superoxide production is derived from NADPH oxidases	69
7.2.3.Dexamethasone upregulates NADPH oxidases and promotes proliferative responses	72
7.2.4.Dexamethasone induces systemic and pulmonary hypertension	74
7.2.5.Dexamethasone induces hypoxia inducible factor 1	77
7.2.6.HIF1 α is involved in dexamethasone-induced pulmonary vascular remodeling	80
7.3. β 3-endonexin as a novel negative regulator of hypoxia inducible factor 1	82
7.3.1. β 3-endonexin expression and localization under hypoxia	82
7.3.2. β 3-endonexin decreases HIF activity and HIF1 α expression under hypoxia	85
7.3.3.Depletion of β 3-endonexin induces NF κ B-driven HIF1 α transcription	87
7.2.4. β 3-endonexin diminishes proliferative and angiogenic responses under hypoxia	90
7.4.The NADPH oxidase NOX4 activates the ATM-CHK2-p53 pathway in response to oxaliplatin	93
7.4.1.Oxaliplatin increases reactive oxygen species in human malignant melanoma cells	93
7.4.2.Oxaliplatin induces double-strand DNA damage response in human melanoma cells	95
7.4.3.Oxaliplatin-induced double-strand DNA damage response is dependent on NOX4	96
7.4.4.Oxaliplatin induces proliferative arrest and senescence	97
8 Discussion	100
8.1.Folic acid protects against hypoxia-induced pulmonary hypertension	100

8.2.Dexamethasone promotes cardiac and pulmonary vascular remodeling <i>via</i> reactive oxygen species and hypoxia inducible factor 1	105
8.3.β3-endonexin as a novel negative regulator of hypoxia inducible factor 1	110
8.4.The NADPH oxidase NOX4 activates the ATM-CHK2-p53 pathway in response to oxaliplatin	113
8.5.Concluding remarks	117
9 Literature	118
10 Appendix	142
11 Acknowledgements	143
12 Curriculum Vitae	144

1 Summary

Oxygen is essential for adequate functioning of all aerobic organisms. Many pathways have been evolved, often governed by the hypoxia inducible factor (HIF) transcription factors, which help to ensure adequate provision of oxygen and to adapt to insufficient oxygen supply, for example by allowing the generation of new vessels. On the other hand, oxygen is easily accepting electrons thus leading to the formation of reactive oxygen species (ROS). ROS in high concentrations are toxic to cellular structures, but act as signaling molecules in lower concentrations, mediating a variety of cellular functions reaching from proliferation to cell death.

Since dysfunction of the complex pathways involved in maintaining oxygen utilization and metabolism can be cause or consequence of various diseases, a better understanding of these pathways and their connection to therapeutically relevant external stimuli is needed.

The aim of this work was thus to explore a) novel pathways involved in the adaptation to hypoxia (parts one and two), and b) to investigate the role of ROS and oxygen-regulated pathways in the response to therapeutically relevant external stimuli (parts three and four).

In the first part, the role of the β 3-integrin binding protein β 3-endonexin, a protein with several variants but insufficiently characterized functions, has been explored in hypoxic endothelial cells. It was shown that β 3-endonexin accumulated in the nucleus under hypoxic conditions where it interfered with NF κ B activation and expression of its target genes including HIF1. Subsequently, β 3-endonexin was identified as novel inhibitor of angiogenesis under hypoxic conditions. Thus, depletion of β 3-endonexin might be a novel strategy to enhance angiogenesis and thus adaptation to hypoxia.

In the second part, the role of nitric oxide (NO) signaling in the response to hypoxia was investigated in hypoxic endothelial cells and in a model of chronic hypoxia-induced pulmonary hypertension. It was found that hypoxia resulted in dysfunction of the NO producing enzyme NO synthase (NOS) leading to the so called uncoupling of this enzyme resulting in the formation of superoxide instead of NO. Mechanistically, hypoxia decreased the expression of dihydrofolate reductase (DHFR), which is important for regeneration of the NOS cofactor BH₄ from BH₂. The subsequent loss of BH₄ in hypoxia resulting in decreased NO availability was prevented by application of folic acid, which restored DHFR levels. In vivo studies in chronic hypoxic mice demonstrated that treatment with folic acid was able to restore BH₄ levels and NO bioavailability and to prevent the development of pulmonary hypertension under these conditions. Thus, folic acid might be an interesting novel therapeutic approach in hypoxia-induced pulmonary hypertension.

In the third part, the role of ROS-generating NADPH oxidases and the HIF signaling pathways in the response to the synthetic glucocorticoid dexamethasone was evaluated in endothelial cells and in a mouse model of chronic low dose dexamethasone treatment. It was found that dexamethasone treatment induced ROS generation by NADPH oxidases, which resulted in activation of the HIF pathway *in vitro* and *in vivo*. Subsequently, dexamethasone increased endothelial proliferation and angiogenesis. *In vivo*, dexamethasone treatment promoted an increase in left ventricular pressure as an indicator of enhanced systemic pressure leading to left ventricular hypertrophy as well as to left ventricular dysfunction. Dexamethasone treatment also resulted in pulmonary vascular remodeling, right ventricular hypertrophy and pulmonary hypertension. These *in vivo* responses were significantly ameliorated in mice with dysfunctional NADPH oxidases or in mice deficient in vascular HIF1 α expression. Thus, inhibition of ROS generation by NADPH oxidases and/or HIF activation might be interesting novel strategies to prevent cardiovascular side effects of dexamethasone treatment.

In the fourth part, the role of NADPH oxidases in the response to double stranded DNA damage (dsDDR) was investigated in a model of oxaliplatin-treated melanoma cells. It was shown, that oxaliplatin induced ROS generation and the expression of the NADPH oxidase NOX4 and subsequently the HIF pathway. NOX4 promoted the activation of oxaliplatin-induced dsDDR by stimulating phosphorylation of the key dsDDR signaling kinase ataxia telangiectasia mutated (ATM), and its downstream targets H2AX and checkpoint kinase 2, as well as by increasing p53 levels. NOX4 was further involved in oxaliplatin-induced reduction of proliferation of melanoma cells, which was not related to programmed cell death but rather to cellular senescence. Importantly, evaluation of tissue samples from patients with metastatic melanoma revealed a high rate of NOX4-positive samples, and the majority of NOX4-positive samples showed signs of active dsDDR. As active dsDDR and the absence of programmed cell death are often found in tumors resistant to chemotherapy, these findings suggest a role for NOX4 in mediating therapy resistance by activating dsDDR in oxaliplatin-treated melanoma.

In summary, this work showed that hypoxia signaling pathways and ROS are involved and interact in various manners mediating not only the adaptation to hypoxia but also contributing to the response to external stimuli with important therapeutic relevance such as glucocorticoids and chemotherapeutics.

2 Zusammenfassung

Sauerstoff ist essentiell für alle aeroben Organismen. Dabei hilft eine Vielzahl von Signalwegen, oft durch Hypoxie-induzierbare Transkriptionsfaktoren (HIF) gesteuert, die notwendige Versorgung mit Sauerstoff zu gewährleisten und sich an ungenügende Sauerstoffversorgung, zum Beispiel durch die Bildung von neuen Gefäßen, anzupassen. Auf der anderen Seite kann Sauerstoff leicht Elektronen akzeptieren und so zur Bildung von reaktiven Sauerstoffspezies (ROS) führen. Hohe Konzentrationen an ROS sind für zelluläre Strukturen toxisch, in niedrigen Konzentrationen können sie jedoch als Signalmoleküle wirken, und so eine Vielzahl von zellulären Funktionen, die von Proliferation bis hin zu Zelltod reichen, regulieren.

Da eine Dysfunktion der komplexen Signalwege, die in die Kontrolle von Sauerstoffnutzung und –metabolismus involviert sind, sowohl Ursache als auch Konsequenz verschiedener Erkrankungen sein kann, ist ein besseres Verständnis dieser Signalwege und deren Verbindung zu therapeutisch relevanten externen Stimuli notwendig. Das Ziel dieser Arbeit war daher, a) neue Signalwege zu erforschen, die in die Anpassung an Hypoxie involviert sind (Teile 1 und 2), und b) die Rolle von ROS und Sauerstoff-regulierten Signalwegen in der Antwort auf therapeutisch relevante externe Stimuli zu untersuchen (Teile 3 und 4).

Im 1. Teil wurde die Rolle des β 3-Integrin-bindenden Proteins β 3-Endonexin, das mehrere Varianten mit ungenügend charakterisierter Funktion besitzt, in hypoxischen Endothelzellen erforscht. Es konnte gezeigt werden, dass β 3-Endonexin im Zellkern unter hypoxischen Bedingungen akkumuliert und dort mit der Aktivierung von NF κ B und der Expression von dessen Zielgenen wie HIF1 interferiert. β 3-Endonexin wurde auch als neuer Angiogeneseinhibitor unter hypoxischen Bedingungen identifiziert. Depletion von β 3-Endonexin könnte daher eine neue Strategie zur Stimulation der Angiogenese und damit der Anpassung an Hypoxie darstellen.

Im 2. Teil wurde die Rolle von Stickstoffmonoxid (NO) als Signal in der Hypoxieantwort in hypoxischen Endothelzellen und in einem Modell der durch chronische Hypoxie induzierten pulmonalen Hypertension untersucht. Es konnte gezeigt werden, dass Hypoxie zu einer Dysfunktion des NO-produzierenden Enzyms NO Synthase (NOS) und damit zum sogenannten Entkoppeln dieses Enzyms führt. Dies resultiert in der Bildung von Superoxid an Stelle von NO. Dabei verminderte Hypoxie die Expression der Dihydrofolatreduktase (DHFR), die für die Regeneration des NOS Kofaktors BH₄ aus BH₂ wichtig ist. Der nachfolgende Verlust von BH₄ unter Hypoxie führte zu verminderter NO Verfügbarkeit, die durch die Anwendung von Folsäure, die die Spiegel an DHFR wieder herstellte, verhindert

werden konnte. In vivo Studien in chronisch hypoxischen Mäusen zeigten ebenfalls, dass Behandlung mit Folsäure die Spiegel an BH₄ und die Bioverfügbarkeit von NO wiederherstellen konnte, und so die Entwicklung einer pulmonalen Hypertension unter diesen Bedingungen verhindern konnte. Folsäure könnte daher ein interessanter neuer therapeutischer Ansatz bei Hypoxie-induzierter pulmonaler Hypertension sein.

Im 3. Teil wurde die Rolle der ROS-bildenden NADPH Oxidasen und der HIF Signalwege in der Antwort auf das synthetische Glukokortikoid Dexamethason in Endothelzellen und in einem Mausmodell mit chronischer Applikation niedriger Dosen von Dexamethason untersucht. Es konnte gezeigt werden, dass Behandlung mit Dexamethason die ROS Bildung durch NADPH Oxidasen induziert. Dies führte zur Aktivierung des HIF Signalwegs *in vitro* und *in vivo*. In der Folge erhöhte Dexamethason die Proliferation von Endothelzellen und die Angiogenese. *In vivo* führte Dexamethasonbehandlung zu einem Anstieg des linksventrikulären Drucks als einem Indikator des erhöhten systemischen Druckes, zu Hypertrophie des linken Ventrikels und linksventrikulärer Dysfunktion. Dexamethasonbehandlung führte auch zu pulmonal-vaskulärem Remodelling, rechtsventrikulärer Hypertrophie und pulmonaler Hypertension. Diese *in vivo* Reaktionen waren in Mäusen mit dysfunktionaler NADPH Oxidase oder in Mäusen, denen vaskuläres HIF1 α fehlte, signifikant vermindert. Die Hemmung der ROS Bildung durch NADPH Oxidasen und/oder der Aktivierung von HIF könnten daher interessante neue Strategien darstellen, um kardiovaskuläre Nebeneffekte einer Dexamethasonbehandlung zu verhindern.

Im 4. Teil wurde die Rolle der NADPH Oxidasen in der Antwort auf Schädigung doppelsträngiger DNA (dsDDR) in einem Modell Oxaliplatin-behandelter Melanomzellen untersucht. Es konnte gezeigt werden, dass Oxaliplatin die Bildung von ROS, die Expression der NADPH Oxidase NOX4 und nachfolgend den HIF Signalweg induziert. NOX4 stimulierte die Aktivierung der Oxaliplatin-induzierten dsDDR durch Phosphorylierung der zentralen dsDDR Signalkinase "ataxia telangiectasia mutated" (ATM) und deren Zielmolekülen H2AX und "checkpoint kinase 2" sowie durch eine Erhöhung der p53 Spiegel. NOX4 trug zudem zur Verminderung der Proliferation von Melanomzellen durch Oxaliplatin bei, die nicht mit programmiertem Zelltod, sondern eher mit Seneszenz in Verbindung stand. Insbesondere die Evaluierung von Gewebeproben von Patienten mit metastasierendem Melanom ergab eine hohe Anzahl an NOX4-positiven Proben, und die Mehrzahl der NOX4-positiven Proben wies Zeichen aktiver dsDDR auf. Da aktive dsDDR und das Fehlen des programmierten Zelltods oft in chemotherapieresistenten Tumoren gefunden werden, lassen diese Befunde eine Rolle von NOX4 bei der Entwicklung der Resistenz auf Oxaliplatinbehandlung von Melanomen durch dsDDR Aktivierung vermuten.

Zusammenfassend zeigte diese Arbeit, dass Hypoxiesignalwege und ROS interagieren können und in verschiedener Hinsicht nicht nur die Anpassung an Hypoxie vermitteln, sondern auch zur Antwort auf externe Stimuli mit wichtiger therapeutischer Relevanz wie Glukokortikoide und Chemotherapeutika beitragen können.

3 List of abbreviations and symbols

Ach – acetylcholine

ActD – actinomycin D

Akt – protein kinase B

L-Arg –L-arginine

Apo – apocynin

ARNT - arylhydrocarbon receptor nuclear translocator

Asc – ascorbic acid

ATR - ataxia telangiectasia and Rad3-related protein kinase

p-ATM - phosphorylated ataxia telangiectasia mutated kinase

BCKDH - branched-chain α -ketoacid dehydrogenase complex

BH₂ - 7',8'-tetrahydrobiopterin

BH₄ - 5',6',7',8'-tetrahydrobiopterin

BM – body mass

BrdU - 5-bromo-2'deoxyuridine

CHK2 - checkpoint kinase 2

CMH - 1-hydroxy-methoxycarbonyl-2,2,5,5-tetramethyl-pyrrolidine hydrochloride

CREB – cyclic adenosine monophosphate [cAMP]-response element-binding (protein)

Ctr - control

DAN - 2, 3-diaminonaphtalene

DAPI - 4', 6-diamidino-2-phenylindole

DDR - DNA damage response

DETC - diethyldithiocarbamate

Dex - dexamethasone

DHE – dihydroethidium

DHFR – dihydrofolate reductase

DMSO - dimethyl sulfoxide

EBM - endothelial basal medium

ECM – extracellular matrix

EDTA - ethylenediaminetetraacetic acid

EGF1 – epidermal growth factor 1
EGTA – ethylene glycol-bis(β -aminoethyl ether)-N,N,N',N'-tetraacetic acid
ELISA - enzyme-linked immunosorbent assay
EN - endonexin
EN-L – endonexin long isoform
EN-S – endonexin short isoform
eNOS – endothelial nitric oxide synthase
EPO - erythropoietin
EPR – electron paramagnetic resonance
ETFQO - electron transfer flavoprotein oxidoreductase
FAD⁺ - flavin adenine dinucleotide
FADH - flavin adenine dinucleotide (half reduced)
FADH₂ - flavin adenine dinucleotide (hydroquinone form)
FCS – fetal calf serum
FFPE – formalin fixed paraffin embedded
FGF β – fibroblast growth factor beta
FIH - factor inhibiting HIF
FMN – flavin mononucleotide
FS - fractional shortening
G3PDH - sn-glycerol-3-phosphate dehydrogenase
GKT – GKT-137831
GR – glucocorticoid receptor
GC – glucocorticoids
GRX - glutaredoxin
GTPCH - GTP cyclohydrolase I
(γ)H2AX - (phospho) histone 2AX
Hb - hemoglobin
HBSS - Hank's balanced salt solution
HIF - hypoxia-inducible factor
HMEC-1 – human microvascular endothelial cells
HPAEC – human pulmonary artery endothelial cells

HPLC – high pressure liquid chromatography
HRE - hypoxia response element
hsp - heat shock protein
Hx - hypoxia
iNOS – inducible nitric oxide synthase
KHB – Krebs-hepes buffer
L-NAME - L-(G)-nitro-L-arginine methyl ester
LY – LY294002 (PI-3K inhibitor)
LV - left ventricle
LVEDD - left ventricular end diastolic diameter
LVESD - left ventricular end systolic diameter
LVH - left ventricular hypertrophy
LVP - left ventricular pressure
MAPK - mitogen-activated protein kinase
MC3T3-E1 – murine osteoblast precursor cell line
MDM2 – mouse double minute 2
MR – mineralocorticoid receptor
mTOR – mammalian target of rapamycin
mtNOS – mitochondrial nitric oxide synthase
NAC – N-acetyl cysteine
NAD⁺ - nicotinamide adenine dinucleotide
NADH - nicotinamide adenine dinucleotide
NADPH - nicotinamide adenine dinucleotide phosphate
NFκB - nuclear factor kappa B
nNOS – neuronal nitric oxide synthase
NO – nitric oxide
NOS - nitric oxide synthase
Nx – normoxia
O₂⁻ - superoxide
ODD – oxygen-dependent degradation domain
ODH - octopine dehydrogenase

Ox - oxaliplatin
Oxy - oxypurinol
PA – pulmonary artery
PAH – pulmonary arterial hypertension
PAI1 – plasminogen activator-inhibitor 1
PARP1 - pro-apoptotic poly (ADP-ribose) polymerase
PASMC – pulmonary artery smooth muscle cells
PBS – phosphate buffered saline
PCD – programmed cell death
PCR - polymerase chain reaction
PDH - pyruvate dehydrogenase
PH – pulmonary hypertension
PI-3K - phosphatidylinositol-4,5-bisphosphate 3-kinase
PHD - prolyl hydroxylases
PTEN - phosphatase and tensin homolog
PTPS - 6-pyruvoyltetrahydropterin synthase
pVHL – protein von Hippel Lindau
PVR – pulmonary vascular remodeling
Q - ubiquinone
QH₂ – ubiquinol
Rac – (Ras-related C3 botulinum toxin substrate) subfamily of the Rho family of GTPases
RAF – (Rapidly accelerated fibrosarcoma) proto-oncogene serine/threonine-protein kinase family
Ras – (Rat sarcoma) protein family of small GTPases
RBC - red blood cell
RDM – right marginal coronary artery
ReOx - reoxygenation
RIV – right descending interventricular artery
ROS – reactive oxygen species
Rot – rotenone
RV – right ventricular
RVH – right ventricular hypertrophy

RVP - right ventricular pressure

RU486 – mifepristone

S - septum

SA – systemic artery

SBE - SMAD3 binding elements

SDS-PAGE – sodium dodecyl sulfate polyacrylamide gel electrophoresis

SDH - succinate dehydrogenase

Ser - serine

shRNA – short hairpin RNA

siRNA – silencing RNA

α -SMA – alpha smooth muscle actin

SMAD3 - *Caenorhabditis elegans Sma* genes and the *Drosophila Mad*, Mothers against decapentaplegic

SOD – superoxide dismutase

SQR - sulfide:quinone oxidoreductase

SR – sepiapterin reductase

SSB – single strand (DNA) breaks

TBM - tetramethylbenzidine

TBS – tris-buffered saline

TBS-T – tris-buffered saline-tween20

TCA - trichloroacetic acid

TF – tissue factor

TGF β 1 – transforming growth factor beta 1

Thr - threonine

TMB - tetramethyl-benzidine

TNF α – tumor necrosis factor alpha

TRX - thioredoxin

TTFA - 2- thenoyltrifluoroactenone

uPAR – urokinase

VEGFA vascular endothelial growth factor A

VHL – von Hippel-Lindau

WGA – wheat germ agglutinin

WHO – World Health Organization

WM1158 - human melanoma cells

4 Introduction

4.1. Oxygen homeostasis

The origin of the aerobic life on Earth is connected to the evolution of photosynthesis – a photochemical process of transducing solar energy into the chemical energy of carbon bonds, characteristic nowadays of virtually all plants, some algae and some bacteria. In this process, carbon dioxide and water are converted into glucose, with molecular oxygen (O_2) generated as a side product of the reaction. Photochemical reaction centers developed in ancestors of green sulfur bacteria enabling them to start photosynthetic reactions some 3 billion years ago – biologically-induced oxygenation of Earth's atmosphere some half a megganium later (Great Oxygenation Event) (1-4).

The increase in atmospheric O_2 was very slow at first and had allowed a gradual evolution of protective mechanisms. Nearly all O_2 produced by early photosynthetic bacteria was used for oxidizing ferrous (Fe^{2+}) (which was found in excess in early oceans) to ferric (Fe^{3+}) state (5). Geological evidence suggests that upon the exhaustion of the ferrous pool, O_2 levels in the atmosphere then began to rise, reaching current levels between 0.5-1.5 billion years ago (5). This shift of O_2 content in the atmosphere was not beneficial for many organisms that inhabited Earth at that time, causing their extinction. On the other hand, raise of oxygen in the atmosphere paved the way for the evolution of the most diverse living organisms on Earth – aerobic *Eukaryota*, that obligatory use oxygen for completion of their metabolic processes. However, the evolution of aerobic eukaryotes would not be able without the appearance of mitochondria, subcellular organelles, about 1.5 billion years ago, in which the end product of glycolysis are further oxidized, thereby extracting significantly higher levels of energy. In this process, reducing equivalents are generated that pass through the mitochondrial respiratory complex, which results in the formation of a proton gradient that is used to drive the synthesis of adenosine 5'-triphosphate (ATP). The electrons transferred through the mitochondrial respiratory chain ultimately react with O_2 to form H_2O , a process that is catalyzed by cytochrome c oxidase (complex IV).

The appearance of the first metazoan organisms (multicellular Eukaryotes) happened ~0.5 billion years ago. Metazoan evolution was dependent on the development of the process of oxidative phosphorylation which, in comparison to glycolysis, produced 18 times as much ATP per glucose molecule (6).

However, as diffusion will only provide sufficient O₂ for cells located < 100 μm from the atmosphere or another source of O₂, specialized systems for O₂ delivery evolved, leading to animals of increasing size and anatomical complexity. Nowadays, terrestrial mammalian life has evolved to perform optimally at an atmospheric partial pressure of oxygen (pO₂) at, or around, 150 mmHg.

In the body, cells exist in highly diverse oxygen environments, and the term hypoxia is usually used to describe low oxygen levels as compared to optimal oxygen levels for a given tissue or organ (7). To illustrate, in humans pO₂ tensions range from 80–100 mmHg in the lung alveoli and arterial blood to 1–2 mmHg in renal papilla (7).

Majorly eukaryotic organisms must maintain oxygen homeostasis, and this requirement is a critical organizing principle of metazoan evolution and biology. *Vertebrata* have evolved complex circulatory, respiratory, and neuroendocrine systems to ensure that oxygen levels are precisely maintained, since an excess or deficiency may result in the death of cells, tissue, or the organism. Thus, when oxygen supply is not adequate, or oxygen is even absent, ATP levels drop, cellular functions cannot be maintained, and – if the insult lasts long enough – cells die.

4.2. Adaptation to hypoxia: hypoxia-inducible transcription factors

The provision of adequate oxygen supply is a challenge faced by all aerobic organisms. This process is especially demanding in multi-cellular organisms. Low or inadequate oxygen provision (hypoxia) is an important feature of many human diseases including ischemic disease, chronic inflammatory disease, and cardiovascular diseases such as pulmonary hypertension, atherosclerosis or myocardial infarction (7). Much scientific attention was given to cellular “oxygen sensing” and hypoxia adaptation mechanisms. The family of hypoxia-inducible transcription factors (HIF) is central in controlling the cellular sensing and response to hypoxia (8-10). Among them, HIF1 is ubiquitously expressed and regulates various genes involved in the adaptation to hypoxia by controlling, among others, cell proliferation and survival, angiogenesis, oxygen transport, glucose metabolism and vascular tone (11, 12).

To date, three HIF family members have been identified. HIF1 was discovered by the identification of a hypoxia response element (HRE; 5-RCGTG-3) in the enhancer of the erythropoietin (EPO) gene, a hormone that stimulates erythrocyte proliferation and undergoes hypoxia induced transcription (13-16). While HIF1 is ubiquitously expressed and widely involved in the cellular process of hypoxic adaptation, HIF2 appears to be more

specifically involved in hypoxia signaling (17-19). HIF3, on the other hand, seems to exert opposing effects (20, 21). HIF transcription factors are α/β -heterodimers that consist of constitutively expressed HIF β , also termed arylhydrocarbon receptor nuclear translocator [ARNT] and a highly regulated α -subunit (22).

Under normoxic conditions, HIF α is hydroxylated at proline residues P402 and P564 (23-27) within the oxygen-dependent degradation (ODD) domain (28) by HIF prolyl hydroxylases (PHD) which comprise 3 different subtypes (PHD1-3) (Figure I) (29). The enzymes belong to the family of 2-oxoglutarate-dependent oxygenases which require oxygen, Fe²⁺ and ascorbic acid for full functionality (24, 25, 27). Proline hydroxylation of HIF α mediates association of the von-Hippel-Lindau protein (pVHL), an E3 ubiquitin ligase complex that sequesters HIF α for proteasomal degradation (24, 30-33). Under hypoxic conditions, PHDs are not functional due to the lack of oxygen, thus leaving HIF α proteins stabilized to bind to ARNT (Figure I). In addition, asparaginyl hydroxylation at the C-terminal transactivation domain by the 2-oxoglutarate-dependent oxygenase FIH (factor inhibiting HIF) regulates binding of p300/CREB coactivators (17, 34). HIF binds to HRE in promoters and/or enhancers of hypoxia-inducible genes and is involved in the hypoxic regulation of glycolysis and other metabolic pathways, angiogenesis, proliferation and apoptosis etc. In addition, various other pathways have been described that modulate the degradation of HIF α irrespective of oxygen (17). These include deubiquitylating enzymes that antagonize pVHL-mediated ubiquitylation,

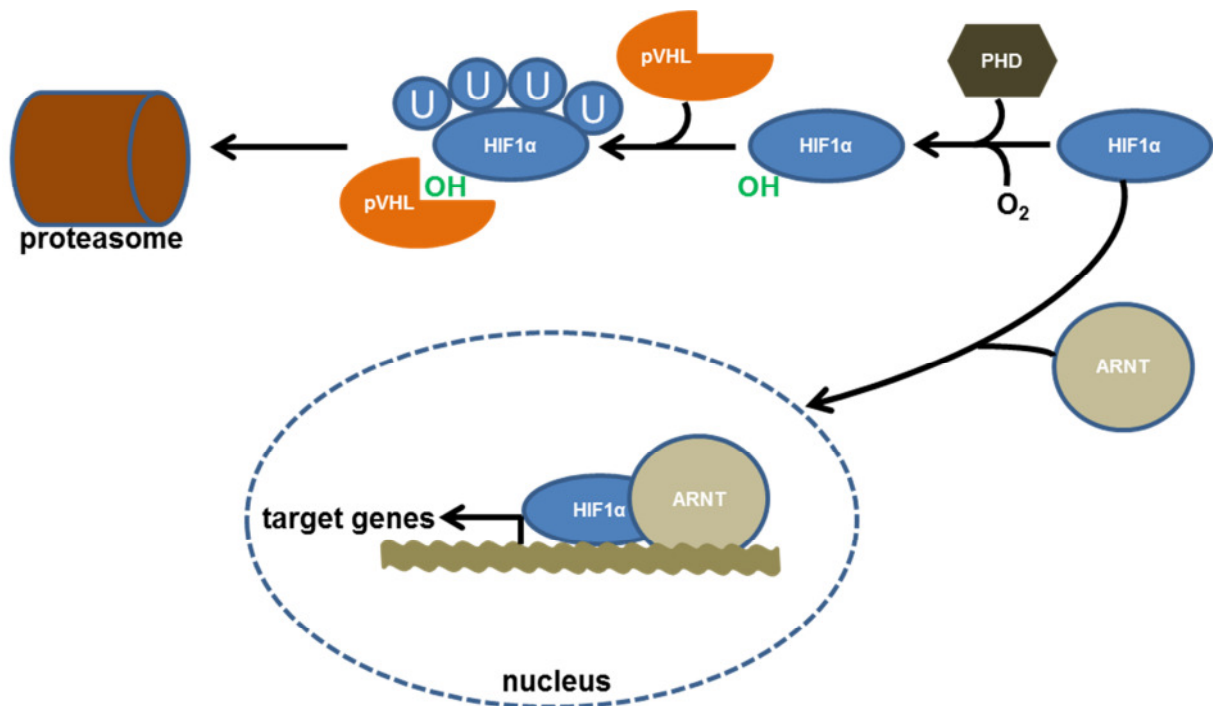


Figure I. Scheme of HIF1 α protein stabilization and degradation. Explanations are given in the text.

alternative ubiquitin ligases that target HIF α domains independently of oxygen, and other modifications that alter HIF α stability, such as sumoylation (7, 35, 36). Control of HIF α synthesis involves both transcriptional and post-transcriptional mechanisms (7). At the transcriptional level, the HIF1 α gene is regulated by nuclear factor kappa B (NF κ B) in response to ROS and cytokines and various other factors (7, 12, 37-39). Translational control is important for the maintenance of steady-state levels of HIF α (7). This is pronounced, in particular, in proliferating cells, where HIF α translation is augmented by mTOR-dependent and mTOR-independent pathways due to activation of the PI-3K/PTEN/AKT and RAS/RAF/MAPK signaling cascades, which lead to the activation of HIF even in the presence of oxygen (7). In hypoxic cells, HIF α subunits escape translation suppression and are synthesized at rates which can even exceed levels of the relevant mRNA (7). This mechanism remains unclear.

4.3.Oxygen toxicity: reactive oxygen species

4.3.1.Chemical properties of oxygen

Although aerobic life depends on oxygen, excess of the latter is toxic to aerobic life forms. The key feature of oxygen that allowed the evolution of aerobic life is the fact that ground-state triplet molecular oxygen (O_2) is a paramagnetic biradical with two electrons occupying separate π^* orbitals (unpaired) with parallel spins. Most of the nonradical organic molecules are diamagnetic having pairs of electrons with opposite spins. Their bonds are in the stable form of two electrons with antiparallel spins. O_2 has an electron spin restriction which only accepts a pair of electrons that has the same spin to fit the vacant spaces in π^* orbitals. Thus, for O_2 to accept a pair of electrons from an organic substrate, one of the electrons of oxygen or one of the electrons from the donating substrate has to invert its spin against which a large thermodynamic barrier exists. As a consequence, oxygen is thus unable to efficiently accept two electrons simultaneously, but rather accepts one electron at a time during redox reactions. This orientation prevents the oxidation by two-electron transfers which is deleterious for the living matter. However, this may be overcome by feeding oxygen with one electron at a time so that each of the unpaired electrons receives a partner, thus, generating oxygen radicals. This can occur e.g. in the respiratory chain when electrons escape and combine with O_2 prematurely, leading to the generation of superoxide anion radicals ($O_2^{\cdot-}$) and other reactive oxygen species (ROS). Furthermore, O_2 in the ground-state can be converted to a more reactive molecular oxygen form by energy transfer - singlet oxygen (1O_2),

which has paired electrons with opposite spins. In this, the spin restriction is removed, increasing the oxidizing capacity of $^1\text{O}_2$ compared to ground-state O_2 .

4.3.2. Chemical properties of ROS

Molecular oxygen can acquire one electron leading to the formation of superoxide anion radical ($\text{O}_2^{\cdot-}$) – a primary ROS. Furthermore, $\text{O}_2^{\cdot-}$ can be reduced either spontaneously or through a reaction with superoxide dismutases (SOD), through the Haber-Weiss reaction (40, 41), or in reaction with nitric oxide radical (NO^{\cdot}) (42) (Figure II). $\text{O}_2^{\cdot-}$ has a half-life of 10^{-9} to 10^{-11} s while in the presence of SOD, the half-life decreases to 10^{-15} s (42). The reaction catalyzed by SOD reduces two $\text{O}_2^{\cdot-}$ radicals to form oxygen and H_2O_2 which in turn can be fully reduced to H_2O and oxygen by peroxidases and catalase. It has a half-life of 10^{-3} s in the absence of catalase and 10^{-8} s in its presence. Alternatively, H_2O_2 can react with reduced transition metals — called the Fenton reaction (43) — to form OH^{\cdot} and OH^- or OOH^{\cdot} and H^+ , when combined with Fe^{2+} or Fe^{3+} , respectively (42). The reaction of $\text{O}_2^{\cdot-}$ with NO^{\cdot} , controlled by the rate of diffusion of both radicals, forms the very potent oxidant peroxynitrite (ONOO^-). ONOO^- in turn is oxidized or reacts with a hydrogen radical (H^{\cdot}) to form the stable HOONO . The latter dismutates quickly into OH^{\cdot} and free nitrogen species (NO_2^{\cdot}). Thus, concentrations of OH^{\cdot} increase by means of H_2O_2 and HOONO dismutation (metal-independent pathway). Alternatively, OH^{\cdot} can be generated through the Haber-Weiss reaction, when superoxide radicals and H_2O_2 molecules spontaneously combine to form molecular oxygen and hydroxyl radicals.

4.3.3. Antioxidant systems

Cells and tissues are protected against the toxicity of ROS and its metabolites by various antioxidant systems. The family of SOD which catalyzes the conversion of $\text{O}_2^{\cdot-}$ to hydrogen peroxide consists of extracellular SOD (SOD3, ecSOD), the MnSOD (SOD2) which is located in the mitochondria (44, 45) and CuZnSOD (SOD3) which is located in the cytosol (46-48). Catalase converts hydrogen peroxide into oxygen and water, and the glutathione redox system (GSH-peroxidase and GSH-reductase) inactivates NO, hydrogen peroxide, and other hydroperoxides (49-51). In addition, on-enzymatic factors are participating in the elimination of oxygen radicals such as: vitamin E (α -tocopherol), vitamin C (ascorbic acid), uric acid, β -carotene, flavonoids, taurine, lactoferrin, albumin, and bilirubin (52). Recent insights into

cellular redox chemistry have revealed the presence of certain specialized proteins such as peroxiredoxins (PRX), thioredoxins (TRX), glutaredoxins (GRX), heme oxygenases and reductases, which are involved in cellular adaptation and protection against an oxidative assault. These molecules usually exert their action at a more subtle level of cellular signaling processes (53).

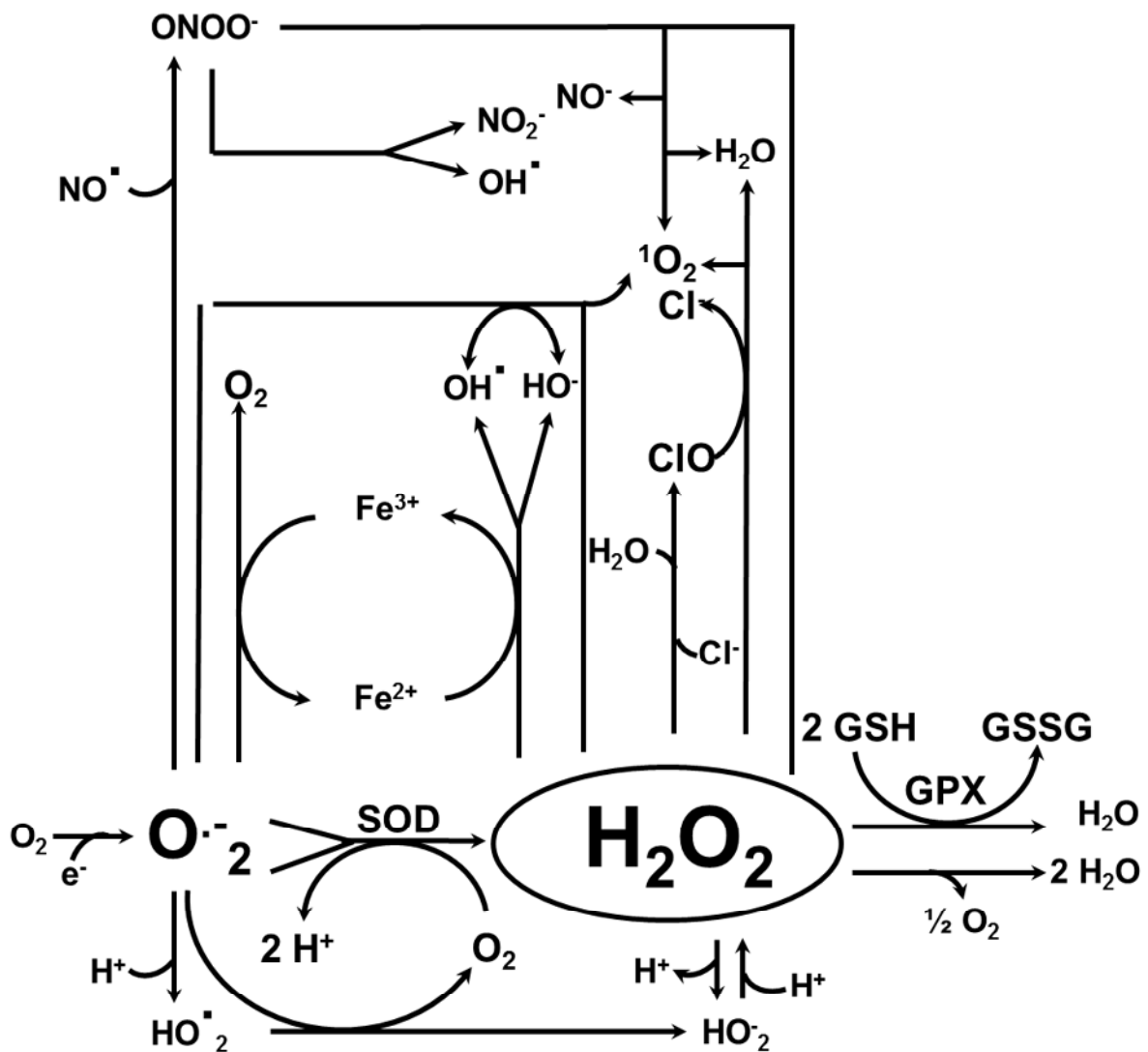


Figure II. Scheme of basic reactive oxygen species and reactions. H^+ hydrogen ion; e^- - electron; 1O_2 - singlet oxygen; ClO^- - hypochlorite; Cl^- - chlorite; HO_2^{\bullet} - perhydroxyl radical; NO_2^- - nitrite; MPX - myeloperoxidase. Explanations are given in the text. (Modified from Kietzman T. and Görlach A., 2005 (54))

4.4.DNA damage response

High levels of ROS either produced endogenously or exogenously, as well as many environmental toxins, irradiation or certain drugs such as chemotherapeutics can attack DNA, leading to formation of adducts that impair base-pairing and/or block DNA replication and/or transcription, base losses, or DNA single-strand breaks (SSBs) (55). When two SSBs arise in proximity, or when the DNA-replication machinery encounters a SSB or other lesions, double-strand breaks (DSBs) are formed, which are difficult to repair and thus extremely toxic (55, 56).

To combat threats posed by DNA damage, cells have evolved mechanisms – collectively termed the DNA-damage response (DDR) – to detect DNA lesions, signal their presence and promote their repair (55, 57, 58). Although responses differ for different classes of DNA lesions, they usually occur by a common general program.

The accumulation of double-strand breaks or adducts induces protective cellular strategies by activating the double strand DNA damage response (dsDDR). The dsDDR consists of a complex set of cell processes involving multiple DNA repair, cell cycle regulation, and cell death/survival pathways thus determining the cellular fate: DNA repair and further proliferation, cellular senescence or programmed cell death (59). dsDDR activity is regulated by the number of DSB, since in the case that the cell cannot maintain its normal DNA repair, it is forced to undergo programmed cell death or to stop proliferation without undergoing cell death - a pathway known as cellular senescence (60, 61). Ataxia telangiectasia mutated kinase (ATM) is the key component of the signal transduction pathways mobilized by dsDNA damage and is essential for safeguarding genomic integrity. It is activated through auto- or trans-phosphorylation on Ser1981 and subsequently phosphorylates downstream targets in multiple signal transduction cascades including the histone variant H2AX, checkpoint kinase 2 (CHK2) and p53. Activation of these checkpoint pathways can arrest progression through the cell cycle until the integrity of DNA is restored by repair mechanisms or allow progression towards programmed cell death.

ATM phosphorylates H2AX at Ser139 in multiple nucleosomes on each side of the DSB (62, 63). Phosphorylation of H2AX is required for the assembly of DNA repair proteins at the sites containing damaged chromatin as well as for activation of checkpoint proteins which arrest the cell cycle progression. H2AX plays thus a critical role in maintaining genome integrity and its loss leads to genomic instability

ATM further activates CHK2 via phosphorylation at Thr68 leading to its dimerization and acquirement of the kinase catalytic activity. Activated CHK2 can undergo dissociation from

chromatin allowing further signal amplification and translocation to soluble substrates. Enzymatically active dimers and monomers of CHK2 can phosphorylate various substrates including Cdc25C and Cdc25A phosphatases which upon activation are responsible for cell arrest at the G₂ to M transition or in G₁ phase, respectively (63).

In addition, ATM phosphorylates p53 protein at Ser15 thereby preventing binding of the mouse double minute 2 (MDM2) and thus degradation of p53. Consequently, a stable nuclear pool of p53 is established in this cascade of events (64). In addition, the active CHK2 enhances tetramerization of p53 by additional phosphorylation at Ser20, thus stabilizing p53 for its functions: It can activate DNA repair machinery when DNA has sustained damage. It can induce growth arrest by holding the cell cycle at the G₁/S regulation point on DNA damage recognition giving time for DNA repair. It can initiate programmed cell death, if DNA damage proves to be irreparable (64, 65).

4.5.ROS signaling

While ROS have been for a long time considered as unwanted by-products of cellular respiration, protein folding, and end products of a number of metabolic reactions, and thought to function exclusively as cellular damaging agents there is now increasing evidence that ROS at low levels can act as signaling molecules mediating varying cellular responses such as cell migration/adhesion, cell proliferation/hypertrophy, endoplasmic reticulum (ER) stress/autophagy, and programmed cell death/senescence. Thus, it appears that ROS are not simply an unwanted product of an imperfect system, but have instead been selected by nature for their specificity in signaling.

Specificity in ROS signaling takes advantage of the distinct biological properties of each oxidant species, which include their chemical reactivity, stability, and lipid diffusion capabilities. Although superoxide alone is not very reactive, it has several cellular effects. It can release iron from Fe/S clusters or can abstract hydrogen atoms from target molecules such as catecholamines, DNA, RNA, fatty acids, or steroid hormones.

The stability and membrane diffusibility of H₂O₂, which has selective reactivity towards cysteine residues, provides an advantage with regard to signaling capacity. Indeed, the best characterized mechanism by which H₂O₂ acts as signaling molecule is through the oxidation of critical cysteine residues within redox-sensitive proteins (66). Susceptible cysteine residues exist as a thiolate anion (S⁻) at physiological pH due their low pK_a, which make them more reactive in comparison to the protonated cysteine thiol group (SH) thus providing selectivity and sensitivity (67). H₂O₂ oxidization of the thiolate anion to the sulfenic form (SO⁻) impinges on cellular signaling by altering protein conformation and activity. In the presence of

high concentrations of H_2O_2 , SO^- is further oxidized to form sulfinic (SO_2^-) and sulfonic (SO_3^-) acids (i.e. hyperoxidation), where SO_3^- generally represents an irreversible oxidative modification. To prevent irreversible cysteine oxidation, the SO^- intermediate is commonly incorporated into a disulfide (S-S) or sulfenic-amide (S-N) bond. These modifications are reversible by the actions of GRX and TRX, which restore protein function; the oxidized protein is returned to its reduced state.

4.6.Sources of reactive oxygen species

Several cellular sources of ROS have been characterized which contribute to the formation of ROS in response to specific stimuli, thus further emphasizing the role of ROS as signaling molecules.

On the one hand, ROS are generated as by-products of the mitochondrial respiratory chain activity, while on the other hand several enzymatic sources of ROS can be either activated or induced to adjust ROS levels to signaling purposes, e.g. NADPH oxidases, xanthine oxidase, lipoxygenases, etc. Among those, only NADPH oxidases are solely prone to generate ROS, thus enabling them to play an important role in ROS signaling. In addition, the generation of NO by several NO synthases contributes by its diffusion-limited reaction with superoxide to peroxynitrite to ROS balance.

4.6.1.Mitochondrial electron transfer chain

Mitochondrial electron transport chain consists of an enzymatic series of electron donors and acceptors with incremental electron affinity, in which energy resulting from electron transfer is used for pumping the H^+ through the inner mitochondrial membrane consequently generating a H^+ gradient which enables ATP synthase to convert the mechanical work into ATP. Within the electron transport chain, energy resulting from electron transfer is used for pumping the H^+ through the inner mitochondrial membrane consequently generating a H^+ gradient which enables ATP synthase to convert the mechanical work into ATP.

Removal of electrons during oxidation is coupled to the reduction of NAD forming NADH which is then oxidized by Complex I (1). Succinate is also oxidized by Krebs cycle enzyme Complex II (succinate dehydrogenase; SDH) producing fumarate and reducing FAD to FADH_2 (1, 68). Electrons from Complex I and II are then passed through a series of prosthetic groups positioned according to increasing affinity for electrons: ubiquinone (Q) is producing ubiquinol (QH_2) which is then oxidized by Complex III (cytochrome bc1 complex)

(1, 69). In addition, electrons are fed into the Q pool by several other enzymes, such as: succinate dehydrogenase (SDH), electron transfer flavoprotein oxidoreductase (ETFQO), proline dehydrogenase, dihydroorotate dehydrogenase, sulfide:quinone oxidoreductase (SQR), and sn-glycerol-3-phosphate dehydrogenase (G3PDH) (70-75). Finally, the electrons are then passed to Complex IV (cytochrome c oxidase) and utilized to reduce O_2 to form H_2O (1). Electron transfer from NADH ($E^\circ = -340$ mV) or $FADH_2$ ($E^\circ = +31$ mV) through the Q pool ($E^\circ = +45$ mV) to O_2 ($E^\circ = +840$ mV) is an energetically favored process and coupled to proton pumping across the mitochondrial inner membrane into the intermembrane space. This creates a transmembrane electrochemical gradient of protons ($\Delta\mu_m$) which is composed of both an electrical ($\Delta\Psi_m$) and chemical (ΔpH) potential (1). F_1F_0 ATP synthase couples the energy liberated from electron transport to the terminal electron acceptor O_2 to the conversion of ADP and P_i into ATP, a process referred to as oxidative phosphorylation (1).

Mitochondria have up to 11 different sources of $O_2^{\cdot-}$ which can be divided into two different subgroups based on the source of redox potential for producing $O_2^{\cdot-}$: (1) NADH/NAD isopotential group and (2) QH_2/Q isopotential group (1, 76). The NADH/NAD isopotential group is reliant on the concentration of NADH and consists of Complex I, octopine dehydrogenase (ODH), pyruvate dehydrogenase (PDH), and branched-chain α -ketoacid dehydrogenase complex (BCKDH). QH_2/Q isopotential group requires reduction of Q to QH_2 and relies on Complex I, II, and III (1, 70, 71, 76-78), but also Q pool can be fed with electrons by SDH, ETFQO, proline dehydrogenase, dihydroorotate dehydrogenase, SQR, and G3PDH (1, 70, 71).

Complex I and III are chief sites for mitochondrial $O_2^{\cdot-}$ production (1). Complex I inhibition by rotenone can increase ROS generation in submitochondrial particles (79-81). At Complex I $O_2^{\cdot-}$ production can occur even when mitochondria are not producing ATP, due to a high proton motive force and reduced coenzyme Q pool, or when there is a high NADH/NAD⁺ ratio in mitochondrial matrix. Complex III funnels electrons from the CoQ pool to cytochrome c, and its blocking by actinomycin produces large amounts of ROS (80, 82, 83).

4.6.2. NADPH oxidases

NADPH oxidases are oxido-reductases which catalyze the transfer of an electron from NADPH to O_2 thus generating $O_2^{\cdot-}$ (84-86). These multiprotein enzyme complexes are “professional” ROS producers, while other enzymes produce ROS only as by-products along with their specific catalytic pathways (86). The prototypic NADPH oxidase has been initially identified in phagocytes localized in the plasma membrane and phagosomes (87, 88) where

it is responsible for generating $O_2^{\cdot-}$ in the respiratory burst as part of the innate immune response (20, 21). It is composed of the catalytic core NOX2 (formerly termed gp91phox) and the smaller subunit p22phox forming the flavocytochrome b558 (89-92) and regulated by the association with the regulatory proteins p47phox (92-94), p67phox (2, 92, 95-97), p40phox (92, 98-101) and the GTPase Rac (96, 100, 102) (Figure III). In the first step, electrons are transferred from NADPH to FAD^+ , a process that is regulated by the activation domain of p67phox (92, 97). In the second step, a single electron is transferred from the reduced flavin $FADH_2$ to the iron center of the inner heme (92). Since the iron of the heme can only accept one electron, the inner heme must donate its electron to the outer heme before the second electron can be accepted from the now partially reduced flavin, $FADH$ (92). The force for the transfer of the second electron, while smaller (31 vs. 79 mV), is still energetically favorable. However, the transfer of the electron from the inner heme to the outer heme is actually against the electromotive force between these two groups (92). To create an energetically favorable state, oxygen must be bound to the outer heme to accept the electron (92, 103-105). The human and mouse NOX2 genes are located on the X chromosome. NOX2 mRNA and protein were found to be expressed besides phagocytic cells in many other tissues, such as: thymus, small intestine, colon, spleen, pancreas, ovary, placenta, prostate, testis, neurons (92, 106), cardiomyocytes (92, 107), skeletal muscle myocytes (92, 108), hepatocytes (92, 109), endothelial cells (110-112), and hematopoietic stem cells (92, 113).

Subsequently, several homologues of NOX2 (NOX1-5) (92, 114-118), and the more distantly related DUOX1/2 (dual oxidases) have been described in non-phagocytic cells (92, 119, 120). NOX1 was the first homolog of NOX2 to be described (92, 121, 122). It shares a high degree of sequence identity with NOX2, both on genomic and protein level (92, 121-123). The human and mouse NOX1 genes are located on the X chromosome. NOX1 mRNA is highly expressed in colon epithelium (92, 122, 123), vascular smooth muscle cells (92, 122, 124), endothelial cells (92, 125, 126), uterus (92, 121, 122), placenta (92, 127), prostate (92, 121, 122), osteoclasts (92, 128), retinal pericytes (92, 129). In addition to its dependence on cytosolic subunits, NOX1 requires the membrane subunit p22phox (92, 130, 131) and the small GTPase Rac for the regulation of NOX1 activity (132-139).

NOX3 shares ~56% amino acid identity with NOX2 (92, 140, 141). The gene for human NOX3 is located on chromosome 6. Sequence alignment and hydropathy plot analysis predict the overall structure of NOX3 to be highly similar to that of NOX1 and NOX2, in terms of transmembrane domains, the length of the extracellular loops, NADPH- and FAD-binding sites, and the localization of the heme-coordinating histidines (92, 114, 115). High NOX3 expression was detected in the inner ear, including the cochlear and vestibular sensory

epithelia and the spiral ganglion (140). Low levels of NOX3 were detected in fetal spleen (115), fetal kidney (114, 140), skull bone, and brain (140).

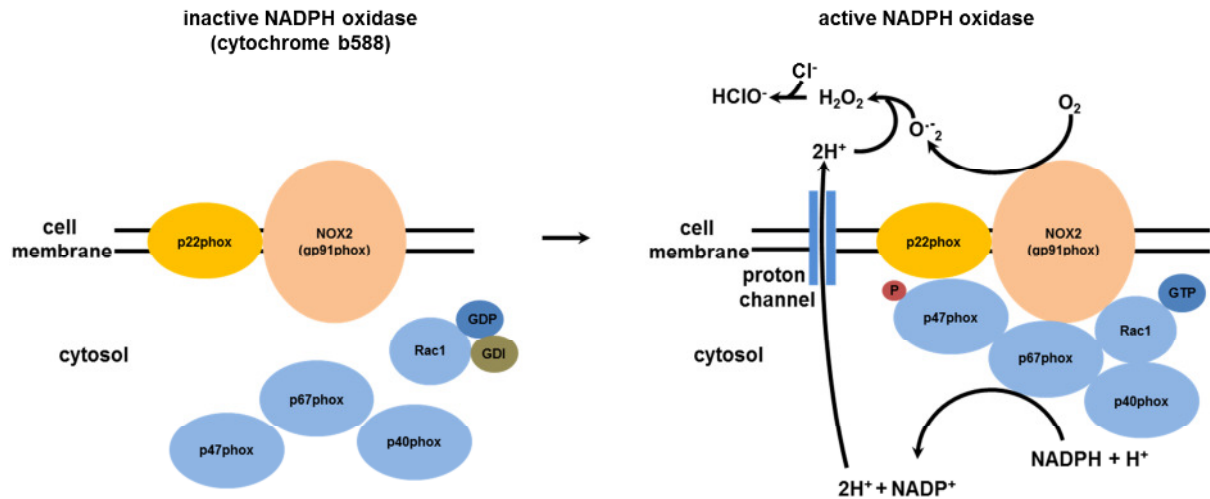


Figure III. NADPH oxidases: Prototypical phagocytic NADPH oxidase containing NOX2. P - phosphate; GDP - guanosine diphosphate; GDI – GDP dissociation inhibitor. Explanations are given in the text.

NOX4 was originally identified as an NADPH oxidase homolog highly expressed in the kidney, hence termed “renox” (92, 116, 117). NOX4 shares only ~39% of the sequential identity to NOX2. The gene for human NOX4 is located on chromosome 11. In addition to its strong expression in the kidney, NOX4 mRNA is also found in osteoclasts (92, 142, 143), endothelial cells (92, 125, 144, 145), smooth muscle cells (92, 146-151), hematopoietic stem cells (92, 113), fibroblasts (103, 152, 153), keratinocytes (154), melanoma cells (92, 155), and neurons (92, 156). NOX4 is a p22phox-dependent enzyme, which does not require cytosolic subunits or Rac for its function (92, 157). Thus, induction or depression of NOX4 expression are considered to be the main regulatory mechanisms of NOX4-dependent ROS production. In fact, various stimuli have been described to upregulate NOX4, including ER stress (92, 150), shear stress (92, 158), carotid artery injury (92, 159), hypoxia and ischemia (92, 156, 160), transforming growth factor β 1 (TGF β 1) and tumor necrosis factor (TNF)- α , angiotensin II (92, 161-163) and thrombin (37, 92).

Human NOX5 gene is located on chromosome 15 (92, 114, 118). The NOX5 isoforms (NOX5 α , - β , - γ , and - δ) distinguish themselves from the NOX1–4 enzymes by the presence of a long intracellular NH₂ terminus containing a Ca²⁺-binding EF hand domain (92, 118, 164, 165). The fifth isoform described by Cheng et al. (NOX5 ϵ or NOX5-S) lacks the EF-hand region and therefore has an overall structure more similar to NOX1–4 (114). On immunoblots, NOX5 is described as an 85-kDa protein (92, 166). This would be consistent

with its predicted molecular mass and suggests that the protein is not glycosylated. As seen for NOX2, NADH cannot replace NADPH as a cytoplasmic electron donor for NOX5 (92, 164, 165). NOX5 does not require p22phox or cytosolic organizer or activator subunits for activity (92, 118, 167); however, the Ca^{2+} -binding domain of NOX5 behaves as an independent folding unit and undergoes conformational changes in response to Ca^{2+} elevations (92, 118, 164, 165). NOX5 mRNA expression is described in testis, spleen, lymph nodes, vascular smooth muscle, bone marrow, pancreas, placenta, ovary, uterus, stomach, and in various fetal tissues, but not in circulating lymphocytes (92, 114, 118, 168).

4.6.3. Nitric oxide synthases

Nitric oxide (NO^{\bullet}) is a free radical due to an unpaired electron with a short half-life *in vivo* (1–5 s) because of its reactivity with hemoglobin and a broad spectrum of other biological compounds (52, 169-172). As a free radical it avidly reacts with other molecules such as oxygen, superoxide radical, or transition metals (52). NO^{\bullet} is a diatomic hydrophobic gas that can permeate various cellular membranes and other hydrophobic structures, and thus it has a high diffusion capacity in a physiological environment. NO^{\bullet} can be produced in biological systems by both enzymatic and non-enzymatic reactions.

Although nitrates and nitrites can serve as immediate sources of NO^{\bullet} , the only enzymatic source of NO^{\bullet} are nitric oxide synthases (NOS) (173-175). The family of NOS enzymes specifically catalyzes the production of NO^{\bullet} radical from L-arginine through a series of redox reactions (174, 175). Three distinct isoforms of NOS have been described in mammals: neuronal NOS (nNOS, NOS1)(176, 177), endothelial NOS (eNOS, NOS3)(178-180) and inducible NOS (iNOS, NOS2) (175, 181-192), with eNOS being the most abundant NOS in vascular endothelial cells (193, 194). Moreover, the existence of a putative mitochondrial NOS (mtNOS) has also been suggested (195).

All three NOS isoforms have been described to catalyze the oxidation of the terminal guanidino nitrogen of L-arginine to produce NO^{\bullet} and L-citrulline (196-198). Several cofactors are required for the reaction including NADPH, flavin adenine dinucleotide (FAD), flavin mononucleotide (FMN), heme, tetrahydrobiopterin and calmodulin (CaM) (199). The constitutively expressed isoforms nNOS and eNOS are Ca^{2+} -dependent, whereas iNOS is Ca^{2+} -independent (200). The K_m value for oxygen of eNOS is 5-23 μM (201, 202), which clearly enables eNOS to be fully functional over a wide range of oxygen concentrations (202). In contrast, K_m values for oxygen of iNOS and nNOS are 125 μM and 350 μM ,

respectively (203, 204), pointing that their generation of NO[•] might be proportional to oxygen availability (202).

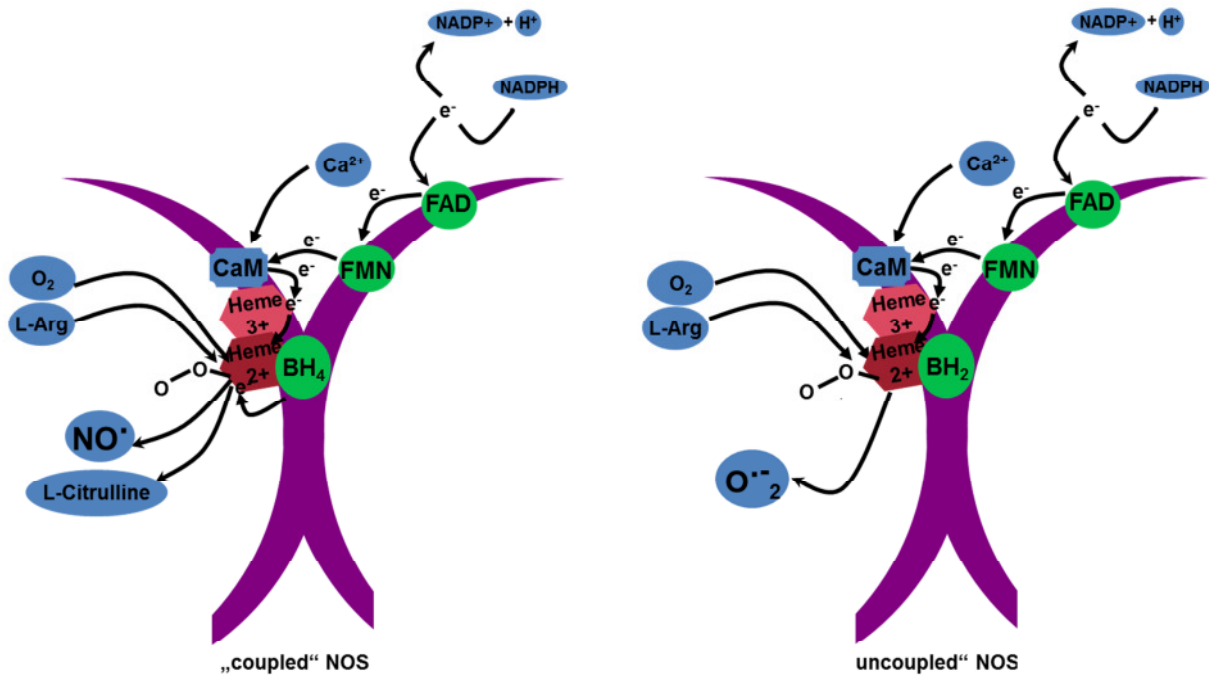


Figure IV. Scheme of “coupled” and “uncoupled” state of endothelial nitric oxide synthase. Explanations are given in the text.

NOS are homodimers comprised of an N-terminal (oxygenase) and a C-terminal (reductase) domain (205) and bind a number of cofactors to convert L-arginine and O₂ to L-citrulline and NO[•] (206) (Figure IV). For completion of the NOS catalytic cycle, two electrons are needed per one produced NO[•] molecule (207, 208). The first electron is derived from the cellular NADPH pool and is transferred *via* flavins (first to FAD, then to FMN) in the reductase domain to the heme group in the oxygenase domain of the opposite monomer, while the second electron is provided by 5',6',7',8'-tetrahydrobiopterin (BH₄) (202, 207, 208). In this way a transitionally formed iron-oxy species in the heme group is used for the oxidation of L-arginine releasing NO[•] and L-citrulline as final products (209, 210). Tetrahydrobiopterin is biosynthesized from guanosine triphosphate (GTP) in a three-step reaction mediated by the enzymes GTP cyclohydrolase I (GTPCH), 6-pyruvoyltetrahydropterin synthase (PTPS), and sepiapterin reductase (SR) (211).

Insufficient availability of L-arginine (212) and some of the cofactors (i.e. BH₄) (213), as well as S-glutathionylation (214) or Thr495 phosphorylation (215, 216) of certain NOS isoforms (e.g. eNOS) may lead to the reduced NO[•] formation and uncoupling of NOS resulting in superoxide production (217). A critical role in modulating NO[•] availability has been related to the cofactor BH₄ (209, 210). In the presence of BH₄, the reduction of molecular oxygen to

form water is coupled to oxidation of L-arginine at the oxygenase domain of NOS to generate NO and L-citrulline. When BH₄ levels are low, electrons are diverted to molecular oxygen rather than to L-arginine, thus transforming eNOS into a pro-oxidant superoxide anion generating enzyme – the so-called “uncoupled” eNOS (202, 218, 219). This transformation of eNOS has been observed in several *in vitro* models, in animal models of cardiovascular diseases, and in patients with cardiovascular risk factors (202, 220).

4.7.Oxygen homeostasis and disease

Disruption of oxygen homeostasis, either by limiting oxygen availability or by modulating ROS levels can lead to diverse adaptive functions and diseases. Interestingly, in many cases, both hypoxia, as well as ROS, contribute to disease progression. For example, an important adaptation to local tissue hypoxia is the formation of new vessels (angiogenesis). However, more recent data also indicate a role of ROS in this process. Exposure to systemic hypoxia results in the development of pulmonary hypertension, a disorder which develops secondary to various insults (221). Also in the pathogenesis of this disease, ROS have been implicated. Furthermore, tumors are characterized by hypoxic regions (222, 223), while tumor cells generate high levels of ROS (224-226), and both cases affect sensitivity to therapy (223, 225, 227).

Finally, the classical systemic stress response is mediated by steroid hormones, although a link to disrupted oxygen homeostasis has not been studied extensively.

4.7.1.Angiogenesis, integrins and vascular homeostasis

The growth of new vessels (angiogenesis) is an important adaptation to local disturbances in oxygen homeostasis. Conditions of low oxygen availability, for example found in proliferating tumors or in ischemic diseases demand a rapid cellular program aiming to overcome these critical conditions by stimulating angiogenesis (228).

After the primary vascular plexus is formed, endothelial cells form new capillaries primarily by sprouting angiogenesis, in which new vessels are formed by outgrowth of endothelial cells from existing vessels. For induction of angiogenesis, endothelial cells, that are normally quiescent, require stimulating cytokines, such as vascular endothelial growth factor (VEGF). VEGF, as a master switch of angiogenesis, causes the detachment of endothelial cells from the parent vessel and their migration to the neighboring stroma – a prerequisite for the new

vessel growth. Hypoxia is one of the principal regulators of VEGF expression, since the latter is a direct transcriptional target of both HIF1 and HIF2 (229).

In addition to pro-angiogenic growth factors, important steps in the angiogenic process are regulated by integrins (230). Integrins are α/β -heterodimeric transmembrane receptors that bind extracellular matrix proteins or other adhesion receptors on neighboring cells (231, 232). Among the many integrins described to date comprising 18 alpha and 8 beta subunits (233), the integrin $\alpha v\beta 3$ has been specifically found to be expressed in activated pro-angiogenic endothelial cells and has been associated with vascular remodeling and tumor angiogenesis (234). The activity of integrins is regulated by modulating receptor binding and/or receptor clustering subsequently affecting the interaction with integrin binding proteins which shuttle into the cytosol thereby mediating the outside signal into the cell. The $\beta 3$ -integrin binding protein $\beta 3$ -endoneixin has been initially characterized as a $\beta 3$ -integrin interaction partner in a yeast 2-hybrid system (235), and was described as a potent regulator of $\beta 3$ -integrin receptor clustering. It has been found to be expressed in various cells, including platelets, mononuclear leukocytes, and vascular cells (235, 236). Several splice variants of $\beta 3$ -endoneixin have been described so far, including the two functionally important isoforms: $\beta 3$ -endoneixin long (EN-L, 170 aa; 19.2 kDa) and $\beta 3$ -endoneixin short (EN-S, 111 aa; 12.6 kDa) (237). While only EN-S has been described to bind to $\beta 3$ -integrin (235), both forms can also interact with other signaling proteins such as cyclin A (238, 239) or the p50/p65 complex of the transcription factor nuclear factor kappa B (NF κ B), thereby acting as inhibitors of the subsequent signaling cascades. In endothelial cells, both $\beta 3$ -endoneixin isoforms have been reported to decrease urokinase-type plasminogen activator receptor (uPAR) promoter activity (240-242). Although uPAR has been found to be regulated by hypoxia and ROS, a role for $\beta 3$ -endoneixin under these conditions has not been described.

4.7.2. Pulmonary hypertension

Pulmonary hypertension is a progressive condition defined as a sustained elevation of pulmonary arterial pressure, which can lead to death due to right ventricular failure (243).

Characteristically, muscularization of small pulmonary capillaries and in some instances increased endothelial cell proliferation result in pulmonary vascular remodelling which together with enhanced pulmonary vascular constriction, and in some cases also *in situ* thrombosis and inflammation lead to enhanced pulmonary vascular resistance and thus to an increase in the pulmonary vascular pressure. Subsequently, the increased demand on the right ventricle leads to right ventricular hypertrophy and eventually right ventricular failure. Pulmonary hypertension is the consequence of various disorders (243). According to World

Health Organization (WHO) classification one can distinguish between WHO group I which includes pulmonary arterial hypertension (PAH), such as idiopathic PAH, and WHO groups II-V, which comprise secondary pulmonary hypertension sub-classified according to the underlying pathological mechanisms: left heart disease (WHO Group II), lung disease and/or hypoxia (WHO Group III), chronic thromboembolic pulmonary events (WHO Group IV) or unclear multifactorial mechanisms (WHO Group V) (244).

Pathophysiologically, endothelial dysfunction due to vascular stresses (injury, shear stress, intoxication, hypoxia) contributes to the increased vascular tone and pulmonary vascular resistance, and has also been implicated in promoting pulmonary vascular remodeling (245, 246). While endothelial dysfunction is often associated with a dysbalance between NO[•] and ROS levels (245, 247) the exact contribution of these reactive species to the pathogenesis of pulmonary hypertension are not fully understood.

Moreover, HIF transcription factors have been found to promote pulmonary hypertension in particular in hypoxia-related pulmonary hypertension. In animal models, exposure to chronic hypoxia for several weeks leads to the development of pulmonary hypertension similar to the situation upon prolonged sojourn at high altitude or cases of lung diseases or some forms of congenital heart disease (246). HIF1 α and HIF2 α have been described to be upregulated in lungs derived from chronic hypoxic animals (248-250), in lungs derived from animal models of congenital heart disease (251) or from patients with pulmonary hypertension due to lung diseases (252), or in hearts from patients with congenital heart disease (253, 254). Moreover, mice heterozygous for HIF1 α or HIF2 α are protected against the development of hypoxia-induced pulmonary hypertension (255, 256). Interestingly, increased levels of HIF1 α have also been observed in some models of non-hypoxic pulmonary hypertension (252, 257), although the exact mechanisms underlying these observations have not been completely identified today.

4.7.3.Cancer

Cancer comprises a heterogeneous group of diseases that are characterized by an abnormal cell proliferation and invasion of distant tissues and organs (metastasis). Douglas Hanahan and Robert Weinberg had postulated in their seminal review „The hallmarks of cancer“ (258) the following common traits of cancer: (1) cancer cells stimulate their own growth (self-sufficiency in growth signals); (2) they resist inhibitory growth signals (insensitivity to anti-growth signals); (3) they resist their programmed cell death; (4) they have a limitless replicative potential; (5) they stimulate angiogenesis to supply nutrients to

tumors; (6) they invade local tissue and spread to distant sites (tissue invasion and metastasis) (258, 259).

Rapid growth of solid tumors creates hypoxic areas in growing cancer tissue due to poor oxygenation of the growing tumor mass (tumor hypoxia). Adaptation of tumor cells to this hypoxic environment is assured by increased angiogenesis as well as metabolic adaptation towards glycolysis. In both cases, HIF signaling plays an important role (260). Tumor hypoxia is well known for its non-beneficial effect in the cancer treatment, such as: resistance to radiotherapy and chemotherapy as well as predisposing for increased tumor metastases (261).

While on the one hand, high levels of ROS have been related to promote cell transformation via DNA damage and genomic instability, many tumor cells show a sustained increase in intrinsic generation of reactive oxygen species which maintains the oncogenic phenotype and drives tumor progression. Although the precise pathways leading to ROS stress in cancer cells remain unclear, several intrinsic and extrinsic mechanisms are thought to cause oxidative stress during cancer development and disease progression (262). Activation of oncogenes, aberrant metabolism, mitochondrial dysfunction and loss of functional p53 are intrinsic factors known to cause increased ROS production in cancer cells (263). The expression of genes that are associated with tumor transformation, such as Ras, Bcr-Abl and c-Myc, were found to induce ROS production, thus contributing to redox adaptation allowing cancer cells to promote survival and to develop resistance to anticancer drugs (226). Increased ROS stress in cancer cells correlates with the aggressiveness of tumors and poor prognosis (262). Compelling evidence suggests that the increased ROS stress in cancer cells has a pivotal role in the acquisition of the hallmarks of cancer (262). However, little is known how an increase in intracellular oxidative stress levels is sensed and transduced into ROS-induced specific intracellular signaling to regulate the expression of survival genes (226).

Therapeutic selectivity is essential in cancer treatment. As cancer cells have elevated ROS generation and are under increased intrinsic oxidative stress, therapeutic approaches to further enhance ROS load by chemotherapeutics or irradiation have been implicated (262). Although ROS-generating agents have been found to be effective in many cases, low clinical response and resistance to those agents were also reported (262). Elevation of certain transcription factors, antioxidants and survival pathways as a result of redox adaptation may explain the drug-resistant phenotype.

4.7.4. Glucocorticoid-dependent stress response

Glucocorticoids are steroid hormones secreted from the adrenal cortex as part of the hypothalamus-pituitary-adrenal axis, and are critical to the stress response, endocrine homeostasis, vascular tone, proliferation, and apoptosis due to their regulatory effects on carbohydrate, lipid and protein metabolism. They also have major regulatory roles in inflammation and the immune response (264).

The actions of glucocorticoids are mediated through an intracellular glucocorticoid receptor (GR), which in the absence of ligand is complexed with hsp90 (2 molecules), hsp70 and hsp56 (265-270). Upon ligand binding activated GR dissociates from hsp90 and hsp56 and translocates to the nucleus where it after dissociation from hsp70, homodimerizes. GR homodimers regulate transcription in several ways: 1) *via* direct binding to specific DNA sequences, glucocorticoid response element (GRE) sites, thereby activating or repressing transcription (271); 2) *via* interaction with other transcription factors; and 3) *via* modulation of the stability of specific mRNAs (271-275).

In humans, the naturally occurring glucocorticoid is hydrocortisone (cortisol), which is synthesized from its precursor cortisone and released in a circadian rhythm. Natural glucocorticoids can act, besides GR, also *via* mineralocorticoid receptor (MR) with a lesser extent and affinity (276).

Various synthetic glucocorticoids have been designed which act more specifically with the GR. Among them, dexamethasone acts almost exclusively *via* the GR receptor and it is 25-fold more potent than natural cortisol (277). Dexamethasone has been used to treat different diseases, such as: rheumatic disorders, skin diseases, allergies, asthma, chronic obstructive lung disease, etc. However, systemic side-effects of dexamethasone treatment are described, among them effects on metabolism, including Cushing syndrome and increased risk of diabetes mellitus type 2. Also, severe adverse effects were recorded in the cardiovascular system, e.g. endothelial dysfunction, systemic hypertension, cardiomyopathy, and atherosclerosis (278, 279). However, the underlying signaling mechanisms are not well understood. Interestingly, while beneficial effects of dexamethasone and other synthetic glucocorticoids have been described in disorders associated with hypoxia or high ROS levels (280), there are more recent reports that dexamethasone and other GC are able to increase ROS levels in different tissues including the vasculature (280-284). While different mechanisms have been described either targeting antioxidant pathways or promoting ROS

generation, the mechanisms and consequences for vascular function are not clearly elucidated.

5 Aims

Oxygen homeostasis is essential for aerobic life. Disruptions of this balance either by inadequate supply of oxygen or by “activation” of oxygen to reactive oxygen species (ROS) can lead to various adverse effects at the local and systemic level. However, the particular interplay between hypoxia and ROS signaling cascades is not completely resolved.

The aim of this work is therefore to further dissect this interplay in vitro and in vivo and to test potentially relevant molecules not yet specifically assigned to the hypoxia/ROS signaling pathways in the cardiovascular system or in tumor cells.

Specifically, the following questions are addressed:

How are nitric oxide (NO) and ROS levels regulated in response to hypoxia in vascular cells in vitro and in vivo?

Is there a role of the novel integrin β 3-binding protein β 3-endonexin in the hypoxic vascular response?

What is the role of ROS and hypoxia signaling cascades in the vascular response to the synthetic glucocorticoid dexamethasone?

Is there a role of the ROS and hypoxia signaling cascades in melanoma cells in response to the clinically relevant chemotherapeutic oxaliplatin?

As hypoxia-inducible (transcription) factor-1 (HIF1) and the ROS-generating enzymes of the NADPH oxidase family are major players in hypoxia and ROS signaling cascades, their direct or indirect contribution to the above mentioned questions will be evaluated.

6 Materials and methods

6.1. Materials

6.1.1. Equipment

Item	Product name	Company
Analytical balance		Sartorius
Autoclave	KSG-116-2-ED KSG	KSG
Autoclave	KSG-25-2-3 KSG	KSG
Balance		Sartorius
Bunsen burner	Vulcan	Heraeus
Centrifuge	Biofuge fresco	Heraeus
Centrifuge	Biofuge pico	Heraeus
Centrifuge	Biofuge stratos	Heraeus
Centrifuge	Megafuge 1.OR	Heraeus
Centrifuge	Varifuge 3.OR	Heraeus
Cryotom	CM 1850	Leica
Deep-freezer (-80°)	Hera freeze	Heraeus
Drying chamber		Heraeus
Fluorescence microscope	IX50	Olympus
Fluorescence microscope	Hg-Lamp U-RFL-T	Olympus
Fluorescence microscope	Camera Controller	Hamamatsu
Fluorescence microscope	Orbit	Improvision
Fluorescence microscope	Hg-Lamp U-RFL-T	Olympus
Liquid-N ₂ -Dewar	Locator 6 Plus	Thermolyne
e-scan		Bruker
Freezer	comfort	Liebherr
Freezer big	comfort	Liebherr
Fridge big	profi line	Liebherr
Fridge small	Premium	Liebherr
Fridge-freezer combination		Liebherr
Gel documentation system	Gel Doc 2000 Bio-Rad	BioRad
Heating block	Thermomixer	
Heatingplate	comfort	Eppendorf
Hypoxia Work Station	CM1850	Leica
Incubator	InVIVO400	IUL Instruments
Incubator	Hera Cell	Heraeus
Incubator	Binder	WTC Binder
Isopropanol freezing box		
Laboratory dishwasher	G7783CD Mielabor	Miele

Laminar airflow cabinet	Hera Safe	Heraeus
Luminometer	AutoLumat plus	Berthold Technologies
Magnetic stirrer + heater	MR3001	Heidolph
Magnetic stirrer without heater	MR3000	Heidolph
Microscope	HAL 100	Zeiss
Microscope	Axiovert 25	Zeiss
Microwave		Whirlpool
Millipore water supply	Milli-Q synthesis	Millipore GmbH
Mini-table-top-centrifuge	Capsulefuge PMC-060	TOMY
pH Meter	pH 540 GLP U-	GLP WTW
Photometer	2001Spectrophotom.	Hitachi
Multifunction Microplate Reader	Tecan Safire	Tecan
Power supply	Power Pac 200	BioRad
Power supply	Power PAC 300	BioRad
Power supply	Power Pac 3000	BioRad
Pump	CVC 2000	Vacuubrand
Roller mixer	RM5 Assistent	Karl Hecht KG
Rotator		Fröbel Labortechnik GmbH
SDS-PAGE	Mini-Protean 2 System	BioRad
SDS-PAGE	Mini-Protean 3 System	BioRad
Shaker	Duomax 1030 IKA-Shaker MTS2 electronic	Heidolph IKA-Werke
Shaker	Polymax 1040	Heidolph
Shaker	C24 Incubator Shaker	New Brunswick Scientific
Shaker-incubator		KGW Isotherm
Standdewar		
Thermocycler	iCycler	BioRad
Thermocycler	PCR System 9700	PE Applied Biosystems
Thermocycler	Rotor-Gene 6000	Corbett
Thermocycler	SDS 7700	Applied Biosystems
UV-Stratalinker	Stratalinker 1800	Stratagene
Vacuum pump		Neuberger
Vortexer		
Water bath	Reax top	Heidolph
Water bath	Vortex-Genie 2	Scientific Industries
Water bath	Grant	SUB

6.1.2.Chemicals

Compound	Company
Acetic acid	Roth
Acetonitrile	Sigma
Agar Agar	Roth
Agarose NEEO	Roth
Amidoblack	Roth
Ammoniumpersulfate	Roth
Ampicilin	Calbiochem
Calciumchloride-dihydrate	Merck
Coumaric acid	Sigma
4',6-Diamidin-2-phenylindol (DAPI)	Invitrogen
Diaminofluorescein-2 diacetate	Alexis
2,3-diaminonaphtalene (DAN)	Sigma
5-(and-6)-chloromethyl-2',7'-dichlorodihydrofluorescein diacetate	MoBiTec
Desferroxamine (DES)	Merck
Diethylpyrocarbonate (DEPC)	Roth
Diethyldithiocarbamate (DETC)	Merck
Dihydroethidium (DHE)	Sigma
Dihydrorhodamine 123	MoBiTec
Diphenyleneiodonium chloride	Alexis
Dimethylsulfoxide (DMSO)	Roth
Dithiothreitol (DTT)	Roth
Ethanol	Merck
Ethidium bromide	Roth
Ethylene diamine tetraacetic acid (EDTA)	Roth
Ethylene glycol tetraacetic acid (EGTA)	Roth
Formaldehyde 37%	Merck
D-Glucose	Merck
Glycerol	Roth
Glycine	Roth
Guanidiniethiocyanate	Roth
Hydrochloric acid	JT Baker
1-hydroxymethoxycarbonyl-2,2,5,5-tetramethyl-pyrrolidine hydrochloride	Noxygen
Iodine	Merck
Isopropanol	JT Baker
Kanamycin sulfate	Calbiochem
Luminol	Sigma
Lucigenin	Sigma
Magnesium carbonate hydroxide	Sigma
Magnesium chloride-Hexahydrate	Roth
Magnesiumsulfat-heptahydrat	Applichem
Manganese-(II)-chloride	Merck
β -Mercaptoethanol	Roth
Methanol	Merck
N-Lauryl-sarcosine	Sigma

Nicotinamide adenine dinucleotide phosphate (NADPH)	Sigma
Nitrate reductase	Sigma
L-(G)-nitro-L-arginine methyl ester (L-NAME)	Sigma
Non-fat dry milk powder	Merck
PBS tablettes	GibCo
Protease inhibitor mix	Calbiochem
Phenylmethanesulfonyl fluoride (PMSF)	Sigma
Ponceau S	Sigma
Potassium chloride	Merck
Potassium dihydrogenphosphate	
Potassium iodine	Merck
Phosphoric acid	
Rotiphorese Gel	Roth
SDS ultra pure	Roth
Sodium acetate	Merck
Sodium chloride	Roth
Sodium citrate	Roth
Sodium dihydrogen phosphate	Sigma
Sodium hydrogen carbonate	
Sodium hydroxide	Merck
N,N,N',N'-Tetramethylethane-1,2-diamine (TEMED)	Roth
Trichloroacetic acid	Sigma
Trifluoroacetic acid	Sigma
Triton®X-100	Sigma
Tris	Roth

6.1.3. Plastic ware

Item	Company
Pipettes (2, 5, 10, 25, 50 ml)	Sarstedt
Cell culture flasks (T25, T75, and T175)	Greiner
Cell culture dish (6, 10, 15 cm)	Sarstedt
Cell culture plates (6-, 12-, 24-, 48- and 96-well)	Greiner
8-well plate	Ibidi
μ -slide (15-well)	Ibidi
Filter tips (10, 100, 200, 1000 ul)	Sarstedt
Combi-tips	Sarstedt
Test tubes (0.5, 1.5 and 2 ml)	Sarstedt
Falcon tubes (15 and 50 ml)	Sarstedt
Cryovials	Greiner

6.1.4.-Primary antibodies

Antibody	Company/Reference	Dilution	
		WB	ICC/ICH
β-actin	Santa Cruz	1:1000	
Caspase 3	Cell Signaling	1:1000	
Caspase 7	Cell Signaling	1:1000	
CD31	DAKO	1:1000	1:100
DHFR	BD Transduction	1:1000	
β3-endonexin	(240, 241)	1:1000	1:100
Endothelial nitric oxide synthase (eNOS)	BD Transduction	1:1000	
p-eNOS (Thr496)	Cell Signaling	1:1000	
p-eNOS (Ser1177)	Cell Signaling	1:100	
HIF1α	Invitrogen	1:100	
HIF1α	BD Transduction	1:100	
HIF2α	Millipore	1:100	
IκBα	Santa Cruz	1:100	
Ki67	DAKO	1:100	1:100
Lamin B1	Cell Signaling	1:100	
NOX1	Eurogentec	1:100	
NOX2 (gp91phox)	Upstate	1:100	
NOX4	Epitomics	1:100	1:100
p21	Cell Signaling	1:100	1:100
p22phox	Santa Cruz	1:100	
p50	Cell Signaling	1:100	
p53DO1	DAKO	1:100	1:100
p53DO7	DAKO	1:100	1:100
p65	Cell Signaling	1:100	
p-ataxia teleangiectasia mutated kinase (p-ATM)	Rockland	1:100	1:100
Poly (ADP-ribose) polymerase (PARP1)	Invitrogen	1:100	1:100
p-check point kinase 2 (p-CHK2)	Invitrogen	1:100	1:100
p-gamma histone 2AX (γH2AX)	Millipore	1:100	1:100
α-smooth muscle actine (α-SMA)	DAKO	1:100	1:100
V5	Cell Signaling	1:100	

6.1.5. Secondary antibodies horse radish peroxidase conjugated

Antibody	Company	Dilution
Goat anti mouse HRP conjugated	Calbiochem	1:10000 in 5% milk/TBST
Goat anti rabbit HRP conjugated	Calbiochem	1:10000 in 5% milk/TBST
Rabbit anti goat HRP conjugated	Calbiochem	1:10000 in 5% milk/TBST

6.1.6. Secondary antibodies fluorescently conjugated

Antibody	Company	Dilution
Mouse IgG Alexa Fluor 488	Molecular Probes/Invitrogen	1:200 5% BSA
Mouse IgG Alexa Fluor 594	Molecular Probes/Invitrogen	1:200 5% BSA
Rabbit IgG Alexa Fluor 488	Molecular Probes/Invitrogen	1:200 5% BSA
Rabbit IgG Alexa Fluor 594	Molecular Probes/Invitrogen	1:200 5% BSA
Goat IgG Alexa Fluor 488	Molecular Probes/Invitrogen	1:200 5% BSA
Goat IgG Alexa Fluor 568	Molecular Probes/Invitrogen	1:200 5% BSA
Goat IgG Alexa Fluor 594	Molecular Probes/Invitrogen	1:200 5% BSA

6.1.7. Cell culture media and additives

Item	Company
L-arginine	Gibco
L-asparagine	Gibco
DMEM	Gibco
EBM-2	Lonza
Fetal calf serum (FCS)	Pan Biotech
Leibovitz	Gibco
MCDB 131-Medium	Gibco
MCDB 153-Medium	Biochrom
Endothelial Basal Medium	PAA
L-glutamine	PAA
Penicillin /Streptomycin	Gibco
SmBm-2 medium	Lonza
SmGm-2 Single Q	Lonza
Trypsin-EDTA	Gibco, PAA
Phosphate buffered saline (PBS)	PAA
HBSS with Mg ⁺⁺ /Ca ⁺⁺	Gibco, PAA
Epidermal growth factor 1 (EGF1)	Invitrogen
Hydrocortisone	Sigma
Insulin	Sigma

6.1.8. Kits

Item	Company
BrdU proliferation assay	Roche
Jetstar Plasmid Maxi Kit	Genomed
Qiagen RNeasy Mini Kit	Qiagen
Qiagen Plasmid Maxi Kit	Qiagen
SuperScript TM III Reverse Transcriptase	Invitrogen
Expand High FidelityPLUS PCR System	Roche
Phusion TM High-Fidelity DNA Polymerase	NewEngland Biolabs

6.2.Methods

6.2.1.Cell lines

6.2.1.1.Human pulmonary artery endothelial cells

Primary human pulmonary aortic endothelial cells (HPAEC) were purchased from Invitrogen and grown according to manufacturer's instructions in endothelial basal medium (EBM) (PAA) supplemented with 1 g/l glucose, 10% fetal calf serum (FCS) (PAA), 100 U/ml penicillin (Invitrogen) and 100 μ g/ml streptomycin (Invitrogen). Cells were maintained at 37°C under the humidified atmosphere of 5% CO₂. 16 h prior to stimulation cells were placed in 1% FCS-containing medium without additives.

6.2.1.2.Human microvascular endothelial cells

Human microvascular endothelial cell line (HMEC-1, ATTC CRL-3243) is an immortalized cell line established by transfection of human dermal microvascular endothelial cells (HMEC) with a PBR-322-based plasmid containing the coding region for the simian virus 40 A gene product, large T antigen (285). HMEC-1 were grown in EBM (PAA) supplemented with 1 g/l glucose, 10% FCS (PAA), 2 mM L-glutamine, 100 U/ml penicillin (Gibco), 100 μ g/ml streptomycin (Gibco), 1 μ g/ml hydrocortisone (Sigma), and 1 μ g/ml human epidermal growth factor (hEGF1) (Invitrogen). Cells were maintained at 37°C under the humidified atmosphere of 5% CO₂. 16 h prior to stimulation cells were placed in 1% FCS-containing medium without additives.

6.2.1.3.Human pulmonary artery smooth muscle cells

Primary human pulmonary artery smooth muscle cells (PASMC, Lonza) were grown in smooth muscle basal medium (SmBM™, Lonza) supplemented by SmGM™-2 SingleQuots™ (Lonza) (containing: FCS, hEGF1, insulin, human fibroblast growth factor B (hFGFB), and gentamicin/amphotericinB). Cells were maintained at 37°C under the humidified atmosphere of 5% CO₂. 16 h prior to stimulation cells were placed in SmBM™ (Lonza) without additives.

6.2.1.4. Human malignant melanoma cells

Human melanoma cell line WM1158 (Wistar) were grown and experiments were performed in medium MCDB 153 (Biochrom): Leibovitz L-15 (Gibco) (4:1), supplemented with 2% FCS, CaCl₂ (1.68 mM), and 5 µg/ml insulin (Sigma). Cells were maintained at 37°C under the humidified atmosphere of 5% CO₂. 16 h prior to stimulation cells were placed in MCDB 153: Leibovitz L-15 (4:1) medium without additives.

6.2.1.5. Cell culture under hypoxia

Cells were set in 1% FCS containing medium 16 h prior to hypoxic stimulation (1% O₂) in a Ruskinn hypoxia work bench for a given experimental design.

6.2.1.6. Storage of cells

For storage of cells in liquid nitrogen, cells were frozen in medium containing 10% dimethylsulfoxide (DMSO) and transferred to cryovials. Thereafter, cells were frozen at -70°C and stored in liquid nitrogen (-196°C).

6.2.2. Animals

The following mouse strains were used:

C57BL/6j mice were obtained from (Charles River). A.B6 Tyr⁺-Cyba^{nmf333}/J (Jackson Laboratories) is a p22phox-deficient mouse strain (nmf333 mutant) carrying a single point mutation in the exon 5 of *Cyba* gene (encoding for p22phox) which causes the substitution of a tyrosine residue (121) to histidine (286). This causes a loss of p22phox protein while mRNA levels are preserved. The nmf333 mice have a specific phenotype characterized by chronic granulomatous disease and balance disorders.

Mice with endothelial- or smooth muscle specific inactivation of HIF1α were generated by cross-breeding either *Tie2-Cre* (B6.Cg-Tg(Tek-cre)12Flv/J; Jackson Laboratories) or *Sm22a-Cre* (B6.Cg-Tg(Tagln-cre)1Her/J; Jackson Laboratories) transgenic mice with *Hif1a*^{+/+} mice homozygous for the *Hif1a* allele with exon 2 flanked by *loxP* sites (B6.129-Hif1a^{tm3Rsj0}/J; Jackson Laboratories) (287).

All animal procedures were performed in accordance with the European directive 86/609/EEC and approved by Government of Upper Bavaria, Munich, Germany as the local legislation on protection of animals: 55.2-2532.Vet_02-17-165; 55.2-1-54-2532-53-2012; and 55.2.2532.Vet_02-15.242.

6.2.3. Transfections, luciferase assays and viral transduction

6.2.3.1. Transfections

For transfections, cells were plated to a density of 50-70%, cultured for 24 h, and transfected by FuGENE HD (Roche) reagent or Lipofectamine™ 2000 (Invitrogen) according to the manufacturers' protocols (202, 228).

6.2.3.2. Luciferase assays

HMEC-1, grown to 50-70% confluency in 24-well plates, were transiently co-transfected with: 400 ng of overexpression constructs, 50 ng of the reporter constructs and 50 ng of pSV- β -galactosidase control vector plasmid (Promega). Transfection with the empty pGL3basic vector (Promega) served as a control. Luciferase assay was performed as described previously (12, 228). In brief, cells were harvested and lysed in Reporter Lysis Buffer (Promega). The plates were placed on a shaker for 30 min and centrifuged at 500 rcf for 5 min at 4°C to remove cell debris. Luciferase activities were, thereafter, measured in a luminometer (Berthold) and β -galactosidase activities were determined spectrophotometrically (Nanodrop) as described in the manufacturer's protocol (Promega). Presented data are normalized to β -galactosidase activities and transfection efficiencies.

6.2.3.3. Plasmids

Plasmid	Reference
EPO-HRE	(228)
HIF1 α 538	(37)
HIF1 α 538m	(37)
I κ Bdn	(B.Dickinson)
NF κ _luc	(288, 289)
p50	(228)
p65	(228)
PAI796	(37)
PAI796m	(37)
pCDNA3.1V5	(228)
pCDNA3.1V5EN-S	(228)

pCDNA3.1V5EN-L	(228)
PH800	(288)
pTF636	(290)
pTF636NFm	(290)
pVHL	(291)
RacT17N	(289)

6.2.3.4. Gene silencing by RNAi

For gene silencing, RNAi technology was used. Cells were transfected with the appropriate siRNA (10 nM) according to the experimental design using LipofectamineTM 2000 (Invitrogen) according to the supplier's protocol. Efficiency of silencing was tested by qPCR or Western blot analysis and ranged from 70-95%. For gene silencing, cells were transfected with corresponding short interfering RNA (siRNA) as previously described (26, 28). siRNAs targeting *p22phox* (SI03078523), *NOX1* (SI03043530), *NOX2* (SI00008736) and *NOX4* (SI05137748) were purchased from Qiagen. In addition, siRNAs against the following genes were designed: *HIF1A*: (5'-UCAAGUUGCUGGUCAUCAGdTdT-3'); *ITGB3BP*: 5'CUGCCUCAGCCUUGGGAGUAGUUDGdG-3' (sense) (ITGB3BP, NCBI Reference Sequence: NM_014288.4) *DHFR*: 5'-CAGUAGAAGGUAAACAGAAdTdT-3' (sense), or control siRNA (5'-GACUACUGGUCGUUGAAGUdTdT-3'). All siRNAs were synthesized by Eurogentec (Köln, Germany).

6.2.3.5. Gene silencing by lentiviral transduction

For *ex vivo* experiments, short hairpin RNA oligonucleotides (shRNA) were used for gene silencing in cultured aortic rings by lentiviral delivery using the BLOCK-iT Inducible H1 Lentiviral RNAi System (Invitrogen) in accordance to the manufacturer's manual. shRNAs against *p22phox* (sense: 5'-CAC CGG TTA ACC CAA TGC CAG TGA CCG AAG TCA CTG GCA TTG GGT TAA CC-3', anti-sense: 5'-AAA AGG TTA ACC CAA TGC CAG TGA CTT CGG TCA CTG GCA TTG GGT TAA CC -3'), *NOX2* (sense: 5'-CAC CGC TGC CAG TGT GTC GAA ATC TCG AAA GAT TTC GAC ACA CTG GCA GC-3', anti-sense: 5'-AAA AGC TGC CAG TGT GTC GAA ATC TTT CGA GAT TTC GAC ACA CTG GCA GC -3') and *NOX4* (sense: 5'-CAC CGT TGG CCA GCC AGC TCC TCC ACG AAT GGA GGA GCT GGC TGG CCA A-3', anti-sense: 5'-AAA ATT GGC CAG CCA GCT CCT CCA TTC GTG GAG GAG CTG GCT GGC CCA AC -3') were generated and cloned into pLenti4 according to the manufacturer's instructions. shRNA against GFP (sense: 5'-CAC CGC AAG CTG ACC CTG AAG TTC ATC GAA ATG AAC TTC AGG GTC AGC TTG C-3', anti-sense: 5'-AAA AGC

AAG CTG ACC CTG AAG TTC ATT TCG ATG AAC TTC AGG GTC AGC TTG C-3') were used. The lentivirus was produced in HEK 293FT cells, and the virus-containing media was harvested for infection of mouse aortic rings. For infection, aortic rings were placed in a 96-well plate (1 ring per well) and supplemented with MCDB131 medium with 1 g/l glucose, 10% FCS (PAA), 100 U/ml penicillin and 100 μ g/ml streptomycin (both Gibco), 1 μ g/ml hydrocortisone (Sigma) and 1 μ g/ml epidermal growth factor - EGF1 (Invitrogen). After 24 h, medium was removed and 110 μ l MCDB131 and hexadimethrine bromide (8 mg/ml, Invitrogen) was added to each well. Subsequently 15 μ l of the appropriate virus-containing media was added to each well. On the following day, medium was exchanged.

6.2.4. Biochemical and molecular biology techniques

6.2.4.1. Protein isolation

Total proteins from cells and macerated tissues were isolated by adding the 1 \times lysis buffer (0.2 M Tris, 1.5 M NaCl, 0.01 uM, 0.1 mM EGTA, 0.025 mM Na₄P₂O₇, 0.01 mM β -glycerophosphate, 0.01 M Na₃VO₄·2H₂O, Triton X). Thereafter, samples were shaking overnight at 4°C. On the following day, samples were centrifuged at 4°C at 10000 rcf and supernatants containing proteins were collected. Thereafter, protein concentration was determined using Nanodrop. For Western Blot analyses, samples were dissolved in 3 \times Laemmli buffer (187 mM Tris, 6% SDS, 30% glycerol, 0.06% bromphenol blue, 15 mM DTT, 60mM EDTA).

Alternatively, cells were lysed by scraping with the cell scraper either in 1.5 \times Laemmli buffer. Samples were centrifuged for 10 min at 10000 rcf. Before performing SDS-poliacrylamide (SDS-PAGE) electrophoresis samples were boiled at 95°C for 5 min, kept on ice for 1 min and spun for 1 min at 3000 rcf.

6.2.4.2. Electrophoretic protein separation and immunoblotting

40 μ g/lane of isolated proteins were separated by 8-12% SDS polyacrylamide gel electrophoresis (SDS PAGE) in 1x running buffer (25 mM Tris, 190 mM glycine, 0.1% SDS, pH 8.3) on a Mini-Protean 3 System (Biorad) and transferred to nitrocellulose Protran membranes (Diagonal) using the Mini Trans-blot System (Biorad) in the ice-cold 1x transfer buffer (25 mM TRIS, 190 mM glycine, 20% methanol, pH 8.3). After transfer, membranes

were rinsed in water and incubated in Ponceau S (Sigma) solution for 1 min for rapid reversible detection of protein bands on nitrocellulose membrane. Thereafter, membranes were rinsed in water and washed for several times in TBS-T buffer (50 mM Tris, 150 mM NaCl, 0.1% tween, pH 7.4-7.6) in order to remove Ponceau S. Next, membranes were incubated for 1 h in TBS-T containing 5% non-dry milk and subsequently incubated for 1 h with corresponding primary antibodies. Next, membranes were washed 3 times for 10 min with TBS-T buffer and incubated with a corresponding horseradish peroxidase-conjugated secondary antibody for 1 h. Finally, blots were washed 3 times for 5 min with TBS-T, protein bands were visualized by the enhanced chemiluminescence (Amersham) on films for autoradiography (FUJI). Films with visualized specific protein bands were scanned and analysed by densitometry using GelDoc software (Biorad).

6.2.4.3. Gene expression analysis

Total RNA was isolated and gene expression was assessed by RT-qPCR as described previously (202, 228). cDNA was synthesized from isolated RNA using high capacity cDNA reverse transcription kit (Applied Biosystems) according to manufacturer's instructions in a 6000 Rotor Gene Real-Time PCR System (Corbett Life Science) (202, 228).

qPCR was performed using gene-specific primers: *p22phox*: 5'-CAC AAA TCA GAC GGC AGC ACT-3' (sense), 5'-CAT CGG GCG TGG TGA ACT C-3' (antisense); *NOX1*: 5'-CAC CCC AAG TCT GTA GTG GGA G-3' (sense), 5'-CCA GAC TGG AAT ATC GGT GAC A-3' (anti-sense); *NOX2*: 5'-GTC ACA CCC TTC GCA TCC ATT CTC AAG TCA GT-3' (sense), 5'-AAC CAC TCA AAG GCA TGT GTG TC-3' (anti-sense); *NOX4*: 5'-CCG GCT GCA TCA GTC TTA ACC-3' (sense), 5'-TCG GCA CAG TAC AGG CAC AA-3' (anti-sense); *HIF1A*: 5'-GAA GAC ATC GCG GGG AC-3' (sense), 5'-TGG CTG CAT CTC GAG ACT TT-3' (anti-sense); *ITGB3BP* (β 3-endonexin consensus sequence): 5'-TCT CCA ACA ACT GGA ACT TGT C-3'(sense), 5'-TCC ATT TCT GTG CTT TTG CTC-3' (anti-sense); *GAPDH*: 5'-GTG AAC ATG AGA AGT ATG ACA AC-3' (sense), 5'-CAT GAG TCC TTC CAC GAT ACC-3' (anti-sense); *VEGFA*: 5'-AGG AGG AGG GCA GAA TCA TCA-3' (sense), 5'-CTC GAT TGG ATG GCA AGT AGC T-3' (anti-sense); *DHFR*: 5'-CAC AAA TCA GAC GGC AGC ACT-3' (sense), 5'-CAT CGG GCG TGG TGA ACT C-3' (antisense); *18S rRNA* 5'-GTA ACC CGT TGA ACC CCA TT-3' (sense), 5'-CCA TCC AAT CGG TAG TAG CG-3' (antisense) (202, 228).

For gene analyses in the murine system, RT-qPCR was performed using murine gene-specific primers: *Itgb3bp* (β 3-endonexin consensus sequence): 5'-GGA ACT TAT CAG TTG AGC CCA TT-3' (sense), 5'-AGT TAC TCC GTT TCC TTG TTTCA-3' (anti-sense); *Hif1a*: 5'-

GCA CTA GAC AAA GTT CAC CCT GAG A-3' (sense), 5'-CGC TAT CCA CAT CAA AGC AA-3' (anti-sense); 18S rRNA 5'-GCA ATT ATT CCC CAT GAA CG-3' (sense), 5'-GGG ACT TAA TCA ACG CAA GC-3' (anti-sense) (228). For each independent experiment, samples were loaded in triplicate for each primer pair, and the value of each sample was normalized to 18S rRNA. All data were analyzed by the system software (Qiagen) (228).

6.2.4.4. Chromatin immunoprecipitation

Chromatin immunoprecipitation to detect p65 binding at the HIF1 α promoter was performed as previously described (37, 228). Specifically, HMEC-1 cells transfected with the expression vector encoding β 3-endonexin long isoform (EN-L) or with control vector (Ctr) were exposed to hypoxia (1% oxygen) for 8 h or remained under normoxia (Ctr). Cells were fixed with formaldehyde, lysed, and sonicated to obtain 500 to 1000 bp DNA fragments. Chromatin was precipitated with an antibody against p65 (Cell Signaling) overnight at 4°C. Real-time PCR was performed to amplify a region of the human HIF1 α promoter containing the NF κ B consensus sequence at -197/188 bp (forward 5'-GCT GAC CGC CTC CTG ATT G-3', reverse 5'-TTC CTC GAG ATC CAA TGG CG-3') using a Rotor-Gene 6000 Real-Time PCR System (Corbett Life Science). A gene-deficient region on chromosome 4 (Untr4) served as a negative control (forward, 5'-CTC CCT CCT GTG CTT CTC AG-3' and reverse, 5'-AAT GAA CGT GTC TCC CAG AA-3'). As a background control, chromatin immunoprecipitation with isotype control antibody (IgG) was performed. Quantification was performed using a standard curve of the input. p65 binding to chromatin was revealed after background subtraction as a relative amount of the input used.

6.2.4.5. Immunofluorescence

β 3-endonexin was detected using indirect immunofluorescence labeling (228). In brief, HMEC-1 cells were grown on uncoated cover slips or on cover slips coated with collagen or fibronectin (both Invitrogen) and fixed in 1:1 methanol-acetone solution, blocked with 2% bovine serum albumin solution for 25 min followed by incubation with the primary β 3-endonexin antibody (1:100) for 1 h at room temperature in a humid chamber. For indirect fluorescent labeling, secondary mouse anti-rabbit antibody conjugated with Alexa fluor 488 (Invitrogen) was applied for 2 h at room temperature in a dark chamber. Cover slips were mounted with Fluorescent mounting medium (DAKO) on objective slides and analyzed on a Zeiss Axiophot microscope (Zeiss) with Axio Vision imaging software (Zeiss). Nuclei were visualized with 4', 6-diamidino-2-phenylindole (DAPI, 1:10000) staining (Invitrogen).

WM1158 melanoma cells were trypsinized and spun down onto positively coated objective slides (Thermo Scientific) and fixed in 1:1 methanol-acetone solution. Slides were blocked with 2% (w/v) bovine serum albumin solution for 25 min. Thereafter, coverslips were incubated with primary antibodies against NOX4 (1:400), p-CHK2 (1:300), γ H2AX (1:300), Ki67 clone MIB (DAKO, Baltimore, USA) (1:150), phospho-ataxia/telangiectasia mutated kinase - p-ATM (Rockland Immunochemicals) (1:250) or p53 clone DO7 (DAKO) (1:150) for 1 h at room temperature in a humid chamber. For indirect fluorescent labelling, secondary mouse anti-rabbit or goat anti-rabbit antibodies conjugated with Alexa fluor 488 (Invitrogen) were applied for 2 h at room temperature in a dark chamber. The nuclei were visualized with 4',6-diamidino-2-phenylindole (DAPI, 1:10000; Invitrogen) staining. The slides were mounted with Fluorescent mounting medium (DAKO) on cover slips and analyzed on a Zeiss Axiophot microscope (Zeiss, Jena, Germany) with Axio Vision imaging software (Zeiss).

6.2.4.6. Immunohistochemistry

Isolated lung tissue samples were immersed in 10% buffered formalin solution for 48 h and subsequently embedded in paraffin (FFPE). FFPE lung sections were stained with an antibody against α -SMA (clone 1A4; DAKO). In brief, slides were heated at 60°C for 1 h before rehydration in decrement alcohol concentration raw. The endogenous peroxidase activity was quenched in 1% hydrogen peroxide solution in methanol. The hydration process was completed by rinsing in DAKO wash buffer (DAKO). Sections were heated in a water bath at 90°C while submerged in antigen retrieval pH 9 epitope retrieval solution (DAKO) for 30 min. Sections were blocked in blocking reagent for 1 h, and then incubated with the antibody 1:100 diluted in M*O*M diluent (Vector M*O*M kit) (Vector Laboratories) for 1 h at room temperature in a humidity chamber. Sections were washed in DAKO wash buffer and secondary antibody was applied (anti-mouse IgG in dilution 1:250). The avidin–biotin complex (Vectastatin Elite Kit) was applied to the slides for 30 min at room temperature. The chromogenic reaction was performed with diaminobenzidine (DAB; DAKO) for 5 min at room temperature. Slides were counterstained with Mayer's hematoxylin for 30 s (Merck), dehydrated in ascending alcohol raw, and mounted with Entelan (Merck). Positive and negative controls were included with each run. Two experienced pathologists scored blindly each tissue section for α -SMA expression based on a semi-quantitative scoring system that measured intensity (0, negative; 1, borderline; 2, weak; 3, moderate; 4, strong) and percentage of positive cells (1–100).

FFPE blocks of tissue samples from metastatic melanoma were retrieved from tissue archives. All patient samples were handled according to the Declaration of Helsinki guidelines. Serial FFPE sections (3 μ m) were attached to positively charged slides (Thermo

Scientific). All slides were heated for 2 h at 60°C and rehydrated. Heat-induced antigen retrieval was performed with Retrieval Solution pH 9 (DAKO). Immunohistochemical (IHC) staining was performed on DAKO Autostainer (DAKO) in a multistep program. In brief, slides were washed in wash buffer (DAKO), followed by incubation with primary antibodies: p-ATM (Rockland Immunochemicals), NOX4 (Epitomics), p-CHK2 (Invitrogen), γ H2AX, p53 clone DO7 (DAKO) and Ki67 (DAKO). After washing with buffer, slides were incubated with EnVision plus polymer anti-mouse and anti-rabbit detection system, followed by a washing step and application of diaminobenzidine substrate (Zytomed) and counterstained with hematoxylin (Merck). All slides were rehydrated and mounted with Entellan (Merck). Representative pictures were taken on Zeiss Axiophot microscope (Zeiss). All IHC slides were scored by semi-quantitative assessment of intensity, whereby signals <10% were considered as absent, signals between 10%-50% were considered as low abundance and signals >50% were considered as high abundance of the marker proteins. dsDDR was considered as active when positive scores for at least p-ATM and γ H2AX were present. dsDDR activity was considered as high when all dsDDR markers were positive.

6.2.5. Physico-chemical techniques

6.2.5.1. Detection of reactive oxygen species

6.2.5.1.1. Detection of superoxide anion radical by electron paramagnetic resonance

Cells or tissues were washed once in 1 \times phospho-buffer saline (PBS) and harvested in 1 \times Krebs–Hepes buffer (KHB: 99 mM NaCl, 4.69 mM KCl, 25 mM NaHCO₃, 1.03 mM KH₂PO₄, 5.6 mM D-glucose, 20 mM Na-HEPES, 2.5 mM CaCl₂, 1.2 mM MgSO₄). Samples were prepared in either hypoxic or normoxic conditions by adding 5 μ M diethyldithiocarbamate (DETC), 25 μ M desferroxamine (DES), and 100 μ M superoxide-specific spin probe (1-hydroxy-methoxycarbonyl-2,2,5,5-tetramethyl-pyrrolidine hydrochloride [CMH]) (Noxygen) (292). Cell suspensions or tissues were placed in airtight glass capillaries and spectra were recorded in an electron paramagnetic resonance (EPR) spectrometer with temperature-controlled resonator Escan (Bruker). EPR settings for CMH spin label were center field 3455 G, sweep width 10 G, frequency 9.7690 GHz, microwave power 23.89 mW, and modulation amplitude 2.93 G. Spectra were recorded over 10 min.

6.2.5.1.2. Detection of reactive oxygen species by high pressure liquid chromatography

Dihydroethidium (DHE) (Sigma) was used for superoxide detection at a final concentration of 50 μM , as described previously (202, 293). Samples were prepared in 1 \times KHB and incubated with DHE (10 μM) at 37°C for 1 h, additionally washed twice with 1 \times KHB, homogenized, and 2-hydroxy-ethidium was extracted in methanol; 2-hydroxy-ethidium was separated on a C18 column (Sulpelco C18 column 4.6 \times 250 mm, 5 μm) and detected by a fluorescence detector (excitation 480 nm and emission 580 nm) in 0.5 ml/ml flow of increased 10–70% gradient of 60% acetonitrile in methanol and 0.1% trifluoroacetic acid. Retention time of 2-hydroxy-ethidium was 37.5 min (202).

6.2.5.2.Detecion of nitric oxide

6.2.5.2.1.Detection of nitric oxide radical by EPR

Freshly prepared iron(2⁺)–diethyldithiocarbamic acid [$\text{Fe}(2^+)\text{DETC}$] colloid complex was used for nitric oxide radical (NO^\cdot) detection at a final concentration of 2 mM (202). Samples were prepared in 1 \times KHB in normoxic or hypoxic conditions. Cell suspensions or tissues were incubated with $\text{Fe}(2^+)\text{DETC}$ in a 1 ml syringe, and then snap-frozen in liquid nitrogen and stored at -80°C . Spectra were recorded by EPR using a Dewar flask filled with liquid nitrogen. EPR settings were center field 3425 G, sweep width 100 G, frequency 9.7704 GHz, power 47.66 mW, and modulation amplitude 10.38 G (202).

6.2.5.2.2.Detection of nitric oxide radical-hemoglobin complex by EPR

Blood collected from mice at death was fractionated to plasma and red blood cell (RBC) fractions. RBC fractions were snap-frozen in 1 ml syringes in liquid nitrogen and loaded for spectral detection by EPR. NO^\cdot -hemoglobin (HbNO) was registered directly by its triple peak. EPR settings for HbNO were center field 3320 G, sweep width 320 G, microwave power 10 mW and modulation amplitude 3 G, time constant 5242 ms, conversion time 655 ms, and number of scans 15 (202).

6.2.5.2.3.Detection of nitrates by HPLC

Nitrites were detected in the cell culture medium supernatant by the reaction with 2, 3-diaminonaphtalene (DAN; Sigma) in acetic conditions (202, 293). 100 μl of the sample was incubated with 10 μl of 0.05 mg/ml of DAN in 6 M HCl for 10 min. Thereafter, the mixture was neutralized by adding 30 μl of 10 M NaOH. Nitrates were reduced to nitrite by nitrate reductase (150 mU/ml) and 0.5 mM of NADPH for 1 h. Nitrated fluorescent DAN adduct was

separated on a C18 column (Sulpelco C18 column 4.6 × 250 mm, 5 μm) and detected by a fluorescence detector (excitation 365 nm and emission 415 nm) in 1 ml/ml flow of 5 mM NaH₂PO₄ in 50% methanol. Retention time of NO₂-DAN was 9.2 min (202, 293).

Blood collected from mice at death was fractionated to plasma and red blood cell (RBC) fractions. RBC fractions were snap-frozen in 1-ml syringes in liquid nitrogen and loaded for spectral detection by EPR. NO-hemoglobin (HbNO) was registered directly by its triple peak. EPR settings for HbNO were center field 3320 G, sweep width 320 G, microwave power 10 mW and modulation amplitude 3 G, time constant 5242 ms, conversion time 655 ms, and number of scans 15 (202).

6.2.5.3. Detection of pterins by HPLC

Cells or tissues were harvested, homogenized in 0.1 M phosphoric acid, 1 mM ethylenediaminetetraacetic acid (EDTA), and 10 mM dithiothreitol (DTT), and incubated on ice in the dark for 20 min (202). After spinning down at 12,000 *g* for 3 min, the supernatant was divided for acidic and alkaline oxidation of BH₄ and incubated either with 2.5% I₂, 10% KI, 0.2 M trichloroacetic acid (TCA; acetic condition) or 5 M NaOH and 0.9% I₂, 1.8% KCl, 0.1 M NaOH (alkaline condition). After incubation for 10 min in the dark, 2% ascorbate and water (acetic condition) or 2 M TCA and 2% ascorbic acid (alkaline condition) were added. Samples were spun down at 30,000 *g* for 10 min and acetic acid was added to stabilize biopterin and pterin. Biopterin and pterin were separated on a C18 column and detected by the fluorescent detector (excitation 350 nm and emission 450 nm) in 1.5 ml/ml flow of 5 mM NaH₂PO₄ in 5% methanol pH 3.5. Retention time of biopterin was 8.6 min (202).

6.2.6. *In vitro* assays

6.2.6.1. BrdU incorporation assay

For assessment of cell proliferative activity 5-bromo-2'-deoxyuridine (BrdU) labeling was used (228). The incorporated BrdU is detected by an immunoassay, using a peroxidase-conjugated antibody that specifically recognizes BrdU bound to denatured DNA. The bound antibody is detected by a peroxidase-catalysed colorimetric reaction, using tetramethylbenzidine (TMB) as a substrate. Cells were seeded in 96-well plates to achieve 50% of confluency. To assess proliferation, cells were then incubated with BrdU (10 μM) for 16 h. Thereafter, cells were fixed for 30 minutes and then incubated for one hour with the peroxidase-conjugated antibody against BrdU. Immunodetection was performed by adding the colorimetric substrate TMB. When the blue color developed, the reaction was stopped

with 1 M H₂SO₄. Absorbance was measured in an ELISA reader (Tecan Safire) at 450 nm with a reference wavelength at 690 nm.

6.2.6.2. Tube formation assay

HMEC-1 cells (5000/well) were seeded on a micro-slide angiogenesis plate (Ibidi) that was mounted with the growth factor-reduced Matrigel (BD Biosciences) (228). Cells were subsequently incubated for 6 h either in hypoxia (1% oxygen) or under control conditions at 37°C, counterstained using Calcein AM (BD Biosciences). Alternatively, HMEC-1 cells were treated with vascular endothelial growth factor (VEGF, 1 µg/µl; Invitrogen). The formation of capillary-like structures was assessed by fluorescence microscopy (Olympus) using the Openlab Modular Software for Scientific Imaging (Improvision) and was quantified for the total tube lengths using Image J software (Wright Cell Imaging Facility).

6.2.7. Ex vivo assays

6.2.7.1. Wire myography

Wire myography on explanted pulmonary artery segments was performed at the Institute for Molecular Genetics (Prague, Czech Republic) as previously described (202). Explanted pulmonary arteries were cut into segments, mounted in a myograph chamber (Dual Wire Myograph System 410A, DMT A/S), and equilibrated for 30 min in oxygenated (5% CO₂, 95% O₂ mixture) physiological salt solution (118.99 mM NaCl, 4.69 mM KCl, 25 mM NaHCO₃, 1.17 mM MgSO₄·7H₂O, 1.18 mM KH₂PO₄, 2.5 mM CaCl₂·2H₂O, 0.03 mM Na₂EDTA, 5.5 mM D-glucose), pH 7.4, at 37°C to achieve a pretension of pulmonary arteries equivalent to an *in vivo* lumen diameter in the relaxed state under a transmural pressure of 100 mmHg. Working parameters for the measurement were then set to 90% of this value. The change in wall tension (active wall tension) was calculated as measured force divided by the double segment length and expressed in mN/mm. Resting wall tension (which arises from the properties of passive elements in the vascular wall) was also determined after the normalization procedure. Forty-five minutes after normalization, modified physiological salt buffer was changed to a buffer, in which NaCl was exchanged for an equimolar concentration of KCl (125 mM) in whole for 2 min followed by washout with modified physiological salt buffer (15 min). Pre-constriction was made by serotonin (1 µM). When the contraction of the

artery reached a steady state, increasing concentrations of acetylcholine (ACh, 0.001–0.3 μ M) were added in an increment manner to perform endothelium-dependent concentration–response curves. The same experiment was done with 20 min of pre-incubation with folic acid (50 μ M) in the bath medium. Data are presented as relative relaxation compared with serotonin-induced pre-constriction.

6.2.7.2. *Ex vivo* hypoxia experiments

For *ex vivo* analyses, lungs were dissected and macerated, or aortae and intact pulmonary arteries were isolated. Isolated tissues were thereafter placed in MCDB131 medium and exposed to hypoxia in a hypoxia work bench (Ruskin) for 24 h.

6.2.8. *In vivo* animal experiments

6.2.8.1. Chronic hypoxia and treatment regimens

For chronic hypoxia experiments, mice were exposed to chronic normobaric hypoxia (10% O₂) in a ventilated chamber (Ing. Humbs, Valley) for 2 weeks. Age-matched control animals breathed room air.

Treatment with folic acid was performed in normoxic and hypoxia-exposed animals by adding folic acid (5 mg/kg/day) as a dietary supplement.

Treatment with dexamethasone was performed by adding dexamethasone (0.3 mg/kg/day) as a water supplement.

All animal procedures were performed in accordance with the European directive 86/609/EEC and approved by the local legislative committee for animal welfare (Government of Upper Bavaria, Munich, Germany).

6.2.8.2. Gross morphology analysis

For analysis of the gross morphologic features of the heart *in situ*, the thoracic wall was opened and RIV and the RDM, as well as the heart apex were visualized. Pictures were taken using an Olympus E520 (Olympus) camera mounted on a compact tripod positioned directly on the dissection table, with 14–42 Olympus ED zoom lens (Olympus), set at a focal length of 30 mm. Subsequently, hearts were explanted and positioned on their right side to visualize alterations of the right chamber. Pictures were taken with the same camera and objective set at the focal length of 40 mm. All images were obtained in high-definition JPG format at a resolution of 10 megapixels and processed in GIMP 2.6.11 software

(www.gimp.org). Angles between the bars marking the RIV and the RDM were measured by a standard transparent manual protractor on A5 printouts of the images and taken as a macroscopic measure of right ventricular hypertrophy. The pictures of the explanted hearts were analyzed for visible protrusion of the right chamber in front of the interventricular sulcus (202).

6.2.8.3. Wheat germ agglutinin assay

To quantify the cardiomyocyte size in both left (LV) and right (RV) ventricle, FFPE heart sections were stained with Wheat Germ Agglutinin–Alexa Fluor 488 (Invitrogen) to delineate cell membranes (294). For each sample 10 different average cardiomyocyte diameters were determined in longitudinally oriented cardiomyocytes by image analysis software (Image J). The nuclei were visualized with DAPI (1:10000) staining (228). Criteria for the short axis of the cardiomyocytes were a circular shape and the visibility of the cell nucleus (294).

6.2.8.4. Right ventricular hypertrophy

Hearts were removed and dissected to isolate the free wall RV from LV and septum (S). The ratio of RV mass to left ventricle plus septum (LV+S) mass (RV/LV+S) (Fulton Index) was used to estimate right ventricle hypertrophy (202). Alternatively, hypertrophy of the respective ventricle was calculated by determining the ratio of the mass of the corresponding ventricle vs. whole body mass (BM). In addition, whole heart sections were dehydrated and stained in 3% Giemsa solution (Merck). Pictures were taken on the Zeiss Axiophot microscope (Zeiss) equipped with a CCD camera. The measurement was done using the Zeiss Axio Vision measurement module. Three measurements of the RV wall were taken per section: one of the center wall thickness and two 1 mm above and 1 mm below the wall midline. All pictures were processed in GIMP 2.6.11 (www.gimp.org).

6.2.8.5. Hemodynamic measurements

Mice were anesthetized by isoflurane, weighed, and the left chest was shaved. RVP was determined hemodynamically in a transthoracic approach (202). Hemodynamic measurements were performed using a 24 G needle connected to a pressure amplifier (Isotec) and recorded using HSE-HA HAEMODYN W software for hemodynamic studies. The catheter was inserted into the LV and then carefully advanced to the RV. The correct position was confirmed by observing the characteristic ventricular waveforms. The pressure

profile was recorded after stabilization for 1 min, and systolic right ventricle pressure (RVP) values were determined. Mice were euthanized in anesthesia by cervical dislocation.

6.2.8.6. Echocardiography

Echocardiography was performed with a Vivid S6 Ultrasound System (General Electrics) and a 12i linear array transducer (12 MHz) as previously described (295, 296). In brief, mice were anesthetized with inhaled 1.4 – 1.6% isoflurane/oxygen mixture and left ventricular end diastolic (LVEDD) and end systolic (LVESD) diameters and wall thicknesses were obtained from M-mode tracings using measurements averaged from 3 separate cardiac cycles. Left ventricular fractional shortening (%) was derived using the equation $FS = [(LVEDD - LVESD) / LVEDD] \times 100$. Cardiac dilation was defined as $LVEDD > 3.5\text{mm}$ and cardiac dysfunction as fractional shortening $< 55\%$.

6.2.8.7. *In vivo* angiogenesis

In vivo matrigel plug assay was performed as previously described (228, 297). HMEC-1 were silenced for $\beta 3$ -endoneixin (siEN) or transfected with scrambled RNA (siCtr). Cells (150000/plug) were mixed with 350 μl of growth factor reduced Matrigel (BD Biosciences) and subcutaneously injected into mice (C5BL/6j, 6 weeks old, male). At 7 days after the injection, matrigel plugs were excised, formalin fixed and paraffin embedded, sectioned, and prepared for immunohistochemistry. The formation of capillary-like structures was assessed by staining with an antibody against CD31 (DAKO) in a 1:50 dilution.

6.2.9. Statistics

All experimental data have been received from independent experiments. Values are presented as mean \pm SD. Results were compared by ANOVA for repeated measurements, followed by Student–Newman–Keuls t-test. $p < 0.05$ was considered statistically significant.

7 Results

7.1.Folic acid protects against hypoxia-induced pulmonary hypertension

Disruption of nitric oxide (NO) and reactive oxygen species (ROS) metabolism under chronic hypoxia has been associated with remodeling in heart and lungs. However, the interplay between these reactive species and the role of functionally competent NO synthase (NOS) under hypoxia alongside their consequences for hypoxia-induced pulmonary hypertension has not been well characterized (202). The data of the following study investigating the role of NO/ROS balance and folic acid in the context of hypoxia induced cardio-pulmonary pathology have been previously published (202). Permission to use the figures and the text of the paper was obtained from *Antioxidants&Redox Signaling* (Appendix, p.143).

7.1.1.Nitric oxide and 5',6',7',8' tetrahydrobiopterin bioavailability are decreased under hypoxia

In order to evaluate the functional competence of NOS under hypoxia, first NO bioavailability under hypoxia was determined (Figure 1A). For this purpose human pulmonary artery endothelial cells (HPAEC) and isolated murine pulmonary arteries were exposed to hypoxia (Hx, 1% oxygen) for 24 h and NO levels were determined by electron paramagnetic resonance (EPR) using iron(2⁺)-diethyldithiocarbamic acid [Fe(2⁺)(DETC)] colloid complex. NO production under hypoxia was decreased in HPAEC and in explanted pulmonary arteries compared to normoxic controls (Figure 1A) (202).

Further on, levels of nitrite, a decomposition product of NO, in the supernatants of normoxic and hypoxic HPAEC were analyzed by high pressure liquid chromatography (HPLC) (202). Nitrite release was decreased in hypoxic samples similar to the situation with NO (Figure 1B). NO formation by NOS requires adequate levels of 5',6',7',8'-tetrahydrobiopterin (BH₄); therefore, levels of BH₄ as well as of its oxidation product 7',8'-dihydrobiopterin (BH₂) were

determined (202). For this purpose HPAEC and explanted pulmonary arteries were exposed to hypoxia (Hx, 1% oxygen) for 24 h and the HPLC based tetrahydrobiopterin assay was performed using supernatants of HPAEC and pulmonary arteries (202). BH₄ levels were reduced in hypoxic HPAEC and pulmonary arteries, while levels of BH₂ were increased under these conditions consequently resulting in a decreased BH₄/BH₂ ratio (Figure 1C) (202). Interestingly, total biopterin levels were not significantly changed in hypoxia, suggesting that hypoxia did not affect biopterin synthesis (Figure 1D) (202).

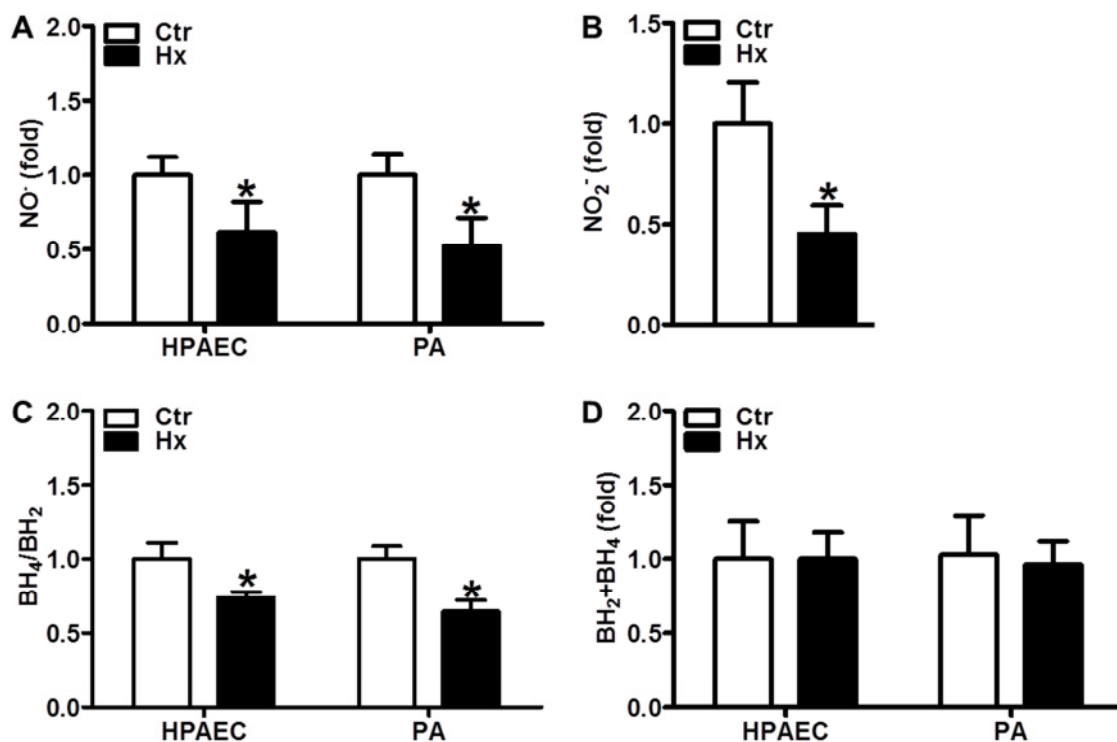


Figure 1. Hypoxia decreases nitric oxide bioavailability. (A–D) Human pulmonary artery endothelial cells (HPAEC) or isolated murine pulmonary arteries (PA) were incubated in hypoxic (Hx, 1% oxygen) or normoxic conditions (Ctr) for 24 h. **(A)** Nitric oxide (NO) levels were measured by electron paramagnetic resonance (EPR) using iron(2⁺)-diethyldithiocarbamic acid [Fe(2⁺)(DETC)] complex as an NO radical-specific spin probe ($n=4$; $*p < 0.05$ vs. Ctr). **(B)** Nitrite levels were determined in the supernatant of HPAEC by high-pressure liquid chromatography (HPLC) ($n=3$; $*p < 0.05$ vs. Ctr). **(C)** 5',6',7',8'-tetrahydrobiopterin (BH₄) and 7',8'-dihydrobiopterin (BH₂) levels were measured in cell and tissue lysates by HPLC ($n=5$; $*p < 0.05$ vs. Ctr). **(D)** The sum of BH₄ and BH₂ levels in HPAEC and PA was calculated. Figure adapted from (202).

7.1.2. Folic acid increases dihydrofolate reductase levels and BH₄ bioavailability under hypoxia

Hypoxia disrupted the balance between BH₄ and BH₂, but did not affect overall biopterin levels. Therefore, it was hypothesized that recycling of BH₄ from BH₂ rather than *de novo* BH₄ synthesis might be affected by hypoxia. Since the conversion of BH₂ to BH₄ is mediated by dihydrofolate reductase (DHFR), DHFR protein levels in HPAEC were determined (202). Compared to normoxia, DHFR protein as well as mRNA levels were reduced under hypoxia (Figure 2A/B) (202). These findings suggest that the decrease in BH₄ and the increase in BH₂ observed under hypoxic conditions might be related to a decreased recycling capacity due to lowered DHFR levels in this setting.

Folic acid has been described to increase the levels of DHFR in the systemic vasculature; hence, in the next step it was evaluated whether folic acid could modulate DHFR levels (298). For this purpose HPAEC were supplemented with folic acid (FA, 50 μM) using a concentration that was previously described to induce DHFR (298). Subsequent exposure to hypoxia for 24 h showed that folic acid supplementation restored hypoxic DHFR protein levels, but also enhanced normoxic DHFR protein levels (Figure 2A) (202). In addition, folic acid enhanced DHFR mRNA levels under normoxic and hypoxic conditions (Figure 2B) (202). Application of actinomycin D (ActD) to normoxic or hypoxic HPAEC treated with folic acid blunted folic acid-mediated induction of DHFR protein levels indicating that folic acid promotes increased transcription of DHFR (Figure 2A) (202).

Next, the effects of folic acid on BH₄ levels were determined. Under hypoxia, the BH₄/BH₂ ratio was restored to normoxic levels in HPAEC and pulmonary arteries treated with folic acid, while it was even further increased under normoxic conditions (Figure 3A/B) (202). Upon brief exposure to normoxia following hypoxia simulating hypoxia–reoxygenation conditions, the BH₄/BH₂ ratio remained low, similar to the situation with hypoxia, but was increased in the presence of folic acid (Figure 3A) (202); however, folic acid did not affect total biopterin levels under normoxia or hypoxia in HPAEC and pulmonary arteries (Figure 3C/D) indicating that it did not act *via de novo* biopterin synthesis.

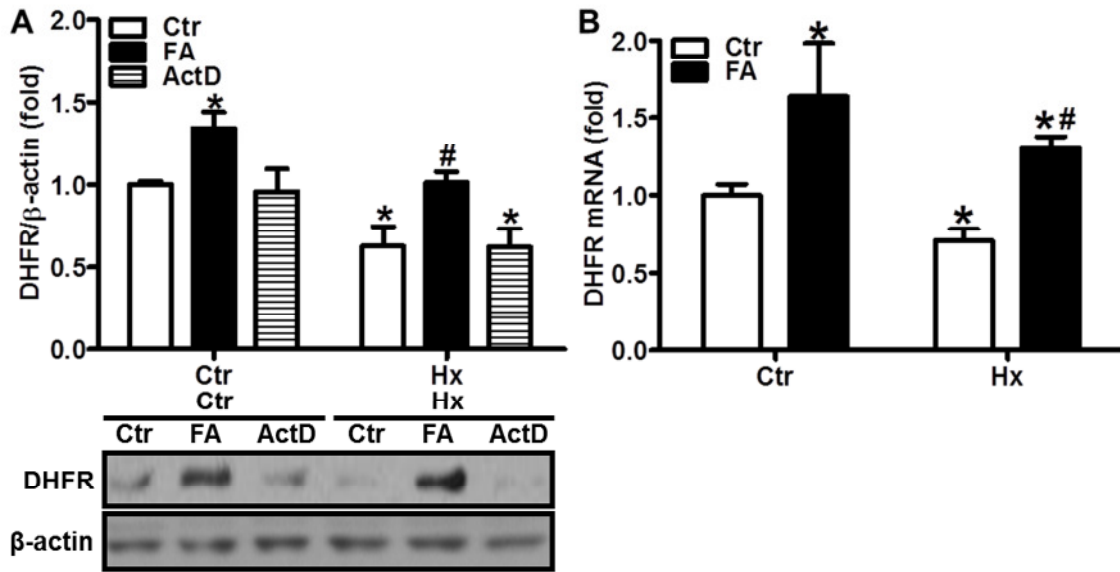


Figure 2. Folic acid restores dihydrofolate reductase expression under hypoxia. (A) HPAEC were incubated in hypoxia (Hx, 1% oxygen) or normoxia (Ctr) for 24 h in the presence or absence of FA (50 μ M) with and without actinomycin D (ActD, 1 μ M). Western blot analysis was performed with an antibody against dihydrofolate reductase (DHFR). β -actin served as loading control ($n = 4$; * $p < 0.05$ vs. CtrCtr; # $p < 0.05$ vs. CtrHx; § $p < 0.05$ vs. FA). **(B)** DHFR mRNA levels were determined by RT-qPCR in normoxic (Ctr) or hypoxic (Hx) HPAEC. 18S rRNA served as a control ($n = 4$; * $p < 0.05$ vs. CtrCtr; # $p < 0.05$ vs. CtrHx). Figure adapted from (202).

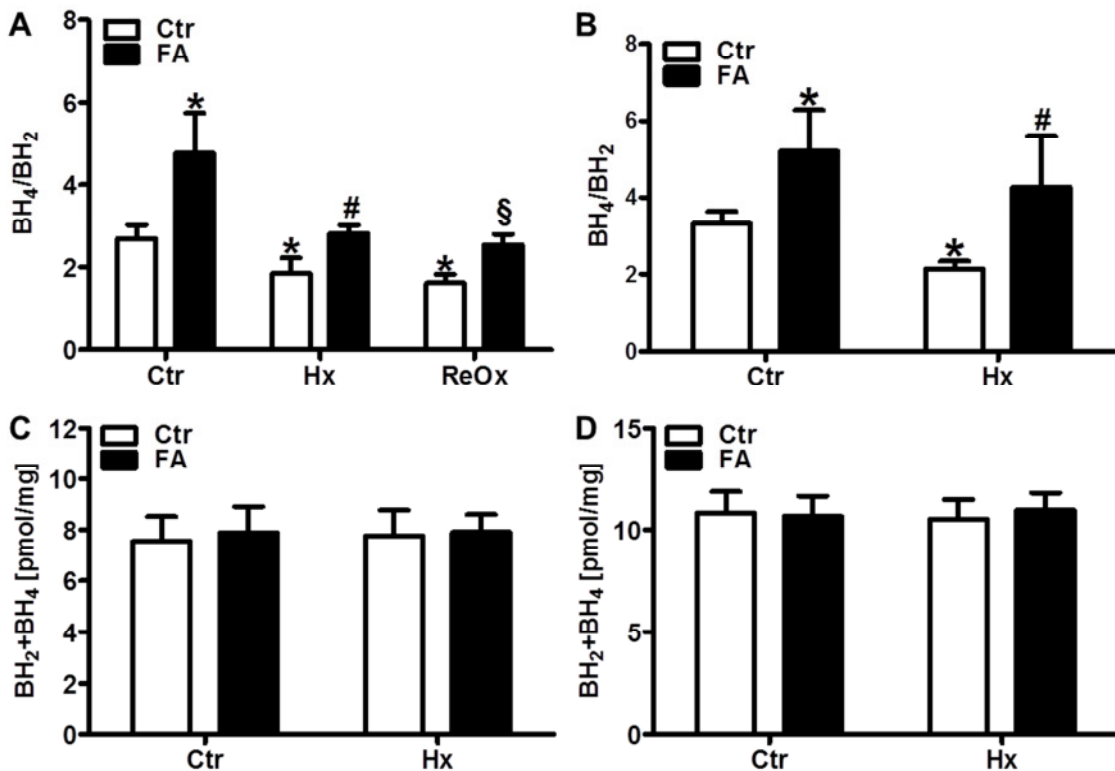


Figure 3. Folic acid restores NO and BH₄/BH₂ balance under hypoxia. (A) HPAEC or **(B)** isolated murine pulmonary arteries (PA) were incubated in hypoxic (Hx) or normoxic (Ctr) conditions for 24 h in the presence or absence of FA (50 μ M). BH₄ and BH₂ levels were measured in cell- and PA

tissue lysates by HPLC under hypoxic or reoxygenated (ReOx) conditions **(A)** or under solely hypoxic conditions **(B)** ($n = 5-6$; $*p < 0.05$ vs. CtrCtr; $^{\#}p < 0.05$ vs. CtrHx, $^{\S}p < 0.05$ vs. CtrReOx). The sum of BH₄ and BH₂ levels was calculated **(C)** in HPAEC and **(D)** in murine PA. Figure adapted from (202).

7.1.3. Folic acid increases hypoxic NO bioavailability

Next, the effects of folic acid on NO availability were determined. In HPAEC, folic acid dose dependently increased NO levels under hypoxia starting at 25 μM (Figure 4A) (202). Since application of more than 50 μM folic acid did not further enhance NO levels under hypoxic conditions, all the following *in vitro* studies were performed at 50 μM concentration (Figure 4A) (202). In fact, 50 μM folic acid increased NO levels under normoxia and restored them to normoxic levels under hypoxic and reoxygenating conditions (Figure 4B). In line, 50 μM folic acid also efficiently restored hypoxic NO levels in pulmonary arteries (Figure 4C) and hypoxic nitrite levels in HPAEC to the respective normoxic levels (Figure 4D) (202).

Similar to the situation with BH₄, NO levels remained low under hypoxia-reoxygenation conditions in HPAEC, but were partially restored by folic acid (Figure 4B) (202).

To confirm that modulation of DHFR levels was indeed involved in the control of NO levels under hypoxia and folic acid treatment, DHFR levels were downregulated by an siRNA approach (Figure 4E/F). While downregulation of DHFR levels did not affect NO levels under normoxic conditions, it further decreased hypoxic NO levels (Figure 4E) (202). However, induction of NO levels by folic acid was blunted in normoxia and hypoxia in DHFR-depleted HPAEC (Figure 4E) indicating that folic acid acts *via* DHFR to improve NO bioavailability.

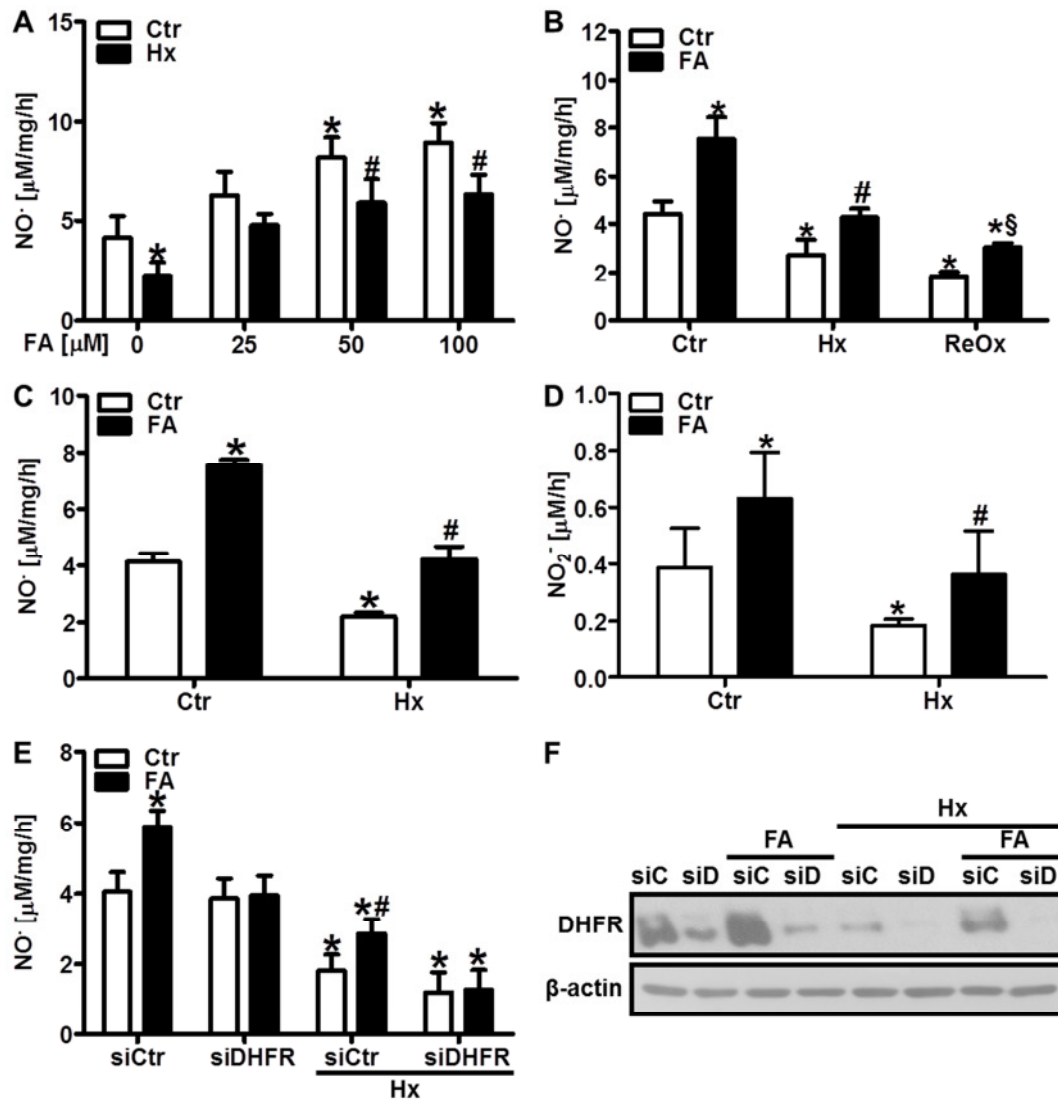


Figure 4. Folic acid restores NO bioavailability under hypoxia. (A) HPAEC were exposed to normoxia (Ctr) or hypoxia (Hx, 1% oxygen) for 24 h in the presence of folic acid (FA, 0-100 μM). NO levels were measured under hypoxic conditions by EPR using [Fe(2+)(DETC)] complex ($n=3$; * $p < 0.05$ vs. CtrCtr; # $p < 0.05$ vs. CtrHx). (B) HPAEC were incubated in hypoxia (1% oxygen, Hx) or normoxia (Ctr) for 24 h in the presence or absence of FA (50 μM) and NO levels were measured under hypoxic or reoxygenated conditions (ReOx) as above ($n=4$; * $p < 0.05$ vs. CtrCtr; # $p < 0.05$ vs. HxCtr; § $p < 0.05$ vs. ReOxCtr). (C) Isolated murine PA were incubated in hypoxia (Hx, 1% oxygen) or normoxia (Ctr) for 24 h in the presence or absence of FA (50 μM) and NO levels were measured under hypoxic or reoxygenated conditions (ReOx) as above ($n=4$; * $p < 0.05$ vs. CtrCtr; # $p < 0.05$ vs. CtrHx; § $p < 0.05$ vs. CtrReOx). (D) Nitrite levels were determined in the supernatant of HPAEC exposed to normoxia (Ctr) or hypoxia (Hx) for 24 h by HPLC ($n=3$; * $p < 0.05$ vs. CtrCtr; # $p < 0.05$ vs. CtrHx). (E-F) HPAEC were transfected with siRNA against DHFR (siDHFR/siD) or scrambled siRNA (siCtrl/siC) and incubated in hypoxia (Hx, 1% oxygen) or normoxia (Ctr) for 24 h in the presence or absence of FA (50 μM). (E) NO levels were measured as above ($n=3$; * $p < 0.05$ vs. siCtrlCtr; # $p < 0.05$ vs. siCtrlFA). (F) Western blot analysis was performed with an antibody against DHFR. β-actin served as loading control. Figure adapted from (202).

7.1.4. Folic acid improves vasoconstriction in pulmonary arteries

Since folic acid has been previously reported to modulate the phosphorylation status of eNOS (299), the levels of Ser1177 phosphorylated eNOS, which renders the enzyme active,

and Thr495 phosphorylated eNOS which results in inactivation of the enzyme were determined (202). In HPAEC, phosphorylation at both sites was increased under hypoxia (Figure 5A) (202). Folic acid also increased the levels of Ser1177 phosphorylated eNOS under normoxic conditions although it did not further increase Ser1177 phosphorylated eNOS levels under hypoxia in HPAEC (Figure 5A) (202).

In contrast, folic acid decreased eNOS phosphorylation at Thr495 under normoxic and hypoxic conditions (Figure 5A) (202). However, folic acid had no effect on unphosphorylated eNOS protein levels under normoxia or hypoxia (Figure 5A). The findings that folic acid is also able to increase NO levels under normoxic conditions due to enhanced BH₄ availability by inducing DHFR-dependent recycling capacity and by modulation of eNOS phosphorylation suggest that basal NO bioavailability in this experimental set-up might be

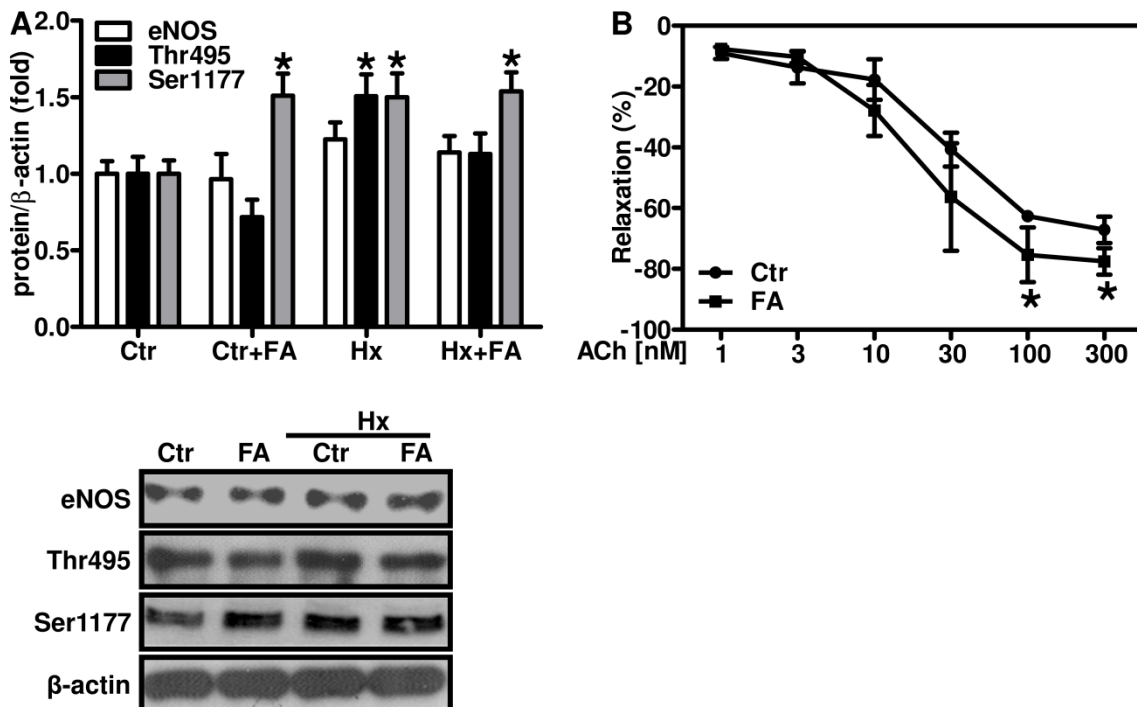


Figure 5. Folic acid increases endothelial nitric oxide synthase phosphorylation and improves vasoconstriction in pulmonary arteries. (A) HPAEC were incubated in hypoxia (Hx, 1% oxygen) or normoxia (Ctr) for 24 h in the presence or absence of folic acid (FA, 50 μM). Western blot analyses were performed in HPAEC lysates using antibodies against native and phosphorylated (Ser1177, Thr495) endothelial nitric oxide synthase (eNOS) ($n=3$; $*p < 0.05$ vs. respective Ctr). β-actin served as a loading control. (B) Explanted pulmonary artery segments were placed in a myograph chamber, pre-constricted with serotonin (1 μM), and increasing concentrations of the vasodilator acetylcholine (ACh, 1-300 nM) were added in the presence or absence of FA (50 μM). Vessel relaxation was determined by wire myography ($n=3$; $*p < 0.05$ vs. respective Ctr). Figure adapted from (202).

limited by insufficient folic acid supply (202). Concomitantly, folic acid was able to improve endothelial-dependent relaxation of isolated pulmonary arteries in response to acetylcholine (Figure 5B); further indicating that folic acid can improve NO bioavailability (202).

7.1.5. Hypoxia uncouples eNOS

Reduced BH₄ levels have been previously associated with uncoupling of NOS (300, 301) and in this study it is shown that hypoxia reduced BH₄ levels in vascular endothelial cells and pulmonary arteries (Figure 1) (202). Since the functional NOS with an intact enzymatic activity is a dimer, determination of NOS monomer/dimer ratio is a good indication of NOS functional activity. Therefore, the eNOS monomer/dimer ratio in HPAEC, aortae and pulmonary arteries was determined (Figure 6A/B)(202). Increased eNOS monomer formation was observed in HPAEC, pulmonary and systemic vessels further confirming that eNOS is uncoupled under hypoxia (Figure 6A/B) (202). eNOS monomer/dimer ratio under hypoxia was however diminished in HPAEC upon treatment with folic acid further indicating recoupling of eNOS (Figure 6A) (202). Uncoupling of NOS leads to the formation of superoxide instead of NO. To evaluate whether uncoupled eNOS contributes to superoxide levels under normoxia or hypoxia, HPAEC and pulmonary arteries were treated with the NOS inhibitor L-(G)-nitro-L-arginine methyl ester (L-NAME) prior to superoxide production measurements. Superoxide production in HPAEC and pulmonary arteries under normoxia and hypoxia was evaluated by EPR using CMH (10 μM) as a spin probe. Importantly, hypoxic cells or vessels were harvested and prepared for superoxide measurements under hypoxic conditions using a hypoxic work bench. Measurements were performed in an air-tight capillary thus preventing any reoxygenation step during sample handling. Under these conditions, cells and tissues exposed for 24 h to hypoxia showed decreased superoxide production compared to normoxia (Figure 6C/D) (202). In contrast, when sample harvesting and preparation was performed under normoxic conditions following 24 h of hypoxia, superoxide production was even more increased than under normoxia (Figure 6C/D) (202). These findings indicate that even short term exposure to normoxia during sample preparation is sufficient to induce a reoxygenation effect. While L-NAME did not affect normoxic or reoxygenated superoxide production, it significantly decreased hypoxic superoxide production (Figure 6C/D) indicating that uncoupling of eNOS contributed to superoxide production under hypoxic conditions.

Recoupling of eNOS by folic acid should not only result in increased NO levels but also in reduced superoxide levels. In fact, in HPAEC, hypoxic and reoxygenated superoxide production was decreased in the presence of folic acid although this effect was less pronounced in pulmonary arteries (Figure 6C/D) (202).

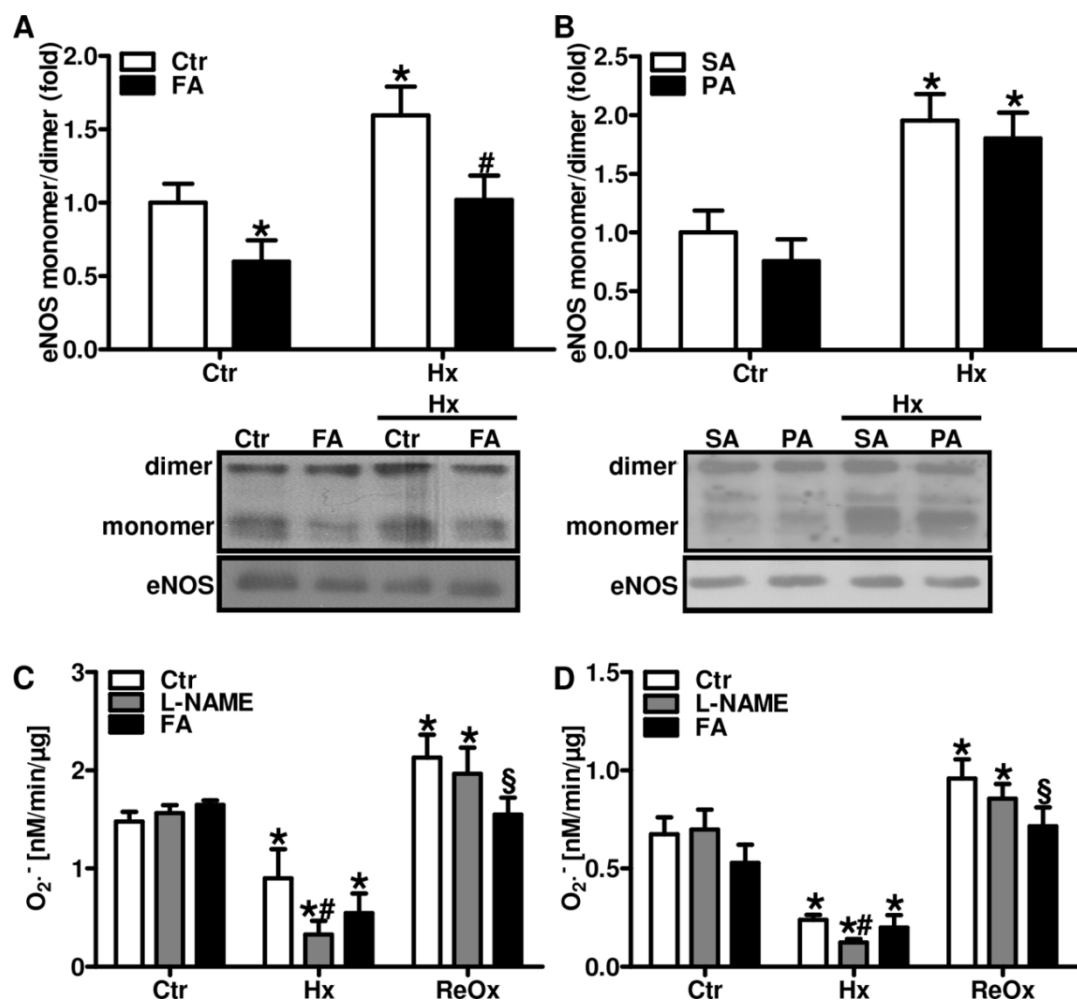


Figure 6. Uncoupled eNOS contributes to hypoxic superoxide production. (A) HPAEC or isolated (B) systemic (SA) or pulmonary arteries (PA) were exposed to hypoxia (Hx, 1% oxygen) and normoxia (Ctr) for 24 h. In addition, pulmonary arteries (A) were supplemented with folic acid (FA, 50 μ M). Total proteins were isolated in non-denaturing conditions and low temperature Western blotting was performed with an antibody against eNOS for the visualization of eNOS monomers and dimers. Standard Western blot with denaturated protein samples was performed for total eNOS levels, which served as a loading control ($n = 3$; * $p < 0.05$ vs. CtrCtr; # $p < 0.05$ vs. CtrHx). (C) HPAEC or (D) isolated murine PA were incubated under normoxic (Ctr) or hypoxic (Hx, 1% oxygen) conditions for 24 h in the presence or absence of the NO synthase inhibitor, L-(G)-nitro-L-arginine methyl ester (L-NAME, 300 μ M), and/or FA (50 μ M). The superoxide production rate was measured by EPR using 1-hydroxy-methoxycarbonyl-2,2,5,5-tetramethyl-pyrrolidine hydrochloride (CMH, 10 μ M) as a spin probe under complete hypoxic (Hx) or normoxic following hypoxic conditions (ReOx) ($n = 5$; * $p < 0.05$ vs. CtrCtr; # $p < 0.05$ vs. CtrHx; § $p < 0.05$ vs. CtrReOx). Figure adapted from (202).

7.1.6. Superoxide production is decreased under hypoxia

Besides uncoupled eNOS, reactive oxygen species (ROS) in vascular cells and tissues may also come from: NADPH oxidases, mitochondrial sources, xanthine oxidase, and virtually from any leaky oxido-reductase. To evaluate the contribution of other ROS sources under these conditions HPAEC were pretreated either with apocynin, an antioxidant, or 2-thenyltrifluoroactenone (TTFA), a mitochondrial complex II inhibitor, or rotenone, a complex

I inhibitor (Figure 7A) (202). While none of the inhibitors significantly affected normoxic superoxide production, apocynin and to a lesser extent the mitochondrial inhibitors decreased hypoxic superoxide levels, similar to the situation with L-NAME. Since NADPH oxidases have been suggested to play a role in the pulmonary vascular response to hypoxia (302), we sought to investigate their role in the hypoxic superoxide generation. For that purpose HPAEC were treated with GKT-137831 which has been described to inhibit NADPH oxidases (202, 303). GKT-137831 treatment decreased normoxic and hypoxic superoxide levels (Figure 7B). These findings indicate that NADPH oxidases also contribute to maintain ROS levels under hypoxia as has been described previously (202, 304). In line, hypoxia induced NOX4 protein levels in HPAEC, while folic acid did not affect NOX4 levels, suggesting that the contribution of NADPH oxidases is independent of NO signaling (Figure 7C/D) (202). Interestingly, under reoxygenated conditions, apocynin and GKT-137831

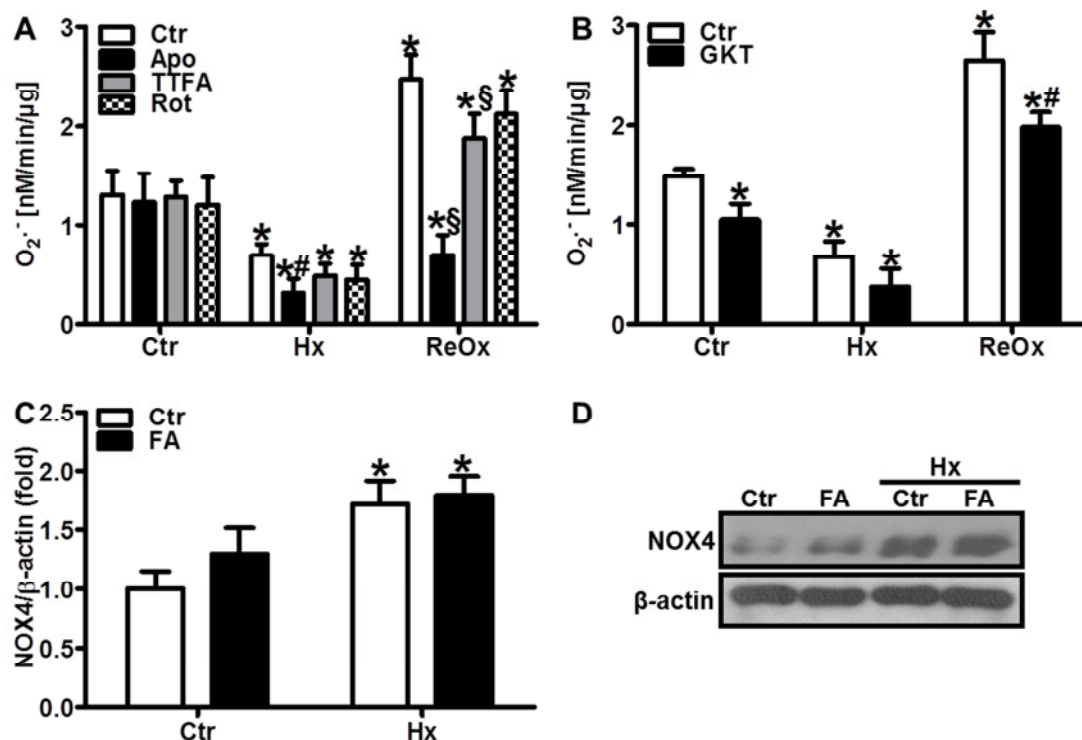


Figure 7. NADPH oxidases contribute to superoxide production under hypoxia. (A) HPAEC were incubated under normoxic (Ctr) or hypoxic (Hx, 1% oxygen) conditions for 24 h in the presence of apocynin (Oxy, 100 μM), or inhibitors of mitochondrial complex II, thenoyltrifluoroacetone (TTFA, 100 μM), or complex I, rotenone (Rot, 100 μM). The superoxide production rate was measured by EPR using 1-hydroxy-methoxycarbonyl-2,2,5,5-tetramethyl-pyrrolidine hydrochloride (CMH, 10 μM) as a spin probe under complete hypoxic (Hx) or normoxic following hypoxic conditions (ReOx) ($n = 3$; * $p < 0.05$ vs. CtrCtr; § $p < 0.05$ vs. CtrHx; # $p < 0.05$ vs. CtrReOx). **(B)** HPAEC were incubated under normoxic (Ctr) or hypoxic (Hx, 1% oxygen) conditions for 24 h in the presence or absence of GKT-137831 (GKT, 50 μM). The superoxide production rate was measured as above ($n = 3$; * $p < 0.05$ vs. CtrCtr; # $p < 0.05$ vs. CtrReOx). **(C/D)** HPAEC were incubated under normoxic (Ctr) or hypoxic (Hx, 1% oxygen) conditions for 24 h in the presence or absence of folic acid (FA, 50 μM) and Western blot analyses were made using an antibody specific for NOX4. β-actin served as a loading control ($n = 3$; * $p < 0.05$ vs. CtrCtr). Representative blots are shown **(D)**. Figure adapted from (202).

reduced superoxide production (Figure 7A/B), while mitochondrial inhibitors, similar to L-NAME pre-treatment (Figure 6C), were not effective, indicating that NADPH oxidases are the major source of ROS under reoxygenated conditions (202).

7.1.7. Folic acid improves hypoxic NO bioavailability *in vivo*

In a next step levels of NO in mice exposed for 2 weeks to hypoxia (10% oxygen) were evaluated by determining NO-hemoglobin levels by EPR (Figure 8A). NO-hemoglobin levels were decreased in chronic hypoxic mice compared to normoxic mice (Figure 8A) (202). In line, the ratio of plasma BH₄/BH₂ was lower in hypoxic than in normoxic mice (Figure 8B) (202). When mice were orally supplemented with folic acid (FA, 5 mg/kg/day) during exposure to hypoxia, NO-hemoglobin levels and plasma BH₄ availability were restored to

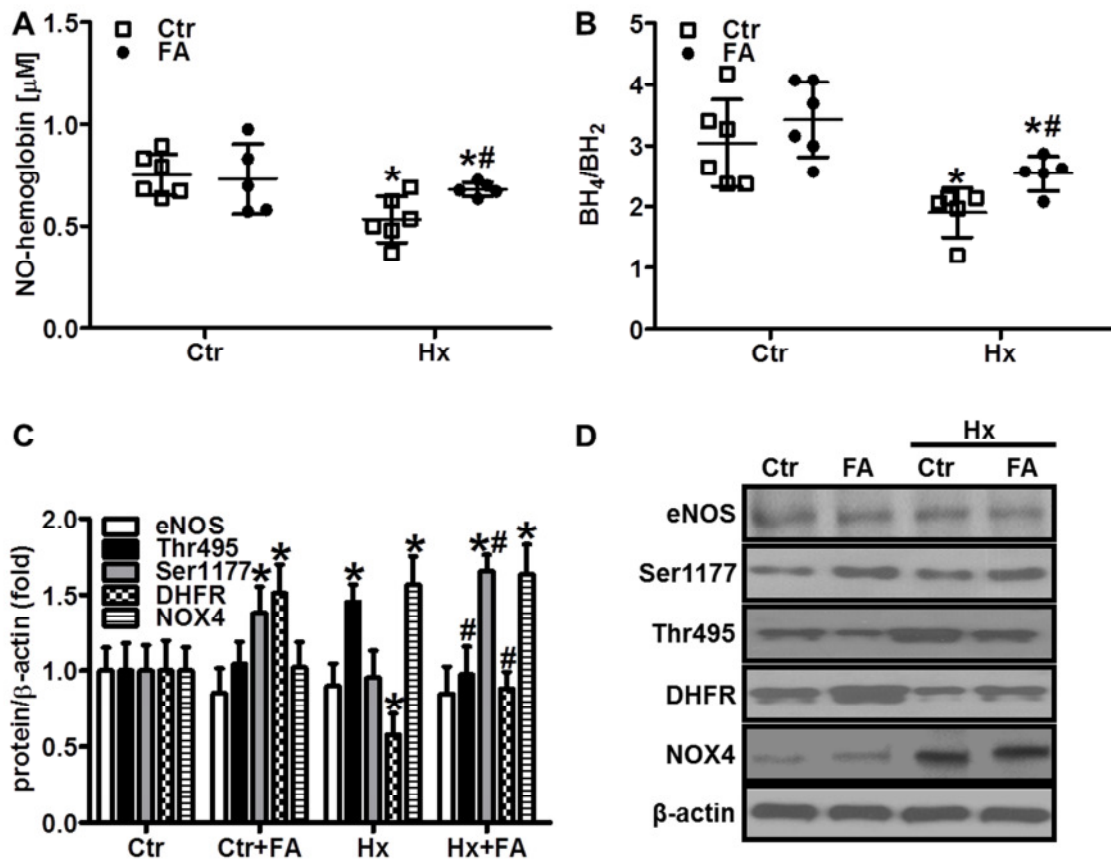


Figure 8. Folic acid prevents the decrease in NO bioavailability in chronic hypoxic mice. CD57BL/6n mice were exposed for 2 weeks to hypoxia (Hx, 10% oxygen) or normoxia (Ctr) with or without supplementation of folic acid (FA, 5 mg/kg/day). **(A)** NO-hemoglobin levels were measured in red blood cell fractions by EPR using CMH ($n=5$; $*p < 0.05$ vs. CtrCtrl; $^{\#}p < 0.05$ vs. CtrHx). **(B)** BH₄ and BH₂ levels were measured in plasma using HPLC, and the BH₄/BH₂ ratio was determined ($n=6$; $*p < 0.05$ vs. CtrCtrl; $^{\#}p < 0.05$ vs. CtrHx). **(C/D)** Western blot analyses were performed in lung tissues using antibodies against eNOS, Ser1177- and Thr495-phosphorylated eNOS, DHFR, and NOX4. β -actin served as a loading control ($n=3$; $*p < 0.05$ vs. CtrCtrl; $^{\#}p < 0.05$ vs. CtrHx). Representative blots are shown **(D)**. Figure adapted from (202).

normoxic levels (Figure 8A/B) (202). Subsequently, decreased pulmonary DHFR levels in hypoxic lungs were restored in folic acid-treated animals (Figure 8C/D) (202). Similar to the situation *in vitro*, pulmonary eNOS protein levels were neither affected by hypoxia nor by folic acid (Figure 8C) (202). However, the levels of Ser1177 phosphorylated eNOS were increased by folic acid under normoxia and hypoxia while the levels of Thr495 phosphorylated eNOS were decreased (Figure 8C/D) indicating that folic acid improves NO bioavailability *in vivo* by several mechanisms (202).

As described previously (304), and suggested by *in vitro* data here, NADPH oxidases might contribute to the increased levels of ROS upon reoxygenation. In line, levels of the NADPH oxidase subunit NOX4 were substantially increased in lung tissues from hypoxic mice compared to normoxic mice (Figure 8D) (202). However, folic acid treatment did not affect NOX4 levels ruling out that the reduction of ROS levels observed in chronic hypoxic mice treated with folic acid was due to downregulation of NOX4 (Figure 8D) (202).

7.1.8. Folic acid decreases hypoxic ROS levels *in vivo*

To evaluate the levels of ROS in chronic hypoxic mice, pulmonary arteries were isolated from normoxic and hypoxic mice under normoxic conditions simulating a reoxygenated state, and superoxide production was determined by EPR. Compared to vessels from normoxic mice vessels from chronic hypoxic mice showed elevated superoxide production (Figure 9A) similar to the *in vitro* situation of hypoxia-reoxygenation (202).

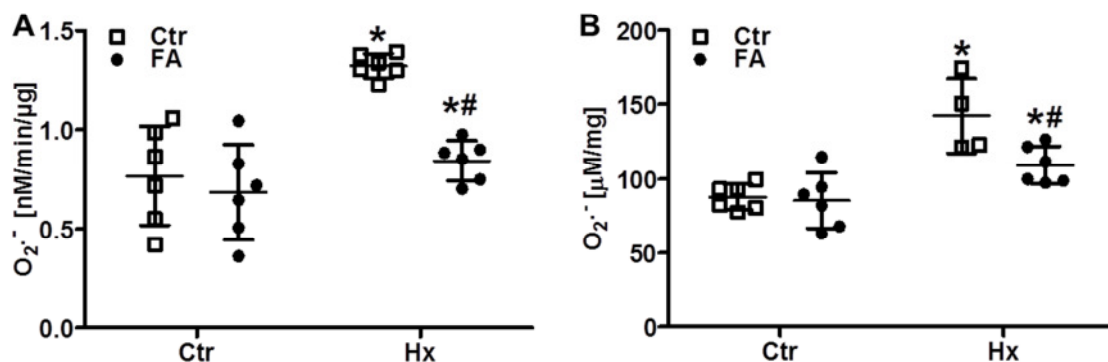


Figure 9. Folic acid reduces superoxide levels in chronic hypoxic mice. CD57BL/6n mice were placed for 2 weeks under hypoxia (Hx, 10% oxygen) or normoxia (Ctr) with or without supplementation of folic acid (FA, 5 mg/kg/day). **(A)** Pulmonary arteries were isolated and superoxide production was measured by EPR using CMH ($n=6$; $*p < 0.05$ vs. CtrCtr; $\#p < 0.05$, vs. CtrHx). **(B)** Whole lung extracts were incubated with dihydroethidium (DHE, 10 μ M), and superoxide levels were determined by measuring DHE fluorescence by HPLC ($n=6$; $*p < 0.05$ vs. CtrCtr; $\#p < 0.05$ vs. CtrHx). Figure adapted from (202).

ROS levels were also determined in lung tissues by HPLC using dihydroethidium as a probe. Similar to the results in pulmonary arteries, ROS levels were increased in lungs derived from hypoxic mice compared to normoxic lungs (Figure 9B) (202).

Treatment with folic acid significantly decreased ROS levels in pulmonary arteries and lung tissues derived from chronic hypoxic mice as determined by EPR or HPLC-based dihydroethidium fluorescence (Figure 9A/B) (202).

These findings are similar to the situation when superoxide production of hypoxic HPAEC was determined under normoxic conditions (Figure 6A).

7.1.9. Folic acid protects against hypoxia-induced right ventricular hypertrophy, right ventricular pressure increase and pulmonary vascular remodeling

Finally, CD57BL6n mice were exposed to chronic hypoxia (Hx, 10% oxygen) for 2 weeks. Control litter-mates breathed room air. Additional two experimental groups of mice either exposed to chronic hypoxia or normoxic conditions were supplemented with folic acid in the drinking water (5 mg/kg/day) for two weeks (Figure 10) (202). In mice exposed to chronic hypoxia, the right ventricle was enlarged as was estimated by determination of the angle between the left descending interventricular artery (RIV) and the right marginal coronary artery (RDM). The angle between RIV and RDM in hearts of normoxic mice was 44°, while it was enlarged to 59° in hearts of chronic hypoxic mice (Figure 10A/B) (202). In line, sections derived from formalin-fixed paraffin-embedded (FFPE) hearts stained with Giemsa showed an increase in right ventricular wall thickness in hypoxic mice compared to normoxic control litter-mates (Figure 10C) (202). Furthermore, staining of FFPE lung sections with an antibody specific for α -smooth muscle cell actin (α -SMA) showed an increased number of muscularized small vessels (diameter <80 μ m) in lungs from hypoxic mice compared to normoxic mice, indicating pulmonary vascular remodeling (Figure 10D/F) (202). In addition, the ratio between right ventricular mass and left ventricular and interseptal mass (Fulton Index) was increased in chronic hypoxic compared to normoxic mice (Figure 10E) indicating the development of right ventricular hypertrophy in chronic hypoxic mice (202).

Folic acid was shown to induce DHFR levels and to enhance DHFR activity, thereby stimulating the regeneration of BH₄ from the inactive oxidized BH₂ (202, 298). Next, the impact of folic acid on pulmonary vascular remodeling, right ventricular hypertrophy and pulmonary hypertension in the context of chronic hypoxia was evaluated.

Treatment with folic acid reduced right ventricular hypertrophy as indicated by a reduction of the angle between RIV and RDM to normoxic values in hearts derived from hypoxic mice treated with folic acid (Figure 10A/B) (202). Under normoxic conditions, however, folic acid treatment had no effect on the size of the right ventricle (Figure 10A/B). Similarly, folic acid

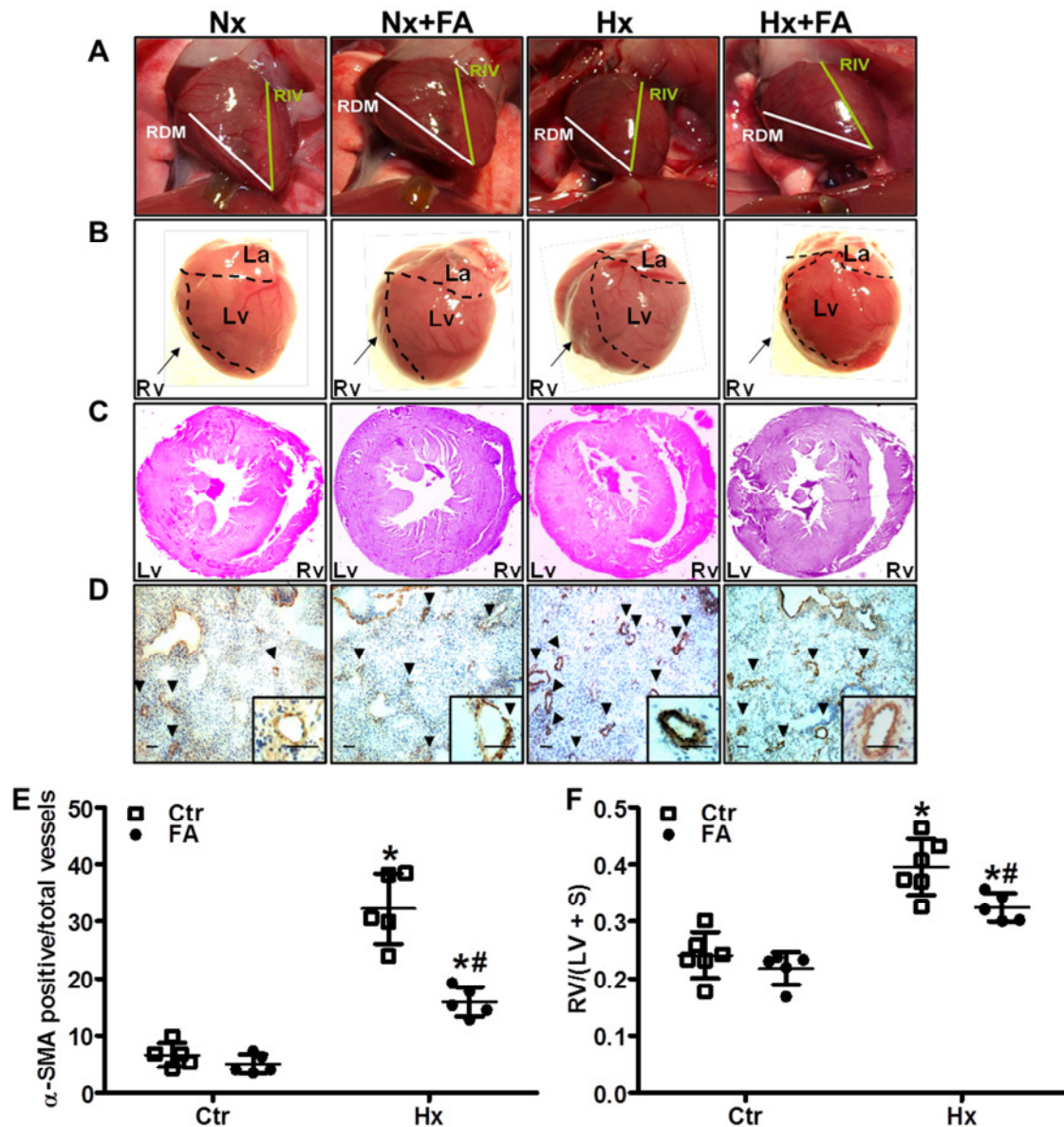


Figure 10. Folic acid decreases hypoxia-induced right ventricular hypertrophy and pulmonary vascular remodeling. CD57BL/6n mice were placed for 2 weeks under hypoxia (Hx, 10% oxygen) or normoxia (Ctr) with or without supplementation of folic acid (FA, 5 mg/kg/day). **(A)** Right ventricular (RV) size was macroscopically estimated by determining the angle between the left descending interventricular artery (RIV) and right marginal coronary artery (RDM). **(B)** Gross heart morphology was macroscopically observed. **(C)** Formalin-fixed paraffin-embedded (FFPE) heart sections were stained with Giemsa. **(D)** FFPE lung sections were stained with an antibody against α -smooth muscle actin (α -SMA). Bar 100 μ m; arrows indicate α -SMA-positive vessels. **(E)** RV was separated from the left ventricle (LV) and septum (S) and mass was determined. The RV/LV+S ratio was calculated ($n=6-8$; $*p < 0.05$ vs. CtrCtr; $\#p < 0.05$ vs. CtrHx). **(F)** α -SMA-positive small- and medium-sized arterioles ($<80 \mu$ m) were counted and related to the total number of arterioles of the same diameter ($n=6$; $*p < 0.05$, vs. CtrCtr; $\#p < 0.05$ vs. CtrHx). Figure adapted from (202).

treatment reduced hypoxia-induced thickening of the right ventricular wall and right ventricle mass (Figure 10C/E) (202). In addition, folic acid treatment decreased the number of small muscularized vessels in hypoxic lungs (Figure 10D/F) (202).

Next, the right ventricular pressure using a hemodynamic transthoracic approach was determined. Hemodynamic measurements showed increased systolic right ventricular pressure in hypoxic control mice (Figure 11), pointing to development of pulmonary hypertension (202), while treatment with folic acid reduced hypoxic increase of the systolic right ventricular pressure (202).

Collectively, these data show that the supplementation of chronic hypoxic mice with folic acid protects against the development of hypoxia-induced pulmonary hypertension by reducing pulmonary vascular remodeling, right ventricular pressure and right ventricular hypertrophy in response to chronic hypoxia (202).

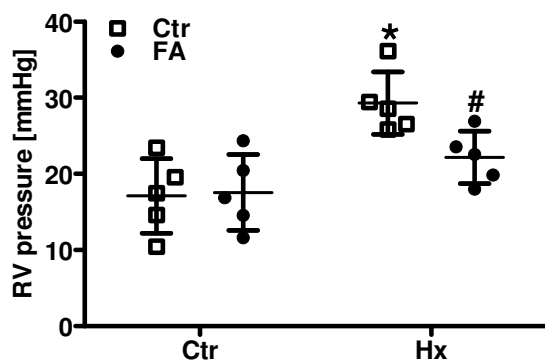


Figure 11. Folic acid decreases hypoxia-induced right ventricular pressure. CD57BL/6n mice were placed for 2 weeks under hypoxia (Hx, 10% oxygen) or normoxia (Ctr) with or without supplementation of folic acid (FA, 5 mg/kg/day). Systolic right ventricular (RV) pressure was determined hemodynamically ($n = 5$; * $p < 0.05$ vs. CtrCtr; # $p < 0.05$ vs. CtrHx). Figure adapted from (202).

7.2.Dexamethasone promotes cardiac and pulmonary vascular remodeling *via* reactive oxygen species and hypoxia inducible factor 1

Reactive oxygen species have been associated with inflammatory and immune reactions. Glucocorticoids have been shown to act immunosuppressive and in certain instances anti-inflammatory. However, how glucocorticoids interfere with ROS metabolism and signaling has not been well understood.

7.2.1.Dexamethasone induces superoxide production in vascular cells and vessels

In order to characterize superoxide production in response to glucocorticoids, human microvascular endothelial cells (HMEC-1) and human pulmonary artery smooth muscle cells (PASMC) were stimulated with different concentrations of the synthetic glucocorticoid dexamethasone (0.1 – 1000 nM) for 4 h, and superoxide production was measured by EPR using CMH as a superoxide-specific spin probe (Figure 12A). In both, HMEC-1 and PASMC, superoxide production was dose-dependently increased starting already at 10 nM dexamethasone. Concomitantly, exposure of HMEC-1 and PASMC to 10 nM dexamethasone for increasing time periods resulted in a significant increase in superoxide production starting 30 min after dexamethasone introduction and remaining sustained even for 8 h (Figure 12B). In addition, dexamethasone induced superoxide production in explanted murine aortae and pulmonary arteries (Figure 12C).

Since actions of glucocorticoids are majorly mediated by the glucocorticoid receptor (GR), it was of interest to determine the role of GR in dexamethasone-induced superoxide production. To this end, HMEC-1 and PASMC were pre-treated with the GR inhibitor mifepristone (RU486, 500 μ M) for 1 h, subsequently treated with dexamethasone and superoxide production was determined by EPR. Indeed, mifepristone addition diminished dexamethasone-induced superoxide production in HMEC-1 (Figure 12D) and in PASMC (Figure 12E).

Since activated GR rapidly binds to the p85 α subunit of phosphatidylinositol-4, 5-bisphosphate 3-kinase (PI-3K) (305), the involvement of this pathway in dexamethasone-induced superoxide generation was tested. Pre-treatment of HMEC-1 with the PI-3K inhibitor LY294002 (LY, 100 μ M) for 1 h attenuated dexamethasone-induced superoxide production (Figure 12F).

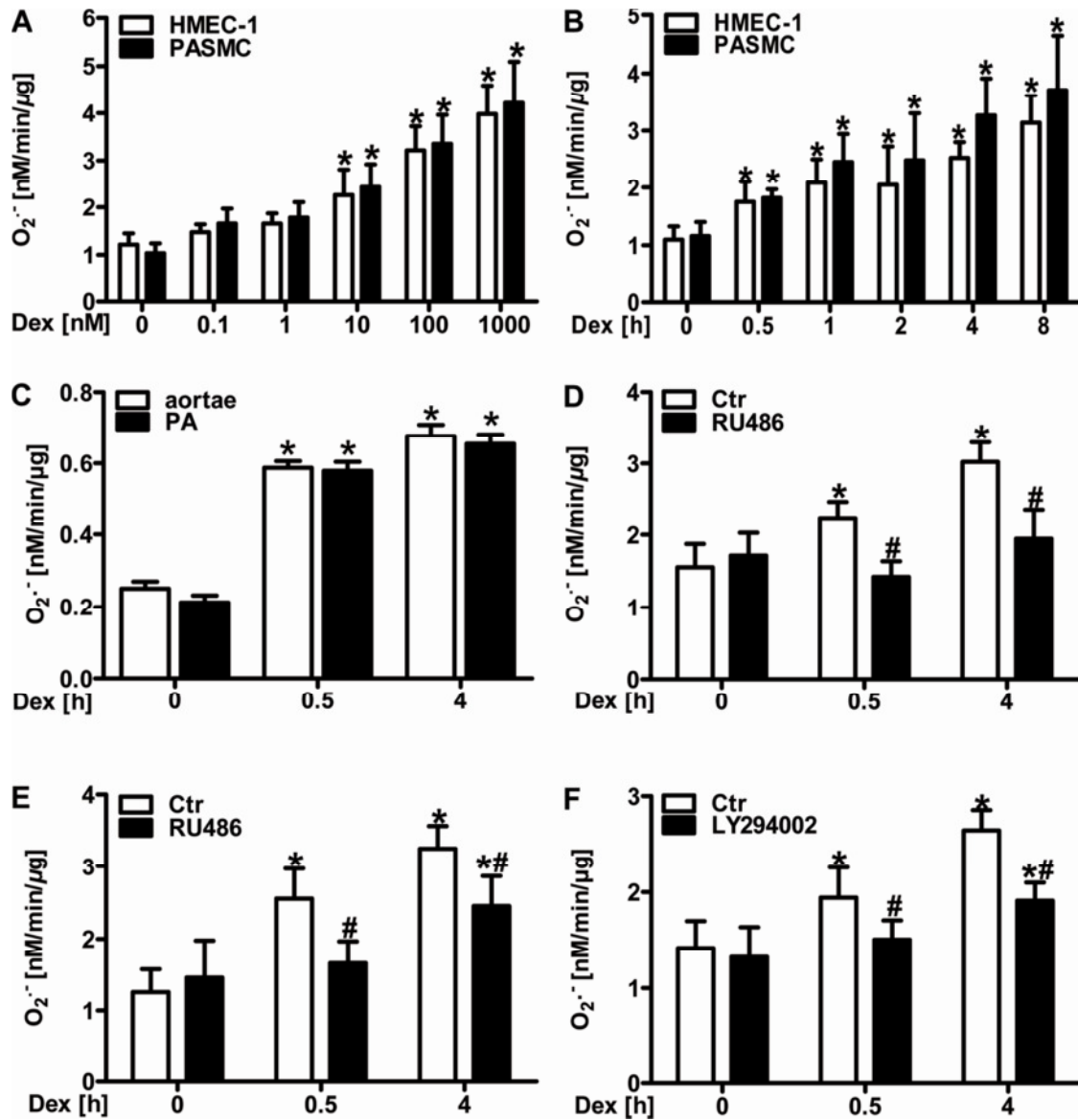


Figure 12. Dexamethasone induces superoxide generation in vascular cells and vessels. (A) Human microvascular endothelial cells (HMEC-1) and pulmonary artery smooth muscle cells (PASMC) were treated with dexamethasone (Dex, 0.1-1000 nM) for 4 h and the superoxide production rate was measured by EPR using CMH ($n=4-6$; $*p<0.05$ vs. Dex 0 nM). (B) HMEC-1 and PASMC were treated with Dex (10 nM) for increasing time periods and the superoxide production rate was measured as above ($n=4-6$; $*p<0.05$ vs. Dex 0 nM). (C) Isolated murine aortic rings and pulmonary arteries (PA) were incubated with Dex (10 nM) *ex vivo* and the superoxide production rate was measured as above ($n=4-6$; $*p<0.05$ vs. Dex 0 nM). (D-E) HMEC-1 (D) and PASMC (E) were pretreated with the glucocorticoid receptor inhibitor – mifepristone (RU486, 500 μ M) for 1 h, subsequently treated with Dex (10 nM) for 0.5 and 4 h and the superoxide production rate was measured as above ($n=4-6$; $*p<0.05$ vs. CtrDex 0 h; $#p<0.05$, vs. CtrDex 0.5 h or CtrDex 4 h). (F) HMEC-1 were pre-treated with inhibitor of phosphatidylinositol-4,5-bisphosphate 3-kinase (LY294002, 100 μ M) and subsequently treated with Dex (10 nM) for 0.5 and 4 h and the superoxide production rate was measured as above ($n=3$; $*p<0.05$ vs. CtrDex 0 h; $#p<0.05$, vs. either CtrDex 0.5 h or CtrDex 4 h).

7.2.2. Dexamethasone-induced superoxide production is derived from NADPH oxidases

To characterize the source of dexamethasone-induced superoxide production, HMEC-1 (Figure 13A) and PASMC (Figure 13B) were treated with the xanthine oxidase inhibitor oxypurinol (Oxy, 100 μ M), as well as with thenoyltrifluoroacetone (TTFA), an inhibitor of the mitochondrial complex II (100 μ M) and rotenone (Rot, 100 μ M), an inhibitor of complex I. However, none of these inhibitors significantly affected dexamethasone-induced superoxide production neither in HMEC-1 nor in PASMC (Figure 13A/B). Similarly, treatment with the eNOS inhibitor L- NAME did not affect dexamethasone-induced ROS production, thus ruling out uncoupled eNOS as a prominent source of ROS in this context (Figure 13A). Treatment with the inhibitor GKT-137831 indicative of NADPH oxidases, however, decreased dexamethasone-induced superoxide production in HMEC-1 (Figure 13A), as well as in PASMC (Figure 13B), thus pointing to NADPH oxidases as a main source of superoxide in vascular cells following dexamethasone treatment.

To further identify subunit(s) of NADPH oxidases involved in superoxide generation in response to dexamethasone treatment, HMEC-1 and PASMC were transfected with specific RNAi to silence either p22phox or NOX1 or NOX2 or NOX4. In both cell types, depletion of NOX4 diminished superoxide generation, while the effect of NOX1 depletion was more pronounced in HMEC-1 compared to PASMC (Figure 13C/D). In addition, silencing of NOX2 and p22phox also prevented dexamethasone-induced superoxide production in HMEC-1 (Figure 13C), as well as in PASMC (Figure 13D). In line, expression of dominant-negative Rac1T17N in HMEC-1 prevented dexamethasone-induced ROS production (Figure 14A).

In support, downregulation of NADPH oxidases by lentiviral delivery of shp22phox, shNOX2 and shNOX4 to explanted murine aortic rings resulted in decreased superoxide production rate upon treatment with dexamethasone (Figure 14B).

Furthermore, aortic rings explanted from a mouse strain deficient in functional p22phox due to a point mutation in the p22phox gene (nmf333 strain) showed reduced superoxide production upon dexamethasone treatment compared to dexamethasone-treated aortic rings from wild type mice (Figure 14C).

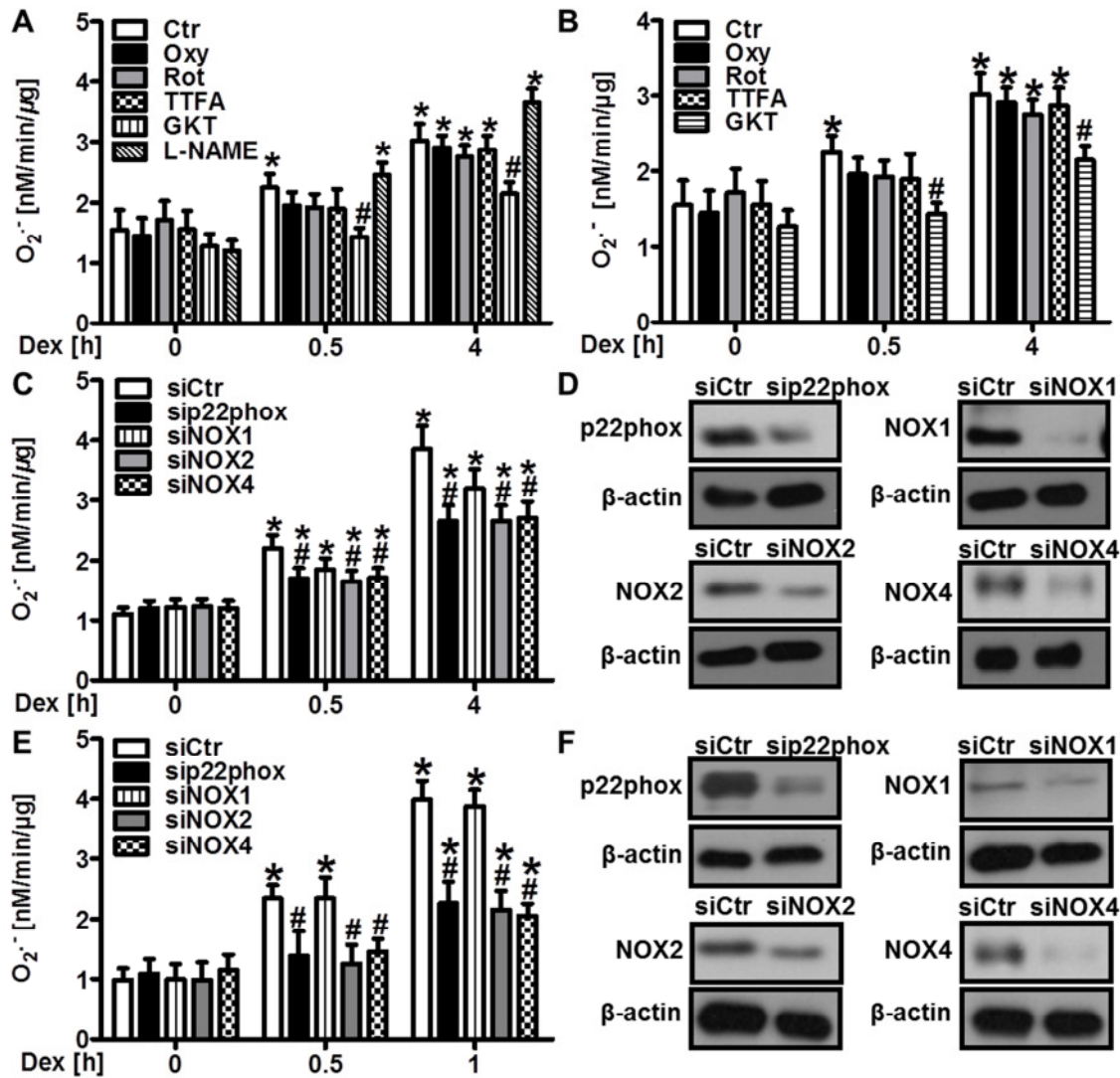


Figure 13. Sources of superoxide production in vascular cells and vessels following the treatment with dexamethasone. (A-B) HMEC-1 (A) and PASM (B) were incubated with dexamethasone (Dex, 10 nM) for 0.5 and 4 h in the presence or absence of the inhibitor of xanthine oxidase – oxypurinol (Oxy, 100 μ M), or inhibitors of mitochondrial complex II, thenoyltrifluoroacetone (TTFA, 100 μ M), or complex I, rotenone (Rot, 100 μ M), or the inhibitor indicative of NADPH oxidases - GKT-137831 (50 μ M) and the nitric oxide synthase inhibitor (only HMEC-1, panel A), L-(G)-nitro-L-arginine methyl ester (L-NAME, 300 μ M). The superoxide production rate was measured by EPR using CMH ($n=3-4$; * $p < 0.05$ vs. CtrDex 0 h; # $p < 0.05$ vs. CtrDex 0.5 h or CtrDex 4 h). (C-D) HMEC-1 (C) and PASM (D) were silenced for either p22phox or NOX1 or NOX2 or NOX4 using RNAi or transfected with siCtr, exposed to Dex (10 nM) for 0.5 and 4 h, and superoxide production was measured as above ($n=3-5$; * $p < 0.05$ vs. CtrDex 0 h; # $p < 0.05$ vs. CtrDex 0.5 h or CtrDex 4 h). Lysates from HMEC-1 and PASM were evaluated by Western blot analysis post EPR measurements for the expression levels of the corresponding silenced NADPH oxidase subunit using antibodies against NOX, NOX2, NOX4 or p22phox. β -actin served as a loading control.

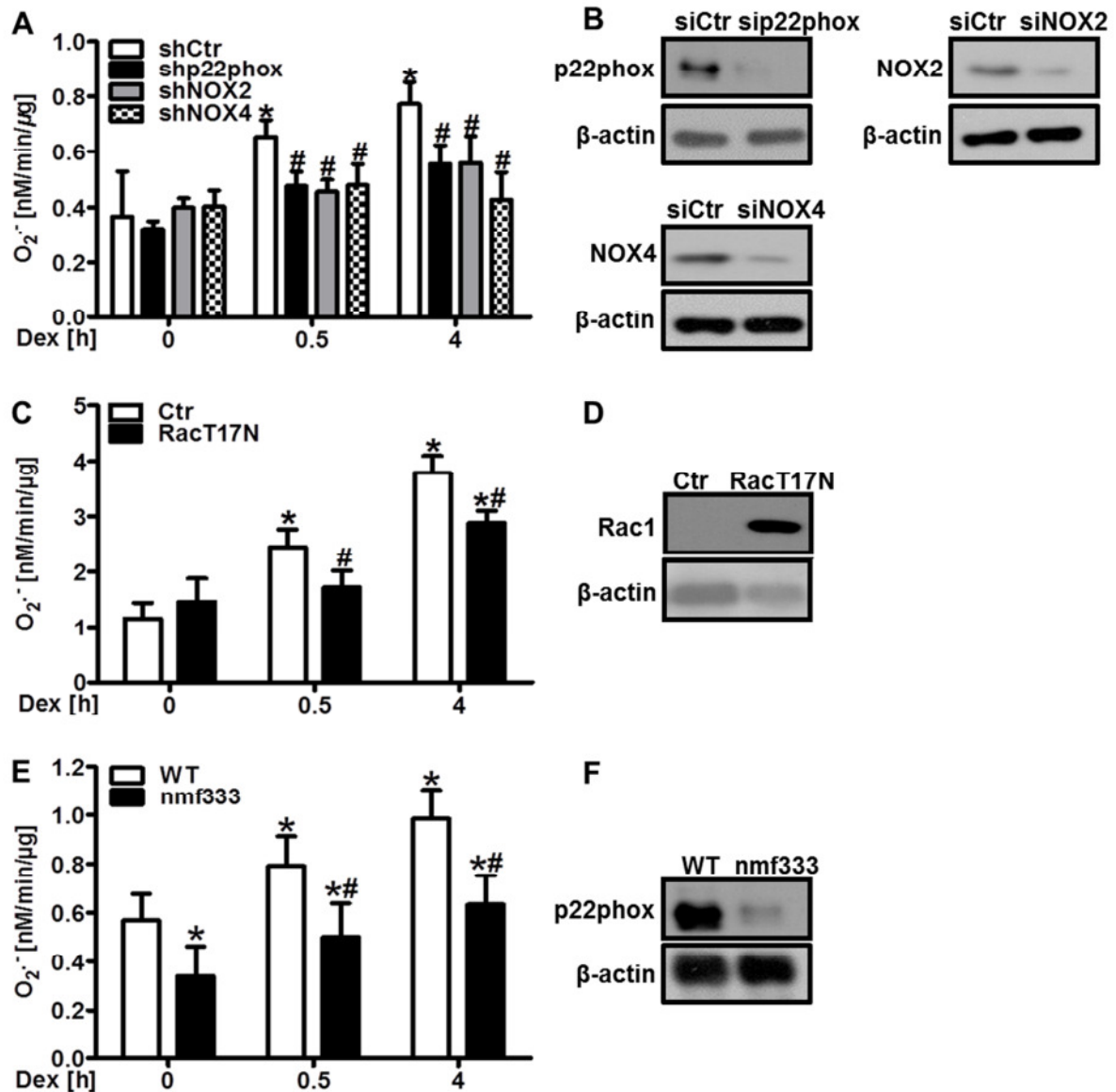


Figure 14. NADPH oxidases are main sources of vascular superoxide production following treatment with dexamethasone. (A) Isolated murine aortic ring were transfected by lentiviral delivery of shRNA targeting either p22phox or NOX2 or NOX4 or transfected with scrambled RNA (shCtrl) and exposed to dexamethasone (Dex, 10 nM) for 0.5 and 4 h. Superoxide production was measured by EPR using CMH (n = 3; *p < 0.05 vs. CtrDex 0 h; #p < 0.05 vs. CtrDex 0.5 h or CtrDex 4 h). (B) Aortic tissue lysates were evaluated by Western blot analysis post EPR measurements p22phox, NOX2 or NOX4 protein levels. β-actin served as loading control. (C) Human microvascular endothelial cells (HMEC-1) were transfected with an the expression vector coding for a dominant-negative Rac1 (RacT17N) and treated with Dex (10 nM) for 0.5 and 4 h. Superoxide production rate was measured by EPR using CMH (n = 3; *p < 0.05 vs. CtrDex 0 h; #p < 0.05 vs. either CtrDex 0.5 h or CtrDex 4 h). (D) Western blot analysis was performed on HMEC-1 lysates for the expression of the V5-tag. β-actin served as loading control. (E) Aortic rings from CD57BL6j (WT) mice and mice lacking p22phox protein due to a point mutation in the cyba gene (nmf333) were exposed to Dex (10 nM) for 0.5 and 4 h and superoxide production was measured as above (n = 3; *p < 0.05 vs. CtrDex 0 h; #p < 0.05 vs. CtrDex 0.5 h or CtrDex 4 h). (F) Aortic tissue lysates were evaluated by Western blot analysis post EPR measurements. β-actin served as a loading control. Representative blots are shown.

7.2.3. Dexamethasone upregulates NADPH oxidases and promotes proliferative responses

Next, it was evaluated whether dexamethasone can modulate the expression of NADPH oxidases. For that purpose, HMEC-1 were stimulated with dexamethasone for increasing time periods and Western blot and RT-qPCR analyses were performed (Figure 15). Exposure to dexamethasone resulted in the upregulation of p22phox and NOX4 both on protein (Figure 15A/B) and mRNA level (Figure 15C). Similar results were observed in lungs of wild type mice orally treated with dexamethasone (Dex, 0.3 mg/kg/day) for 12 weeks (Figure 15D).

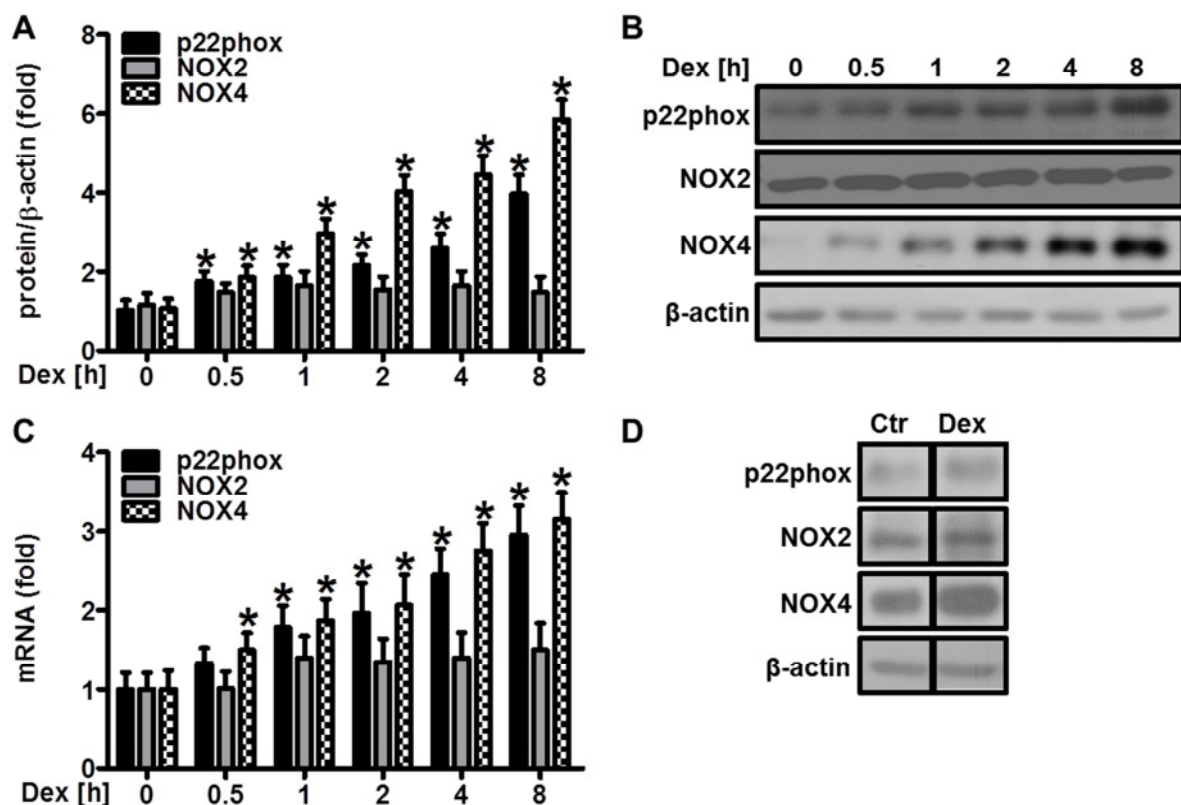


Figure 15. Dexamethasone upregulates NADPH oxidase expression in vascular cells and murine lungs. (A-B) HMEC-1 were stimulated with dexamethasone (Dex, 10 nM) for increasing time periods as indicated, and Western blot (A/B) and RT-qPCR (C) analyses were performed using antibodies against- or gene-specific primers for p22phox, NOX2 and NOX4, respectively ($n=3$, $*p<0.05$ vs. Dex 0 h). β -actin or 18S rRNA served as loading controls, respectively. (D) CD57BL6j mice were orally supplemented in the drinking water with Dex (0.3 mg/kg/day) for 12 weeks. Control litter-mates drunk normal water (Ctr). Western blot analyses were performed on murine lung tissues using antibodies against p22phox, NOX2 and NOX4. β -actin served as a loading control.

Since ROS derived from NADPH oxidases have been implicated to promote vascular proliferation and angiogenesis (306, 307), HMEC-1 were depleted of p22phox, NOX2 and NOX4 and proliferation was determined by 5-bromo-2'deoxyuridine (BrdU) incorporation assay (Figure 16A). Dexamethasone-induced proliferation in HMEC-1 was not observed in the absence of p22phox, NOX2 and NOX4 (Figure 16A).

Next, we determined whether dexamethasone affects tube formation in an *in vitro* matrigel assay as an indicator of angiogenesis. Indeed, dexamethasone treatment enhanced tube

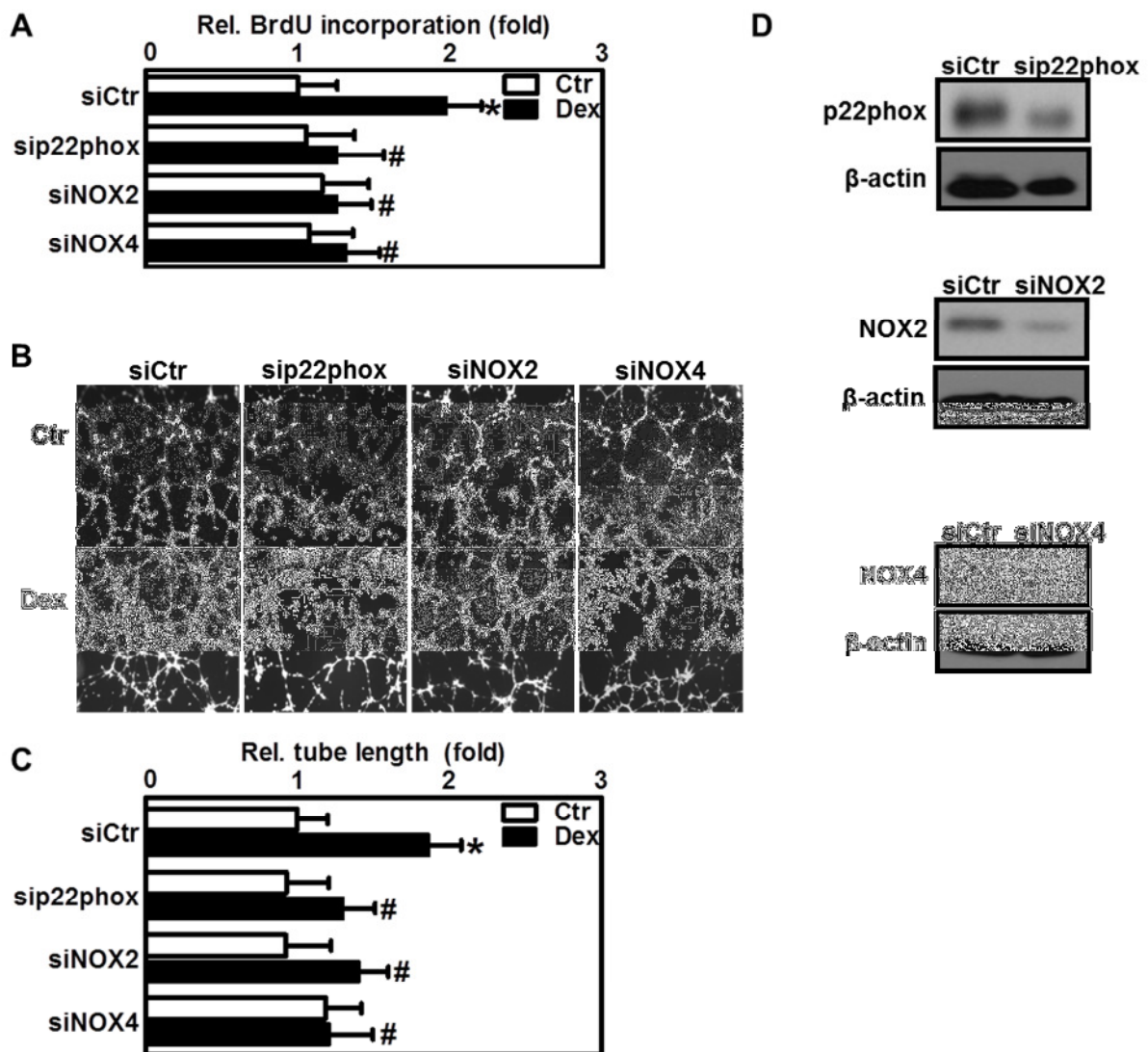


Figure 16. Dexamethasone promotes proliferative and angiogenic responses via NADPH oxidases in endothelial cells. (A-D) HMEC-1 were transfected with siRNA against either p22phox or NOX2 or NOX4 or scrambled RNA (siCtr). **(A)** HMEC-1 were exposed to dexamethasone, (Dex, 10 nM) for 24 h or remained untreated (Ctr), and a 5-bromo-2'deoxyuridine (BrdU) incorporation assay was performed ($n=3, *p<0.05$ vs. siCtrCtr; $\#p<0.05$ vs. siCtrDex). Alternatively, **(B/C)** HMEC-1 were seeded on matrigel for an *in vitro* tube formation assay, subsequently exposed to Dex (10 nM) for 6 h or remained untreated (Ctr). **(C)** For quantification of tube formation assays, total tube lengths were evaluated ($n=3, *p<0.05$ vs. siCtrCtr; $\#p<0.05$ vs. siCtrDex). Representative figures are shown **(D)**.

formation in HMEC-1 (Figure 16B/C). HMEC-1 silenced for either p22phox, NOX2 and NOX4 showed a decrease in *in vitro* tube formation in response to dexamethasone treatment (Figure 16B/C).

7.2.4.Dexamethasone induces systemic and pulmonary hypertension

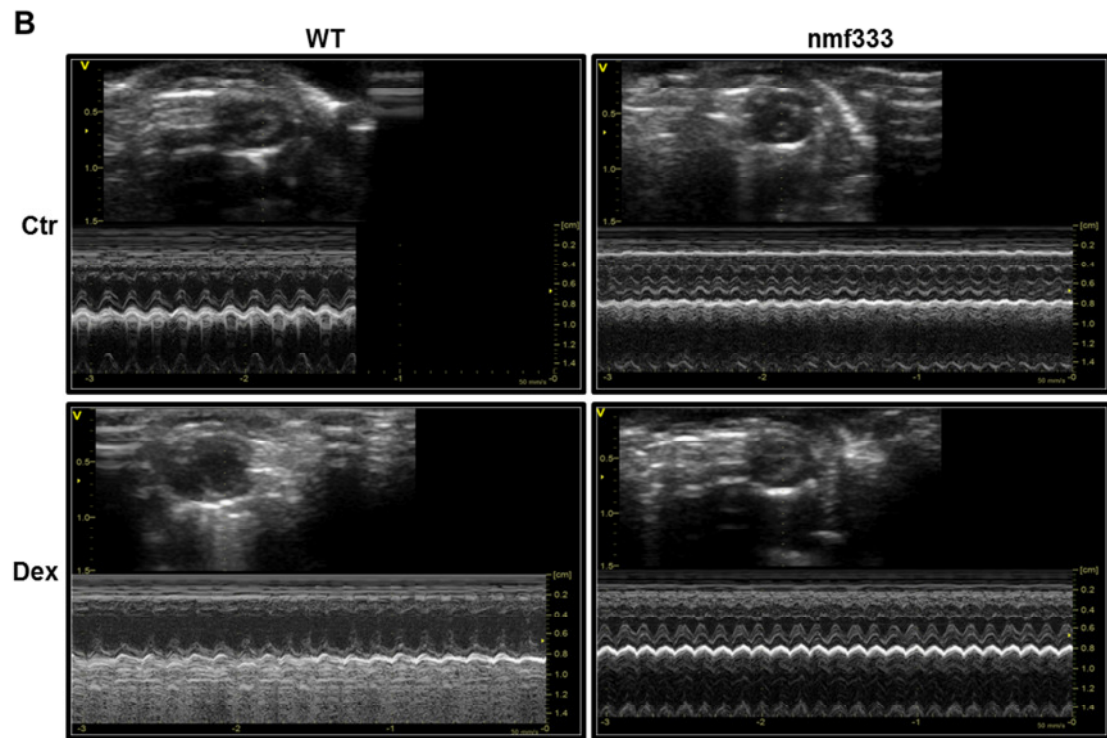
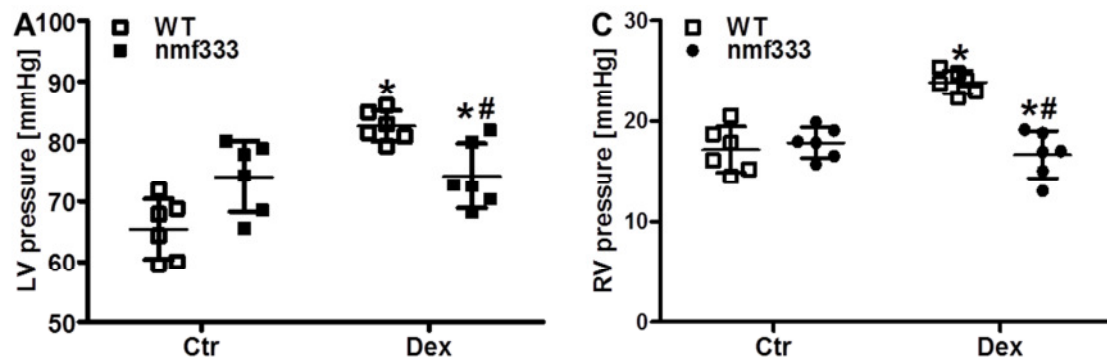
To evaluate whether NADPH oxidases are involved in the systemic cardiovascular effects of dexamethasone treatment mice carrying a point mutation in the p22phox gene thus leading to a loss of p22phox protein (nmf333) and wild type mice were orally supplemented with dexamethasone (Dex, 0.3 mg/kg/day) in the drinking water for 12 weeks. As increased ROS in the vasculature and dexamethasone have been associated with hypertension (308-311), left ventricular pressure (LVP) was hemodynamically evaluated using a transthoracic approach (Figure 17A).

In fact, dexamethasone treatment significantly increased left ventricular pressure in wild type mice, but not in nmf333 mice lacking p22phox (Figure 17A).

Echocardiography showed, that dexamethasone-treated wild type mice, but not nmf333 mice, had decreased left ventricular wall thickness (LVPWd) and increased left-ventricular end-diastolic diameter (LVEDD) and left-ventricular end-systolic diameter (LVESD) as well as decreased left-ventricular fractional shortening (FS), all of which are indicative of left ventricular dysfunction (Figure 17A/B).

Interestingly, in addition to the effects on the left ventricle dexamethasone treatment also resulted in increased right ventricular pressure in wild type mice, but not in nmf333 mice (Figure 17C).

In order to evaluate ventricular size masses, the ratios between right and left ventricular mass and the body mass were determined (Figure 18A/B). Similar to the situation with functional cardiac parameters, dexamethasone treatment increased both relative left and right ventricular mass as compared to body mass in wild type mice (Figure 18A/B). nmf333 mice showed increased ratios between right and left ventricular mass and the body mass, respectively, in response to dexamethasone treatment; however, significantly lower than those of dexamethasone-treated wild type mice (Figure 18A/B).



	Ctr		p*	Dex		p**	p#
	WT	nmf333		WT	nmf333		
n	3	4		4	3		
RR (ms)	140.5±31.5	145.9±40.3	n.s.	158.9±31.7	141.3±12.0	n.s.	n.s.
HR	422.9±94.1	436.6±118.1	n.s.	389.0±76.7	428.2±40.4	n.s.	n.s.
IVSd (cm)	0.076±0.01	0.065±0.006	n.s.	0.06±0.01	0.08±0.01	n.s.	n.s.
LVPWd (cm)	0.09±0.02	0.07±0.005	n.s.	0.06±0.01	0.09±0.005	0.0455	0.0054
LVEDD (cm)	0.20±0.04	0.27±0.04	n.s.	0.41±0.04	0.3±0.01	0.0081	0.0061
LVESD (cm)	0.12±0.01	0.15±0.03	n.s.	0.26±0.03	0.13±0.02	0.0006	0.0013
FS (%)	56.8±6.1	46.6±7.1	n.s.	36.3±4.3	58.3±6.7	0.0033	0.0031

Figure 17. Dexamethasone-induced hypertension and left ventricular remodeling is p22phox-dependent. (A-C) CD57BL6j (WT) and mice deficient of p22phox due to a point mutation (nmf333) were orally supplemented in the drinking water with Dex (0.3 mg/kg/day) for 12 weeks. Control litter-mates drunk normal water (Ctr). Left ventricular (LV) pressure (A) and right ventricular (RV) pressure (RVP) (B) were determined hemodynamically ($n=5-8$; * $p < 0.05$ vs. WT Ctr; # $p < 0.05$ vs. WT Dex). (C) Echocardiography was performed in M-mode. Representative echocardiography figures are shown. Echocardiography was performed in M-mode (* $p < 0.05$ WT Ctr vs. nmf333 Ctr; ** $p < 0.05$ WT Ctr vs. WT Dex; # $p < 0.05$ WT Dex vs. nmf333 Dex); n.s. - not significant; n – number of mice; RR – interval duration; HR – heart rate; IVSd - intraventricular septal width (diastole); LVPWd - left ventricular posterior wall (diastole); LVEDD - left ventricular end diastolic diameter; LVESD - left ventricular end systolic diameter; FS - fractional shortening.

To assess whether cardiomyocyte hypertrophy might be responsible for ventricular enlargement in response to dexamethasone treatment FFPE heart sections from both left and right ventricle were stained with WGA to determine cardiomyocyte diameters. Indeed, cardiomyocyte diameters were increased both in the left and right ventricle in dexamethasone treated wild type mice (Figure 18C/D).

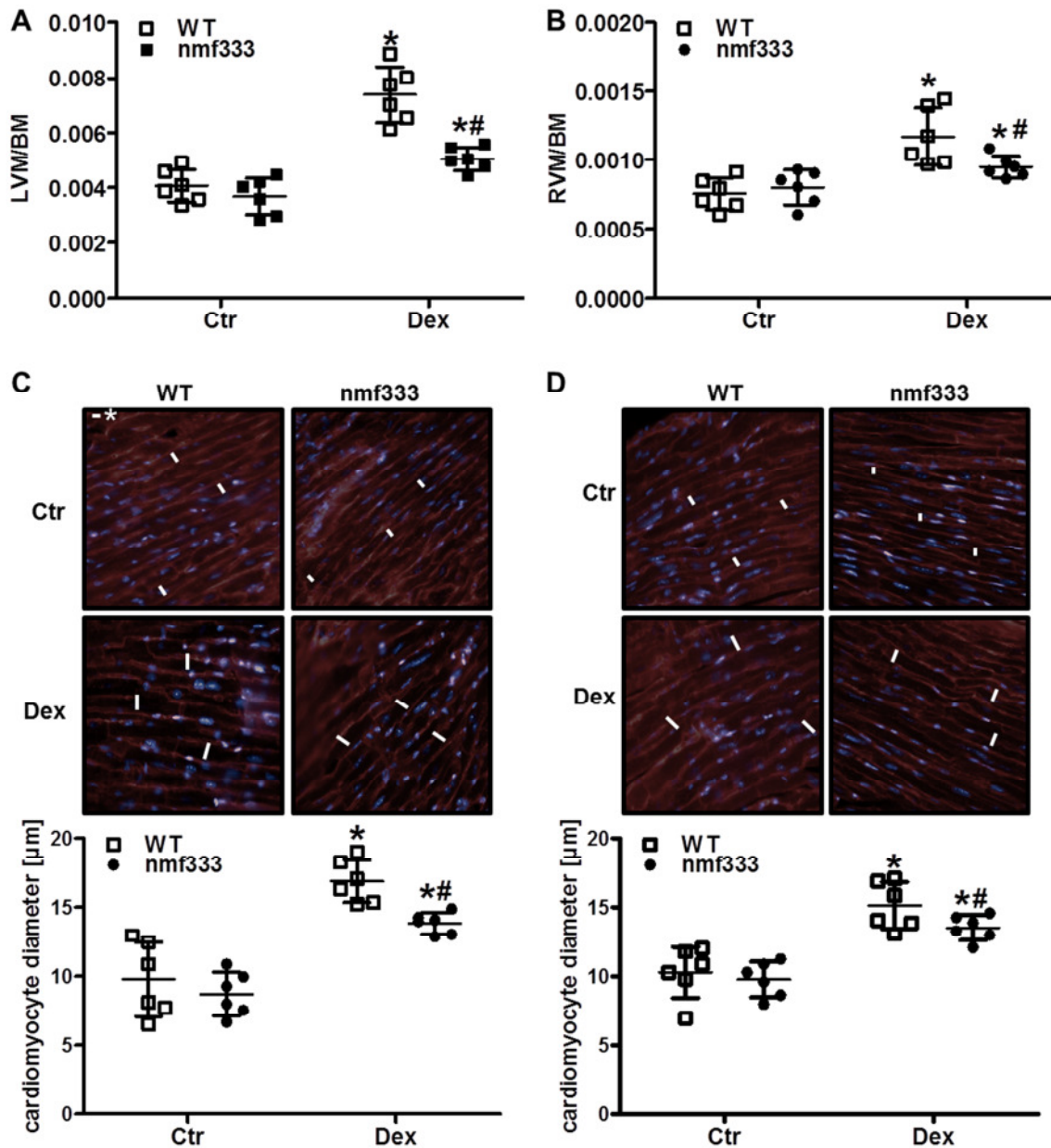


Figure 18. Dexamethasone-induced ventricular remodeling is p22phox-dependent. (A-D) CD57BL6j (WT) and nmf333 mice were orally supplemented in the drinking water with dexamethasone (Dex, 0.3 mg/kg/day) for 12 weeks. Control litter-mates drunk normal water (Ctr). (A-B) Body mass (BM), left ventricle and septum mass (LVM), and right ventricle mass (RVM) were evaluated and LVM/BM (A) and RVM/BM (B) ratios were determined ($n=3-5$; * $p < 0.05$, vs. WT Ctr; # $p < 0.05$ vs. WT Dex). (C-D) FFPE sections were stained with wheat germ agglutinin and average left (C) and right (D) ventricle cardiomyocyte diameters were determined ($n=3-5$; * $p < 0.05$, vs. WT Ctr; # $p < 0.05$ vs. WT Dex).

Similar to the situation with increased ventricular masses, *nmf333* mice showed increased cardiomyocyte diameters following dexamethasone treatment; yet, significantly lower than those of dexamethasone-treated control litter-mates (Figure 18C/D). As increased right ventricular pressure and right ventricular hypertrophy are signs of pulmonary hypertension, it was evaluated whether dexamethasone treatment would affect pulmonary vascular remodeling, another hallmark of pulmonary hypertension. Immunohistochemistry with an antibody against smooth muscle actin revealed an increased number of small muscularized vessels in lungs indicative of pulmonary vascular remodeling (Figure 19). However, similar to the situation with the cardiac remodeling, vascular remodeling was reduced in lungs derived from dexamethasone-treated *nmf333* mice (Figure 19).

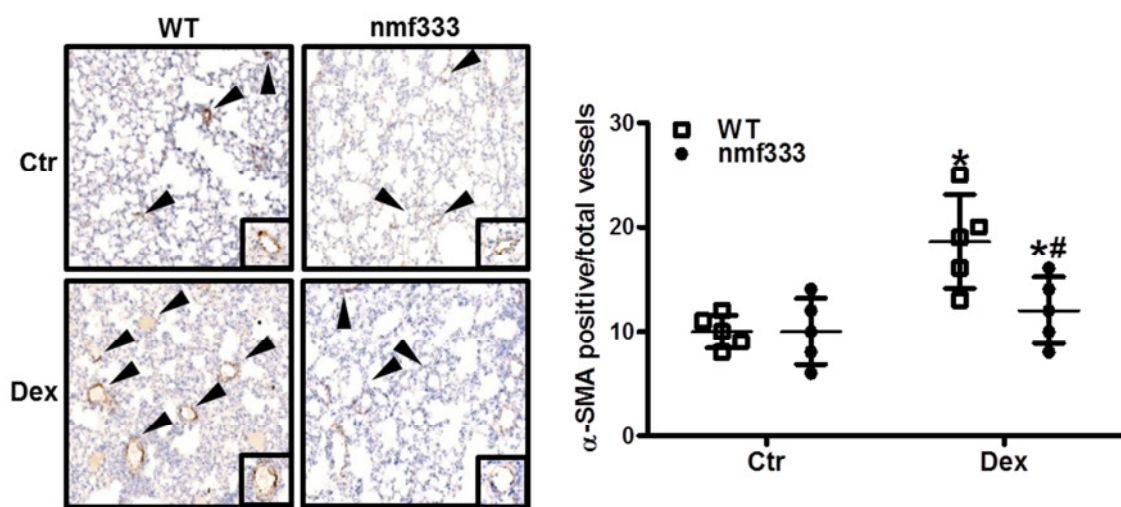


Figure 19. Dexamethasone-induced pulmonary vascular remodeling is p22phox-dependent. CD57BL6j (WT) and *nmf333* mice were orally supplemented in the drinking water with dexamethasone (Dex, 0.3 mg/kg/day) for 12 weeks. Control litter-mates drunk normal water (Ctr). FFPE lung sections were stained with an antibody against α -SMA, and α -SMA-positive small- and medium-sized arterioles ($<80\ \mu\text{m}$) were counted and related to the total number of arterioles of the same diameter ($n = 3-5$; $*p < 0.05$, vs. WT Ctr; $^{\#}p < 0.05$ vs. WT Dex).

7.2.5. Dexamethasone induces hypoxia inducible factor 1

To assess possible mediators downstream of NADPH oxidases which might contribute to the cardiovascular dexamethasone effects the involvement of the transcription factor hypoxia inducible factor 1 (HIF1) was evaluated. HIF1 has been identified to be involved in the control of angiogenesis and vascular proliferation and to contribute to the development of hypoxia-induced pulmonary hypertension (312, 313).

In fact, dexamethasone increased HIF activity in HMEC-1 as was determined by a reporter gene assay (Figure 20A). Dexamethasone treatment further increased the levels of HIF1 α , the inducible subunit of HIF1, in a time-dependent manner in HMEC-1 (Figure 20B) and

PASMC (Figure 20C). Similarly, dexamethasone also increased protein levels of the HIF-target gene plasminogen activator inhibitor 1 (PAI1) in HMEC-1 (Figure 20B) and PASMC (Figure 20C). HIF1 α protein levels were also increased in lungs from wild type mice orally supplemented with dexamethasone (0.3 mg/kg/day) for 12 weeks (Figure 20D).

However, dexamethasone had no effect on HIF1 promoter activity (Figure 20E), suggesting a post-transcriptional pathway involved in HIF1 α protein upregulation.

As dexamethasone increased ROS production via the glucocorticoid receptor and NADPH oxidases, it was tested whether this pathway was also involved in upregulation of HIF1 α by dexamethasone. Indeed, pretreatment with RU486 diminished induction of HIF1 α by

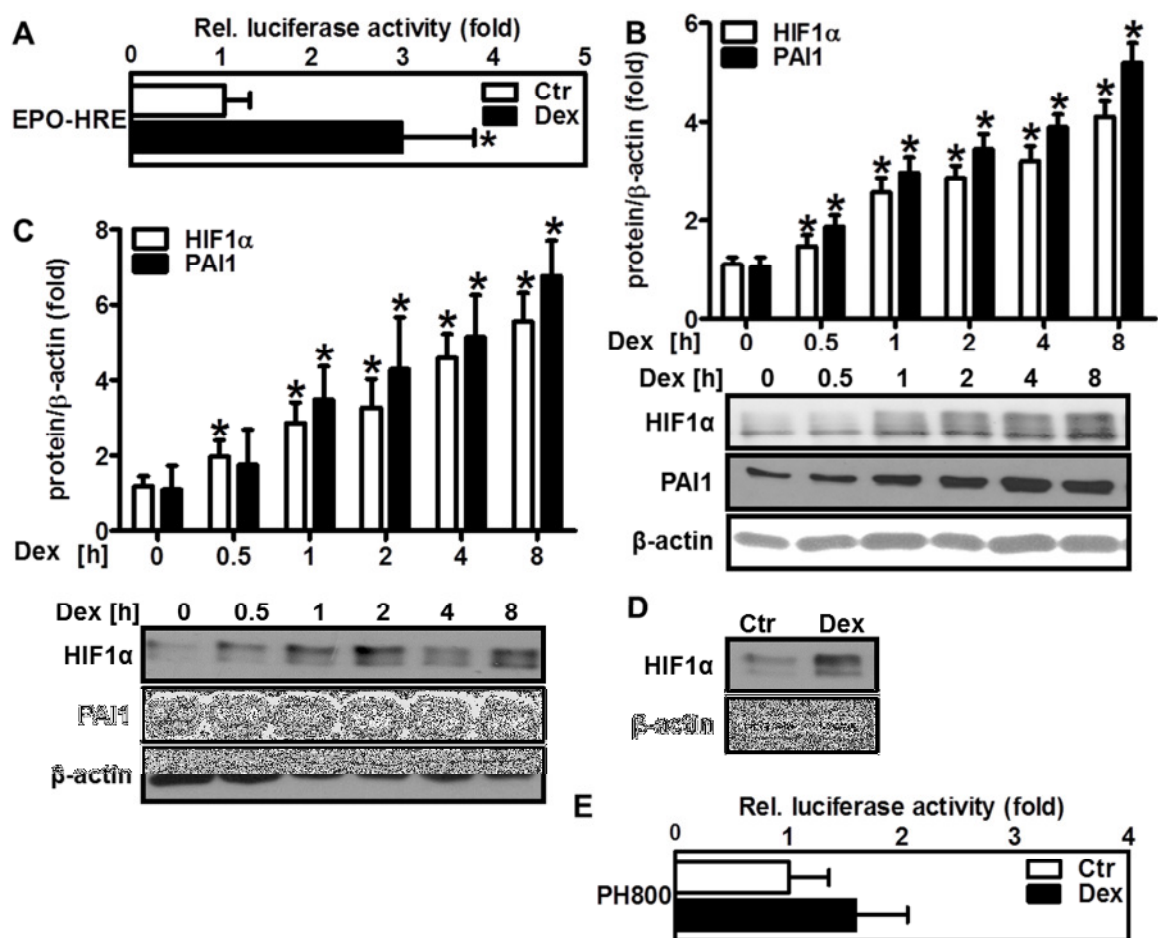


Figure 20. Dexamethasone induces HIF1 α protein levels. (A) HMEC-1 were transfected with a luciferase construct either driven by three hypoxia-response elements (HRE) from the erythropoietin gene (EPO-HRE), exposed to Dex (10 nM) for 8 h, and luciferase assay was performed. HMEC-1 (B) and PASMC (C) were exposed to Dex (10 nM) as indicated on the graph and Western blot analyses were performed using antibodies against HIF1 α and plasminogen activator inhibitor 1 (PAI1). β -actin served as a loading control (n=3, * p < 0.05 vs. Ctr) (D) CD57BL6j mice were orally supplemented in the drinking water with Dex (0.3 mg/kg/day) for 12 weeks. Control litter-mates drunk normal water. Western blot analyses were performed in lung tissue lysates using antibodies against HIF1 α and p22phox. β -actin served as a loading control. (E) HMEC-1 were transfected with a luciferase construct containing HIF1 α promoter (PH800), exposed to Dex (10 nM) for 8 h, and luciferase assay was performed (n=3, * p < 0.05 vs. Ctr).

dexamethasone (Figure 21A) indicating an involvement of the glucocorticoid receptor.

Moreover, HMEC-1 were treated with the NADPH oxidase inhibitor GKT-137831 (Figure 21A). In fact, HIF1 α protein levels were diminished by this inhibitor in dexamethasone-treated HMEC-1.

Furthermore, in order to test whether NADPH oxidases are involved in the control of HIF1 α by dexamethasone, HMEC-1 were depleted of p22phox and NOX4. Compared to control cells, HIF1 α protein levels were significantly decreased in p22phox- and NOX4-deficient HMEC-1 stimulated with dexamethasone (Figure 21B/C).

In line, HIF1 α protein levels were decreased in lungs of dexamethasone-treated nmf333 mice compared to wildtype mice thus proving also *in vivo* the importance of NADPH oxidases for the regulation of HIF1 α protein by dexamethasone (Figure 21D).

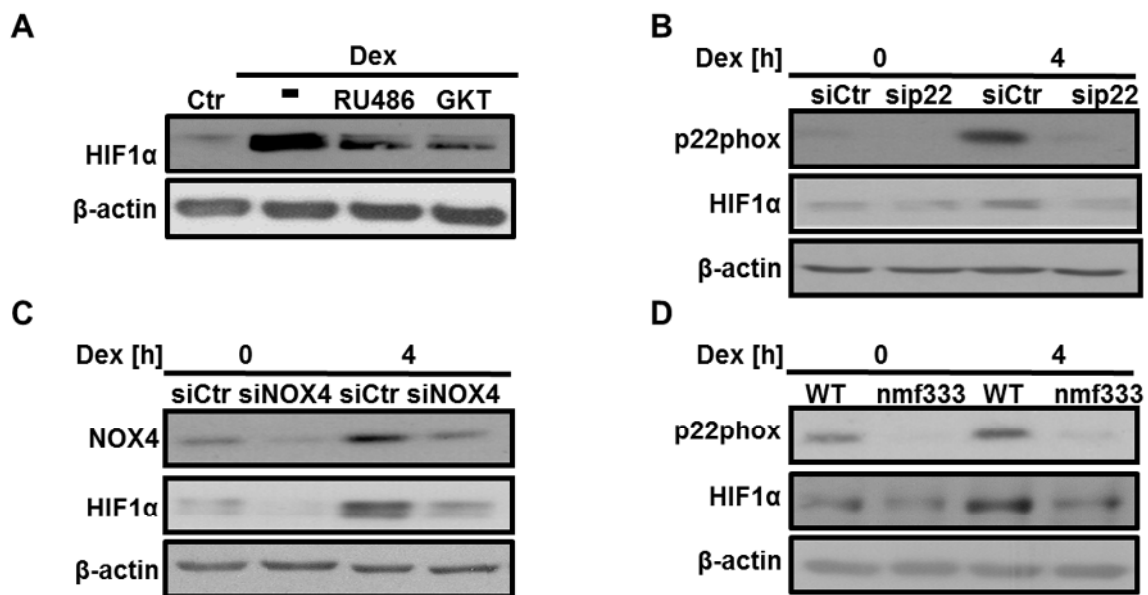


Figure 21. Dexamethasone stabilization of HIF1 α protein levels is dependent on ROS derived from NADPH oxidases. (A) HMEC-1 were treated or not (Ctr) with either RU486 (500 μ M), or GKT-137831 (50 μ M) for 1 h, subsequently exposed to dexamethasone (Dex, 10 nM) for 4 h and Western blot analyses were performed using an antibody against HIF1 α . β -actin served as a loading control ($n=3$, representative blots are shown). (B-C) HMEC-1 were either transfected with siRNA against p22phox or siCtr (B) or with siRNA against NOX4 or siCtr (C) and exposed to Dex (10 nM) for 4 h and Western blot analyses were performed using antibodies against p22phox and NOX4 respectively. β -actin served as a loading control ($n=3$, representative blots are shown). (D) CD57BL6j (WT) and nmf333 mice were orally supplemented in the drinking water with Dex (0.3 mg/kg/day) for 12 weeks. Control litter-mates drunk normal water. Western blot analyses were performed in lung tissue lysates using antibodies against HIF1 α and p22phox. β -actin served as a loading control ($n=3$, representative blots are shown).

7.2.6. HIF1 α is involved in dexamethasone-induced pulmonary vascular remodeling

As NADPH oxidases promoted the angiogenic response towards dexamethasone, the involvement of HIF1 α in this response was tested using HMEC-1 depleted of HIF1 α by siRNA (Figure 22A).

In fact, *in vitro* tube formation induced by dexamethasone was decreased in HMEC-1 depleted of HIF1 α (Figure 22A/B). In addition, depletion of HIF1 α also decreased dexamethasone-induced proliferation of HMEC-1 (Figure 22C/D).

Furthermore, compared to control mice, pulmonary vascular remodeling was decreased in mice deficient of HIF1 α in endothelial cells (Tie2CreHIF1 α) or smooth muscle cells (Sm22CreHIF1 α) treated with dexamethasone for 12 weeks similar to the situation with nmf333 mice (Figure 23).

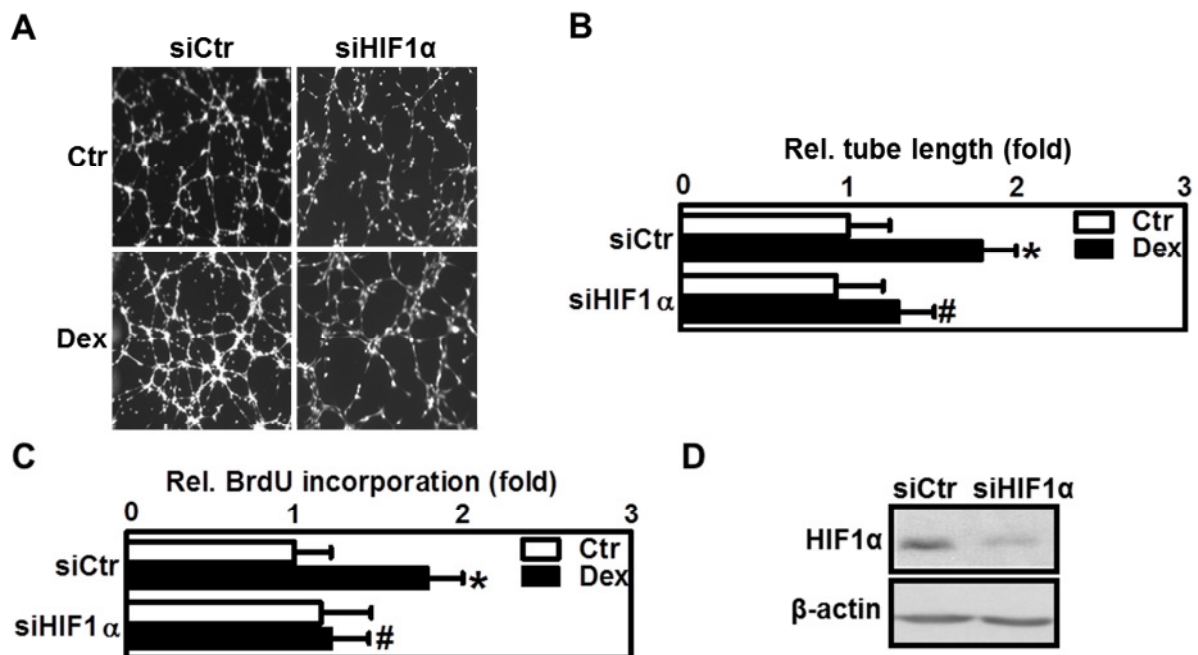


Figure 22. HIF1 α mediates dexamethasone-induced proliferative responses in endothelial cells. HMEC-1 were transfected with siRNA against HIF1 α (siHIF1 α) or scrambled RNA (siCtrl). Cells were seeded either (**A/B**) on matrigel for an *in vitro* tube formation assay or (**C**) for BrdU incorporation assay, subsequently exposed to dexamethasone (Dex, 10 nM) for 6 h or remained untreated (Ctr). (**A/B**) For quantification of tube formation assays, total tube lengths were evaluated ($n=3$, * $p<0.05$ vs. siCtrlCtr; # $p<0.05$ vs. siCtrlDex). Representative figures are shown. (**C**) for BrdU incorporation assay (**D**) Western blot analyses on cellular lysates were performed for the expression levels of HIF1 α . β -actin served as a loading control.

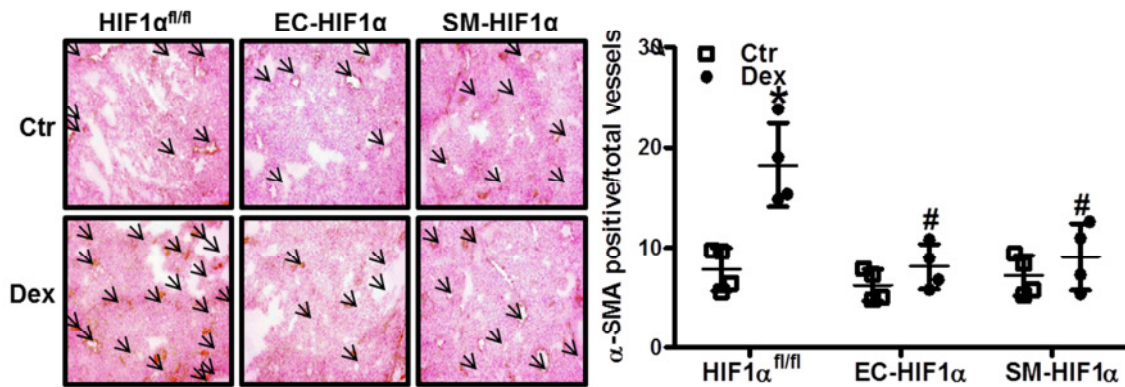


Figure 23. Dexamethasone-induced pulmonary vascular remodeling is HIF1α-dependent. Tie2CreHIF1α (EC-HIF1α), Sm2CreHIF1α (SM-HIF1α) or HIF1α^{fl/fl} mice were orally supplemented in the drinking water with Dex (0.3 mg/kg/day) for 12 weeks. Control litter-mates drunk normal water. FFPE lung tissue sections were stained with an α-SMA antibody to visualize vascular remodeling. α-SMA-positive small- and medium-sized arterioles (<80 μm) were counted and related to the total number of arterioles of the same diameter (n=4; *p<0.05, vs. HIF1α^{fl/fl} Ctr; #p<0.05 vs. HIF1α^{fl/fl} Dex).

7.3.β3-endonexin as a novel negative regulator of hypoxia inducible factor 1

The family of integrins regulate key processes in the vasculature such as proliferation and angiogenesis by mediating extracellular signals into cells (outside in signaling) as well as by directing intracellular signals to the cell surface (inside out signaling) (314, 315). These functions are conducted by several interacting molecules which can shuttle between cell membrane and intracellular organelles. The β3-integrin binding protein β3-endonexin has been suggested to regulate the function of β3-integrin and to contribute to atherosclerosis (241). The data of the following study investigating the role of β3-endonexin in the context of hypoxia have been previously published (228). Permission to use the figures and the text of the paper was obtained from *Antioxidants&Redox Signaling* (Appendix, p.143).

7.3.1.β3-endonexin expression and localization under hypoxia

To evaluate the effects of hypoxia on the expression patterns of the β3-integrin binding protein β3-endonexin in endothelial cells, HMEC-1 were exposed to hypoxia (1% oxygen) for increasing time periods and endogenous levels of β3-endonexin were subsequently identified by Western blot analysis using an antibody that detects the short (EN-S, 12.6 kDa) as well as the long (EN-L, 19.2 kDa) isoforms of β3-endonexin (228). Western blot analyses revealed that protein levels of neither of the β3-endonexin splice variants were significantly affected within 24 h of hypoxic exposure, although HIF1α protein levels were upregulated under hypoxia peaking at 4 to 8 h of exposure (Figure 24 A/B) (228). In line, β3-endonexin mRNA levels were not affected by short- and intermediate-term hypoxia, while prolonged hypoxia over 16 h significantly increased β3-endonexin mRNA levels (Figure 24C) (228). β3-endonexin mRNA levels were also increased in lungs from mice exposed for 2 weeks to hypoxia (10% oxygen) (Figure 24D) (228). In contrast, HIF1α mRNA transcripts rapidly but transiently increased in response to hypoxia followed by a decline to levels below the initial normoxic values (Figure 24C) (228).

Indirect immunofluorescent labeling in HMEC-1 showed that β3-endonexin was primarily localized in the cytoplasm and plasma membrane in normoxia, while in hypoxia, β3-endonexin accumulated predominantly in the nucleus (Figure 25A) (228). In line, Western blot analysis showed that β3-endonexin was primarily present in the cytoplasmic fraction under normoxic conditions, while it accumulated in the nuclear fraction under hypoxia (Figure 25B) indicating that β3-endonexin translocates to the nucleus on exposure to hypoxia (228).

β 3-endonexin has been identified as a β 3-integrin binding protein (235), suggesting that the distribution of β 3-endonexin might be in relation to integrin-linked signaling. Hence, for purpose of evaluating the role of integrin signaling in the distribution of β 3-endonexin under hypoxia, HMEC-1 were seeded on cover slips coated either with collagen or fibronectin and exposed to hypoxia, and β 3-endonexin localization was assessed by immunofluorescence (Figure 25C). However, in both cases, β 3-endonexin accumulated in the nucleus similar to the situation without coating, indicating that this response was independent of integrin signaling (Figure 25C) (228).

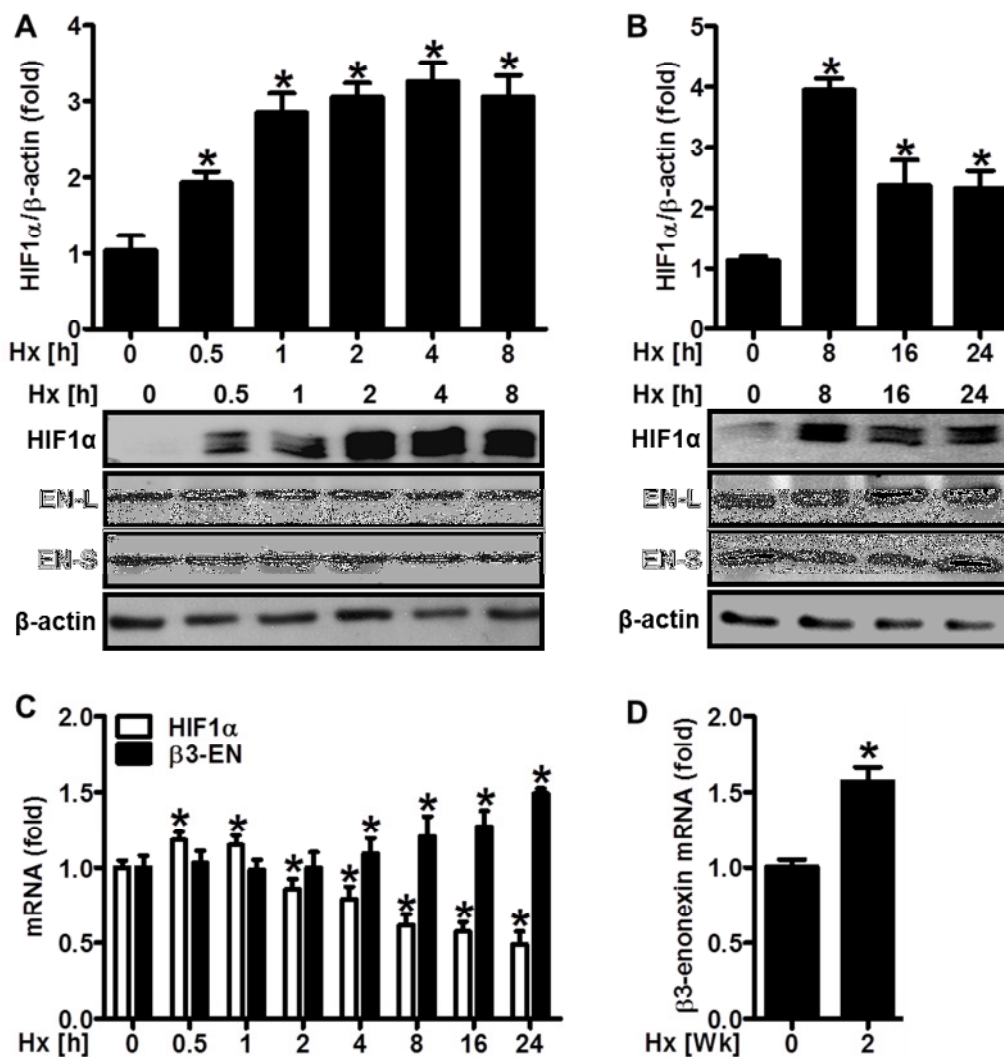


Figure 24. Hypoxic regulation of β 3-endonexin and HIF1 α expression. (A–C) HMEC-1 were exposed to hypoxia (Hx, 1% oxygen) or normoxic conditions (Hx 0 h) for increasing time points. (A/B) Western blot analyses were performed with antibodies against HIF1 α and β 3-endonexin. β -actin staining served as loading control ($n=3$, $*p<0.05$ vs. Hx 0 h). (C) RT-qPCR was performed with primers amplifying human β 3-endonexin and HIF1 α . 18S rRNA served as a control ($n=3$, $*p<0.05$ vs. 0 h). (D) Mice were exposed to chronic hypoxia (Hx, 10% oxygen) for 2 weeks. Control litter-mates breathed room air. RT-qPCR was performed in samples from murine lung tissue with primers amplifying murine β 3-endonexin. 18S rRNA served as a control ($n=3$, $*p<0.05$ vs. Hx 0 Wk). Figure adapted from (228).

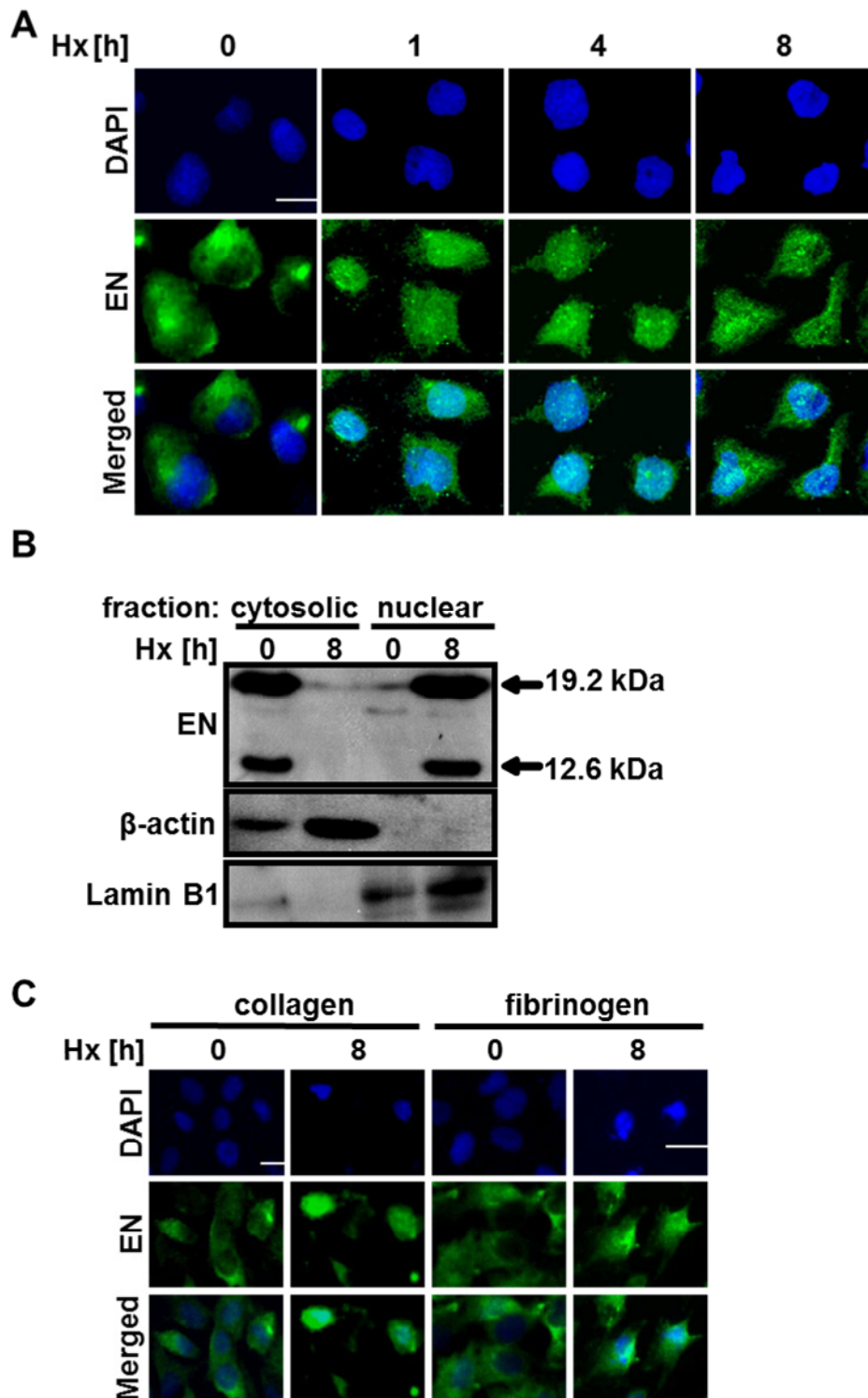


Figure 25. β 3-endonexin translocates to the nucleus under hypoxia. (A) HMEC-1 were seeded on uncoated coverslips and exposed to hypoxia (Hx) or normoxia (Hx 0 h) for increasing time periods. Cells were fixed, and immunostaining was performed with an antibody against β 3-endonexin and a secondary antibody conjugated with Alexa fluor 488. Nuclei were visualized by 4', 6-diamidino-2-phenylindole (DAPI) staining. Scale bars represent 10 μ m. (B) HMEC-1 were exposed to hypoxia (Hx) for 8 h or remained under normoxia (Hx 0 h). Western blot analyses were performed on nuclear and cytosolic fractions using antibodies against HIF1 α and β 3-endonexin isoforms. β -actin and lamin B served as cytosolic and nuclear fraction loading control, respectively. (C) HMEC-1 were seeded on coverslips coated with collagen or fibronectin and immunostaining for β 3-endonexin was performed as above. Figure adapted from (228).

7.3.2. β 3-endonexin decreases HIF activity and HIF1 α expression under hypoxia

In order to evaluate the possibility that β 3-endonexin may interfere with the HIF system under hypoxia, it was first assessed whether β 3-endonexin affects HIF transactivation. For this purpose, HMEC-1 were co-transfected with a EPO-HRE luciferase construct and expression vectors coding for either β 3-endonexin short or long isoforms (Figure 26A) (228). Indeed, hypoxia-induced HIF activity was completely abolished in cells overexpressing either of the β 3-endonexin isoforms compared to control (Figure 26A) (228).

Next, protein levels of HIF1 α under hypoxia were assessed in the context of β 3-endonexin abundance. Overexpression of either of the β 3-endonexin isoforms decreased hypoxic HIF1 α protein levels (Figure 26B) (228). Oppositely, in HMEC-1 silenced for β 3-endonexin by RNAi, hypoxic HIF activity was enhanced (Figure 26A) (228). This effect was accompanied by a further increase in hypoxic HIF1 α protein levels (Figure 26C) (228).

Regulation of HIF1 α by β 3-endonexin was specific to HIF1 α since the induction of HIF2 α protein levels by hypoxia was not affected in β 3-endonexin-depleted endothelial cells (Figure 26C) (228).

Interestingly, while silencing of β 3-endonexin decreased its mRNA levels by more than 75% (Figure 26D), it enhanced hypoxic HIF1 α mRNA levels (Figure 26C) (228). To further confirm this observation, the effects of β 3-endonexin on well-defined HIF1 α target genes, such as glyceraldehyde phosphate dehydrogenase (GAPDH) and vascular endothelial growth factor-A (VEGF-A) were evaluated (Figure 27A/B) (228). For that purpose, HMEC-1 were exposed to hypoxia for increasing time periods and mRNA levels of VEGF-A and GAPDH were determined by RT-qPCR. Indeed, both VEGF-A and GAPDH mRNA were regulated in a similar fashion as HIF1 α ; i.e. the silencing of β 3-endonexin further enhanced hypoxic induction of VEGF-A and GAPDH (228).

In addition, overexpression of either of the β 3-endonexin isoforms prevented hypoxic induction of PAI1 promoter activity (Figure 27C) (228). Silencing of β 3-endonexin enhanced hypoxic induction of PAI1 promoter activity; while this effect was abrogated when the HIF binding site in the PAI1 promoter was mutated, indicating that β 3-endonexin reduces hypoxic PAI1 expression *via* an HIF-dependent mechanism (228).

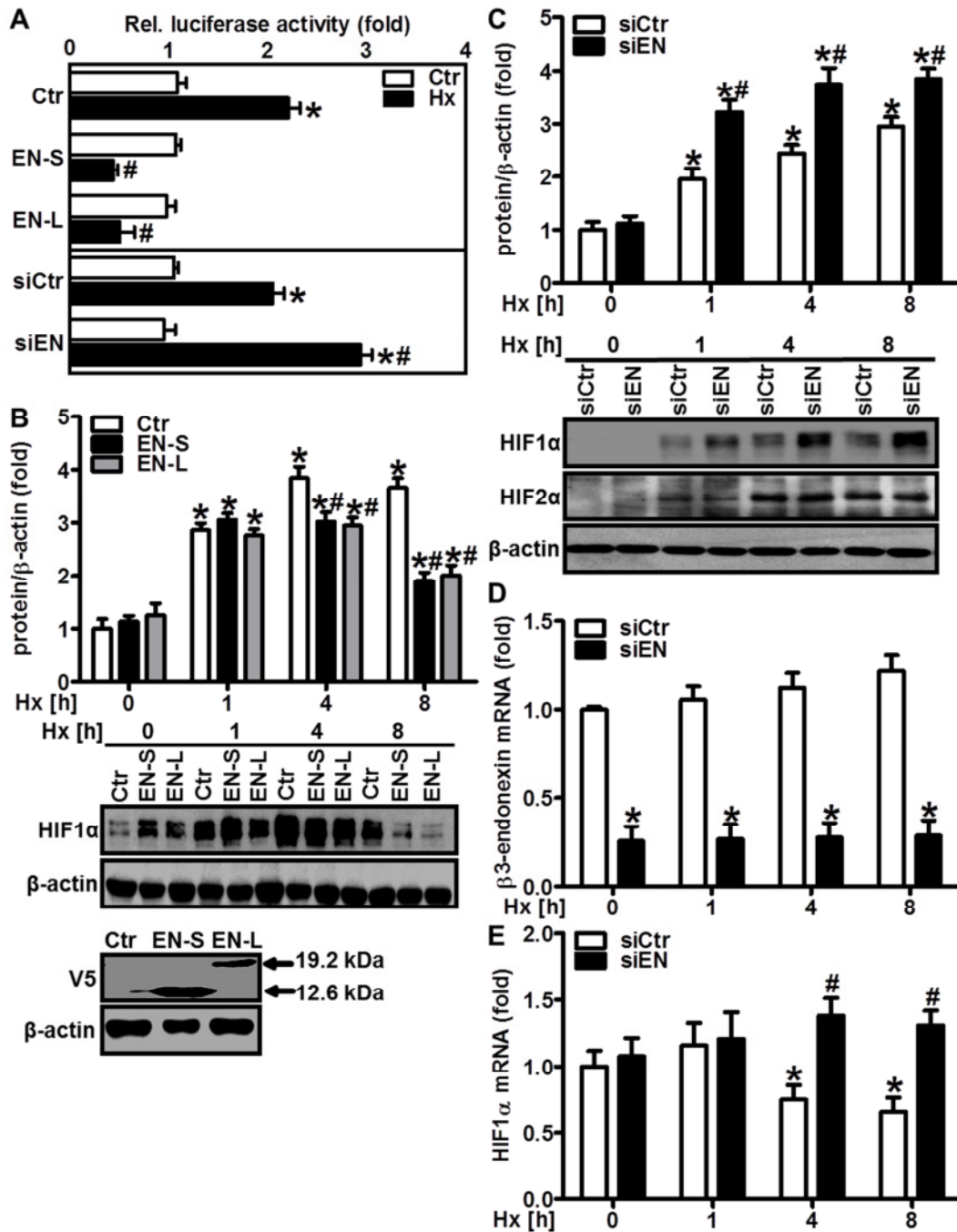


Figure 26. β 3-endonexin decreases hypoxic HIF activity and HIF1 α protein levels. (A) HMEC-1 were co-transfected with EPO-HRE luciferase construct and expression vectors coding for either β 3-endonexin short (EN-S) or long (EN-L) isoforms or with control vector (Ctr) or with RNAi against β 3-endonexin (siEN) or with scrambled RNA (siCtr), exposed to hypoxia (Hx, 1% oxygen) for 8 h, and luciferase assays were performed ($n=3$, $*p<0.05$ vs. CtrCtr or siCtrCtr; $\#p<0.05$ vs. siCtrHx). (B) HMEC-1 were transfected with either EN-S or EN-L or with control expression vector (Ctr) and exposed to hypoxia. Western blot analyses were performed with an antibody against HIF1 α . β -actin served as a loading control ($n=3$, $*p<0.05$ vs. Ctr 0 h; $\#p<0.05$ vs. CtrHx 1, 4 or 8 h). Expression of EN-S or EN-L constructs was validated by Western blotting using a V5 antibody. β -actin served as a loading control. (C-E) HMEC-1 were transfected with siEN or with scrambled RNA (siCtr) and exposed to hypoxia. (C) Western blot analyses were performed with antibodies against HIF1 α and HIF2 α . β -actin levels served as loading control ($n=3$, $*p<0.05$ vs. siCtr 0 h; $\#p<0.05$ vs. siCtrHx 1, 4, or 8 h). (D-E) RT-qPCR analyses were performed with primers amplifying either human β 3-endonexin (D) or HIF1 α (E). 18S rRNA served as a control ($n=3$, $*p<0.05$ vs. siCtr 0 h; $\#p<0.05$ vs. siCtr 1, 4, or 8 h). Figure adapted from (228).

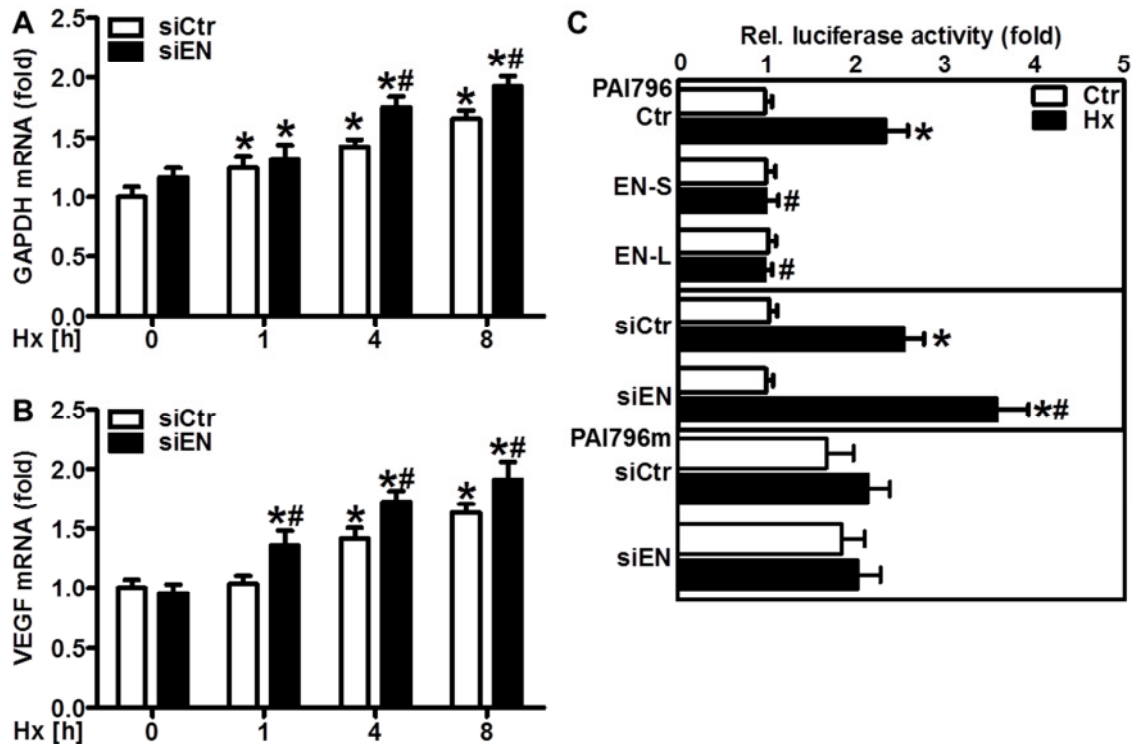


Figure 27. β 3-endonexin regulates HIF1 α -target genes. (A–B) HMEC-1 were transfected with siEN or with scrambled RNA (siCtr) and exposed to hypoxia as indicated on the graph. RT-qPCR analyses were performed with primers amplifying either human glyceraldehyde-3-phosphate dehydrogenase (GAPDH) **(A)** or vascular endothelial growth factor-A (VEGF) **(B)**. 18S rRNA served as a control ($n=3$, $*p<0.05$ vs. siCtrHx 0 h; $\#p<0.05$ vs. siCtrHx 1, 4, or 8 h). **(C)** HMEC-1 were co-transfected with a luciferase construct driven by the wild-type plasminogen activator inhibitor-1 (PAI1) promoter (PAI796) or the PAI1 promoter mutated at the HRE (PAI796m) and expression vectors coding for either β 3-endonexin short (EN-S) or long (EN-L) isoforms or with control vector (Ctr) or with siRNA against β 3-endonexin (siEN) or scrambled RNA (siCtr). Cells were exposed to hypoxia (Hx) for 8 h or remained under normoxia (Ctr), and luciferase assays were performed ($n=3$, $*p<0.05$ vs. siCtrCtr; $\#p<0.05$ vs. siCtrHx). Figure adapted from (228).

7.3.3. Depletion of β 3-endonexin induces NF κ B-driven HIF1 α transcription

HIF1 α was shown to be regulated not only at the level of protein stability but also at the level of transcription as a direct target gene of NF κ B (12, 37, 38). Hence, in this study the possibility that β 3-endonexin might be involved in the transcriptional regulation of HIF1 α by NF κ B was evaluated.

In fact, hypoxia increased NF κ B-dependent luciferase activity in HMEC-1, and this response was prevented by the overexpression of either β 3-endonexin isoform (Figure 28A) (228). In contrast, the depletion of β 3-endonexin further enhanced the hypoxic NF κ B response (Figure 28A), indicating that β 3-endonexin diminishes hypoxic NF κ B activation.

Overexpression of the NF κ B subunits p50 and p65 increased HIF1 α mRNA levels under hypoxia (Figure 28B) similar to the situation with the depletion of β 3-endonexin (Figure 28A), while it did not affect β 3-endonexin mRNA levels (Figure 28C) (228).

Moreover, co-expression of dominant-negative I κ B α (I κ Bdn) that inhibits NF κ B activation, prevented the up-regulation of HIF1 α mRNA in β 3-endonexin-depleted cells under hypoxia

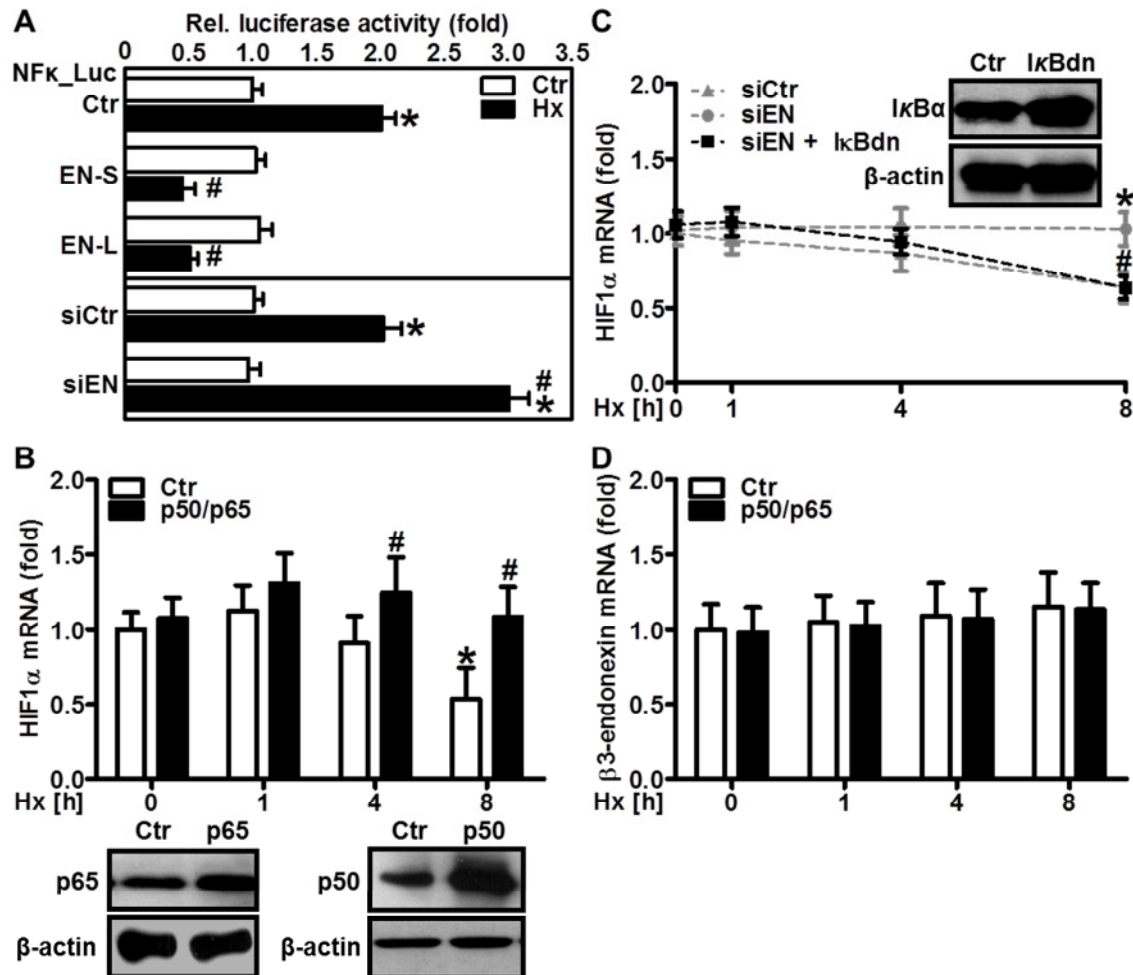


Figure 28. β 3-endonexin modulates NF κ B activity. (A) HMEC-1 were co-transfected with a luciferase construct driven by five NF κ B binding-sites (NF κ B-Luc) and expression vectors coding for either EN-S or EN-L or with control vector (Ctr) or with siEN or siCtr. HMEC-1 were exposed to hypoxia (Hx, 1% oxygen) for 8 h or remained at normoxia (Ctr), and luciferase assays were performed. ($n=3$, $*p<0.05$ vs. CtrCtr or siCtrCtr; $\#p<0.05$ vs. CtrHx or siCtrHx). (B/C) HMEC-1 were co-transfected with expression vectors encoding for the NF κ B subunits p50 and p65 or with control vector (Ctr) and exposed to hypoxia as indicated on the graph or cultivated under normoxia (Hx 0 h). RT-qPCR was performed using gene-specific primers for either HIF1 α (B) or β 3-endonexin (C). 18S rRNA served as a control. Western blot analyses were performed using antibodies against p50 and p65. β -actin levels served as a loading control ($n=3$, $*p<0.05$ vs. CtrHx 0 h; $\#p<0.05$ vs. CtrHx 4 or 8 h or vs. siENHx). (D) HMEC-1 were co-transfected with siEN or siCtr and with an expression vector coding for dominant-negative I κ B α (I κ Bdn) and exposed to hypoxia as indicated on the graph or normoxia (Hx 0 h). RT-qPCR was performed using gene-specific primers for HIF1 α . 18S rRNA served as a control. Western blot analyses were performed using antibody against I κ B α . β -actin served as a loading control ($n=3$, $*p<0.05$ vs. siCtrHx 0 h; $\#p<0.05$ vs. siCtrHx 1, 4, or 8 h). Figure adapted from (228).

(Figure 28D), suggesting that β 3-endonexin might act on HIF1 α mRNA expression *via* NF κ B (228). In line, depletion of β 3-endonexin further enhanced the hypoxic induction of HIF1 α promoter activity (Figure 29A), while the overexpression of β 3-endonexin isoforms had opposite effects. Interestingly, depletion of β 3-endonexin had no effect on luciferase activity driven by the HIF1 α promoter mutated at the NF κ B-binding site at -197/188 bp (37, 38, 228); further

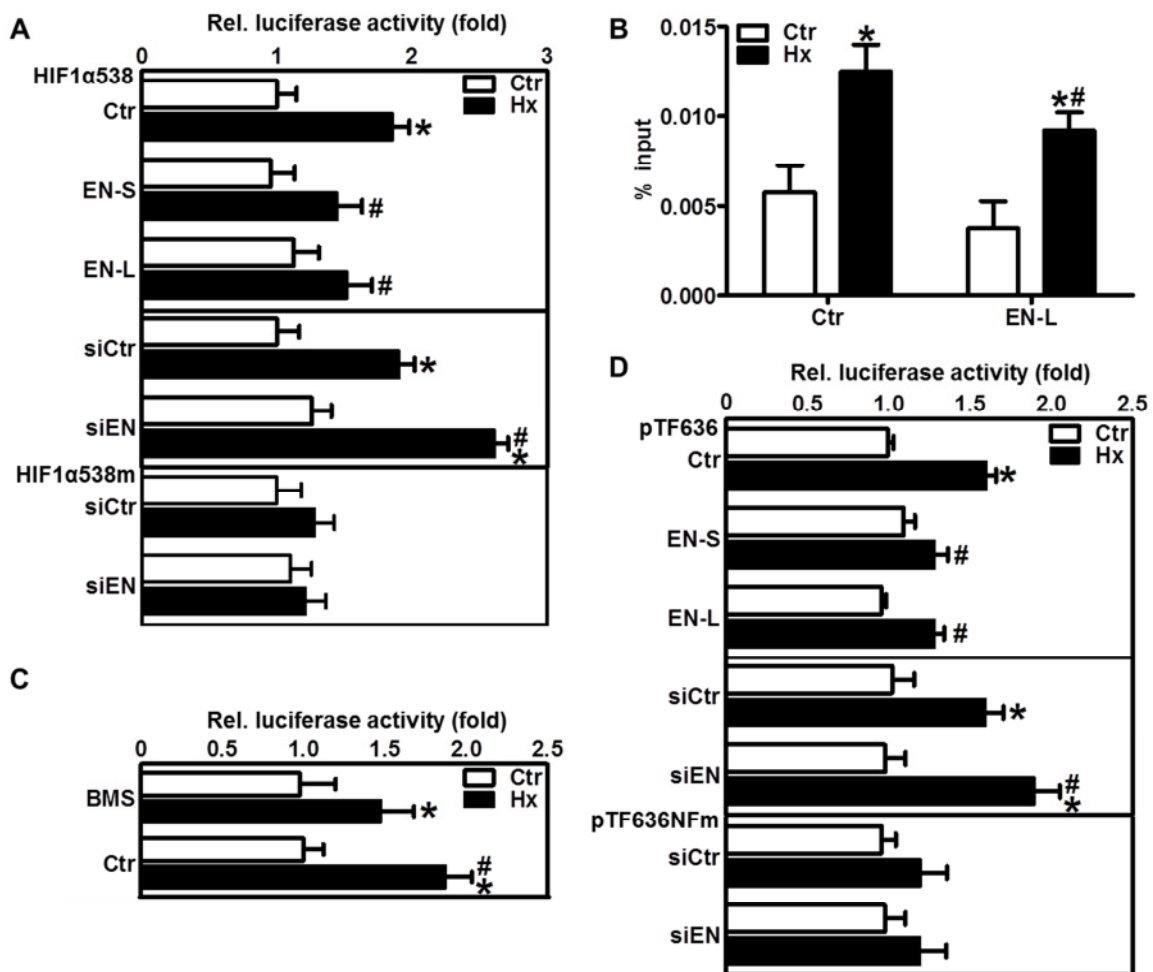


Figure 29. β 3-endonexin regulates hypoxic NF κ B-driven HIF1 α transcription. (A) HMEC-1 were transfected with HIF1 α promoter luciferase constructs containing either the wild-type NF κ B-binding site (HIF1 α 538) or a mutated NF κ B-binding site (HIF1 α 538m) and with siEN or siCtr or with EN-S or EN-L or with control vector (Ctr). Cells were exposed to Hx (1% oxygen) for 8 h or remained under normoxia (Ctr), and luciferase assays were performed. (B) HMEC-1 were transfected with EN-L or control vector (Ctr). Cells were exposed to Hx (1% oxygen) for 8 h or remained under normoxia (Ctr). Chromatin immunoprecipitation assay was performed using an antibody against p65 and RT-qPCR was performed using primers amplifying the region of the human HIF1 α promoter containing the NF κ B-binding site at -197/188 bp. (C) HMEC-1 transfected with HIF1 α 538 were pretreated with the I κ B kinase inhibitor BMS-345541 (BMS, 100 μ M) and exposed to Hx (1% oxygen) for 8 h or remained under normoxia (Ctr), and luciferase assays were performed. (D) HMEC-1 were co-transfected with a luciferase construct driven by the wild-type tissue factor (TF) promoter (pTF636) or the TF promoter mutated at the NF κ B site (pTF636NFm) and either EN-S or EN-L or with control vector (Ctr) or siEN or siCtr. Cells were exposed to Hx (1% oxygen) for 8 h or remained under normoxia (Ctr), and luciferase assays were performed. ($n=3$, * $p<0.05$ vs. CtrCtr or siCtrCtr; # $p<0.05$ vs. CtrHx or siCtrHx). Figure adapted from (228).

indicating that β 3-endonexin interferes with the regulation of HIF1 α by NF κ B. In support, application of the I κ B kinase inhibitor BMS-345541 (BMS, 100 μ M) (316) decreased HIF1 α promoter activity (Figure 29B) (228). To evaluate whether β 3-endonexin would affect NF κ B binding to the HIF1 α promoter, chromatin immunoprecipitation assays in HMEC-1 overexpressing EN-L was performed. While hypoxia increased the binding of p65 to the HIF1 α promoter in cells transfected with control vector, the overexpression of EN-L significantly decreased occupation of the HIF1 α promoter by p65 under hypoxic conditions (Figure 29C), indicating that β 3-endonexin interferes with NF κ B binding to the HIF1 α promoter under hypoxic conditions and thereby inhibits HIF1 α transcription under these conditions (228).

In addition to modifying the HIF1 α expression and activity under hypoxia, β 3-endonexin was also able to modulate hypoxic induction of the NF κ B-target gene - tissue factor (TF) (317) (228). The overexpression of both β 3-endonexin forms prevented the hypoxic induction of TF promoter activity (Figure 29D) (228). Oppositely, the silencing of β 3-endonexin further enhanced hypoxic TF promoter activity (Figure 29D) (228). However, this response was blunted when the NF κ B-binding site in the TF promoter was mutated, suggesting that β 3-endonexin can act as a negative regulator of NF κ B-dependent genes under hypoxia (228).

7.2.4. β 3-endonexin diminishes proliferative and angiogenic responses under hypoxia

In the next step, it was tested whether β 3-endonexin is involved in endothelial proliferative and angiogenic responses under hypoxia. The expression of either of the β 3-endonexin isoforms did not affect endothelial proliferation under normoxia as was determined by 5-bromo-2'-deoxyuridine (BrdU) incorporation assay (Figure 30A) but prevented hypoxic induction of proliferation (228). In contrast, HMEC-1 silenced for β 3-endonexin showed a further increase in proliferative activity under hypoxia (Figure 30A) (228). However, co-expression of I κ Bdn that inhibits the activation of NF κ B, decreased proliferative activity under hypoxia in control cells and β 3-endonexin depleted cells. Similarly, depletion of HIF1 α prevented the hypoxic induction of proliferation in these cells (Figure 30A), indicating that HIF1 α and NF κ B are involved in the inhibition of endothelial proliferation by β 3-endonexin (228). Next, it was tested whether β 3-endonexin affects tube formation using an *in vitro* matrigel assay as an indicator of angiogenesis. While under normoxic conditions, the

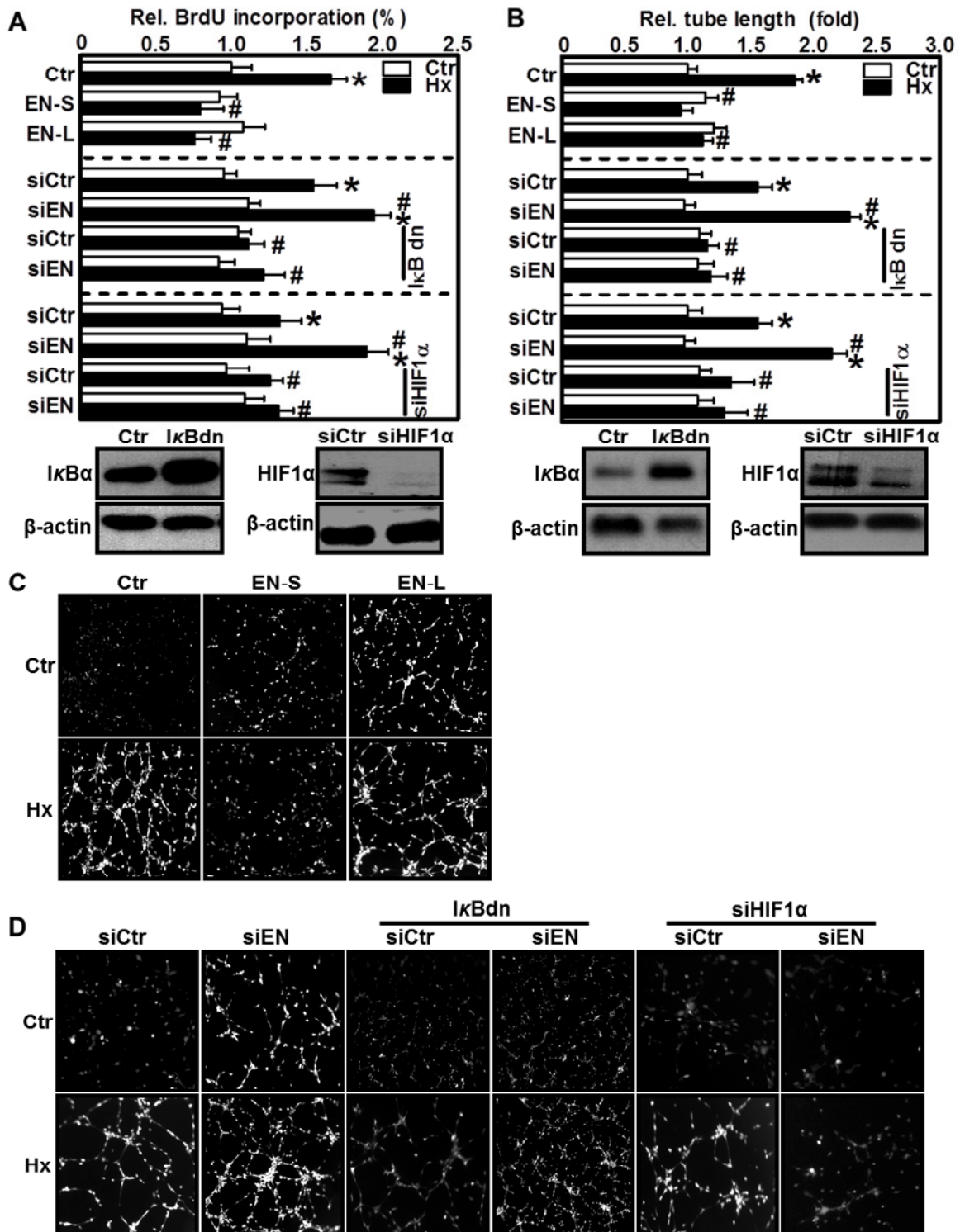


Figure 30. β 3-endonexin affects endothelial hypoxic proliferative responses. (A-D) HMEC-1 were transfected with expression vectors coding for either β 3-endonexin short (EN-S) or long (EN-L) isoform or with control vector (Ctr), or with siRNA against β 3-endonexin (siEN) or scrambled RNA (siCtr). Alternatively, HMEC-1 were transfected with siRNA against β 3-endonexin (siEN) or scrambled RNA (siCtr) and, in addition, transfected with an expression vector coding for I κ Bdn or with control vector (Ctr) or with siRNA against HIF1 α (siHIF1 α). Cells were exposed to hypoxia (1% oxygen, Hx) for 24 h and BrdU incorporation assay was performed **(A)**. Alternatively, cells were seeded on matrigel and exposed to hypoxia (Hx, 1% oxygen) **(B-D)**. Controls remained under normoxia (Ctr) **(A-D)**. **(B)** Total tube lengths were evaluated. Western blot analyses were performed with antibodies against I κ B α and HIF1 α . β -actin levels served as loading control ($n=3$, * $p<0.05$ vs. siCtrCtr; # $p<0.05$ vs. CtrHx or siCtrHx). **(C/D)** Representative figures are shown. Figure adapted from (228).

modulation of β 3-endonexin levels did not affect tube formation, the hypoxic induction of tube formation was diminished upon overexpression of β 3-endonexin isoforms (Figure 30B/C) (228). In contrast, silencing of β 3-endonexin further enhanced hypoxic tube formation (Figure 30B/D) (228). However, in the presence of I κ Bdn or upon depletion of HIF1 α , the effect of β 3-endonexin silencing on hypoxic tube formation was abrogated (Figure 30B/D) (228). Similarly, the expression of EN-L was also able to decrease tube formation in response to the HIF target gene VEGF-A (Figure 31A), indicating that β 3-endonexin negatively affects tube formation by interfering with NF κ B and HIF1 α (228). Similar to our *in vitro* model, the silencing of β 3-endonexin significantly increased CD31 staining in an *in vivo* matrigel plug assay as an indicator of the angiogenic response (Figure 31B). This further supports the concept that β 3-endonexin is a negative regulator of endothelial proliferative and angiogenic processes (228).

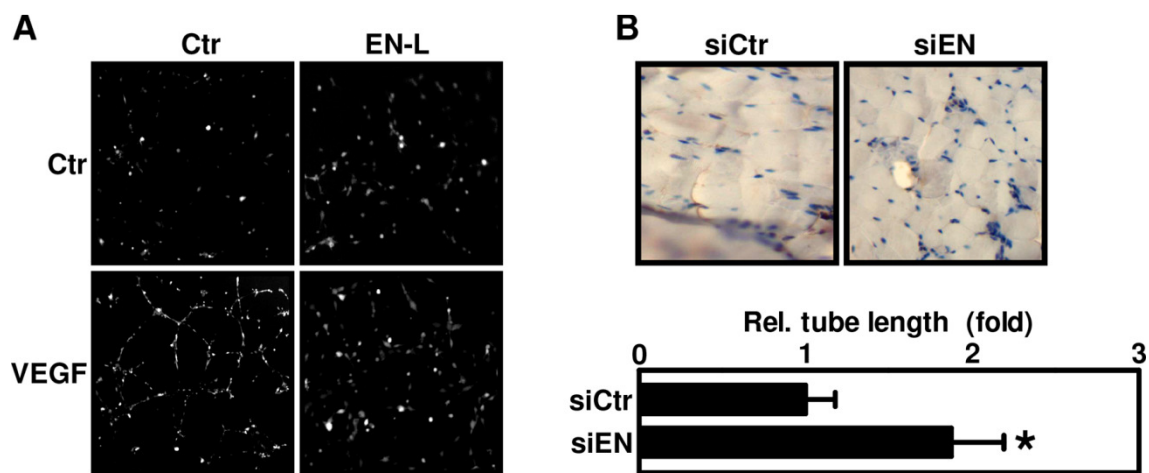


Figure 31. β 3-endonexin decreases the angiogenic response *in vivo*. (A) HMEC-1 were transfected with an expression vector for β 3-endonexin long (EN-L) or control vector (Ctr), seeded on matrigel, and exposed to VEGF-A (VEGF, 1 μ g/ μ l) for 6 h or remained untreated (Ctr). A representative figure is shown ($n=3$). (B) HMEC-1 transfected with RNAi against β 3-endonexin (siEN) or with scrambled RNA (siCtrl) were mixed with matrigel. Plugs were injected subcutaneously in mice and excised after 7 days. Immunohistochemistry was performed with an antibody against CD31 to stain for human endothelial cells. Representative figures are shown ($n=3$, $*p<0.05$ vs. siCtrl). Figure adapted from (228).

7.4.The NADPH oxidase NOX4 activates the ATM-CHK2-p53 pathway in response to oxaliplatin

Application of chemotherapeutics has been associated with the generation of ROS in tumor cells. However, their exact role in this context is not completely understood. NADPH oxidases besides playing an important role in physiological and pathological signalling in the vasculature were shown to be an active site of ROS production in many cancer pathologies both *in vitro* and in patients (155, 318-320). NOX1 and NOX4 have been most frequently observed in several tumor cell lines (124, 320-326). Many observations point to a critical role of NOX4 in apoptosis resistance and sustained tumor cell proliferation in various types of cancer cells including: malignant metastatic melanoma (155, 318, 319), glioma (320), renal cell carcinoma (327, 328) and pancreatic cancer cells (329). The platinum chemotherapeutic oxaliplatin is used in the treatment of melanoma; however, the success of this treatment regimen is often limited due to the development of chemoresistance (330). Whether ROS and NADPH oxidases might play a role in this reaction is not well understood.

7.4.1.Oxaliplatin increases reactive oxygen species in human malignant melanoma cells

In order to evaluate the effects of oxaliplatin on superoxide anion radical generation, human melanoma cells (WM1158) were treated with 250 nM oxaliplatin for increasing time periods and superoxide production was assessed by EPR using CMH (Figure 32A). Oxaliplatin time-dependently increased superoxide generation in WM1158 peaking at 16 h, and returning to baseline at 48 h (Figure 32A). Subsequently, WM1158 were pretreated with the unspecific inhibitor of NADPH oxidases – apocynin (Apo, 100 μ M) for 1 h prior to stimulation with oxaliplatin for increasing time periods up to 48 h (Figure 32A). Superoxide production rate was significantly decreased in apocynin-treated WM1158 compared to controls (Figure 32A). Addition of polyethylene glycol-superoxide dismutase (PEG-SOD, 50 U/ml) diminished the oxaliplatin-induced response confirming the detection of superoxide anion radical in this assay (Figure 32B). To further evaluate a role of NADPH oxidases in the generation of superoxide towards oxaliplatin treatment, melanoma WM1158 were silenced for NOX1 and NOX4 using RNAi. Cells were subsequently exposed to oxaliplatin for increasing time periods and superoxide production was measured by EPR (Figure 32C). Depletion of NOX4 robustly decreased superoxide production rate in response to oxaliplatin treatment in WM1158, while NOX1 depletion had no effect (Figure 32C). In support, oxaliplatin treatment increased NOX4 mRNA and protein levels in a time-dependent manner in WM1158 as was

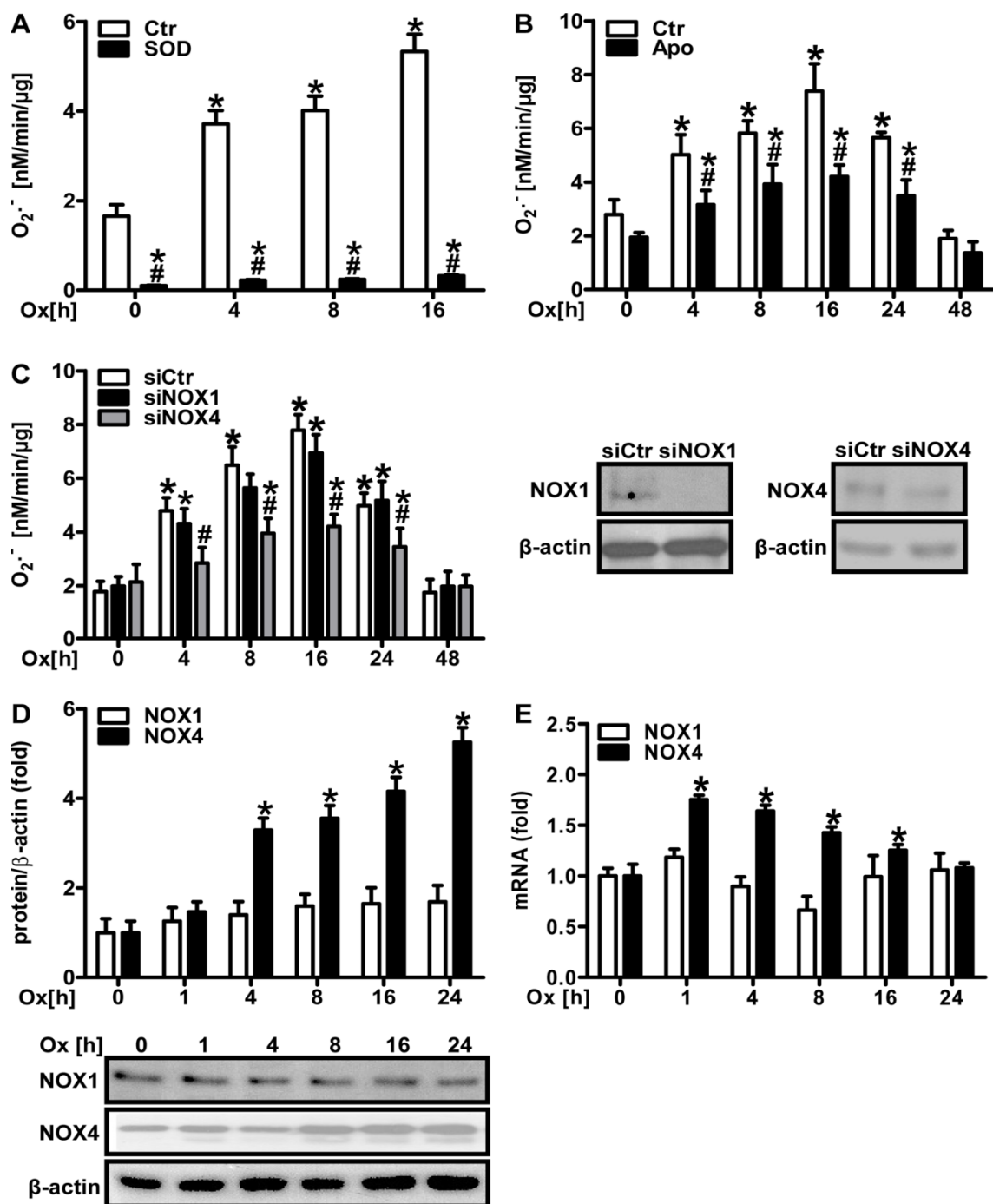


Figure 32. NOX4 contributes to oxaliplatin-induced superoxide production in human melanoma cells. (A) Human melanoma cells (WM1158) were treated with oxaliplatin (Ox, 250 nM) for increasing time periods and superoxide production rate was measured by EPR using CMH (10 μM) by adding polyethylene-glycol superoxide dismutase (SOD, 50 U/ml) or not (Ctr) ($n=3$; $*p<0.05$ vs. Ox 0h, $\#p<0.05$ vs. corr.Ox). (B) WM1158 were pre-treated with apocynin (Apo, 100 μM) or not (Ctr) for 1 h, and subsequently treated with Ox (250 nM) and superoxide production rate was measured as above ($n=3$; $*p<0.05$ vs. 0 h Ctr, $\#p<0.05$ vs. Ctr). (C) WM1158 were transfected with either siNOX1 or siNOX4 or with siCtr, treated with oxaliplatin (Ox, 250 nM) for the indicated time points and superoxide production rate was measured as above ($n=3$; $*p<0.05$ vs. 0h siCtr, $\#p<0.05$ vs. siCtr). Western blots were performed using antibodies against NOX1 and NOX4. β-actin served as loading control. (D/E) WM1158 were treated with oxaliplatin (Ox, 250 nM) as indicated on the graph ($*p<0.05$ vs. 0h Ox). (D) Western blot analyses were performed using antibodies detecting NOX1 and NOX4. β-actin served as loading control ($n=3$; $*p<0.05$ vs. 0h Ox). (E) RTqPCR analyses were performed using gene-specific primers for NOX1 or NOX4. 18S rRNA served as a control ($n=3$; $*p<0.05$ vs. 0h Ox).

determined by RT-qPCR and Western blot analysis (Figure 32D/E). In contrast NOX1 mRNA and protein levels were not affected by oxaliplatin treatment (Figure 32D/E).

7.4.2. Oxaliplatin induces double-strand DNA damage response in human melanoma cells

Double-strand breaks (DSBs) are highly deleterious lesions in genomic DNA (331-333). They can be generated by ionizing irradiation and a variety of chemical agents, e.g. chemotherapeutics (334, 335), heavy metal ions, and ROS (333, 336-338). Accumulated DSBs stop the replicative fork and cell cycle inducing a pro-survival response - double-strand DNA damage response (dsDDR) (331-333). In addition, platinum salts (e.g. carboplatin, cisplatin, oxaliplatin), were shown to induce DSBs (335, 339). Hence, in the next step it was evaluated whether oxaliplatin induces dsDDR in human melanoma cells.

For this purpose, WM1158 were exposed to oxaliplatin (Ox, 250 nM) for increasing time periods and Western blot analyses were performed for dsDDR markers, such as phospho-histone 2AX (γ H2AX), phospho-check point kinase 2 (p-CHK2) and the dsDDR effector p53.

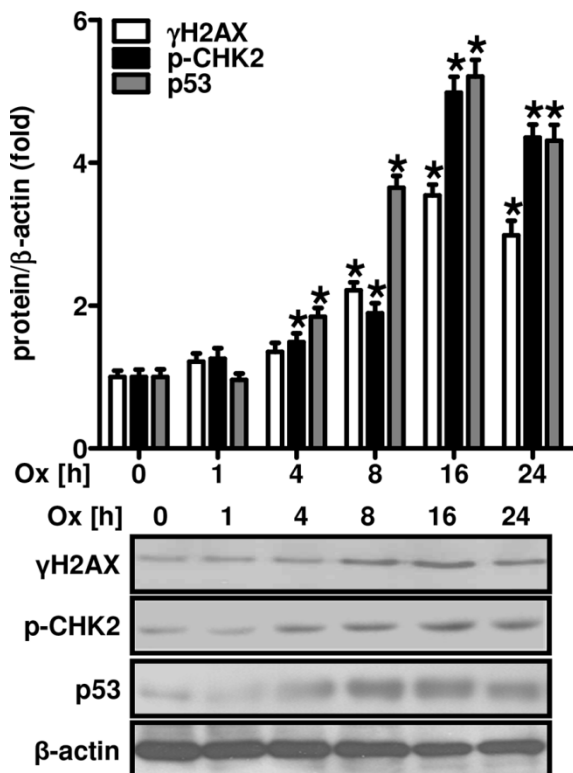


Figure 33. Oxaliplatin induces double stranded DNA damage response in human melanoma cells. WM1158 were treated with oxaliplatin (Ox, 250 nM) or not (Ctr) for increasing time periods and Western blot analyses were performed using antibodies against phospho-histone 2AX (γ H2AX), phospho-check point kinase 2 (p-CHK2) or p53. β -actin served as a loading control ($n=3$; * $p < 0.05$ vs. 0h).

Indeed, oxaliplatin treatment time-dependently increased p-CHK2 and p53 levels starting at 4 h and γ H2AX levels starting at 8 h of treatment (Figure 33). In addition, WM1158 were treated with oxaliplatin (Ox, 250 nM), spun down onto coverslips and stained with an antibody against the dsDDR sensor phosphorylated ataxia telangiectasia mutated kinase (p-ATM). Compared to control cells, oxaliplatin time dependently increased p-ATM stainings in WM1158 cytopins (Figure 34A/B).

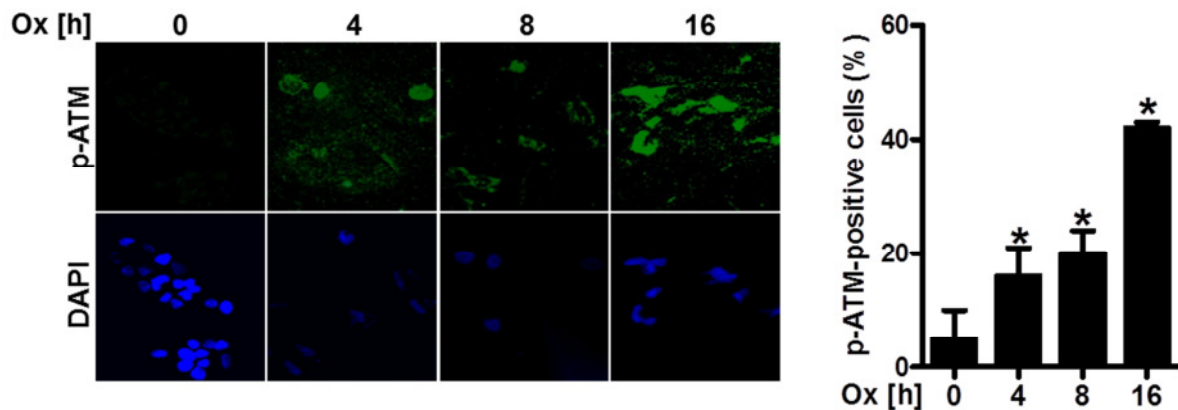


Figure 34. Oxaliplatin induces ataxia telangiectasia mutated kinase phosphorylation in human melanoma cells. WM1158 were treated with oxaliplatin (Ox, 250 nM) or not (Ctr) for increasing time periods, trypsinized and spun down onto coverslips and incubated with an antibody against phospho-ataxia/telangiectasia mutated kinase (p-ATM), and subsequently fluorescently labelled with a secondary antibody conjugated with Alexa fluor 488. Quantification represents number of positive cells in a visible field (1 cm²) (*n*=3; **p*<0.05 vs. Ox 0h). Nuclei were visualized by DAPI staining.

7.4.3. Oxaliplatin-induced double-strand DNA damage response is dependent on NOX4

For evaluation of the role of ROS in oxaliplatin-induced dsDDR, WM1158 were pre-treated with the antioxidant ascorbic acid (Asc, 100 μ M) 1 h prior to oxaliplatin treatment (Ox, 250 nM) for increasing time periods and Western blot analyses for the dsDDR markers γ H2AX, p-CHK2 and p53 were performed (Figure 35A). Pre-treatment with ascorbic acid diminished phosphorylation of H2AX and CHK2 and decreased the levels of p53 in response to oxaliplatin indicating that ROS are involved in this response (Figure 35A).

Next, WM1158 were silenced for NOX4 using RNAi and subsequently treated with oxaliplatin, and Western blot analyses for dsDDR markers were performed (Figure 35B). Silencing of NOX4 diminished the induction of phosphorylated H2AX and CHK2 and decreased p53 levels upon oxaliplatin treatment. In addition, immunocytochemical staining of cytopins in WM1158 showed that the oxaliplatin-induced phosphorylation of ATM was

reduced in WM1158 depleted of NOX4, suggesting that NOX4 is important in controlling the dsDDR upon oxaliplatin treatment in melanoma cells (Figure 36C).

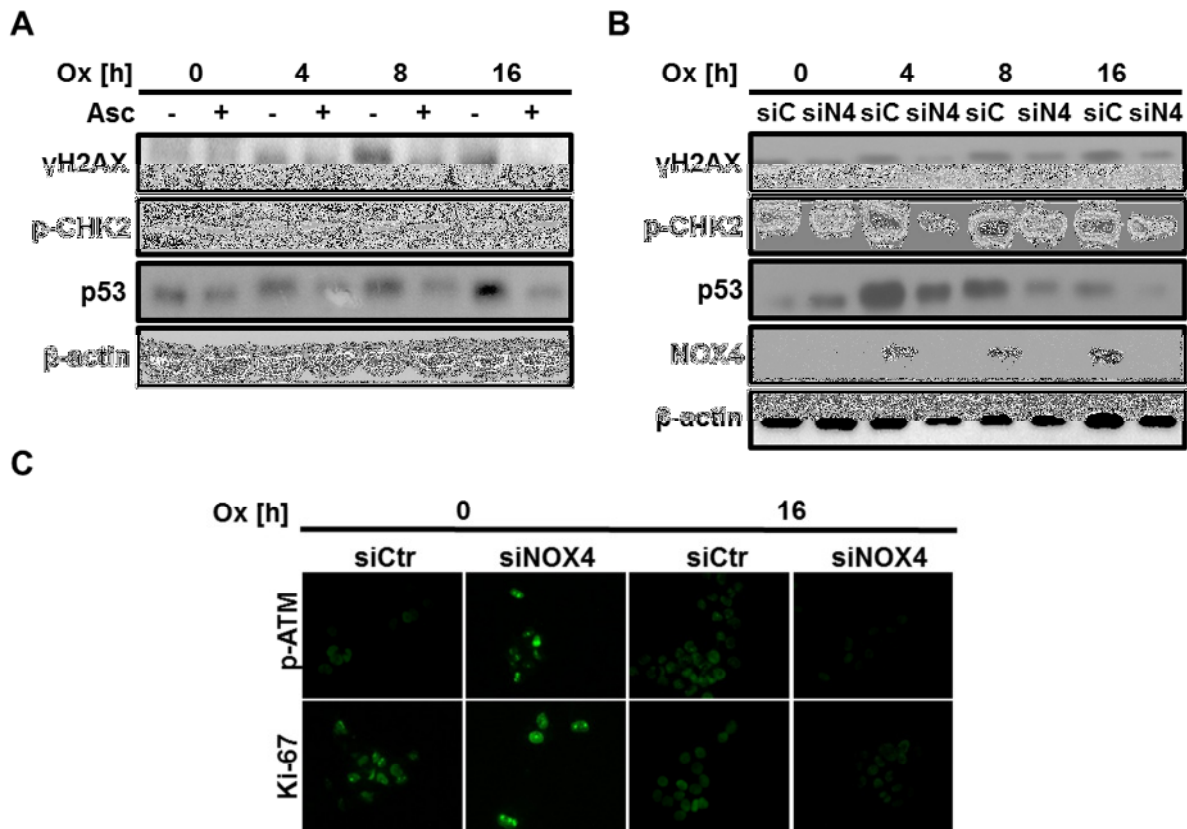


Figure 35. NOX4 promotes oxaliplatin-induced double stranded DNA damage response in human melanoma cells. (A) WM1158 were pre-treated or not (Ctr) with the unspecific scavenger of reactive oxygen species – ascorbic acid (Asc, 100 μ M) for 1 h, subsequently treated with oxaliplatin (Ox, 250 nM) as indicated and Western blot analyses were performed using antibodies against: γ H2AX, p-CHK2 or p53 DO7. β -actin served as a loading control. **(B)** WM1158 were silenced either for NOX4 (siN4) using RNAi or transfected with scramble RNA (siC), subsequently treated with oxaliplatin (Ox, 250 nM) as indicated and Western blot analyses were performed using antibodies against: γ H2AX, p-CHK2 or p53 DO7. β -actin served as a loading control. **(C)** WM1158 were silenced either for NOX4 (siNOX4) using RNAi or transfected with scrambled RNAi (siCtr), subsequently treated with oxaliplatin (Ox, 250 nM) for 16 h or not (0 h), trypsinized and spun down onto coverslips, incubated with an antibody against p-ATM, and subsequently fluorescently labelled with a secondary antibody conjugated with Alexa fluor 488.

7.4.4. Oxaliplatin induces proliferative arrest and senescence

Induction of dsDDR markers, in particular p-CHK2, as demonstrated here in response to oxaliplatin treatment, is usually a strong indication of cellular proliferative arrest (340). To further support this notion, WM1158 were treated with oxaliplatin (Ox, 250 nM) for increasing time points, and cytopins were stained for the proliferative marker Ki67 (Figure 36A). Upon prolonged treatment with oxaliplatin, staining for Ki67 decreased (Figure 36A). Moreover, DNA synthesis as determined by BrdU incorporation decreased upon exposure to higher

concentrations of oxaliplatin (1000 nM) (Figure 36B). While Western blot analyses did not show evidence for cleavage of the pro-apoptotic poly (ADP-ribose) polymerase (PARP1) protein (Figure 36C) oxaliplatin time-dependently increased the levels of p21 in WM1158, a marker for cell senescence, suggesting that oxaliplatin might induce senescence in this set-up (Figure 36C).

Due to the close link between ROS, NOX4 and HIF1 α with NOX4 being a HIF1 target gene (302, 304, 341, 342), as well as upregulation of HIF1 α by ROS and NOX4 (37, 343-348) the levels of HIF1 α were evaluated in WM1158. To this end, WM1158 were treated with oxaliplatin and Western blot analyses were performed using a HIF1 α antibody (Figure 37A).

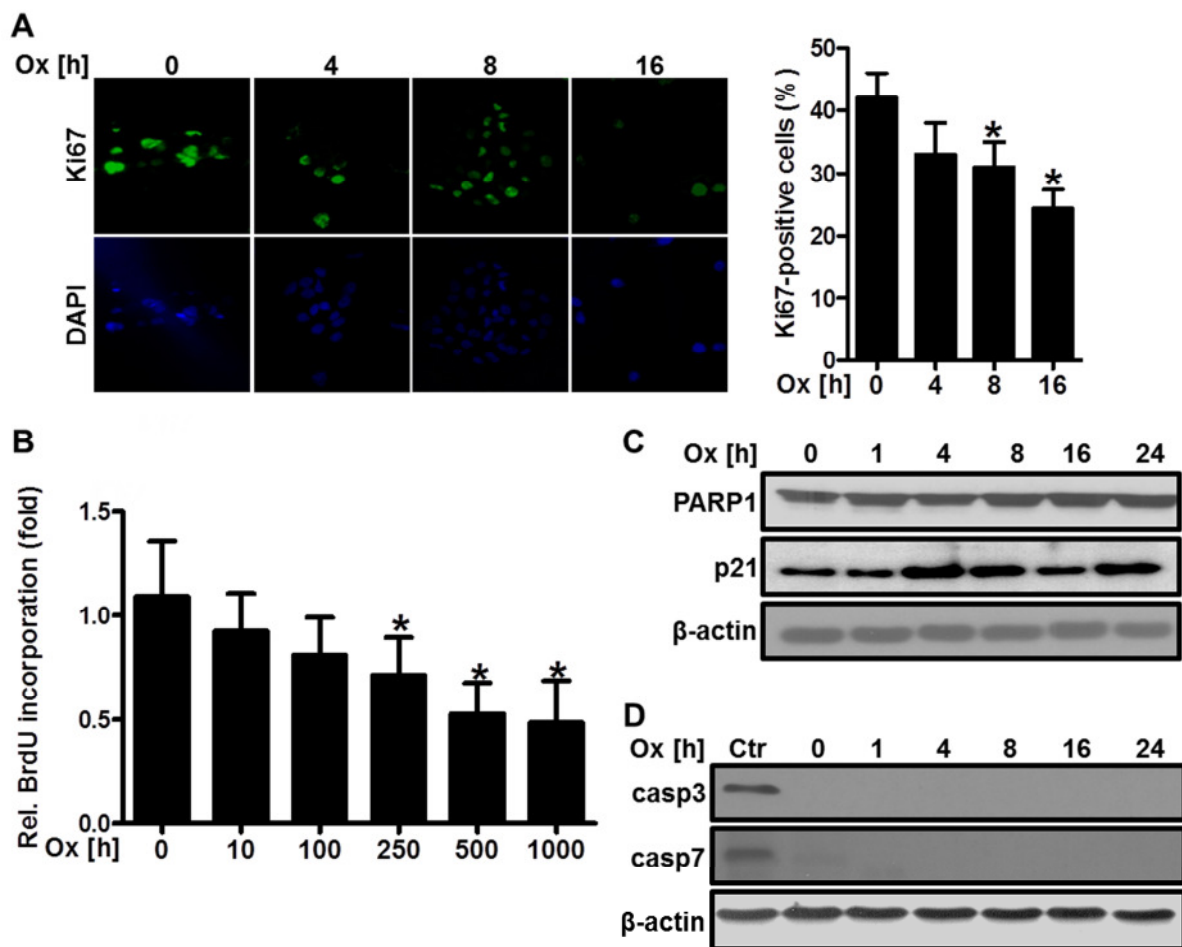


Figure 36. NOX4 promotes oxaliplatin-induced double strand DNA damage response in human melanoma cells. (A) WM1158 were treated with oxaliplatin (Ox, 250 nM) or not (0 h) for increasing time periods, trypsinized and spun down onto coverslips and incubated with an antibody against Ki67 and subsequently fluorescently labelled with a secondary antibody conjugated with Alexa fluor 488. Nuclei were visualized by DAPI staining. Quantification represents the number of positive cells for Ki67 in a visible field (1 cm²) ($n=3$; * $p<0.05$ vs. Ox 0h). **(B)** WM1158 were treated with different concentrations of Ox (0-1000 nM) for 24 h and BrdU incorporation assay was performed ($n=3$; * $p<0.05$ vs. Ox 0h). **(C-D)** WM1158 were treated with oxaliplatin (Ox, 250 nM) as indicated on the graph, and Western blot analyses were performed using antibodies against: poly (ADP-ribose) polymerase (PARP1) and p21 **(C)**, as well as cleaved caspase 3 and 7 (casp3, casp7) **(D)**. As control (Ctr) for cleaved levels of caspases 3 and 7 WM1158 treated with doxorubicin (1 μ M) for 8 h were used. β -actin served as a loading control.

Indeed, HIF1 α was upregulated in a time-dependent manner in WM1158 following oxaliplatin treatment (Figure 37A).

In order to decipher the temporal regulation between NOX4 and HIF1 α , WM1158 were silenced either for NOX4 or HIF1 α and subsequently treated with oxaliplatin (Figure 37B/C). Depletion of HIF1 α decreased NOX4 levels in response to oxaliplatin treatment (Figure 37B). However, depletion of NOX4 did not affect HIF1 α levels (Figure 37C), indicating that induction of HIF1 α is upstream of NOX4 in response to oxaliplatin in WM1158.

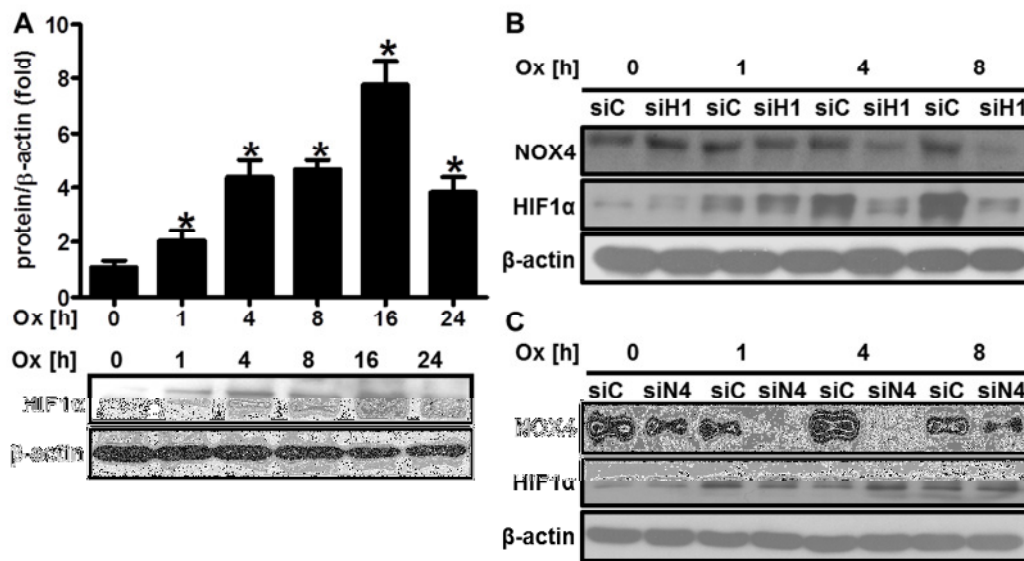


Figure 37. Oxaliplatin induces HIF1 α in human melanoma cells. (A) WM1158 were treated with oxaliplatin (Ox, 250 nM) for increasing time periods, and Western blot analyses were performed using an antibody against HIF1 α . β -actin served as a loading control ($n=3$; $*p<0.05$ vs. Ox 0h). (B/C) WM1158 were silenced either for HIF1 α (siH1) (B) or for NOX4 (siN4) (C) using RNAi or transfected with scramble RNA (siC), subsequently treated with Ox (250 nM) for increasing time periods and Western blot analyses were performed using antibodies against HIF1 α and NOX4. β -actin served as a loading control.

8 Discussion

8.1. Folic acid protects against hypoxia-induced pulmonary hypertension

The data of the following study investigating the role of NO/ROS balance and folic acid in the context of hypoxia induced cardio-pulmonary pathology have been previously published (202). Permission to use the figures and the text of the article was obtained from *Antioxidants&Redox Signaling* (Appendix, p.143).

Pulmonary hypertension has been associated with dysfunction in ROS and NO metabolism (349-356). In this study the interplay between these reactive species under hypoxia and the consequences for hypoxia-induced pulmonary hypertension have been characterized (202). It was found that: a) hypoxia leads to uncoupling of eNOS due to downregulation of dihydrofolate reductase (DHFR) and subsequent failure to recycle 7',8'-dihydrobiopterin (BH₂) to 5',6',7',8'-tetrahydrobiopterin (BH₄); b) treatment with folic acid restored NO bioavailability by upregulating DHFR expression, and improving the recycling of dihydrobiopterin to tetrahydrobiopterin; c) treatment with folic acid protected chronic hypoxic mice from right ventricular hypertrophy, right ventricular pressure increase and pulmonary vascular remodeling – hallmarks of pulmonary hypertension - by restoring, and subsequently increasing the NO bioavailability (202).

Measurements of NO levels in endothelial cells and *in vivo* showed that hypoxia decreased NO availability although eNOS protein levels remained unchanged (202). In contrast, several studies reported increased NO levels in response to hypoxia (357-360). Concomitantly, hypoxia was reported to increase eNOS expression in endothelial cells and *in vivo* in rats and mice concomitant with increased NO bioavailability (301, 357-360). Disconcordant findings might relate to differences in model systems, timing, and severity of hypoxia, as well as to variations in secondary effects associated with hypoxia in particular in the *in vivo* situation (361).

Similar to our study, there are many studies that show decreased NO bioavailability in hypoxia *in vitro* and *in vivo* (361-365) although decreased NO levels were not always related to decreased levels of eNOS (366).

This indicates that other mechanisms apart from modulation of eNOS expression contribute to the adaptation of NO metabolism to hypoxia (366). In line, hypoxia induced phosphorylation of eNOS at Thr495, which acts inhibitory on eNOS activity thus explaining the reduced NO levels under hypoxia (202). In support of this study, increased Thr495

phosphorylation of eNOS under hypoxia has been reported (364, 367, 368). However, hypoxia also increased phosphorylation of eNOS at Ser1177 in HPAEC (202), which has been associated with Akt-induced activation of this enzyme although NO levels were reduced.

While the role of Ser1177 phosphorylation of eNOS under hypoxia has been controversially reported, showing increased (357), unchanged (369), or decreased (364, 367, 370) phosphorylation of eNOS at Ser1177, in the absence of BH₄, eNOS Ser1177 phosphorylation has been associated with increased superoxide rather than with NO production due to uncoupling of eNOS (371). Since Akt can be activated under hypoxic conditions, and BH₄ and NO levels were decreased under hypoxia (202), phosphorylation of eNOS at Ser1177 seen in response to hypoxia might be linked to superoxide rather than to NO generation (371).

Furthermore, L-NAME decreased ROS production under hypoxia and monomer formation of eNOS by hypoxia was increased (202) further pointing to uncoupled eNOS under these conditions.

In line, decreased NO bioavailability was accompanied by decreased BH₄/BH₂ ratio that reflected decreased levels of BH₄ and increased levels of BH₂ both *in vitro* and *in vivo* (202). BH₄ levels are considered to be an important determinant of the functional enzymatic competence of eNOS, since decreased BH₄ levels also lead to eNOS uncoupling (372, 373). Similar to this study, decreased BH₄ levels have been described in other *in vivo* models of chronic hypoxia, although the levels of superoxide or other ROS have not been evaluated (202, 300, 301). In contrast, hypoxia has been reported to increase the BH₄/BH₂ ratio due to increased *de novo* synthesis of biopterins, an assumption which was based on elevated levels of GTPCH-1 (374); however, this study did not find evidence that *de novo* synthesis of biopterins was altered under hypoxia (202). Instead, here decreased levels of DHFR under hypoxia were observed (202, 375). DHFR has been described to recycle BH₂ to BH₄, thereby maintaining the BH₄ pool required for adequate NOS function (202, 375). However, a study conducted in a similar model of chronic hypoxia showed increased BH₄ levels and eNOS expression in lungs, without modifying BH₂, GTPCH-1 or DHFR levels (374).

ROS levels under hypoxia are a matter of ongoing debate since the literature shows conflicting data that reflect the fact that both increased and decreased levels of ROS in hypoxia were reported (202, 376).

This study reports a clear decrease in ROS levels under hypoxic stimulation (202). When the sample handling and superoxide measurements were performed under hypoxic conditions, superoxide generation was decreased compared to normoxic conditions (202).

However, when superoxide measurements were performed under normoxia following exposure to hypoxia, thus mimicking hypoxia–reoxygenation, superoxide levels were increased (202), as has been shown previously (304). Even short exposure of HPAEC or pulmonary arteries to normoxia was sufficient to increase superoxide generation (202, 376). These findings could account for at least some of the divergent results regarding ROS levels under hypoxia.

However, in contrast to the hypoxic setting, L-NAME did not affect superoxide production under reoxygenated conditions in HPAEC, indicating that uncoupled eNOS did not contribute to increased ROS levels in this setting (202). Application of inhibitors of mitochondrial ROS generation and NADPH oxidases, however, pointed to NADPH oxidases as the source of ROS in reoxygenated conditions (202).

Although eNOS uncoupling (377) and mitochondrial ROS production (378, 379) have been described in a situation of hypoxia–reoxygenation in endothelial cells, findings in this study and earlier reports showed that expression of the NADPH oxidase subunit, NOX4, is increased under hypoxia *in vitro* and *in vivo* (302, 304). Together with findings that hypoxic induction of NOX4 promotes ROS generation upon reoxygenation (304) the data presented here point to NOX4 and NADPH oxidases as source of ROS under hypoxia-reoxygenation conditions.

In pulmonary vessels and lung tissues explanted from chronic hypoxic mice ROS levels were increased (202), which is in concordance with previously described results in similar *in vivo* models (380-382). However, preparation of pulmonary arteries and lung tissue lysates from chronic hypoxic mice was performed in normoxia (202); hence, it is likely that the increase in ROS was the consequence of reoxygenation rather than hypoxia. This conclusion is supported by *in vitro* and *ex vivo* data in this study (202). Thus, observations that ROS levels are increased in chronic hypoxic mice (380, 381) might not reflect the real *in vivo* situation, but can be the result of reoxygenation effects.

In line, previous studies showed that ROS generation was also decreased in hypoxic lung tissues derived from NOX2 knock out mice (380, 381), further supporting the observation that NADPH oxidases might contribute to ROS generation upon reoxygenation (202).

Under hypoxia–reoxygenation conditions NO levels, in contrast to superoxide, remained decreased, which might relate to the view that increased superoxide levels scavenge NO, thereby lowering overall NO levels (202). In addition, the BH₄/BH₂ ratio remained reduced under hypoxia–reoxygenation conditions (202), which might also relate to increased levels of superoxide under these conditions since oxidation of BH₄ to BH₂ and consequent reduction of NO generation can increase superoxide levels (383).

Application of folic acid, however, restored BH₄ bioavailability and NO generation under hypoxia and hypoxia–reoxygenation conditions, while, consequently reducing superoxide levels under reoxygenation conditions (202).

Folic acid, which has been previously shown to upregulate DHFR levels under normoxic conditions (298), effectively increased hypoxic DHFR levels (202). Importantly, folic acid restored BH₄ levels and enhanced NO and nitrite levels under normoxia and hypoxia as well as under reoxygenation, and this effect was dependent on DHFR, further indicating that the folic acid-induced increase in NO and BH₄ levels is promoted by improved BH₂ to BH₄ recycling (202). Furthermore, folic acid reversed eNOS monomerization under hypoxia, thus indicating recoupling of eNOS (202).

In line, beneficial effects of folic acid on BH₄ availability and eNOS uncoupling have been reported (202, 298, 384).

In line, folic acid reduced hypoxia-induced phosphorylation of eNOS at Thr495, thus increasing eNOS activity under these conditions (202). Folic acid has been shown to dephosphorylate eNOS at Thr495 in porcine aortic endothelial cells (202, 299)., and *in vivo* studies suggested that Thr495-phosphorylated eNOS can uncouple eNOS (215), further indicating that hypoxia results in eNOS uncoupling with folic acid being able to recouple this enzyme (202).

However, folic acid increased phosphorylation of eNOS at Ser1177 under normoxic conditions as well as under hypoxic conditions in particular *in vivo* (202). This finding has been supported by a recent study demonstrating that folic acid activates the PI-3 kinase/Akt pathway (299) and thus Ser1177 phosphorylation of eNOS, indicating that folic acid acts beneficially on NO availability *via* different mechanisms. Moreover, in the presence of folic acid, BH₄ bioavailability increased, which might allow the Ser1177-phosphorylated enzyme to generate NO again also under hypoxic conditions (202).

Thus, folic acid appears to have an important function in restoring and maintaining the balance between NO and ROS (202) which could counteract endothelial dysfunction and other adverse effects under these conditions. In support, our data show that supplementation with folic acid improved acetylcholine-dependent vasorelaxation in murine pulmonary vessels (202) although other studies failed to link the beneficial effect of folic acid on endothelial dysfunction to the regeneration or stabilization of BH₄ (385).

Importantly, this study showed that folic acid application to chronic hypoxic mice not only improved BH₄ recycling capacity and recoupling of eNOS (202), but also effectively protected against the development of pulmonary hypertension under hypoxia, as indicated by decreased right ventricular pressure, pulmonary vascular remodeling, and right ventricular

hypertrophy. In contrast, it was recently reported that treatment with sepiapterin, a commercially available modified BH₂, did not ameliorate pulmonary vascular remodeling in mice in response to chronic hypoxia (202, 374). However, since BH₄ levels seemed to be increased under hypoxic conditions in this study, further increasing biopterin levels through application of sepiapterin might possibly be less efficient. Moreover, since sepiapterin needs to be converted to BH₄ by DHFR to be fully active, the decreased capacity to recycle BH₂ to BH₄ under hypoxic conditions might limit this therapeutic approach (202). However, a recent study suggested that supplementation with tetrahydrobiopterin might also have beneficial effects on pulmonary hypertension induced by chronic hypoxia (300), although the mechanisms underlying this effect have not been analyzed in this study.

Although folic acid has been shown to have beneficial effects in coronary artery disease and other cardiovascular disorders associated with hypoxia and reoxygenation (384, 386, 387), several clinical trials indicated controversial outcomes with regard to cardiovascular disease risk and mortality (202, 387-389). While multiple reasons have been indicated for the negative results in some studies (390), increasing evidence suggests that folic acid might be more beneficial in primary prevention in subjects with low folic acid levels (202, 391). A recent, large clinical trial indicated a substantially reduced risk for stroke in hypertensive patients taking folic acid (202, 392, 393).

While the results of this study in an animal model suggest that folic acid might be able to prevent the development of PH in conditions of hypoxia, such as a high altitude sojourn, or in hypoxemic patients at risk to develop PH; clearly, clinical trials will be required to assess the potential of folic acid as a preventive or treatment option for PH associated with low oxygen availability (202).

Collectively, findings of this study indicate that disruption of the BH₄ to BH₂ balance due to reduction of DHFR levels under hypoxia uncouples eNOS thus decreasing NO bioavailability, subsequently promoting right ventricular hypertrophy and pulmonary vascular remodeling and the development of pulmonary hypertension (202). Since supplementation with folic acid restored NO metabolism under hypoxia and protected against the development of pulmonary vascular remodeling and right ventricular hypertrophy and lowered right ventricular pressure, folic acid may provide an efficient and cost-effective therapeutic strategy to combat pulmonary hypertension (202).

8.2. Dexamethasone promotes cardiac and pulmonary vascular remodeling *via* reactive oxygen species and hypoxia inducible factor 1

In this study it was shown that dexamethasone increased NADPH oxidase dependent superoxide production in vascular cells and tissues, which promoted a HIF-dependent pathway leading to endothelial proliferation and angiogenesis. Moreover, *in vivo* studies indicated that chronic treatment with dexamethasone promoted an increase in systemic, but also pulmonary pressure associated with left ventricular dysfunction as well as right ventricular hypertrophy and pulmonary vascular remodeling, respectively, which were dependent on NADPH oxidase regulated pathways.

Interestingly, while initial studies reported that dexamethasone decreases ROS generation (394, 395), there is now an increasing awareness that dexamethasone promotes ROS production in endothelial cells (281), macrophages (283), dendritic cells (283), pancreatic cells (282), osteoblasts (284), MC3T3-E1 pre-osteoblasts (396), and HepG2 cells (397).

Data here now clearly identified NADPH oxidases as source of ROS in vascular cells and isolated vessels. Importantly, dexamethasone-induced ROS generation was abolished in isolated vessels from mice deficient in p22phox thus demonstrating for the first time the *in vivo* relevance of this pathway.

p22phox is required for the function of NOX1, NOX2 and NOX4, and our data indicate that dependent on the cell type, all three NADPH oxidases might be able to generate ROS in response to dexamethasone. Mechanistically, this response was mediated by the glucocorticoid receptor and involved PI3 kinase and Rac1 which is required for NOX2 or NOX1 activity. In addition, dexamethasone not only increased the expression of p22phox, but also of NOX4 in vascular cells as well as in the lungs, a highly vascularized tissue. Previous studies have shown that NOX4 can be induced by dexamethasone in MC3T3-E1 cells (396) and rat pancreatic β -cell line (INS-1) (282). Furthermore, dexamethasone treatment has been reported to increase the expression of p47phox which is required for NOX2 activity, in macrophages (283), and to increase NOX1 mRNA levels in vascular smooth muscle cells (398).

These data now clearly demonstrate that dexamethasone can increase ROS generation in vascular cells and intact vessels by activating and/or upregulating different NADPH oxidases in a cell type specific context. ROS production by NADPH oxidases further promoted proliferation of vascular cells and angiogenic activity in response to dexamethasone.

However, dexamethasone has been previously reported to decrease proliferation and/or increase apoptosis or necrosis in different cellular models (399, 400). Moreover, dexamethasone has been described to decrease angiogenesis in different models such as tumors, inflammatory neovascularization or wound healing (401). Several mechanisms have been described including GR-mediated alterations in cytoskeletal structure, induction of the anti-angiogenic TSP-1 (401), inhibition of paracrine angiogenic factors such as VEGF (401-404) or prostaglandin production (405, 406). While the reasons for these conflicting data are not conclusively resolved they at one point seem to be related to the concentration applied where application of micromolar concentrations inhibited proliferation while in this study dexamethasone was used in nanomolar concentrations. Moreover, dexamethasone seems to act differently in a disease context in comparison to application in healthy conditions. In line, increased proliferation in response to dexamethasone has been observed in smooth muscle cells (407), human corneal epithelial cells (408) and prostate derived fibroblasts (409) or in human umbilical vein endothelial cells (410).

In support, dexamethasone exposure promoted angiogenesis in the chick yolk sac membrane model (410).

Mechanistically, this study showed that dexamethasone-induced proliferation of vascular cells was mediated by NADPH oxidase dependent activation of the HIF pathway. HIF transcription factors are master regulators of angiogenesis under hypoxic conditions, but also promote vascular proliferation and angiogenesis under normoxic conditions (10, 411). Thereby dexamethasone increased HIF1 α protein levels dependent on ROS and NADPH oxidases. In line, HIF transcription factors have been shown previously to be induced and activated in a ROS-dependent manner, involving NADPH oxidases (37, 343, 344).

Moreover, this study indicates the involvement of pVHL in upregulation of HIF1 α by dexamethasone. pVHL can bind to hydroxylated HIF1 α mostly under normoxic conditions, thereby promoting its degradation. In line, overexpression of pVHL prevented the induction of HIF1 α by dexamethasone. In addition, dexamethasone decreased pVHL levels in endothelial cells which subsequently might allow HIF1 α stabilization. In support, it has been previously reported that dexamethasone can decrease pVHL levels thereby increasing protein stability of HIF1 α (412).

In contrast, several studies showed that dexamethasone inhibits HIF1 α or HIF activity in different cellular models (280, 413-415). Again, these studies were carried out under hypoxic, but not under normoxic conditions. However, in line with this study, demonstrating enhanced levels of HIF1 α in vascular tissues in dexamethasone-treated mice, the glucocorticoid prednisolone has recently been shown to increase HIF1 α levels in the liver of humans and

zebrafish (412). While the reasons for these conflicting data are not clear in detail, these data suggest that the HIF pathway responds differently to glucocorticoids under normoxic, unstimulated conditions than under conditions of hypoxia or other stimuli.

Interestingly, depletion of HIF1 α also decreased dexamethasone-induced ROS production and prevented upregulation of NOX4, a known HIF target gene. These findings suggest a positive feed back mechanism whereby dexamethasone rapidly increased ROS production by activation of Rac-dependent NADPH oxidases such as NOX2 or NOX1 possibly mediated by PI-3 kinase. PI-3 kinase has been previously reported to be activated by the glucocorticoid receptor (305) and to mediate activation of Rac (416). In line, application of a PI3 kinase inhibitor as well as expression of dominant-negative Rac1 decreased dexamethasone-induced ROS production. Dexamethasone-induced ROS production then increases HIF1 α protein levels and activity leading to the upregulation of HIF target genes such as PAI1, which is known to promote vascular proliferation, and NOX4 which further helps to sustain increased ROS production.

Increased ROS production has been previously suggested to contribute to vascular dysfunction and hypertension as a frequent complication of dexamethasone treatment in animal models and in humans (281, 308-311).

In support, treatment with antioxidants such as N-acetylcysteine, tempol, lactoferrin or apocynin, prevented or reversed the development of systemic hypertension in response to dexamethasone treatment (417-420).

In this study NADPH oxidases could be identified as sources of ROS mediating a hypertensive response towards chronic treatment with low dose dexamethasone as this treatment increased left ventricular pressure indicative of systemic hypertension in wildtype mice, but not in p22phox-deficient mice. Moreover, dexamethasone treated wildtype mice, but not p22phox-deficient mice, showed an increase in left ventricular mass and increased cardiomyocyte diameter. In addition, echocardiography revealed a thinned left ventricular wall associated with increased left ventricular diastolic and systolic diameter and impaired fractional shortening as indicator of ejection fraction in dexamethasone treated wildtype mice resembling a dilated cardiomyopathy (421). However, p22phox-deficient mice were fully protected from the cardiac effects of dexamethasone.

While these responses might be secondary to the dexamethasone effects on the systemic pressure, it has been reported that dexamethasone can also induce hypertrophy of cultured cardiomyocytes (422) arguing that dexamethasone also exerts direct effects on cardiomyocytes (422, 423). In fact, the symptoms observed in chronically dexamethasone treated mice resemble dilated cardiomyopathies described in patients with Cushing

syndrome (424). In addition, cardiomyopathy has been reported as complication of dexamethasone treatment in particular in preterm infants (425).

In addition to alterations in left ventricular function, chronic dexamethasone treatment also resulted in increased right ventricular pressure, increased right ventricular cardiomyocyte size and pulmonary vascular remodeling as indicators of pulmonary hypertension in wildtype mice, while p22phox-deficient mice were protected. Moreover, pulmonary vascular remodeling, which is associated with increased proliferation of vascular cells, was also blunted in dexamethasone treated mice deficient in HIF1 α in endothelial or smooth muscle cells further emphasizing the importance of the NADPH oxidase-HIF signaling axis in the cardiovascular response to chronic dexamethasone treatment.

Pulmonary hypertension secondary to left-sided heart disease (WHO Group II) is a frequent complication of heart failure, and increased pulmonary artery pressure in patients with heart failure often represents a combination of increased left-sided filling pressures (“passive” component) and elevated pulmonary vascular resistance due to functional and structural abnormalities of the pulmonary vascular bed (“reactive” component) (426).

Initiation of pulmonary vascular remodeling has been associated with endothelial dysfunction and vascular damage, and ROS have been implicated in these responses. Increased ROS generation by NADPH oxidases has been suggested to lead to pulmonary vascular remodeling in response to monocrotaline, a pulmonary toxin (427, 428). Moreover, HIF1 α has been described to contribute to pulmonary vascular remodeling in response to hypoxia (256, 429, 430), and in several models of non-hypoxic pulmonary hypertension (251, 431). Thus, one might speculate that chronic exposure to dexamethasone would elicit endothelial dysfunction and vascular damage, due to an increased ROS load, leading to pulmonary vascular remodeling by activating the HIF pathway and subsequently to pulmonary hypertension.

In contrast, dexamethasone has been described to act beneficially in different models of pulmonary hypertension (400, 432, 433). While the reasons for these discrepant findings are not fully elucidated they might be in close relation to the findings that dexamethasone exerts clearly different action in normal “healthy” cells and tissues compared to diseased, predamaged cells and tissues. Moreover, most studies only covered rather short term periods of dexamethasone treatment which might have not been sufficiently long for pulmonary hypertension to develop as a secondary event to left ventricular dysfunction.

In conclusion, this study identified NADPH oxidases and the HIF pathway as targets of dexamethasone in the cardiovascular system where they promote proliferative responses at

the cellular level and induce hypertension, dilated cardiomyopathy and pulmonary hypertension upon long term systemic treatment with dexamethasone.

Thus, application of NADPH oxidase or HIF inhibitors might be interesting strategies to prevent long term complications of dexamethasone treatment.

8.3.β3-endonexin as a novel negative regulator of hypoxia inducible factor 1

The data of the following study investigating the role of β3-endonexin in the context of hypoxia have been previously published (228). Permission to use the figures and the text of the paper was obtained from *Antioxidants&Redox Signaling* (Appendix, p.143).

The family of integrins regulates key processes in the vasculature which are important for hypoxic survival such as proliferation and angiogenesis. The β3-integrin binding protein β3-endonexin has been suggested to regulate the function of β3-integrin under normoxia. This study demonstrates that β3-endonexin acts as a novel anti-angiogenic and anti-proliferative molecule under hypoxic conditions (228). Mechanistically, β3-endonexin accumulated in the nucleus following exposure to hypoxia where it decreased NFκB activation thus contributing to the decline in HIF1α mRNA and HIF1α protein levels after the onset of prolonged hypoxia (228).

αβ3-integrins were suggested to play an important role in the control of angiogenesis, although the precise mechanisms of action remain under dispute (234). It has been suggested that αβ3-integrins may interact with multiple players in the angiogenic pathway and, depending on the interaction, have either pro-angiogenic or anti-angiogenic effects (228, 434).

In this study, it is shown that the β3-integrin binding protein β3-endonexin is able to negatively control endothelial proliferation and angiogenic responses both *in vitro* and *in vivo* under hypoxic conditions (228).

β3-endonexin has been initially reported to exist in two alternatively spliced isoforms: the long (EN-L) and short (EN-S) (235). However, only EN-S has been identified as a binding protein to the cytoplasmic tail of β3-integrin (235), while both EN-S and EN-L have been shown to bind cyclin A (238, 239). Similarly, in this study, EN-S as well as EN-L were able to decrease the angiogenic response toward hypoxia, indicating that β3-endonexin isoforms can act as anti-angiogenic molecules beyond their functions in regulating avidity and, thus, ligand-binding affinity of β3-integrin (228).

Furthermore the anti-angiogenic function of β3-endonexin was linked to the family of HIFs (228, 411), which have been described to promote angiogenesis under hypoxia due to up-regulation of important proangiogenic factors such as VEGF and PAI1 (228, 411). In fact, VEGF and PAI1 expression was enhanced in hypoxic β3-endonexin-deficient cells (228). Moreover, the depletion of HIF1α prevented enhanced tube formation in β3-endonexin-

deficient cells under hypoxia, while the overexpression of β 3-endonexin diminished hypoxic as well as VEGF-induced tube formation, indicating a close link between the HIF pathway and β 3-endonexin in the angiogenic response (228).

In fact, this study indicated that β 3-endonexin can act as a negative regulator of HIF activity under hypoxic conditions, as hypoxic HIF activity and HIF1 α protein levels were decreased in endothelial cells overexpressing either EN-L or EN-S (228). On the contrary, in β 3-endonexin-deficient cells, the hypoxic induction of HIF activity and HIF1 α protein levels was further enhanced (228). Interestingly, this effect was specific to HIF1 α , as the induction of HIF2 α by hypoxia was not affected by the depletion of β 3-endonexin (228). Moreover, in contrast to HIF1 α or HIF2 α , the protein as well as mRNA levels of β 3-endonexin remained constant over a period of intermediate hypoxia, indicating that the inhibitory effect of β 3-endonexin on the HIF pathway in this timeframe was not primarily mediated by increased expression of EN-L or EN-S under hypoxic conditions (228). However, upon onset of prolonged hypoxia or in an animal model of chronic hypoxia, β 3-endonexin mRNA levels were elevated (228). While one cannot rule out that upon prolonged hypoxic stress, up-regulation of β 3-endonexin expression might also be relevant for its response to hypoxia, this study clearly showed that the primary response of β 3-endonexin to hypoxia is translocation to and accumulation in the nucleus (228). This mechanism was independent of integrin binding and might be facilitated by the presence of a nuclear localization sequence in the β 3-endonexin protein (228, 235).

While HIF1 α levels are predominantly regulated by hypoxia *via* a complex mechanism of protein stabilization, HIF1 α mRNA levels seem to be differentially affected by hypoxia in different cellular and organismal systems (435). Besides this study, others have reported that hypoxia induces a rapid but transient increase in HIF1 α mRNA levels followed by a decline in prolonged hypoxia in smooth muscle and other cells (12, 38). Interestingly, a similar response to hypoxia in endothelial cells was observed in this study (228). However, when cells were depleted from β 3-endonexin, the decline in HIF1 α mRNA levels on prolonged exposure to hypoxia was abrogated (228). These novel findings indicated that β 3-endonexin might be involved in regulating HIF1 α mRNA levels under hypoxia (228).

It was previously shown that HIF1 α is a NF κ B target gene (12, 37), an observation that has been confirmed in inflammatory conditions both *in vitro* and *in vivo* (38). Furthermore, it was shown that NF κ B contributes to the transient induction of HIF1 α mRNA in response to hypoxia (12, 228). In support, this study demonstrated that hypoxia increased NF κ B transcriptional activity in endothelial cells but β 3-endonexin was able to prevent the activation of NF κ B by hypoxia (228). Importantly, β 3-endonexin was able to negatively affect NF κ B-mediated HIF1 α transcription under hypoxia (228). This assumption was supported by

findings of this study - forced expression of p50/p65 not only enhanced hypoxic HIF1 α mRNA levels but also prevented its decline on prolonged hypoxic exposure; while expression of an I κ Bdn that prevents activation of NF κ B not only diminished the hypoxic up-regulation of HIF1 α mRNA levels in the absence of β 3-endonexin, but also prevented endothelial proliferation and angiogenesis in β 3-endonexin-deficient hypoxic cells (228). Moreover, the increase in hypoxic HIF1 α promoter activity upon depletion of β 3-endonexin was completely blunted when the NF κ B-binding site within the HIF1 α promoter that binds a p50/p65 complex (12, 38) was mutated (228). Importantly, hypoxic binding of the NF κ B protein p65 to the HIF1 α promoter was decreased upon overexpression of EN-L, suggesting that NF κ B binding to the HIF1 α promoter is prevented by β 3-endonexin (228). In line, β 3-endonexin has been reported to inhibit NF κ B activity by binding and sterically blocking the active p50/p65 complex (228, 240). These findings support a model by which under hypoxic conditions β 3-endonexin translocates to the nucleus, binds to the p50/p65 complex, and, subsequently, prevents HIF1 α transcription and induction of HIF1 α mRNA (228). These findings also indicate that β 3-endonexin is a novel regulator of the hypoxic response in endothelial cells by modulating the induction and activation of HIF1 α (228).

Although transcriptional regulation and *de novo* synthesis of HIF1 α take place under various conditions, in many cases regulated by NF κ B (12, 38), this pathway may be less favourable under hypoxic conditions, where protein synthesis is limited (228). By activation of β 3-endonexin as an endogenous inhibitor of HIF1 α transcription under hypoxic conditions, the stabilization of HIF1 α protein due to the inhibition of prolyl hydroxylases (PHD) activity will be favored, thus enabling a rapid and efficient provision of HIF1 α not affecting protein synthesis machinery (228). Since HIF1 α mRNA levels will not be replenished due to β 3-endonexin blockade of NF κ B as a major transcription factor regulating HIF1 α , HIF1 α mRNA levels will decline on prolonged exposure to hypoxia, a situation that might be overcome by enhanced levels of p50 and p65 exceeding the levels of β 3-endonexin (228).

This study further suggest that the inhibition of NF κ B-dependent transcription under hypoxia by β 3-endonexin might not only be limited to HIF1 α , as this protein is also able to negatively regulate hypoxic activation of the NF κ B target gene - tissue factor (TF) (228). Along with the findings of this study that under hypoxic conditions β 3-endonexin accumulates in the nucleus, these data suggest that this protein might be a negative regulator of NF κ B-dependent gene expression under hypoxia (228).

Taken together, this study indicates that β 3-endonexin is a novel anti-angiogenic factor which is specifically important in the response to hypoxia due to the inhibition of NF κ B-dependent up-regulation of HIF1 α and, subsequently, HIF1 activity and HIF1-dependent pro-angiogenic target gene expression (228).

8.4. The NADPH oxidase NOX4 activates the ATM-CHK2-p53 pathway in response to oxaliplatin

The therapeutic success of common chemotherapy drugs, such as oxaliplatin, is often limited as resistance to therapy can occur. This study showed that oxaliplatin can induce ROS generation involving the NADPH oxidase NOX4. Subsequently, this pathway resulted in activation of the ATM-dependent canonical double-strand DNA damage response (dsDDR) in melanoma cells. This assumption was based on findings that oxaliplatin-treated melanoma cells showed increased NOX4-dependent ROS generation in conjunction with elevated NOX4 levels, which were mediated by the transcription factor HIF1. Oxaliplatin increased phosphorylation of ATM and CHK2 and elevated the levels of p53 and γ H2AX dependent on NOX4 and ROS generation. Subsequently, oxaliplatin decreased DNA synthesis and the levels of the proliferation marker Ki67. However, no evidence for cleavage of PARP1, caspase 3 or caspase 7 as markers for programmed cell death was observed. Instead, oxaliplatin increased p21 levels indicative of cellular senescence

Previously, high concentrations of platinum salts, in particular cisplatin have been shown to increase ROS levels in several tumor cell lines (436-438) including melanoma cells (438). More recently, also newer platinum compounds such as oxaliplatin which differs from cisplatin in that the amine groups of cisplatin are replaced by diaminocyclohexane (dach) (439) have been described to promote ROS generation in colon cancer cells (440, 441), liver cancer cells or neuroblastoma cells (442, 443).

However, compared to our study in melanoma cells, oxaliplatin concentrations applied were at least 10 times higher than in our study.

In addition, ROS generation was maximal only after 16 h and could be inhibited by the unspecific NADPH oxidase inhibitor apocynin. In fact, oxaliplatin induced NOX4, but not NOX1 levels, concomitant with decreased ROS generation by NOX4 depletion and to a much lesser extent by NOX1 depletion. These data strongly indicate that induction of NOX4 is primarily responsible for the delayed and regulated ROS response elicited by oxaliplatin. In melanoma cells, NOX4 depletion has been shown to decrease spontaneous ROS generation (319), although in this study depletion of NOX4 or NOX1 did not result in a significant decrease in superoxide levels in non-treated cells. In contrast, in colon cancer cells, NOX1 was reported to mediate oxaliplatin-induced ROS generation (444), while NOX4 has been linked to ROS production in response to cisplatin in renal cancer cells (445). In the ear, both NOX1 and NOX4 contributed to cisplatin induced ROS generation (446). These findings

strongly suggest that NADPH oxidases are important players in the response to platinum salts in tumor and non-tumor cells.

Concomitant with the NOX4 protein increase in oxaliplatin-treated melanoma cells HIF1 α protein was increased as well. While depletion of HIF1 α reduced NOX4 expression, NOX4 did not affect HIF1 α protein levels, indicating that HIF1 is upstream of NOX4. In line previous studies identified NOX4 as a genuine HIF1 target gene (304). This study further shows that oxaliplatin not only time-dependently increased the levels of NOX4, but concomitantly induced the levels of phosphorylated ATM, H2AX and CHK2, as well as of p53 indicating that NOX4 induction is closely associated with activation of dsDDR. In line, proteomic studies predicted DDR as a primary response to oxaliplatin in colon cancer cells (447).

A direct involvement of NOX4-derived ROS in the dsDDR was confirmed by findings in this study, that not only the antioxidant ascorbate but also depletion of NOX4 prevented upregulation of p-ATM, γ H2AX and p-CHK2, as well as of p53, in the response to oxaliplatin. Previous studies showed that silencing NOX4 by siRNA inhibited psoralidin-induced ROS generation and DNA damage response (448).

Although recent data suggest that ATM is important not only for DNA damage responses but also for maintenance of cellular redox homeostasis and can be directly oxidized (449) this is the first study showing that NOX4 is involved in ATM phosphorylation in response to oxaliplatin.

Interestingly, ATM has been shown to regulate NOX4 thus suggesting a positive feedback loop in the initiation of dsDDR (450).

While CHK2 phosphorylation has not been linked to NOX4 to date in melanoma models, recent data showed that downregulation of NOX4 decreased γ H2AX levels in thyrocytes or human embryonic lung fibroblasts overexpressing oncogenic Ras (451, 452). Together, these data clearly demonstrate that NOX4 plays an important role in controlling activation and promotion of dsDDR also in a clinically relevant model of chemotherapeutic response.

In line with this assumption this study shows that NOX4 was also involved in the upregulation of p53 since depletion of NOX4 prevented induction of this protein by oxaliplatin. In support, NOX4 depletion decreased the levels of p53 in fibroblasts overexpressing active Ras (451), and in epithelial cells, dominant-negative NOX4 prevented induction of p53 by high glucose (453). In contrast, depletion of NOX4 enhanced p53 levels in PDGF-treated HS68 cells (454) indicating that NOX4 is involved in the cell and stimulus dependent fine tuning of p53.

The p53 tumor suppressor was initially identified as the 'guardian of the genome' based on its ability to mediate a G1 arrest following DNA damage. However, p53 is now known to act

in many cellular processes, including cell-cycle checkpoints, DNA repair, senescence, and programmed cell death (455).

Interestingly, p53 wildtype caused dose-dependent suppression of NOX4 transcription by TGF β while mutated p53 increased NOX4 expression via binding to SMAD3 binding elements (SBE) and p53 response elements in a TGF β -dependent manner (456). These findings further suggest a negative feedback loop where increased (wild type) p53 levels following NOX4 activation would downregulate this pathway again. However, in the context of p53 mutations in tumors this control pathway might be non-functional thus leading to tumor progression.

Reciprocal to the induction of NOX4, p53 and the dsDDR markers in the course of oxaliplatin treatment the levels of Ki67 which indicates active cell cycle and mitosis, were decreased. Concomitantly, DNA synthesis was decreased upon exposure to higher concentrations of oxaliplatin.

However, there was no evidence for cleavage of poly (ADP-ribose) polymerase (PARP1) protein or caspases 3 or 7. In support with findings that low concentrations of oxaliplatin induce a proliferative halt but not programmed cell death, PARP1 cleavage has been suggested to require high concentrations of oxaliplatin in several tumor cell lines and has been associated with decreased p53 levels in melanoma (457, 458). Moreover, oxaliplatin increased the levels of p21, a cyclin-dependent kinase inhibitor which is able to inhibit cyclin/CDK complexes. As a major target of p53, it thus links DNA damage to cell cycle arrest (459). In line, upregulation of p21 and induction of senescence by oxaliplatin has been observed in liver cancer cells (460). Further studies will have to confirm that oxaliplatin also induces senescence in melanoma cells.

Furthermore, while depletion of NOX4 decreased oxaliplatin induction of p53, Ki67 levels did not decrease in NOX4-depleted cells, but remained unchanged or even increased, suggesting that NOX4 promoted dsDDR to induce a proliferative halt rather than programmed cell death.

In contrast, depletion of NOX4 has been associated with decreased growth and enhanced cytotoxicity towards platinum salts in glioma and renal cancer cells (320, 445). NOX4 was suggested to promote proliferation of melanoma cells, due to activation of cdc25 and CDK1 (cdc2) kinase and subsequently G₂-M cell cycle progression although a link to p53 has not been demonstrated (319, 461).

However, in support with findings of this study, in models of oncogenic growth arrest induced by overexpression of active H-Ras in non-tumor cells, depletion of NOX4 or NOX1 partially

prevented growth arrest concomitant with decreased levels of γ H2AX, p53 and p21, and partially counteracted H-RasV12 induced senescence (453, 462).

Taken together, this study provides evidence that NOX4 is essentially modulating the ATM-CHK2-p53 axis of dsDDR in oxaliplatin treated cells thereby promoting a proliferative halt without effect on PCD. Since NOX4 expression has been described in metastatic melanoma cells NOX4 might serve as an interesting stratification marker towards oxaliplatin and possibly other DNA-damaging therapeutic regimens in melanoma or other tumor entities.

8.5. Concluding remarks

These studies show complexity and many facets of oxygen signaling. Low oxygen tension (hypoxia) induces the stabilization of HIF1 α thus directly promoting proliferative and angiogenic responses in endothelial cells. On the other hand, these studies show that HIF1 α can be regulated by a variety of stimuli through redox signaling involving HIF1 α protein stabilization or modulation of transcriptional regulation and is even linked to alterations in cell adhesion receptors (e.g. integrins). Furthermore in normoxic conditions dexamethasone was able to promote these responses by inducing the ROS production from NADPH oxidases which in turn stabilized HIF1 α protein levels. Hypoxia, however, decreased NO production in endothelial cells by uncoupling eNOS thus limiting the hypoxic ROS production to this source, and consequently decreased hypoxic ROS levels.

ROS signaling was involved in the in vivo cardiopulmonary response towards chronic hypoxia and dexamethasone treatment. While HIF signaling has been previously associated with hypoxia-induced pulmonary hypertension, this study now shows that HIF is closely linked to redox signaling also in the response to dexamethasone. That HIF1 α and ROS signaling have a strong importance in the cellular response to a variety of stressors was further confirmed in cancer cells, as the chemotherapeutic oxaliplatin was shown to induce HIF1 α *via* ROS in melanoma cells.

From a translational side these studies show the value of folic acid supplementation in conditions where local hypoxia and disturbed ROS/NO balance play a role, such as in pulmonary hypertension. In addition, a novel anti-angiogenic protein β 3-endonexin was described which may serve to combat pathologies in which angiogenesis plays an important role such as in cancer. Moreover, evidence was provided that chronic treatment with dexamethasone, one of the most widely used drugs on the market, can have side effects not only in the systemic but also in the pulmonary vasculature, and that treatment with NADPH oxidase inhibitors which are currently extensively searched for, might help to prevent these side effects. Finally, findings in this study that NOX4 expression correlates with dsDDR marker expression in response to oxaliplatin point to the potential of NOX4 as a surrogate stratification marker for this treatment regimen in melanoma and possibly other cancer entities.

9 Literature

1. Mailloux RJ. Teaching the fundamentals of electron transfer reactions in mitochondria and the production and detection of reactive oxygen species. *Redox biology*. 2015;4:381-98.
2. Han CH, Freeman JL, Lee T, Motalebi SA, Lambeth JD. Regulation of the neutrophil respiratory burst oxidase. Identification of an activation domain in p67(phox). *The Journal of biological chemistry*. 1998;273(27):16663-8.
3. Sosa Torres ME, Saucedo-Vazquez JP, Kroneck PM. The magic of dioxygen. *Metal ions in life sciences*. 2015;15:1-12.
4. Lesser MP. Oxidative stress in marine environments: biochemistry and physiological ecology. *Annual review of physiology*. 2006;68:253-78.
5. Bruce Alberts AJ, Julian Lewis, Martin Raff, Keith Roberts, and Peter Walter. *Molecular Biology of the Cell*. 4th ed 2002 2002.
6. Semenza GL. Life with oxygen. *Science*. 2007;318(5847):62-4.
7. Bishop T, Ratcliffe PJ. Signaling hypoxia by hypoxia-inducible factor protein hydroxylases: a historical overview and future perspectives. *Hypoxia*. 2014;2:197-213.
8. Wang GL, Semenza GL. Purification and characterization of hypoxia-inducible factor 1. *The Journal of biological chemistry*. 1995;270(3):1230-7.
9. Semenza GL, Roth PH, Fang HM, Wang GL. Transcriptional regulation of genes encoding glycolytic enzymes by hypoxia-inducible factor 1. *The Journal of biological chemistry*. 1994;269(38):23757-63.
10. Semenza GL. Hypoxia. Cross talk between oxygen sensing and the cell cycle machinery. *American journal of physiology Cell physiology*. 2011;301(3):C550-2.
11. Hirota K, Semenza GL. Regulation of angiogenesis by hypoxia-inducible factor 1. *Critical reviews in oncology/hematology*. 2006;59(1):15-26.
12. Belaiba RS, Bonello S, Zahringer C, Schmidt S, Hess J, Kietzmann T, et al. Hypoxia up-regulates hypoxia-inducible factor-1alpha transcription by involving phosphatidylinositol 3-kinase and nuclear factor kappaB in pulmonary artery smooth muscle cells. *Molecular biology of the cell*. 2007;18(12):4691-7.
13. Goldberg MA, Dunning SP, Bunn HF. Regulation of the erythropoietin gene: evidence that the oxygen sensor is a heme protein. *Science*. 1988;242(4884):1412-5.
14. Semenza GL. Hypoxia-inducible factor 1: master regulator of O₂ homeostasis. *Current opinion in genetics & development*. 1998;8(5):588-94.
15. Semenza GL, Neifelt MK, Chi SM, Antonarakis SE. Hypoxia-inducible nuclear factors bind to an enhancer element located 3' to the human erythropoietin gene. *Proceedings of the National Academy of Sciences of the United States of America*. 1991;88(13):5680-4.
16. Ke Q, Costa M. Hypoxia-inducible factor-1 (HIF-1). *Mol Pharmacol*. 2006;70(5):1469-80.
17. Ratcliffe PJ. HIF-1 and HIF-2: working alone or together in hypoxia? *The Journal of clinical investigation*. 2007;117(4):862-5.
18. Tian H, McKnight SL, Russell DW. Endothelial PAS domain protein 1 (EPAS1), a transcription factor selectively expressed in endothelial cells. *Genes & development*. 1997;11(1):72-82.
19. O'Rourke JF, Tian YM, Ratcliffe PJ, Pugh CW. Oxygen-regulated and transactivating domains in endothelial PAS protein 1: comparison with hypoxia-inducible factor-1alpha. *The Journal of biological chemistry*. 1999;274(4):2060-71.
20. Gu YZ, Moran SM, Hogenesch JB, Wartman L, Bradfield CA. Molecular characterization and chromosomal localization of a third alpha-class hypoxia inducible factor subunit, HIF3alpha. *Gene expression*. 1998;7(3):205-13.
21. Makino Y, Cao R, Svensson K, Bertilsson G, Asman M, Tanaka H, et al. Inhibitory PAS domain protein is a negative regulator of hypoxia-inducible gene expression. *Nature*. 2001;414(6863):550-4.

22. Wang GL, Jiang BH, Rue EA, Semenza GL. Hypoxia-inducible factor 1 is a basic-helix-loop-helix-PAS heterodimer regulated by cellular O₂ tension. *Proceedings of the National Academy of Sciences of the United States of America*. 1995;92(12):5510-4.
23. Hirsila M, Koivunen P, Gunzler V, Kivirikko KI, Myllyharju J. Characterization of the human prolyl 4-hydroxylases that modify the hypoxia-inducible factor. *The Journal of biological chemistry*. 2003;278(33):30772-80.
24. Ivan M, Kondo K, Yang H, Kim W, Valiando J, Ohh M, et al. HIF α targeted for VHL-mediated destruction by proline hydroxylation: implications for O₂ sensing. *Science*. 2001;292(5516):464-8.
25. Jaakkola P, Mole DR, Tian YM, Wilson MI, Gielbert J, Gaskell SJ, et al. Targeting of HIF- α to the von Hippel-Lindau ubiquitylation complex by O₂-regulated prolyl hydroxylation. *Science*. 2001;292(5516):468-72.
26. Masson N, Willam C, Maxwell PH, Pugh CW, Ratcliffe PJ. Independent function of two destruction domains in hypoxia-inducible factor- α chains activated by prolyl hydroxylation. *The EMBO journal*. 2001;20(18):5197-206.
27. Yu F, White SB, Zhao Q, Lee FS. HIF-1 α binding to VHL is regulated by stimulus-sensitive proline hydroxylation. *Proceedings of the National Academy of Sciences of the United States of America*. 2001;98(17):9630-5.
28. Srinivas V, Zhang LP, Zhu XH, Caro J. Characterization of an oxygen/redox-dependent degradation domain of hypoxia-inducible factor α (HIF- α) proteins. *Biochemical and biophysical research communications*. 1999;260(2):557-61.
29. Epstein AC, Gleadle JM, McNeill LA, Hewitson KS, O'Rourke J, Mole DR, et al. *C. elegans* EGL-9 and mammalian homologs define a family of dioxygenases that regulate HIF by prolyl hydroxylation. *Cell*. 2001;107(1):43-54.
30. Maxwell PH, Wiesener MS, Chang GW, Clifford SC, Vaux EC, Cockman ME, et al. The tumour suppressor protein VHL targets hypoxia-inducible factors for oxygen-dependent proteolysis. *Nature*. 1999;399(6733):271-5.
31. Cockman ME, Masson N, Mole DR, Jaakkola P, Chang GW, Clifford SC, et al. Hypoxia inducible factor- α binding and ubiquitylation by the von Hippel-Lindau tumor suppressor protein. *The Journal of biological chemistry*. 2000;275(33):25733-41.
32. Ohh M, Park CW, Ivan M, Hoffman MA, Kim TY, Huang LE, et al. Ubiquitination of hypoxia-inducible factor requires direct binding to the beta-domain of the von Hippel-Lindau protein. *Nature cell biology*. 2000;2(7):423-7.
33. Tanimoto K, Makino Y, Pereira T, Poellinger L. Mechanism of regulation of the hypoxia-inducible factor-1 α by the von Hippel-Lindau tumor suppressor protein. *The EMBO journal*. 2000;19(16):4298-309.
34. Lando D, Peet DJ, Gorman JJ, Whelan DA, Whitelaw ML, Bruick RK. FIH-1 is an asparaginyl hydroxylase enzyme that regulates the transcriptional activity of hypoxia-inducible factor. *Genes & development*. 2002;16(12):1466-71.
35. Kaelin WG, Jr., Ratcliffe PJ. Oxygen sensing by metazoans: the central role of the HIF hydroxylase pathway. *Molecular cell*. 2008;30(4):393-402.
36. Semenza GL. Regulation of cancer cell metabolism by hypoxia-inducible factor 1. *Seminars in cancer biology*. 2009;19(1):12-6.
37. Bonello S, Zahringer C, BelAiba RS, Djordjevic T, Hess J, Michiels C, et al. Reactive oxygen species activate the HIF-1 α promoter via a functional NF κ B site. *Arteriosclerosis, thrombosis, and vascular biology*. 2007;27(4):755-61.
38. Rius J, Guma M, Schachtrup C, Akassoglou K, Zinkernagel AS, Nizet V, et al. NF- κ B links innate immunity to the hypoxic response through transcriptional regulation of HIF-1 α . *Nature*. 2008;453(7196):807-11.
39. Gorlach A, Bonello S. The cross-talk between NF- κ B and HIF-1: further evidence for a significant liaison. *The Biochemical journal*. 2008;412(3):e17-9.
40. Kehrer JP. The Haber-Weiss reaction and mechanisms of toxicity. *Toxicology*. 2000;149(1):43-50.
41. Haber F. WJ. Über die Katalyse des Hydroperoxydes *Naturwissenschaften*. 1932;20(51):948-50.

42. Droge W. Free radicals in the physiological control of cell function. *Physiological reviews*. 2002;82(1):47-95.
43. Fenton HJH. Oxidation of tartaric acid in presence of iron. *Journal of the Chemical Society, Transactions*. 1894;65:899-910.
44. Fridovich I, Freeman B. Antioxidant defenses in the lung. *Annual review of physiology*. 1986;48:693-702.
45. Weisiger RA, Fridovich I. Superoxide dismutase. Organelle specificity. *The Journal of biological chemistry*. 1973;248(10):3582-92.
46. Crapo JD, Oury T, Rabouille C, Slot JW, Chang LY. Copper,zinc superoxide dismutase is primarily a cytosolic protein in human cells. *Proceedings of the National Academy of Sciences of the United States of America*. 1992;89(21):10405-9.
47. Okado-Matsumoto A, Fridovich I. Subcellular distribution of superoxide dismutases (SOD) in rat liver: Cu,Zn-SOD in mitochondria. *The Journal of biological chemistry*. 2001;276(42):38388-93.
48. Sturtz LA, Diekert K, Jensen LT, Lill R, Culotta VC. A fraction of yeast Cu,Zn-superoxide dismutase and its metallochaperone, CCS, localize to the intermembrane space of mitochondria. A physiological role for SOD1 in guarding against mitochondrial oxidative damage. *The Journal of biological chemistry*. 2001;276(41):38084-9.
49. Flohe L. Glutathione peroxidase. *Basic life sciences*. 1988;49:663-8.
50. Arthur JR. The glutathione peroxidases. *Cellular and molecular life sciences : CMLS*. 2000;57(13-14):1825-35.
51. Chu FF, Doroshov JH, Esworthy RS. Expression, characterization, and tissue distribution of a new cellular selenium-dependent glutathione peroxidase, GSHPx-GI. *The Journal of biological chemistry*. 1993;268(4):2571-6.
52. Ricciardolo FL, Sterk PJ, Gaston B, Folkerts G. Nitric oxide in health and disease of the respiratory system. *Physiological reviews*. 2004;84(3):731-65.
53. Rahman I, Biswas SK, Kode A. Oxidant and antioxidant balance in the airways and airway diseases. *European journal of pharmacology*. 2006;533(1-3):222-39.
54. Kietzmann T, Gorkach A. Reactive oxygen species in the control of hypoxia-inducible factor-mediated gene expression. *Seminars in cell & developmental biology*. 2005;16(4-5):474-86.
55. Jackson SP, Bartek J. The DNA-damage response in human biology and disease. *Nature*. 2009;461(7267):1071-8.
56. Khanna KK, Jackson SP. DNA double-strand breaks: signaling, repair and the cancer connection. *Nature genetics*. 2001;27(3):247-54.
57. Harper JW, Elledge SJ. The DNA damage response: ten years after. *Molecular cell*. 2007;28(5):739-45.
58. Harrison JC, Haber JE. Surviving the breakup: the DNA damage checkpoint. *Annual review of genetics*. 2006;40:209-35.
59. Jackson SP. Sensing and repairing DNA double-strand breaks. *Carcinogenesis*. 2002;23(5):687-96.
60. Serrano M, Blasco MA. Putting the stress on senescence. *Current opinion in cell biology*. 2001;13(6):748-53.
61. Chen Z, Trotman LC, Shaffer D, Lin HK, Dotan ZA, Niki M, et al. Crucial role of p53-dependent cellular senescence in suppression of Pten-deficient tumorigenesis. *Nature*. 2005;436(7051):725-30.
62. Burma S, Chen BP, Murphy M, Kurimasa A, Chen DJ. ATM phosphorylates histone H2AX in response to DNA double-strand breaks. *The Journal of biological chemistry*. 2001;276(45):42462-7.
63. Tanaka T, Kurose A, Huang X, Dai W, Darzynkiewicz Z. ATM activation and histone H2AX phosphorylation as indicators of DNA damage by DNA topoisomerase I inhibitor topotecan and during apoptosis. *Cell Prolif*. 2006;39(1):49-60.
64. Bartkova J, Horejsi Z, Koed K, Kramer A, Tort F, Zieger K, et al. DNA damage response as a candidate anti-cancer barrier in early human tumorigenesis. *Nature*. 2005;434(7035):864-70.

65. Nuciforo PG, Luise C, Capra M, Pelosi G, d'Adda di Fagagna F. Complex engagement of DNA damage response pathways in human cancer and in lung tumor progression. *Carcinogenesis*. 2007;28(10):2082-8.
66. D'Autreaux B, Toledano MB. ROS as signalling molecules: mechanisms that generate specificity in ROS homeostasis. *Nature reviews Molecular cell biology*. 2007;8(10):813-24.
67. Finkel T. From sulfenylation to sulfhydration: what a thiolate needs to tolerate. *Science signaling*. 2012;5(215):pe10.
68. Chen YR, Zweier JL. Cardiac mitochondria and reactive oxygen species generation. *Circulation research*. 2014;114(3):524-37.
69. Nicholls DG. Mitochondrial ion circuits. *Essays in biochemistry*. 2010;47:25-35.
70. Goncalves RL, Rothschild DE, Quinlan CL, Scott GK, Benz CC, Brand MD. Sources of superoxide/H₂O₂ during mitochondrial proline oxidation. *Redox biology*. 2014;2:901-9.
71. Hey-Mogensen M, Goncalves RL, Orr AL, Brand MD. Production of superoxide/H₂O₂ by dihydroorotate dehydrogenase in rat skeletal muscle mitochondria. *Free radical biology & medicine*. 2014;72:149-55.
72. Quinlan CL, Orr AL, Perevoshchikova IV, Treberg JR, Ackrell BA, Brand MD. Mitochondrial complex II can generate reactive oxygen species at high rates in both the forward and reverse reactions. *The Journal of biological chemistry*. 2012;287(32):27255-64.
73. Zhang J, Ferman FE, Kim JJ. Structure of electron transfer flavoprotein-ubiquinone oxidoreductase and electron transfer to the mitochondrial ubiquinone pool. *Proceedings of the National Academy of Sciences of the United States of America*. 2006;103(44):16212-7.
74. Shabalina IG, Vrbacky M, Pecinova A, Kalinovich AV, Drahota Z, Houstek J, et al. ROS production in brown adipose tissue mitochondria: the question of UCP1-dependence. *Biochimica et biophysica acta*. 2014;1837(12):2017-30.
75. Lagoutte E, Mimoun S, Andriamihaja M, Chaumontet C, Blachier F, Bouillaud F. Oxidation of hydrogen sulfide remains a priority in mammalian cells and causes reverse electron transfer in colonocytes. *Biochimica et biophysica acta*. 2010;1797(8):1500-11.
76. Quinlan CL, Goncalves RL, Hey-Mogensen M, Yadava N, Bunik VI, Brand MD. The 2-oxoacid dehydrogenase complexes in mitochondria can produce superoxide/hydrogen peroxide at much higher rates than complex I. *The Journal of biological chemistry*. 2014;289(12):8312-25.
77. Quinlan CL, Perevoshchikova IV, Hey-Mogensen M, Orr AL, Brand MD. Sites of reactive oxygen species generation by mitochondria oxidizing different substrates. *Redox biology*. 2013;1:304-12.
78. Perevoshchikova IV, Quinlan CL, Orr AL, Gerencser AA, Brand MD. Sites of superoxide and hydrogen peroxide production during fatty acid oxidation in rat skeletal muscle mitochondria. *Free radical biology & medicine*. 2013;61:298-309.
79. Turrens JF, Boveris A. Generation of superoxide anion by the NADH dehydrogenase of bovine heart mitochondria. *The Biochemical journal*. 1980;191(2):421-7.
80. Turrens JF, Alexandre A, Lehninger AL. Ubisemiquinone is the electron donor for superoxide formation by complex III of heart mitochondria. *Archives of biochemistry and biophysics*. 1985;237(2):408-14.
81. Chen Q, Vazquez EJ, Moghaddas S, Hoppel CL, Lesnefsky EJ. Production of reactive oxygen species by mitochondria: central role of complex III. *The Journal of biological chemistry*. 2003;278(38):36027-31.
82. Herrero A, Barja G. Sites and mechanisms responsible for the low rate of free radical production of heart mitochondria in the long-lived pigeon. *Mechanisms of ageing and development*. 1997;98(2):95-111.
83. St-Pierre J, Buckingham JA, Roebuck SJ, Brand MD. Topology of superoxide production from different sites in the mitochondrial electron transport chain. *The Journal of biological chemistry*. 2002;277(47):44784-90.
84. Gorlach A, Kietzmann T, Hess J. Redox signaling through NADPH oxidases: involvement in vascular proliferation and coagulation. *Annals of the New York Academy of Sciences*. 2002;973:505-7.
85. Lambeth JD, Kawahara T, Diebold B. Regulation of Nox and Duox enzymatic activity and expression. *Free radical biology & medicine*. 2007;43(3):319-31.

86. Lambeth JD. NOX enzymes and the biology of reactive oxygen. *Nature reviews Immunology*. 2004;4(3):181-9.
87. Royer-Pokora B, Kunkel LM, Monaco AP, Goff SC, Newburger PE, Baehner RL, et al. Cloning the gene for an inherited human disorder--chronic granulomatous disease--on the basis of its chromosomal location. *Nature*. 1986;322(6074):32-8.
88. Teahan C, Rowe P, Parker P, Totty N, Segal AW. The X-linked chronic granulomatous disease gene codes for the beta-chain of cytochrome b-245. *Nature*. 1987;327(6124):720-1.
89. Parkos CA, Dinauer MC, Jesaitis AJ, Orkin SH, Curnutte JT. Absence of both the 91kD and 22kD subunits of human neutrophil cytochrome b in two genetic forms of chronic granulomatous disease. *Blood*. 1989;73(6):1416-20.
90. Dinauer MC, Pierce EA, Bruns GA, Curnutte JT, Orkin SH. Human neutrophil cytochrome b light chain (p22-phox). Gene structure, chromosomal location, and mutations in cytochrome-negative autosomal recessive chronic granulomatous disease. *The Journal of clinical investigation*. 1990;86(5):1729-37.
91. Stasia MJ, Bordigoni P, Martel C, Morel F. A novel and unusual case of chronic granulomatous disease in a child with a homozygous 36-bp deletion in the CYBA gene (A22(0)) leading to the activation of a cryptic splice site in intron 4. *Human genetics*. 2002;110(5):444-50.
92. Sumimoto H, Hata K, Mizuki K, Ito T, Kage Y, Sakaki Y, et al. Assembly and activation of the phagocyte NADPH oxidase. Specific interaction of the N-terminal Src homology 3 domain of p47phox with p22phox is required for activation of the NADPH oxidase. *The Journal of biological chemistry*. 1996;271(36):22152-8.
93. Groemping Y, Lapouge K, Smerdon SJ, Rittinger K. Molecular basis of phosphorylation-induced activation of the NADPH oxidase. *Cell*. 2003;113(3):343-55.
94. Koga H, Terasawa H, Nuno H, Takeshige K, Inagaki F, Sumimoto H. Tetratricopeptide repeat (TPR) motifs of p67(phox) participate in interaction with the small GTPase Rac and activation of the phagocyte NADPH oxidase. *The Journal of biological chemistry*. 1999;274(35):25051-60.
95. Lapouge K, Smith SJ, Walker PA, Gamblin SJ, Smerdon SJ, Rittinger K. Structure of the TPR domain of p67phox in complex with Rac.GTP. *Molecular cell*. 2000;6(4):899-907.
96. Nisimoto Y, Motalebi S, Han CH, Lambeth JD. The p67(phox) activation domain regulates electron flow from NADPH to flavin in flavocytochrome b(558). *The Journal of biological chemistry*. 1999;274(33):22999-3005.
97. Wientjes FB, Hsuan JJ, Totty NF, Segal AW. p40phox, a third cytosolic component of the activation complex of the NADPH oxidase to contain src homology 3 domains. *The Biochemical journal*. 1993;296 (Pt 3):557-61.
98. Tsunawaki S, Mizunari H, Nagata M, Tatsuzawa O, Kuratsuji T. A novel cytosolic component, p40phox, of respiratory burst oxidase associates with p67phox and is absent in patients with chronic granulomatous disease who lack p67phox. *Biochemical and biophysical research communications*. 1994;199(3):1378-87.
99. Prigmore E, Ahmed S, Best A, Kozma R, Manser E, Segal AW, et al. A 68-kDa kinase and NADPH oxidase component p67phox are targets for Cdc42Hs and Rac1 in neutrophils. *The Journal of biological chemistry*. 1995;270(18):10717-22.
100. Fuchs A, Dagher MC, Vignais PV. Mapping the domains of interaction of p40phox with both p47phox and p67phox of the neutrophil oxidase complex using the two-hybrid system. *The Journal of biological chemistry*. 1995;270(11):5695-7.
101. Diebold BA, Bokoch GM. Molecular basis for Rac2 regulation of phagocyte NADPH oxidase. *Nature immunology*. 2001;2(3):211-5.
102. Bedard K, Krause KH. The NOX family of ROS-generating NADPH oxidases: physiology and pathophysiology. *Physiological reviews*. 2007;87(1):245-313.
103. Cross AR, Segal AW. The NADPH oxidase of professional phagocytes--prototype of the NOX electron transport chain systems. *Biochimica et biophysica acta*. 2004;1657(1):1-22.

104. Doussiere J, Gaillard J, Vignais PV. Electron transfer across the O₂- generating flavocytochrome b of neutrophils. Evidence for a transition from a low-spin state to a high-spin state of the heme iron component. *Biochemistry*. 1996;35(41):13400-10.
105. Vignais PV. The superoxide-generating NADPH oxidase: structural aspects and activation mechanism. *Cellular and molecular life sciences : CMLS*. 2002;59(9):1428-59.
106. Serrano F, Kolluri NS, Wientjes FB, Card JP, Klann E. NADPH oxidase immunoreactivity in the mouse brain. *Brain research*. 2003;988(1-2):193-8.
107. Heymes C, Bendall JK, Ratajczak P, Cave AC, Samuel JL, Hasenfuss G, et al. Increased myocardial NADPH oxidase activity in human heart failure. *Journal of the American College of Cardiology*. 2003;41(12):2164-71.
108. Javeshghani D, Magder SA, Barreiro E, Quinn MT, Hussain SN. Molecular characterization of a superoxide-generating NAD(P)H oxidase in the ventilatory muscles. *American journal of respiratory and critical care medicine*. 2002;165(3):412-8.
109. Reinehr R, Becker S, Eberle A, Grether-Beck S, Haussinger D. Involvement of NADPH oxidase isoforms and Src family kinases in CD95-dependent hepatocyte apoptosis. *The Journal of biological chemistry*. 2005;280(29):27179-94.
110. Gorlach A, Brandes RP, Nguyen K, Amidi M, Dehghani F, Busse R. A gp91phox containing NADPH oxidase selectively expressed in endothelial cells is a major source of oxygen radical generation in the arterial wall. *Circulation research*. 2000;87(1):26-32.
111. Jones SA, O'Donnell VB, Wood JD, Broughton JP, Hughes EJ, Jones OT. Expression of phagocyte NADPH oxidase components in human endothelial cells. *The American journal of physiology*. 1996;271(4 Pt 2):H1626-34.
112. Li JM, Shah AM. Intracellular localization and preassembly of the NADPH oxidase complex in cultured endothelial cells. *The Journal of biological chemistry*. 2002;277(22):19952-60.
113. Piccoli C, Ria R, Scrima R, Cela O, D'Aprile A, Boffoli D, et al. Characterization of mitochondrial and extra-mitochondrial oxygen consuming reactions in human hematopoietic stem cells. Novel evidence of the occurrence of NAD(P)H oxidase activity. *The Journal of biological chemistry*. 2005;280(28):26467-76.
114. Cheng G, Cao Z, Xu X, van Meir EG, Lambeth JD. Homologs of gp91phox: cloning and tissue expression of Nox3, Nox4, and Nox5. *Gene*. 2001;269(1-2):131-40.
115. Kikuchi H, Hikage M, Miyashita H, Fukumoto M. NADPH oxidase subunit, gp91(phox) homologue, preferentially expressed in human colon epithelial cells. *Gene*. 2000;254(1-2):237-43.
116. Geiszt M, Kopp JB, Varnai P, Leto TL. Identification of renox, an NAD(P)H oxidase in kidney. *Proceedings of the National Academy of Sciences of the United States of America*. 2000;97(14):8010-4.
117. Shiose A, Kuroda J, Tsuruya K, Hirai M, Hirakata H, Naito S, et al. A novel superoxide-producing NAD(P)H oxidase in kidney. *The Journal of biological chemistry*. 2001;276(2):1417-23.
118. Banfi B, Molnar G, Maturana A, Steger K, Hegedus B, Demaurex N, et al. A Ca⁽²⁺⁾-activated NADPH oxidase in testis, spleen, and lymph nodes. *The Journal of biological chemistry*. 2001;276(40):37594-601.
119. De Deken X, Wang D, Many MC, Costagliola S, Libert F, Vassart G, et al. Cloning of two human thyroid cDNAs encoding new members of the NADPH oxidase family. *The Journal of biological chemistry*. 2000;275(30):23227-33.
120. Dupuy C, Ohayon R, Valent A, Noel-Hudson MS, Deme D, Virion A. Purification of a novel flavoprotein involved in the thyroid NADPH oxidase. Cloning of the porcine and human cdnas. *The Journal of biological chemistry*. 1999;274(52):37265-9.
121. Banfi B, Maturana A, Jaconi S, Arnaudeau S, Laforge T, Sinha B, et al. A mammalian H⁺ channel generated through alternative splicing of the NADPH oxidase homolog NOH-1. *Science*. 2000;287(5450):138-42.
122. Suh YA, Arnold RS, Lassegue B, Shi J, Xu X, Sorescu D, et al. Cell transformation by the superoxide-generating oxidase Mox1. *Nature*. 1999;401(6748):79-82.

123. Banfi B, Clark RA, Steger K, Krause KH. Two novel proteins activate superoxide generation by the NADPH oxidase NOX1. *The Journal of biological chemistry*. 2003;278(6):3510-3.
124. Szanto I, Rubbia-Brandt L, Kiss P, Steger K, Banfi B, Kovari E, et al. Expression of NOX1, a superoxide-generating NADPH oxidase, in colon cancer and inflammatory bowel disease. *The Journal of pathology*. 2005;207(2):164-76.
125. Ago T, Kitazono T, Kuroda J, Kumai Y, Kamouchi M, Ooboshi H, et al. NAD(P)H oxidases in rat basilar arterial endothelial cells. *Stroke*. 2005;36(5):1040-6.
126. Kobayashi S, Nojima Y, Shibuya M, Maru Y. Nox1 regulates apoptosis and potentially stimulates branching morphogenesis in sinusoidal endothelial cells. *Experimental cell research*. 2004;300(2):455-62.
127. Cui XL, Brockman D, Campos B, Myatt L. Expression of NADPH oxidase isoform 1 (Nox1) in human placenta: involvement in preeclampsia. *Placenta*. 2006;27(4-5):422-31.
128. Lee NK, Choi YG, Baik JY, Han SY, Jeong DW, Bae YS, et al. A crucial role for reactive oxygen species in RANKL-induced osteoclast differentiation. *Blood*. 2005;106(3):852-9.
129. Manea A, Raicu M, Simionescu M. Expression of functionally phagocyte-type NAD(P)H oxidase in pericytes: effect of angiotensin II and high glucose. *Biology of the cell*. 2005;97(9):723-34.
130. Kawahara T, Ritsick D, Cheng G, Lambeth JD. Point mutations in the proline-rich region of p22phox are dominant inhibitors of Nox1- and Nox2-dependent reactive oxygen generation. *The Journal of biological chemistry*. 2005;280(36):31859-69.
131. Ambasta RK, Kumar P, Griending KK, Schmidt HH, Busse R, Brandes RP. Direct interaction of the novel Nox proteins with p22phox is required for the formation of a functionally active NADPH oxidase. *The Journal of biological chemistry*. 2004;279(44):45935-41.
132. Cheng G, Diebold BA, Hughes Y, Lambeth JD. Nox1-dependent reactive oxygen generation is regulated by Rac1. *The Journal of biological chemistry*. 2006;281(26):17718-26.
133. Kawahara T, Kohjima M, Kuwano Y, Mino H, Teshima-Kondo S, Takeya R, et al. *Helicobacter pylori* lipopolysaccharide activates Rac1 and transcription of NADPH oxidase Nox1 and its organizer NOXO1 in guinea pig gastric mucosal cells. *American journal of physiology Cell physiology*. 2005;288(2):C450-7.
134. Miyano K, Ueno N, Takeya R, Sumimoto H. Direct involvement of the small GTPase Rac in activation of the superoxide-producing NADPH oxidase Nox1. *The Journal of biological chemistry*. 2006;281(31):21857-68.
135. Park HS, Lee SH, Park D, Lee JS, Ryu SH, Lee WJ, et al. Sequential activation of phosphatidylinositol 3-kinase, beta Pix, Rac1, and Nox1 in growth factor-induced production of H₂O₂. *Molecular and cellular biology*. 2004;24(10):4384-94.
136. Sun C, Sellers KW, Sumners C, Raizada MK. NAD(P)H oxidase inhibition attenuates neuronal chronotropic actions of angiotensin II. *Circulation research*. 2005;96(6):659-66.
137. Takeya R, Ueno N, Kami K, Taura M, Kohjima M, Izaki T, et al. Novel human homologues of p47phox and p67phox participate in activation of superoxide-producing NADPH oxidases. *The Journal of biological chemistry*. 2003;278(27):25234-46.
138. Takeya R, Ueno N, Kami K, Taura M, Kohjima M, Izaki T, et al. Novel human homologues of p47phox and p67phox participate in activation of superoxide-producing NADPH oxidases. *The Journal of biological chemistry*. 2015;290(10):6003.
139. Ueyama T, Geiszt M, Leto TL. Involvement of Rac1 in activation of multicomponent Nox1- and Nox3-based NADPH oxidases. *Molecular and cellular biology*. 2006;26(6):2160-74.
140. Banfi B, Malgrange B, Knisz J, Steger K, Dubois-Dauphin M, Krause KH. NOX3, a superoxide-generating NADPH oxidase of the inner ear. *The Journal of biological chemistry*. 2004;279(44):46065-72.
141. Paffenholz R, Bergstrom RA, Pasutto F, Wabnitz P, Munroe RJ, Jagla W, et al. Vestibular defects in head-tilt mice result from mutations in Nox3, encoding an NADPH oxidase. *Genes & development*. 2004;18(5):486-91.

142. Yang S, Madyastha P, Bingel S, Ries W, Key L. A new superoxide-generating oxidase in murine osteoclasts. *The Journal of biological chemistry*. 2001;276(8):5452-8.
143. Yang S, Zhang Y, Ries W, Key L. Expression of Nox4 in osteoclasts. *Journal of cellular biochemistry*. 2004;92(2):238-48.
144. Hu T, Ramachandrarao SP, Siva S, Valancius C, Zhu Y, Mahadev K, et al. Reactive oxygen species production via NADPH oxidase mediates TGF-beta-induced cytoskeletal alterations in endothelial cells. *American journal of physiology Renal physiology*. 2005;289(4):F816-25.
145. Van Buul JD, Fernandez-Borja M, Anthony EC, Hordijk PL. Expression and localization of NOX2 and NOX4 in primary human endothelial cells. *Antioxidants & redox signaling*. 2005;7(3-4):308-17.
146. Ellmark SH, Dusting GJ, Fui MN, Guzzo-Pernell N, Drummond GR. The contribution of Nox4 to NADPH oxidase activity in mouse vascular smooth muscle. *Cardiovascular research*. 2005;65(2):495-504.
147. Hoidal JR, Brar SS, Sturrock AB, Sanders KA, Dinger B, Fidone S, et al. The role of endogenous NADPH oxidases in airway and pulmonary vascular smooth muscle function. *Antioxidants & redox signaling*. 2003;5(6):751-8.
148. Janiszewski M, Lopes LR, Carmo AO, Pedro MA, Brandes RP, Santos CX, et al. Regulation of NAD(P)H oxidase by associated protein disulfide isomerase in vascular smooth muscle cells. *The Journal of biological chemistry*. 2005;280(49):40813-9.
149. Lassegue B, Sorescu D, Szocs K, Yin Q, Akers M, Zhang Y, et al. Novel gp91(phox) homologues in vascular smooth muscle cells : nox1 mediates angiotensin II-induced superoxide formation and redox-sensitive signaling pathways. *Circulation research*. 2001;88(9):888-94.
150. Pedruzzi E, Guichard C, Ollivier V, Driss F, Fay M, Prunet C, et al. NAD(P)H oxidase Nox-4 mediates 7-ketocholesterol-induced endoplasmic reticulum stress and apoptosis in human aortic smooth muscle cells. *Molecular and cellular biology*. 2004;24(24):10703-17.
151. Sturrock A, Cahill B, Norman K, Huecksteadt TP, Hill K, Sanders K, et al. Transforming growth factor-beta1 induces Nox4 NAD(P)H oxidase and reactive oxygen species-dependent proliferation in human pulmonary artery smooth muscle cells. *American journal of physiology Lung cellular and molecular physiology*. 2006;290(4):L661-L73.
152. Colston JT, de la Rosa SD, Strader JR, Anderson MA, Freeman GL. H₂O₂ activates Nox4 through PLA2-dependent arachidonic acid production in adult cardiac fibroblasts. *FEBS letters*. 2005;579(11):2533-40.
153. Dhaunsi GS, Paintlia MK, Kaur J, Turner RB. NADPH oxidase in human lung fibroblasts. *Journal of biomedical science*. 2004;11(5):617-22.
154. Chamulitrat W, Stremmel W, Kawahara T, Rokutan K, Fujii H, Wingler K, et al. A constitutive NADPH oxidase-like system containing gp91phox homologs in human keratinocytes. *The Journal of investigative dermatology*. 2004;122(4):1000-9.
155. Brar SS, Kennedy TP, Sturrock AB, Huecksteadt TP, Quinn MT, Whorton AR, et al. An NAD(P)H oxidase regulates growth and transcription in melanoma cells. *American journal of physiology Cell physiology*. 2002;282(6):C1212-24.
156. Vallet P, Charnay Y, Steger K, Ogier-Denis E, Kovari E, Herrmann F, et al. Neuronal expression of the NADPH oxidase NOX4, and its regulation in mouse experimental brain ischemia. *Neuroscience*. 2005;132(2):233-8.
157. Martyn KD, Frederick LM, von Loehneysen K, Dinauer MC, Knaus UG. Functional analysis of Nox4 reveals unique characteristics compared to other NADPH oxidases. *Cellular signalling*. 2006;18(1):69-82.
158. Hwang J, Ing MH, Salazar A, Lassegue B, Griending K, Navab M, et al. Pulsatile versus oscillatory shear stress regulates NADPH oxidase subunit expression: implication for native LDL oxidation. *Circulation research*. 2003;93(12):1225-32.
159. Szocs K, Lassegue B, Sorescu D, Hilenski LL, Valppu L, Couse TL, et al. Upregulation of Nox-based NAD(P)H oxidases in restenosis after carotid injury. *Arteriosclerosis, thrombosis, and vascular biology*. 2002;22(1):21-7.
160. Suliman HB, Ali M, Piantadosi CA. Superoxide dismutase-3 promotes full expression of the EPO response to hypoxia. *Blood*. 2004;104(1):43-50.

161. Higashi M, Shimokawa H, Hattori T, Hiroki J, Mukai Y, Morikawa K, et al. Long-term inhibition of Rho-kinase suppresses angiotensin II-induced cardiovascular hypertrophy in rats in vivo: effect on endothelial NAD(P)H oxidase system. *Circulation research*. 2003;93(8):767-75.
162. Winkler K, Wunsch S, Kreutz R, Rothermund L, Paul M, Schmidt HH. Upregulation of the vascular NAD(P)H-oxidase isoforms Nox1 and Nox4 by the renin-angiotensin system in vitro and in vivo. *Free radical biology & medicine*. 2001;31(11):1456-64.
163. Yamagishi S, Nakamura K, Ueda S, Kato S, Imaizumi T. Pigment epithelium-derived factor (PEDF) blocks angiotensin II signaling in endothelial cells via suppression of NADPH oxidase: a novel anti-oxidative mechanism of PEDF. *Cell and tissue research*. 2005;320(3):437-45.
164. Banfi B, Tirone F, Durussel I, Knisz J, Moskwa P, Molnar GZ, et al. Mechanism of Ca²⁺ activation of the NADPH oxidase 5 (NOX5). *The Journal of biological chemistry*. 2004;279(18):18583-91.
165. Petrushanko IY, Lobachev VM, Kononikhin AS, Makarov AA, Devred F, Kovacic H, et al. Oxidation of capital ES, Cyrillicsmall a, Cyrillic2+-Binding Domain of NADPH Oxidase 5 (NOX5): Toward Understanding the Mechanism of Inactivation of NOX5 by ROS. *PloS one*. 2016;11(7):e0158726.
166. Brar SS, Corbin Z, Kennedy TP, Hemendinger R, Thornton L, Bommarius B, et al. NOX5 NAD(P)H oxidase regulates growth and apoptosis in DU 145 prostate cancer cells. *American journal of physiology Cell physiology*. 2003;285(2):C353-69.
167. BelAiba RS, Djordjevic T, Petry A, Diemer K, Bonello S, Banfi B, et al. NOX5 variants are functionally active in endothelial cells. *Free radical biology & medicine*. 2007;42(4):446-59.
168. Salles N, Szanto I, Herrmann F, Armenian B, Stumm M, Stauffer E, et al. Expression of mRNA for ROS-generating NADPH oxidases in the aging stomach. *Experimental gerontology*. 2005;40(4):353-7.
169. Kelm M, Schrader J. Control of coronary vascular tone by nitric oxide. *Circulation research*. 1990;66(6):1561-75.
170. Liu X, Miller MJ, Joshi MS, Sadowska-Krowicka H, Clark DA, Lancaster JR, Jr. Diffusion-limited reaction of free nitric oxide with erythrocytes. *The Journal of biological chemistry*. 1998;273(30):18709-13.
171. Thomas DD, Liu X, Kantrow SP, Lancaster JR, Jr. The biological lifetime of nitric oxide: implications for the perivascular dynamics of NO and O₂. *Proceedings of the National Academy of Sciences of the United States of America*. 2001;98(1):355-60.
172. al-Ali MK, Howarth PH. Nitric oxide and the respiratory system in health and disease. *Respiratory medicine*. 1998;92(5):701-15.
173. Panesar NS. Downsides to the nitrate-nitrite-nitric oxide pathway in physiology and therapeutics? *Nature reviews Drug discovery*. 2008;7(8):710; author reply
174. Lundberg JO, Weitzberg E, Gladwin MT. The nitrate-nitrite-nitric oxide pathway in physiology and therapeutics. *Nature reviews Drug discovery*. 2008;7(2):156-67.
175. Forstermann U, Sessa WC. Nitric oxide synthases: regulation and function. *European heart journal*. 2012;33(7):829-37, 37a-37d.
176. Bredt DS, Snyder SH. Isolation of nitric oxide synthetase, a calmodulin-requiring enzyme. *Proceedings of the National Academy of Sciences of the United States of America*. 1990;87(2):682-5.
177. Bredt DS, Hwang PM, Glatt CE, Lowenstein C, Reed RR, Snyder SH. Cloned and expressed nitric oxide synthase structurally resembles cytochrome P-450 reductase. *Nature*. 1991;351(6329):714-8.
178. Pollock JS, Forstermann U, Mitchell JA, Warner TD, Schmidt HH, Nakane M, et al. Purification and characterization of particulate endothelium-derived relaxing factor synthase from cultured and native bovine aortic endothelial cells. *Proceedings of the National Academy of Sciences of the United States of America*. 1991;88(23):10480-4.
179. Pollock JS, Nakane M, BATTERY LD, Martinez A, Springall D, Polak JM, et al. Characterization and localization of endothelial nitric oxide synthase using specific monoclonal antibodies. *The American journal of physiology*. 1993;265(5 Pt 1):C1379-87.

180. Sessa WC, Harrison JK, Barber CM, Zeng D, Durieux ME, D'Angelo DD, et al. Molecular cloning and expression of a cDNA encoding endothelial cell nitric oxide synthase. *The Journal of biological chemistry*. 1992;267(22):15274-6.
181. Knowles RG, Palacios M, Palmer RM, Moncada S. Formation of nitric oxide from L-arginine in the central nervous system: a transduction mechanism for stimulation of the soluble guanylate cyclase. *Proceedings of the National Academy of Sciences of the United States of America*. 1989;86(13):5159-62.
182. Mayer B, Schmidt K, Humbert P, Bohme E. Biosynthesis of endothelium-derived relaxing factor: a cytosolic enzyme in porcine aortic endothelial cells Ca²⁺-dependently converts L-arginine into an activator of soluble guanylyl cyclase. *Biochemical and biophysical research communications*. 1989;164(2):678-85.
183. Mulsch A, Bassenge E, Busse R. Nitric oxide synthesis in endothelial cytosol: evidence for a calcium-dependent and a calcium-independent mechanism. *Naunyn-Schmiedeberg's archives of pharmacology*. 1989;340(6 Pt 2):767-70.
184. Palacios M, Knowles RG, Palmer RM, Moncada S. Nitric oxide from L-arginine stimulates the soluble guanylate cyclase in adrenal glands. *Biochemical and biophysical research communications*. 1989;165(2):802-9.
185. Palmer RM, Moncada S. A novel citrulline-forming enzyme implicated in the formation of nitric oxide by vascular endothelial cells. *Biochemical and biophysical research communications*. 1989;158(1):348-52.
186. Stuehr DJ, Kwon NS, Gross SS, Thiel BA, Levi R, Nathan CF. Synthesis of nitrogen oxides from L-arginine by macrophage cytosol: requirement for inducible and constitutive components. *Biochemical and biophysical research communications*. 1989;161(2):420-6.
187. Moncada S, Palmer RM, Higgs EA. Biosynthesis of nitric oxide from L-arginine. A pathway for the regulation of cell function and communication. *Biochemical pharmacology*. 1989;38(11):1709-15.
188. Nakane M, Schmidt HH, Pollock JS, Forstermann U, Murad F. Cloned human brain nitric oxide synthase is highly expressed in skeletal muscle. *FEBS letters*. 1993;316(2):175-80.
189. Zhou L, Zhu DY. Neuronal nitric oxide synthase: structure, subcellular localization, regulation, and clinical implications. *Nitric oxide : biology and chemistry*. 2009;20(4):223-30.
190. Forstermann U, Closs EI, Pollock JS, Nakane M, Schwarz P, Gath I, et al. Nitric oxide synthase isozymes. Characterization, purification, molecular cloning, and functions. *Hypertension*. 1994;23(6 Pt 2):1121-31.
191. Lyons CR, Orloff GJ, Cunningham JM. Molecular cloning and functional expression of an inducible nitric oxide synthase from a murine macrophage cell line. *The Journal of biological chemistry*. 1992;267(9):6370-4.
192. Yui Y, Hattori R, Kosuga K, Eizawa H, Hiki K, Kawai C. Purification of nitric oxide synthase from rat macrophages. *The Journal of biological chemistry*. 1991;266(19):12544-7.
193. Wood CE, Chen GF, Keller-Wood M. Expression of nitric oxide synthase isoforms is reduced in late-gestation ovine fetal brainstem. *American journal of physiology Regulatory, integrative and comparative physiology*. 2005;289(2):R613-R9.
194. Matouk CC, Marsden PA. Epigenetic regulation of vascular endothelial gene expression. *Circulation research*. 2008;102(8):873-87.
195. Zaobornyj T, Ghafourifar P. Strategic localization of heart mitochondrial NOS: a review of the evidence. *American journal of physiology Heart and circulatory physiology*. 2012;303(11):H1283-93.
196. Castillo L, deRojas TC, Chapman TE, Vogt J, Burke JF, Tannenbaum SR, et al. Splanchnic metabolism of dietary arginine in relation to nitric oxide synthesis in normal adult man. *Proceedings of the National Academy of Sciences of the United States of America*. 1993;90(1):193-7.
197. Leaf CD, Wishnok JS, Tannenbaum SR. L-arginine is a precursor for nitrate biosynthesis in humans. *Biochemical and biophysical research communications*. 1989;163(2):1032-7.

198. Leaf CD, Wishnok JS, Hurley JP, Rosenblad WD, Fox JG, Tannenbaum SR. Nitrate biosynthesis in rats, ferrets and humans. Precursor studies with L-arginine. *Carcinogenesis*. 1990;11(5):855-8.
199. Bredt DS, Snyder SH. Nitric oxide: a physiologic messenger molecule. *Annual review of biochemistry*. 1994;63:175-95.
200. Moncada S, Palmer RM, Higgs EA. Nitric oxide: physiology, pathophysiology, and pharmacology. *Pharmacological reviews*. 1991;43(2):109-42.
201. Rengasamy A, Johns RA. Determination of Km for oxygen of nitric oxide synthase isoforms. *The Journal of pharmacology and experimental therapeutics*. 1996;276(1):30-3.
202. Chalupsky K, Kracun D, Kanchev I, Bertram K, Grolach A. Folic Acid Promotes Recycling of Tetrahydrobiopterin and Protects Against Hypoxia-Induced Pulmonary Hypertension by Recoupling Endothelial Nitric Oxide Synthase. *Antioxidants & redox signaling*. 2015;23(14):1076-91.
203. Stuehr DJ, Santolini J, Wang ZQ, Wei CC, Adak S. Update on mechanism and catalytic regulation in the NO synthases. *The Journal of biological chemistry*. 2004;279(35):36167-70.
204. Fosen KM, Thom SR. Hyperbaric oxygen, vasculogenic stem cells, and wound healing. *Antioxidants & redox signaling*. 2014;21(11):1634-47.
205. Venema RC, Ju H, Zou R, Ryan JW, Venema VJ. Subunit interactions of endothelial nitric-oxide synthase. Comparisons to the neuronal and inducible nitric-oxide synthase isoforms. *The Journal of biological chemistry*. 1997;272(2):1276-82.
206. Shaul PW, North AJ, Brannon TS, Ujiie K, Wells LB, Nisen PA, et al. Prolonged in vivo hypoxia enhances nitric oxide synthase type I and type III gene expression in adult rat lung. *American journal of respiratory cell and molecular biology*. 1995;13(2):167-74.
207. Pritchard KA, Jr., Shi Y, Konduri GG. Tetrahydrobiopterin in pulmonary hypertension: pulmonary hypertension in guanosine triphosphate-cyclohydrolase-deficient mice. *Circulation*. 2005;111(16):2022-4.
208. Bredt DS. Endogenous nitric oxide synthesis: biological functions and pathophysiology. *Free radical research*. 1999;31(6):577-96.
209. Alp NJ, Channon KM. Regulation of endothelial nitric oxide synthase by tetrahydrobiopterin in vascular disease. *Arteriosclerosis, thrombosis, and vascular biology*. 2004;24(3):413-20.
210. Stuehr DJ. Mammalian nitric oxide synthases. *Biochimica et biophysica acta*. 1999;1411(2-3):217-30.
211. Bendall JK, Douglas G, McNeill E, Channon KM, Crabtree MJ. Tetrahydrobiopterin in cardiovascular health and disease. *Antioxidants & redox signaling*. 2014;20(18):3040-77.
212. Berkowitz DE, White R, Li D, Minhas KM, Cernetich A, Kim S, et al. Arginase reciprocally regulates nitric oxide synthase activity and contributes to endothelial dysfunction in aging blood vessels. *Circulation*. 2003;108(16):2000-6.
213. Vasquez-Vivar J, Kalyanaraman B, Martasek P, Hogg N, Masters BS, Karoui H, et al. Superoxide generation by endothelial nitric oxide synthase: the influence of cofactors. *Proceedings of the National Academy of Sciences of the United States of America*. 1998;95(16):9220-5.
214. Chen CA, Wang TY, Varadharaj S, Reyes LA, Hemann C, Talukder MA, et al. S-glutathionylation uncouples eNOS and regulates its cellular and vascular function. *Nature*. 2010;468(7327):1115-8.
215. Lin MI, Fulton D, Babbitt R, Fleming I, Busse R, Pritchard KA, Jr., et al. Phosphorylation of threonine 497 in endothelial nitric-oxide synthase coordinates the coupling of L-arginine metabolism to efficient nitric oxide production. *The Journal of biological chemistry*. 2003;278(45):44719-26.
216. Fleming I, Fisslthaler B, Dimmeler S, Kemp BE, Busse R. Phosphorylation of Thr(495) regulates Ca(2+)/calmodulin-dependent endothelial nitric oxide synthase activity. *Circulation research*. 2001;88(11):E68-75.
217. Forstermann U, Li H. Therapeutic effect of enhancing endothelial nitric oxide synthase (eNOS) expression and preventing eNOS uncoupling. *British journal of pharmacology*. 2011;164(2):213-23.

218. Stroes E, Hijmering M, van Zandvoort M, Wever R, Rabelink TJ, van Faassen EE. Origin of superoxide production by endothelial nitric oxide synthase. *FEBS letters*. 1998;438(3):161-4.
219. Thum T, Fraccarollo D, Schultheiss M, Froese S, Galuppo P, Widder JD, et al. Endothelial nitric oxide synthase uncoupling impairs endothelial progenitor cell mobilization and function in diabetes. *Diabetes*. 2007;56(3):666-74.
220. Gielis JF, Lin JY, Wingler K, Van Schil PE, Schmidt HH, Moens AL. Pathogenetic role of eNOS uncoupling in cardiopulmonary disorders. *Free radical biology & medicine*. 2011;50(7):765-76.
221. Simonneau G, Galie N, Rubin LJ, Langleben D, Seeger W, Domenighetti G, et al. Clinical classification of pulmonary hypertension. *Journal of the American College of Cardiology*. 2004;43(12 Suppl S):5S-12S.
222. Eales KL, Hollinshead KE, Tennant DA. Hypoxia and metabolic adaptation of cancer cells. *Oncogenesis*. 2016;5:e190.
223. Semenza GL. Hypoxia-inducible factors: mediators of cancer progression and targets for cancer therapy. *Trends in pharmacological sciences*. 2012;33(4):207-14.
224. Schumacker PT. Reactive oxygen species in cancer: a dance with the devil. *Cancer cell*. 2015;27(2):156-7.
225. de Sa Junior PL, Camara DAD, Porcacchia AS, Fonseca PMM, Jorge SD, Araldi RP, et al. The Roles of ROS in Cancer Heterogeneity and Therapy. *Oxidative medicine and cellular longevity*. 2017;2017:2467940.
226. Liou GY, Storz P. Reactive oxygen species in cancer. *Free radical research*. 2010;44(5):479-96.
227. Paolicchi E, Gemignani F, Krstic-Demonacos M, Dedhar S, Mutti L, Landi S. Targeting hypoxic response for cancer therapy. *Oncotarget*. 2016;7(12):13464-78.
228. Kracun D, Riess F, Kanchev I, Gawaz M, Gorchach A. The beta3-integrin binding protein beta3-endonexin is a novel negative regulator of hypoxia-inducible factor-1. *Antioxidants & redox signaling*. 2014;20(13):1964-76.
229. Krock BL, Skuli N, Simon MC. Hypoxia-induced angiogenesis: good and evil. *Genes & cancer*. 2011;2(12):1117-33.
230. Contois L, Akalu A, Brooks PC. Integrins as "functional hubs" in the regulation of pathological angiogenesis. *Seminars in cancer biology*. 2009;19(5):318-28.
231. Hynes RO. Integrins: versatility, modulation, and signaling in cell adhesion. *Cell*. 1992;69(1):11-25.
232. Sastry SK, Horwitz AF. Integrin cytoplasmic domains: mediators of cytoskeletal linkages and extra- and intracellular initiated transmembrane signaling. *Current opinion in cell biology*. 1993;5(5):819-31.
233. Longmate W, DiPersio CM. Beyond adhesion: emerging roles for integrins in control of the tumor microenvironment. *F1000Research*. 2017;6:1612.
234. Brooks PC, Stromblad S, Klemke R, Visscher D, Sarkar FH, Cheresch DA. Antiintegrin alpha v beta 3 blocks human breast cancer growth and angiogenesis in human skin. *The Journal of clinical investigation*. 1995;96(4):1815-22.
235. Shattil SJ, O'Toole T, Eigenthaler M, Thon V, Williams M, Babior BM, et al. Beta 3-endonexin, a novel polypeptide that interacts specifically with the cytoplasmic tail of the integrin beta 3 subunit. *The Journal of cell biology*. 1995;131(3):807-16.
236. Byzova TV, Plow EF. Activation of alphaVbeta3 on vascular cells controls recognition of prothrombin. *The Journal of cell biology*. 1998;143(7):2081-92.
237. Fujimoto TT, Katsutani S, Shimomura T, Fujimura K. Novel alternatively spliced form of beta(3)-endonexin. *Thrombosis research*. 2002;105(1):63-70.
238. Ohtoshi A, Ohtoshi H. Analysis of beta3-endonexin mutants for their ability to interact with cyclin A. *Molecular genetics and genomics : MGG*. 2001;266(4):664-71.
239. Ohtoshi A, Maeda T, Higashi H, Ashizawa S, Yamada M, Hatakeyama M. beta3-endonexin as a novel inhibitor of cyclin A-associated kinase. *Biochemical and biophysical research communications*. 2000;267(3):947-52.

240. Besta F, Massberg S, Brand K, Muller E, Page S, Gruner S, et al. Role of beta(3)-endoneixin in the regulation of NF-kappaB-dependent expression of urokinase-type plasminogen activator receptor. *Journal of cell science*. 2002;115(Pt 20):3879-88.
241. Besta F, Muller I, Lorenz M, Massberg S, Bultmann A, Cabeza N, et al. Reduced beta3-endoneixin levels are associated with enhanced urokinase-type plasminogen activator receptor expression in ApoE^{-/-} mice. *Thrombosis research*. 2004;114(4):283-92.
242. Hapke S, Gawaz M, Dehne K, Kohler J, Marshall JF, Graeff H, et al. beta(3)A-integrin downregulates the urokinase-type plasminogen activator receptor (u-PAR) through a PEA3/ets transcriptional silencing element in the u-PAR promoter. *Molecular and cellular biology*. 2001;21(6):2118-32.
243. Humbert M, Lau EM, Montani D, Jais X, Sitbon O, Simonneau G. Advances in therapeutic interventions for patients with pulmonary arterial hypertension. *Circulation*. 2014;130(24):2189-208.
244. Simonneau G, Gatzoulis MA, Adatia I, Celermajer D, Denton C, Ghofrani A, et al. Updated clinical classification of pulmonary hypertension. *Journal of the American College of Cardiology*. 2013;62(25 Suppl):D34-41.
245. Budhiraja R, Tuder RM, Hassoun PM. Endothelial dysfunction in pulmonary hypertension. *Circulation*. 2004;109(2):159-65.
246. Tuder RM, Archer SL, Dorfmueller P, Erzurum SC, Guignabert C, Michelakis E, et al. Relevant issues in the pathology and pathobiology of pulmonary hypertension. *Journal of the American College of Cardiology*. 2013;62(25 Suppl):D4-12.
247. Giaid A. Nitric oxide and endothelin-1 in pulmonary hypertension. *Chest*. 1998;114(3 Suppl):208S-12S.
248. Ema M, Taya S, Yokotani N, Sogawa K, Matsuda Y, Fujii-Kuriyama Y. A novel bHLH-PAS factor with close sequence similarity to hypoxia-inducible factor 1alpha regulates the VEGF expression and is potentially involved in lung and vascular development. *Proceedings of the National Academy of Sciences of the United States of America*. 1997;94(9):4273-8.
249. Flamme I, Frohlich T, von Reutern M, Kappel A, Damert A, Risau W. HRF, a putative basic helix-loop-helix-PAS-domain transcription factor is closely related to hypoxia-inducible factor-1 alpha and developmentally expressed in blood vessels. *Mechanisms of development*. 1997;63(1):51-60.
250. Compennolle V, Brusselmans K, Acker T, Hoet P, Tjwa M, Beck H, et al. Loss of HIF-2alpha and inhibition of VEGF impair fetal lung maturation, whereas treatment with VEGF prevents fatal respiratory distress in premature mice. *Nature medicine*. 2002;8(7):702-10.
251. Diebold I, Petry A, Djordjevic T, Belaiba RS, Fineman J, Black S, et al. Reciprocal regulation of Rac1 and PAK-1 by HIF-1alpha: a positive-feedback loop promoting pulmonary vascular remodeling. *Antioxidants & redox signaling*. 2010;13(4):399-412.
252. Shimoda LA, Semenza GL. HIF and the lung: role of hypoxia-inducible factors in pulmonary development and disease. *American journal of respiratory and critical care medicine*. 2011;183(2):152-6.
253. Qing M, Gorchach A, Schumacher K, Woltje M, Vazquez-Jimenez JF, Hess J, et al. The hypoxia-inducible factor HIF-1 promotes intramyocardial expression of VEGF in infants with congenital cardiac defects. *Basic research in cardiology*. 2007;102(3):224-32.
254. Yin HL, Luo CW, Dai ZK, Shaw KP, Chai CY, Wu CC. Hypoxia-inducible factor-1alpha, vascular endothelial growth factor, inducible nitric oxide synthase, and endothelin-1 expression correlates with angiogenesis in congenital heart disease. *The Kaohsiung journal of medical sciences*. 2016;32(7):348-55.
255. Brusselmans K, Compennolle V, Tjwa M, Wiesener MS, Maxwell PH, Collen D, et al. Heterozygous deficiency of hypoxia-inducible factor-2alpha protects mice against pulmonary hypertension and right ventricular dysfunction during prolonged hypoxia. *The Journal of clinical investigation*. 2003;111(10):1519-27.
256. Yu AY, Shimoda LA, Iyer NV, Huso DL, Sun X, McWilliams R, et al. Impaired physiological responses to chronic hypoxia in mice partially deficient for hypoxia-inducible factor 1alpha. *The Journal of clinical investigation*. 1999;103(5):691-6.
257. Tuder RM, Chacon M, Alger L, Wang J, Taraseviciene-Stewart L, Kasahara Y, et al. Expression of angiogenesis-related molecules in plexiform lesions in severe pulmonary

- hypertension: evidence for a process of disordered angiogenesis. *The Journal of pathology*. 2001;195(3):367-74.
258. Hanahan D, Weinberg RA. The hallmarks of cancer. *Cell*. 2000;100(1):57-70.
259. Hanahan D, Weinberg RA. Hallmarks of cancer: the next generation. *Cell*. 2011;144(5):646-74.
260. Schito L, Semenza GL. Hypoxia-Inducible Factors: Master Regulators of Cancer Progression. *Trends in cancer*. 2016;2(12):758-70.
261. Brown JM. Tumor hypoxia in cancer therapy. *Methods in enzymology*. 2007;435:297-321.
262. Trachootham D, Alexandre J, Huang P. Targeting cancer cells by ROS-mediated mechanisms: a radical therapeutic approach? *Nature reviews Drug discovery*. 2009;8(7):579-91.
263. Barrera G. Oxidative stress and lipid peroxidation products in cancer progression and therapy. *ISRN oncology*. 2012;2012:137289.
264. Kadmiel M, Cidlowski JA. Glucocorticoid receptor signaling in health and disease. *Trends in pharmacological sciences*. 2013;34(9):518-30.
265. van der Velden VH. Glucocorticoids: mechanisms of action and anti-inflammatory potential in asthma. *Mediators of inflammation*. 1998;7(4):229-37.
266. Gustafsson JA, Carlstedt-Duke J, Poellinger L, Okret S, Wikstrom AC, Bronnegard M, et al. Biochemistry, molecular biology, and physiology of the glucocorticoid receptor. *Endocrine reviews*. 1987;8(2):185-234.
267. Mendel DB, Orti E. Isoform composition and stoichiometry of the approximately 90-kDa heat shock protein associated with glucocorticoid receptors. *The Journal of biological chemistry*. 1988;263(14):6695-702.
268. Smith DF, Stensgard BA, Welch WJ, Toft DO. Assembly of progesterone receptor with heat shock proteins and receptor activation are ATP mediated events. *The Journal of biological chemistry*. 1992;267(2):1350-6.
269. Sanchez ER. Hsp56: a novel heat shock protein associated with untransformed steroid receptor complexes. *The Journal of biological chemistry*. 1990;265(36):22067-70.
270. Lebeau MC, Massol N, Herrick J, Faber LE, Renoir JM, Radanyi C, et al. P59, an hsp 90-binding protein. Cloning and sequencing of its cDNA and preparation of a peptide-directed polyclonal antibody. *The Journal of biological chemistry*. 1992;267(7):4281-4.
271. Beato M. Gene regulation by steroid hormones. *Cell*. 1989;56(3):335-44.
272. Truss M, Beato M. Steroid hormone receptors: interaction with deoxyribonucleic acid and transcription factors. *Endocrine reviews*. 1993;14(4):459-79.
273. Schule R, Rangarajan P, Kliewer S, Ransone LJ, Bolado J, Yang N, et al. Functional antagonism between oncoprotein c-Jun and the glucocorticoid receptor. *Cell*. 1990;62(6):1217-26.
274. Strahle U, Schmid W, Schutz G. Synergistic action of the glucocorticoid receptor with transcription factors. *The EMBO journal*. 1988;7(11):3389-95.
275. Didonato JA, Saatcioglu F, Karin M. Molecular mechanisms of immunosuppression and anti-inflammatory activities by glucocorticoids. *American journal of respiratory and critical care medicine*. 1996;154(2 Pt 2):S11-5.
276. Gomez-Sanchez E, Gomez-Sanchez CE. The multifaceted mineralocorticoid receptor. *Comprehensive Physiology*. 2014;4(3):965-94.
277. Melby JC. Drug spotlight program: systemic corticosteroid therapy: pharmacology and endocrinologic considerations. *Annals of internal medicine*. 1974;81(4):505-12.
278. Walker BR. Glucocorticoids and cardiovascular disease. *European journal of endocrinology*. 2007;157(5):545-59.
279. Goodwin JE, Geller DS. Glucocorticoid-induced hypertension. *Pediatric nephrology*. 2012;27(7):1059-66.
280. Wagner AE, Huck G, Stiehl DP, Jelkmann W, Hellwig-Burgel T. Dexamethasone impairs hypoxia-inducible factor-1 function. *Biochemical and biophysical research communications*. 2008;372(2):336-40.

281. Iuchi T, Akaike M, Mitsui T, Ohshima Y, Shintani Y, Azuma H, et al. Glucocorticoid excess induces superoxide production in vascular endothelial cells and elicits vascular endothelial dysfunction. *Circulation research*. 2003;92(1):81-7.
282. Guo B, Zhang W, Xu S, Lou J, Wang S, Men X. GSK-3 β mediates dexamethasone-induced pancreatic beta cell apoptosis. *Life sciences*. 2016;144:1-7.
283. Kraaij MD, van der Kooij SW, Reinders ME, Koekkoek K, Rabelink TJ, van Kooten C, et al. Dexamethasone increases ROS production and T cell suppressive capacity by anti-inflammatory macrophages. *Molecular immunology*. 2011;49(3):549-57.
284. Zhu FB, Wang JY, Zhang YL, Quan RF, Yue ZS, Zeng LR, et al. Curculigoside regulates proliferation, differentiation, and pro-inflammatory cytokines levels in dexamethasone-induced rat calvarial osteoblasts. *International journal of clinical and experimental medicine*. 2015;8(8):12337-46.
285. Ades EW, Candal FJ, Swerlick RA, George VG, Summers S, Bosse DC, et al. HMEC-1: establishment of an immortalized human microvascular endothelial cell line. *The Journal of investigative dermatology*. 1992;99(6):683-90.
286. Nakano Y, Longo-Guess CM, Bergstrom DE, Nauseef WM, Jones SM, Banfi B. Mutation of the *Cyba* gene encoding p22phox causes vestibular and immune defects in mice. *The Journal of clinical investigation*. 2008;118(3):1176-85.
287. Ryan HE, Poloni M, McNulty W, Elson D, Gassmann M, Arbeit JM, et al. Hypoxia-inducible factor-1 α is a positive factor in solid tumor growth. *Cancer Res*. 2000;60(15):4010-5.
288. Minet E, Mottet D, Michel G, Roland I, Raes M, Remacle J, et al. Hypoxia-induced activation of HIF-1: role of HIF-1 α -Hsp90 interaction. *FEBS letters*. 1999;460(2):251-6.
289. Djordjevic T, Hess J, Herkert O, Gorkach A, BelAiba RS. Rac regulates thrombin-induced tissue factor expression in pulmonary artery smooth muscle cells involving the nuclear factor-kappaB pathway. *Antioxidants & redox signaling*. 2004;6(4):713-20.
290. BelAiba RS, Djordjevic T, Bonello S, Artunc F, Lang F, Hess J, et al. The serum- and glucocorticoid-inducible kinase Sgk-1 is involved in pulmonary vascular remodeling: role in redox-sensitive regulation of tissue factor by thrombin. *Circulation research*. 2006;98(6):828-36.
291. Ampofo E, Kietzmann T, Zimmer A, Jakupovic M, Montenarh M, Gotz C. Phosphorylation of the von Hippel-Lindau protein (VHL) by protein kinase CK2 reduces its protein stability and affects p53 and HIF-1 α mediated transcription. *The international journal of biochemistry & cell biology*. 2010;42(10):1729-35.
292. Dikalov SI, Kirilyuk IA, Voinov M, Grigor'ev IA. EPR detection of cellular and mitochondrial superoxide using cyclic hydroxylamines. *Free radical research*. 2011;45(4):417-30.
293. Fernandes DC, Wosniak J, Jr., Pescatore LA, Bertoline MA, Liberman M, Laurindo FR, et al. Analysis of DHE-derived oxidation products by HPLC in the assessment of superoxide production and NADPH oxidase activity in vascular systems. *American journal of physiology Cell physiology*. 2007;292(1):C413-22.
294. Coelho-Filho OR, Shah RV, Mitchell R, Neilan TG, Moreno H, Jr., Simonson B, et al. Quantification of cardiomyocyte hypertrophy by cardiac magnetic resonance: implications for early cardiac remodeling. *Circulation*. 2013;128(11):1225-33.
295. Wolf CM, Moskowitz IP, Arno S, Branco DM, Semsarian C, Bernstein SA, et al. Somatic events modify hypertrophic cardiomyopathy pathology and link hypertrophy to arrhythmia. *Proceedings of the National Academy of Sciences of the United States of America*. 2005;102(50):18123-8.
296. Wolf CM, Wang L, Alcalai R, Pizard A, Burgon PG, Ahmad F, et al. Lamin A/C haploinsufficiency causes dilated cardiomyopathy and apoptosis-triggered cardiac conduction system disease. *Journal of molecular and cellular cardiology*. 2008;44(2):293-303.
297. Diebold I, Djordjevic T, Petry A, Hatzelmann A, Tenor H, Hess J, et al. Phosphodiesterase 2 mediates redox-sensitive endothelial cell proliferation and angiogenesis by thrombin via Rac1 and NADPH oxidase 2. *Circulation research*. 2009;104(10):1169-77.

298. Gao L, Chalupsky K, Stefani E, Cai H. Mechanistic insights into folic acid-dependent vascular protection: dihydrofolate reductase (DHFR)-mediated reduction in oxidant stress in endothelial cells and angiotensin II-infused mice: a novel HPLC-based fluorescent assay for DHFR activity. *Journal of molecular and cellular cardiology*. 2009;47(6):752-60.
299. Taylor SY, Dixon HM, Yoganayagam S, Price N, Lang D. Folic acid modulates eNOS activity via effects on posttranslational modifications and protein-protein interactions. *European journal of pharmacology*. 2013;714(1-3):193-201.
300. Francis BN, Hale A, Channon KM, Wilkins MR, Zhao L. Effects of tetrahydrobiopterin oral treatment in hypoxia-induced pulmonary hypertension in rat. *Pulmonary circulation*. 2014;4(3):462-70.
301. Koubsky K, Durisova J, Mikova D, Herget J. Chronic hypoxia inhibits tetrahydrobiopterin-induced NO production in rat lungs. *Respiratory physiology & neurobiology*. 2013;185(3):547-52.
302. Mittal M, Roth M, Konig P, Hofmann S, Dony E, Goyal P, et al. Hypoxia-dependent regulation of nonphagocytic NADPH oxidase subunit NOX4 in the pulmonary vasculature. *Circulation research*. 2007;101(3):258-67.
303. Altenhofer S, Radermacher KA, Kleikers PW, Wingler K, Schmidt HH. Evolution of NADPH Oxidase Inhibitors: Selectivity and Mechanisms for Target Engagement. *Antioxidants & redox signaling*. 2015;23(5):406-27.
304. Diebold I, Petry A, Hess J, Gorlach A. The NADPH oxidase subunit NOX4 is a new target gene of the hypoxia-inducible factor-1. *Molecular biology of the cell*. 2010;21(12):2087-96.
305. Limbourg FP, Liao JK. Nontranscriptional actions of the glucocorticoid receptor. *Journal of molecular medicine*. 2003;81(3):168-74.
306. Ushio-Fukai M. Redox signaling in angiogenesis: role of NADPH oxidase. *Cardiovascular research*. 2006;71(2):226-35.
307. Abid MR, Kachra Z, Spokes KC, Aird WC. NADPH oxidase activity is required for endothelial cell proliferation and migration. *FEBS letters*. 2000;486(3):252-6.
308. Souverein PC, Berard A, Van Staa TP, Cooper C, Egberts AC, Leufkens HG, et al. Use of oral glucocorticoids and risk of cardiovascular and cerebrovascular disease in a population based case-control study. *Heart*. 2004;90(8):859-65.
309. Davis JM, 3rd, Maradit Kremers H, Crowson CS, Nicola PJ, Ballman KV, Thorneau TM, et al. Glucocorticoids and cardiovascular events in rheumatoid arthritis: a population-based cohort study. *Arthritis and rheumatism*. 2007;56(3):820-30.
310. Panoulas VF, Douglas KM, Stavropoulos-Kalinoglou A, Metsios GS, Nightingale P, Kita MD, et al. Long-term exposure to medium-dose glucocorticoid therapy associates with hypertension in patients with rheumatoid arthritis. *Rheumatology*. 2008;47(1):72-5.
311. Soto-Pina AE, Franklin C, Rani CS, Gottlieb H, Hinojosa-Laborde C, Strong R. A Novel Model of Dexamethasone-Induced Hypertension: Use in Investigating the Role of Tyrosine Hydroxylase. *The Journal of pharmacology and experimental therapeutics*. 2016;358(3):528-36.
312. Greijer AE, van der Groep P, Kemming D, Shvarts A, Semenza GL, Meijer GA, et al. Up-regulation of gene expression by hypoxia is mediated predominantly by hypoxia-inducible factor 1 (HIF-1). *The Journal of pathology*. 2005;206(3):291-304.
313. Semenza GL. Angiogenesis in ischemic and neoplastic disorders. *Annual review of medicine*. 2003;54:17-28.
314. Shen B, Delaney MK, Du X. Inside-out, outside-in, and inside-outside-in: G protein signaling in integrin-mediated cell adhesion, spreading, and retraction. *Current opinion in cell biology*. 2012;24(5):600-6.
315. Wrighton KH. Cell adhesion: the 'ins' and 'outs' of integrin signalling. *Nature reviews Molecular cell biology*. 2013;14(12):752.
316. Burke JR, Pattoli MA, Gregor KR, Brassil PJ, MacMaster JF, McIntyre KW, et al. BMS-345541 is a highly selective inhibitor of I kappa B kinase that binds at an allosteric site of the enzyme and blocks NF-kappa B-dependent transcription in mice. *The Journal of biological chemistry*. 2003;278(3):1450-6.

317. Mackman N, Brand K, Edgington TS. Lipopolysaccharide-mediated transcriptional activation of the human tissue factor gene in THP-1 monocytic cells requires both activator protein 1 and nuclear factor kappa B binding sites. *The Journal of experimental medicine*. 1991;174(6):1517-26.
318. Liu F, Gomez Garcia AM, Meyskens FL, Jr. NADPH oxidase 1 overexpression enhances invasion via matrix metalloproteinase-2 and epithelial-mesenchymal transition in melanoma cells. *J Invest Dermatol*. 2012;132(8):2033-41.
319. Yamaura M, Mitsushita J, Furuta S, Kiniwa Y, Ashida A, Goto Y, et al. NADPH oxidase 4 contributes to transformation phenotype of melanoma cells by regulating G2-M cell cycle progression. *Cancer Res*. 2009;69(6):2647-54.
320. Shono T, Yokoyama N, Uesaka T, Kuroda J, Takeya R, Yamasaki T, et al. Enhanced expression of NADPH oxidase Nox4 in human gliomas and its roles in cell proliferation and survival. *Int J Cancer*. 2008;123(4):787-92.
321. Juhasz A, Markel S, Gaur S, Liu H, Lu J, Jiang G, et al. NADPH oxidase 1 supports proliferation of colon cancer cells by modulating reactive oxygen species-dependent signal transduction. *The Journal of biological chemistry*. 2017;292(19):7866-87.
322. Laurent E, McCoy JW, 3rd, Macina RA, Liu W, Cheng G, Robine S, et al. Nox1 is over-expressed in human colon cancers and correlates with activating mutations in K-Ras. *Int J Cancer*. 2008;123(1):100-7.
323. Juhasz A, Ge Y, Markel S, Chiu A, Matsumoto L, van Balgooy J, et al. Expression of NADPH oxidase homologues and accessory genes in human cancer cell lines, tumours and adjacent normal tissues. *Free radical research*. 2009;43(6):523-32.
324. Kamata T. Roles of Nox1 and other Nox isoforms in cancer development. *Cancer science*. 2009;100(8):1382-8.
325. Lin XL, Yang L, Fu SW, Lin WF, Gao YJ, Chen HY, et al. Overexpression of NOX4 predicts poor prognosis and promotes tumor progression in human colorectal cancer. *Oncotarget*. 2017;8(20):33586-600.
326. Meitzler JL, Makhoulouf HR, Antony S, Wu Y, Butcher D, Jiang G, et al. Decoding NADPH oxidase 4 expression in human tumors. *Redox biology*. 2017;13:182-95.
327. Fitzgerald JP, Nayak B, Shanmugasundaram K, Friedrichs W, Sudarshan S, Eid AA, et al. Nox4 mediates renal cell carcinoma cell invasion through hypoxia-induced interleukin 6- and 8- production. *PloS one*. 2012;7(1):e30712.
328. Gregg JL, Turner RM, 2nd, Chang G, Joshi D, Zhan Y, Chen L, et al. NADPH oxidase NOX4 supports renal tumorigenesis by promoting the expression and nuclear accumulation of HIF2alpha. *Cancer Res*. 2014;74(13):3501-11.
329. Vaquero EC, Edderkaoui M, Pandol SJ, Gukovsky I, Gukovskaya AS. Reactive oxygen species produced by NAD(P)H oxidase inhibit apoptosis in pancreatic cancer cells. *The Journal of biological chemistry*. 2004;279(33):34643-54.
330. Martinez-Balibrea E, Martinez-Cardus A, Gines A, Ruiz de Porras V, Moutinho C, Layos L, et al. Tumor-Related Molecular Mechanisms of Oxaliplatin Resistance. *Molecular cancer therapeutics*. 2015;14(8):1767-76.
331. Scott SP, Pandita TK. The cellular control of DNA double-strand breaks. *Journal of cellular biochemistry*. 2006;99(6):1463-75.
332. Mills KD, Ferguson DO, Alt FW. The role of DNA breaks in genomic instability and tumorigenesis. *Immunological reviews*. 2003;194:77-95.
333. Smart DJ, Halicka HD, Schmuck G, Traganos F, Darzynkiewicz Z, Williams GM. Assessment of DNA double-strand breaks and gammaH2AX induced by the topoisomerase II poisons etoposide and mitoxantrone. *Mutation research*. 2008;641(1-2):43-7.
334. Frankenberg-Schwager M, Kirchermeier D, Greif G, Baer K, Becker M, Frankenberg D. Cisplatin-mediated DNA double-strand breaks in replicating but not in quiescent cells of the yeast *Saccharomyces cerevisiae*. *Toxicology*. 2005;212(2-3):175-84.
335. Woods D, Turchi JJ. Chemotherapy induced DNA damage response: convergence of drugs and pathways. *Cancer biology & therapy*. 2013;14(5):379-89.
336. Olive PL, Banath JP. Detection of DNA double-strand breaks through the cell cycle after exposure to X-rays, bleomycin, etoposide and 125I dUrd. *International journal of radiation biology*. 1993;64(4):349-58.

337. Kurose A, Tanaka T, Huang X, Halicka HD, Traganos F, Dai W, et al. Assessment of ATM phosphorylation on Ser-1981 induced by DNA topoisomerase I and II inhibitors in relation to Ser-139-histone H2AX phosphorylation, cell cycle phase, and apoptosis. *Cytometry Part A : the journal of the International Society for Analytical Cytology*. 2005;68(1):1-9.
338. Ayene IS, Koch CJ, Krisch RE. DNA strand breakage by bivalent metal ions and ionizing radiation. *International journal of radiation biology*. 2007;83(3):195-210.
339. Faivre S, Chan D, Salinas R, Woynarowska B, Woynarowski JM. DNA strand breaks and apoptosis induced by oxaliplatin in cancer cells. *Biochemical pharmacology*. 2003;66(2):225-37.
340. Sherman MH, Bassing CH, Teitell MA. Regulation of cell differentiation by the DNA damage response. *Trends in cell biology*. 2011;21(5):312-9.
341. Diebold I, Petry A, Sabrane K, Djordjevic T, Hess J, Gorch A. The HIF1 target gene NOX2 promotes angiogenesis through urotensin-II. *Journal of cell science*. 2012;125(Pt 4):956-64.
342. Li J, Wang JJ, Yu Q, Chen K, Mahadev K, Zhang SX. Inhibition of reactive oxygen species by Lovastatin downregulates vascular endothelial growth factor expression and ameliorates blood-retinal barrier breakdown in db/db mice: role of NADPH oxidase 4. *Diabetes*. 2010;59(6):1528-38.
343. BelAiba RS, Djordjevic T, Bonello S, Flugel D, Hess J, Kietzmann T, et al. Redox-sensitive regulation of the HIF pathway under non-hypoxic conditions in pulmonary artery smooth muscle cells. *Biological chemistry*. 2004;385(3-4):249-57.
344. Diebold I, Flugel D, Becht S, Belaiba RS, Bonello S, Hess J, et al. The hypoxia-inducible factor-2alpha is stabilized by oxidative stress involving NOX4. *Antioxidants & redox signaling*. 2010;13(4):425-36.
345. Gorch A, Diebold I, Schini-Kerth VB, Berchner-Pfannschmidt U, Roth U, Brandes RP, et al. Thrombin activates the hypoxia-inducible factor-1 signaling pathway in vascular smooth muscle cells: Role of the p22(phox)-containing NADPH oxidase. *Circulation research*. 2001;89(1):47-54.
346. Qutub AA, Popel AS. Reactive oxygen species regulate hypoxia-inducible factor 1alpha differentially in cancer and ischemia. *Molecular and cellular biology*. 2008;28(16):5106-19.
347. Tafani M, Sansone L, Limana F, Arcangeli T, De Santis E, Polese M, et al. The Interplay of Reactive Oxygen Species, Hypoxia, Inflammation, and Sirtuins in Cancer Initiation and Progression. *Oxidative medicine and cellular longevity*. 2016;2016:3907147.
348. Chandel NS, McClintock DS, Feliciano CE, Wood TM, Melendez JA, Rodriguez AM, et al. Reactive oxygen species generated at mitochondrial complex III stabilize hypoxia-inducible factor-1alpha during hypoxia: a mechanism of O2 sensing. *The Journal of biological chemistry*. 2000;275(33):25130-8.
349. Hoshikawa Y, Ono S, Suzuki S, Tanita T, Chida M, Song C, et al. Generation of oxidative stress contributes to the development of pulmonary hypertension induced by hypoxia. *Journal of applied physiology*. 2001;90(4):1299-306.
350. Brennan LA, Steinhorn RH, Wedgwood S, Mata-Greenwood E, Roark EA, Russell JA, et al. Increased superoxide generation is associated with pulmonary hypertension in fetal lambs: a role for NADPH oxidase. *Circulation research*. 2003;92(6):683-91.
351. Li H, Forstermann U. Nitric oxide in the pathogenesis of vascular disease. *The Journal of pathology*. 2000;190(3):244-54.
352. Rabinovitch M. Molecular pathogenesis of pulmonary arterial hypertension. *The Journal of clinical investigation*. 2008;118(7):2372-9.
353. Mandegar M, Fung YC, Huang W, Remillard CV, Rubin LJ, Yuan JX. Cellular and molecular mechanisms of pulmonary vascular remodeling: role in the development of pulmonary hypertension. *Microvascular research*. 2004;68(2):75-103.
354. Grobe AC, Wells SM, Benavidez E, Oishi P, Azakie A, Fineman JR, et al. Increased oxidative stress in lambs with increased pulmonary blood flow and pulmonary hypertension: role of NADPH oxidase and endothelial NO synthase. *American journal of physiology Lung cellular and molecular physiology*. 2006;290(6):L1069-77.

355. Khoo JP, Zhao L, Alp NJ, Bendall JK, Nicoli T, Rockett K, et al. Pivotal role for endothelial tetrahydrobiopterin in pulmonary hypertension. *Circulation*. 2005;111(16):2126-33.
356. Lai YL, Wu HD, Chen CF. Antioxidants attenuate chronic hypoxic pulmonary hypertension. *Journal of cardiovascular pharmacology*. 1998;32(5):714-20.
357. Chen JX, Meyrick B. Hypoxia increases Hsp90 binding to eNOS via PI3K-Akt in porcine coronary artery endothelium. *Laboratory investigation; a journal of technical methods and pathology*. 2004;84(2):182-90.
358. Justice JM, Tanner MA, Myers PR. Endothelial cell regulation of nitric oxide production during hypoxia in coronary microvessels and epicardial arteries. *Journal of cellular physiology*. 2000;182(3):359-65.
359. Le Cras TD, McMurtry IF. Nitric oxide production in the hypoxic lung. *American journal of physiology Lung cellular and molecular physiology*. 2001;280(4):L575-82.
360. Strijdom H, Friedrich SO, Hattingh S, Chamane N, Lochner A. Hypoxia-induced regulation of nitric oxide synthase in cardiac endothelial cells and myocytes and the role of the PI3-K/PKB pathway. *Molecular and cellular biochemistry*. 2009;321(1-2):23-35.
361. Ho JJ, Man HS, Marsden PA. Nitric oxide signaling in hypoxia. *Journal of molecular medicine*. 2012;90(3):217-31.
362. Fago A, Jensen FB, Tota B, Feelisch M, Olson KR, Helbo S, et al. Integrating nitric oxide, nitrite and hydrogen sulfide signaling in the physiological adaptations to hypoxia: A comparative approach. *Comparative biochemistry and physiology Part A, Molecular & integrative physiology*. 2012;162(1):1-6.
363. Laufs U, Fata VL, Liao JK. Inhibition of 3-hydroxy-3-methylglutaryl (HMG)-CoA reductase blocks hypoxia-mediated down-regulation of endothelial nitric oxide synthase. *The Journal of biological chemistry*. 1997;272(50):31725-9.
364. Ostergaard L, Stankevicius E, Andersen MR, Eskildsen-Helmond Y, Ledet T, Mulvany MJ, et al. Diminished NO release in chronic hypoxic human endothelial cells. *American journal of physiology Heart and circulatory physiology*. 2007;293(5):H2894-903.
365. Umbrello M, Dyson A, Feelisch M, Singer M. The key role of nitric oxide in hypoxia: hypoxic vasodilation and energy supply-demand matching. *Antioxidants & redox signaling*. 2013;19(14):1690-710.
366. Zuckerbraun BS, George P, Gladwin MT. Nitrite in pulmonary arterial hypertension: therapeutic avenues in the setting of dysregulated arginine/nitric oxide signalling. *Cardiovascular research*. 2011;89(3):542-52.
367. Prieto CP, Krause BJ, Quezada C, San Martin R, Sobrevia L, Casanello P. Hypoxia-reduced nitric oxide synthase activity is partially explained by higher arginase-2 activity and cellular redistribution in human umbilical vein endothelium. *Placenta*. 2011;32(12):932-40.
368. Heiss EH, Dirsch VM. Regulation of eNOS enzyme activity by posttranslational modification. *Current pharmaceutical design*. 2014;20(22):3503-13.
369. Bauer PM, Bauer EM, Rogers NM, Yao M, Feijoo-Cuaresma M, Pilewski JM, et al. Activated CD47 promotes pulmonary arterial hypertension through targeting caveolin-1. *Cardiovascular research*. 2012;93(4):682-93.
370. Murata T, Sato K, Hori M, Ozaki H, Karaki H. Decreased endothelial nitric-oxide synthase (eNOS) activity resulting from abnormal interaction between eNOS and its regulatory proteins in hypoxia-induced pulmonary hypertension. *The Journal of biological chemistry*. 2002;277(46):44085-92.
371. Chen CA, Druhan LJ, Varadharaj S, Chen YR, Zweier JL. Phosphorylation of endothelial nitric-oxide synthase regulates superoxide generation from the enzyme. *The Journal of biological chemistry*. 2008;283(40):27038-47.
372. Bendall JK, Alp NJ, Warrick N, Cai S, Adlam D, Rockett K, et al. Stoichiometric relationships between endothelial tetrahydrobiopterin, endothelial NO synthase (eNOS) activity, and eNOS coupling in vivo: insights from transgenic mice with endothelial-targeted GTP cyclohydrolase 1 and eNOS overexpression. *Circulation research*. 2005;97(9):864-71.
373. Crabtree MJ, Tatham AL, Al-Wakeel Y, Warrick N, Hale AB, Cai S, et al. Quantitative regulation of intracellular endothelial nitric-oxide synthase (eNOS) coupling by both tetrahydrobiopterin-eNOS stoichiometry and biopterin redox status: insights from cells with

- tet-regulated GTP cyclohydrolase I expression. *The Journal of biological chemistry*. 2009;284(2):1136-44.
374. Dubois M, Delannoy E, Duluc L, Closs E, Li H, Toussaint C, et al. Biopterin metabolism and eNOS expression during hypoxic pulmonary hypertension in mice. *PloS one*. 2013;8(11):e82594.
375. Crabtree MJ, Channon KM. Synthesis and recycling of tetrahydrobiopterin in endothelial function and vascular disease. *Nitric oxide : biology and chemistry*. 2011;25(2):81-8.
376. Gorlach A, Kietzmann T. Superoxide and derived reactive oxygen species in the regulation of hypoxia-inducible factors. *Methods in enzymology*. 2007;435:421-46.
377. De Pascali F, Hemann C, Samons K, Chen CA, Zweier JL. Hypoxia and reoxygenation induce endothelial nitric oxide synthase uncoupling in endothelial cells through tetrahydrobiopterin depletion and S-glutathionylation. *Biochemistry*. 2014;53(22):3679-88.
378. Zhang DX, Gutterman DD. Mitochondrial reactive oxygen species-mediated signaling in endothelial cells. *American journal of physiology Heart and circulatory physiology*. 2007;292(5):H2023-31.
379. Therade-Matharan S, Laemmel E, Carpentier S, Obata Y, Levade T, Duranteau J, et al. Reactive oxygen species production by mitochondria in endothelial cells exposed to reoxygenation after hypoxia and glucose depletion is mediated by ceramide. *American journal of physiology Regulatory, integrative and comparative physiology*. 2005;289(6):R1756-62.
380. Fresquet F, Pourageaud F, Leblais V, Brandes RP, Savineau JP, Marthan R, et al. Role of reactive oxygen species and gp91phox in endothelial dysfunction of pulmonary arteries induced by chronic hypoxia. *British journal of pharmacology*. 2006;148(5):714-23.
381. Liu JQ, Zelko IN, Erbynn EM, Sham JS, Folz RJ. Hypoxic pulmonary hypertension: role of superoxide and NADPH oxidase (gp91phox). *American journal of physiology Lung cellular and molecular physiology*. 2006;290(1):L2-10.
382. Matsui H, Shimosawa T, Itakura K, Guanqun X, Ando K, Fujita T. Adrenomedullin can protect against pulmonary vascular remodeling induced by hypoxia. *Circulation*. 2004;109(18):2246-51.
383. Crabtree MJ, Tatham AL, Hale AB, Alp NJ, Channon KM. Critical role for tetrahydrobiopterin recycling by dihydrofolate reductase in regulation of endothelial nitric-oxide synthase coupling: relative importance of the de novo biopterin synthesis versus salvage pathways. *The Journal of biological chemistry*. 2009;284(41):28128-36.
384. Moens AL, Vrints CJ, Claeys MJ, Timmermans JP, Champion HC, Kass DA. Mechanisms and potential therapeutic targets for folic acid in cardiovascular disease. *American journal of physiology Heart and circulatory physiology*. 2008;294(5):H1971-7.
385. Moat SJ, Clarke ZL, Madhavan AK, Lewis MJ, Lang D. Folic acid reverses endothelial dysfunction induced by inhibition of tetrahydrobiopterin biosynthesis. *European journal of pharmacology*. 2006;530(3):250-8.
386. Shirodaria C, Antoniadou C, Lee J, Jackson CE, Robson MD, Francis JM, et al. Global improvement of vascular function and redox state with low-dose folic acid: implications for folate therapy in patients with coronary artery disease. *Circulation*. 2007;115(17):2262-70.
387. Stanger O. Physiology of folic acid in health and disease. *Current drug metabolism*. 2002;3(2):211-23.
388. Yang HT, Lee M, Hong KS, Ovbiagele B, Saver JL. Efficacy of folic acid supplementation in cardiovascular disease prevention: an updated meta-analysis of randomized controlled trials. *European journal of internal medicine*. 2012;23(8):745-54.
389. Cui R, Iso H, Date C, Kikuchi S, Tamakoshi A, Japan Collaborative Cohort Study G. Dietary folate and vitamin b6 and B12 intake in relation to mortality from cardiovascular diseases: Japan collaborative cohort study. *Stroke*. 2010;41(6):1285-9.
390. Stampfer M, Willett W. Folate supplements for stroke prevention: targeted trial trumps the rest. *Jama*. 2015;313(13):1321-2.
391. Holmes MV, Newcombe P, Hubacek JA, Sofat R, Ricketts SL, Cooper J, et al. Effect modification by population dietary folate on the association between MTHFR genotype,

- homocysteine, and stroke risk: a meta-analysis of genetic studies and randomised trials. *Lancet*. 2011;378(9791):584-94.
392. Huo Y, Li J, Qin X, Huang Y, Wang X, Gottesman RF, et al. Efficacy of folic acid therapy in primary prevention of stroke among adults with hypertension in China: the CSPPT randomized clinical trial. *Jama*. 2015;313(13):1325-35.
393. Wang X, Qin X, Demirtas H, Li J, Mao G, Huo Y, et al. Efficacy of folic acid supplementation in stroke prevention: a meta-analysis. *Lancet*. 2007;369(9576):1876-82.
394. Huo Y, Rangarajan P, Ling EA, Dheen ST. Dexamethasone inhibits the Nox-dependent ROS production via suppression of MKP-1-dependent MAPK pathways in activated microglia. *BMC neuroscience*. 2011;12:49.
395. Condino-Neto A, Whitney C, Newburger PE. Dexamethasone but not indomethacin inhibits human phagocyte nicotinamide adenine dinucleotide phosphate oxidase activity by down-regulating expression of genes encoding oxidase components. *Journal of immunology*. 1998;161(9):4960-7.
396. Li J, He C, Tong W, Zou Y, Li D, Zhang C, et al. Tanshinone IIA blocks dexamethasone-induced apoptosis in osteoblasts through inhibiting Nox4-derived ROS production. *International journal of clinical and experimental pathology*. 2015;8(10):13695-706.
397. Park GB, Choi Y, Kim YS, Lee HK, Kim D, Hur DY. ROS and ERK1/2-mediated caspase-9 activation increases XAF1 expression in dexamethasone-induced apoptosis of EBV-transformed B cells. *International journal of oncology*. 2013;43(1):29-38.
398. Siuda D, Tobias S, Rus A, Xia N, Forstermann U, Li H. Dexamethasone upregulates Nox1 expression in vascular smooth muscle cells. *Pharmacology*. 2014;94(1-2):13-20.
399. Chen WL, Lin CT, Yao CC, Huang YH, Chou YB, Yin HS, et al. In-vitro effects of dexamethasone on cellular proliferation, apoptosis, and Na⁺-K⁺-ATPase activity of bovine corneal endothelial cells. *Ocular immunology and inflammation*. 2006;14(4):215-23.
400. Price LC, Shao D, Meng C, Perros F, Garfield BE, Zhu J, et al. Dexamethasone induces apoptosis in pulmonary arterial smooth muscle cells. *Respiratory research*. 2015;16:114.
401. Logie JJ, Ali S, Marshall KM, Heck MM, Walker BR, Hadoke PW. Glucocorticoid-mediated inhibition of angiogenic changes in human endothelial cells is not caused by reductions in cell proliferation or migration. *PloS one*. 2010;5(12):e14476.
402. Folkman J, Langer R, Linhardt RJ, Haudenschild C, Taylor S. Angiogenesis inhibition and tumor regression caused by heparin or a heparin fragment in the presence of cortisone. *Science*. 1983;221(4612):719-25.
403. Harada I. [The effects of glucocorticoids on angiogenesis in vitro]. *Nihon Seikeigeka Gakkai zasshi*. 1992;66(7):763-70.
404. Yano A, Fujii Y, Iwai A, Kageyama Y, Kihara K. Glucocorticoids suppress tumor angiogenesis and in vivo growth of prostate cancer cells. *Clinical cancer research : an official journal of the American Association for Cancer Research*. 2006;12(10):3003-9.
405. Colville-Nash PR, Scott DL. Angiogenesis and rheumatoid arthritis: pathogenic and therapeutic implications. *Annals of the rheumatic diseases*. 1992;51(7):919-25.
406. Luo JC, Shin VY, Liu ES, Ye YN, Wu WK, So WH, et al. Dexamethasone delays ulcer healing by inhibition of angiogenesis in rat stomachs. *European journal of pharmacology*. 2004;485(1-3):275-81.
407. Volk KA, Roghair RD, Jung F, Scholz TD, Lamb FS, Segar JL. Coronary endothelial function and vascular smooth muscle proliferation are programmed by early-gestation dexamethasone exposure in sheep. *American journal of physiology Regulatory, integrative and comparative physiology*. 2010;298(6):R1607-14.
408. Bourcier T, Forgez P, Borderie V, Scheer S, Rostene W, Laroche L. Regulation of human corneal epithelial cell proliferation and apoptosis by dexamethasone. *Investigative ophthalmology & visual science*. 2000;41(13):4133-41.
409. Albrecht M, Janssen M, Konrad L, Renneberg H, Aumuller G. Effects of dexamethasone on proliferation of and fibronectin synthesis by human primary prostatic stromal cells in vitro. *Andrologia*. 2002;34(1):11-21.

410. Cheng X, Yan Y, Chen JL, Ma ZL, Yang RH, Wang G, et al. Dexamethasone Exposure Accelerates Endochondral Ossification of Chick Embryos Via Angiogenesis. *Toxicological sciences : an official journal of the Society of Toxicology*. 2016;149(1):167-77.
411. Rey S, Semenza GL. Hypoxia-inducible factor-1-dependent mechanisms of vascularization and vascular remodelling. *Cardiovascular research*. 2010;86(2):236-42.
412. Vettori A, Greenald D, Wilson GK, Peron M, Facchinello N, Markham E, et al. Glucocorticoids promote Von Hippel Lindau degradation and Hif-1alpha stabilization. *Proceedings of the National Academy of Sciences of the United States of America*. 2017;114(37):9948-53.
413. Lim W, Park C, Shim MK, Lee YH, Lee YM, Lee Y. Glucocorticoids suppress hypoxia-induced COX-2 and hypoxia inducible factor-1alpha expression through the induction of glucocorticoid-induced leucine zipper. *British journal of pharmacology*. 2014;171(3):735-45.
414. Gaber T, Schellmann S, Erekul KB, Fangradt M, Tykwinska K, Hahne M, et al. Macrophage migration inhibitory factor counterregulates dexamethasone-mediated suppression of hypoxia-inducible factor-1 alpha function and differentially influences human CD4+ T cell proliferation under hypoxia. *Journal of immunology*. 2011;186(2):764-74.
415. Simko V, Takacova M, Debreova M, Laposova K, Ondriskova-Panisova E, Pastorekova S, et al. Dexamethasone downregulates expression of carbonic anhydrase IX via HIF-1alpha and NF-kappaB-dependent mechanisms. *International journal of oncology*. 2016;49(4):1277-88.
416. Pan J, Kao YL, Joshi S, Jeetendran S, Dipette D, Singh US. Activation of Rac1 by phosphatidylinositol 3-kinase in vivo: role in activation of mitogen-activated protein kinase (MAPK) pathways and retinoic acid-induced neuronal differentiation of SH-SY5Y cells. *Journal of neurochemistry*. 2005;93(3):571-83.
417. Zhang Y, Croft KD, Mori TA, Schyvens CG, McKenzie KU, Whitworth JA. The antioxidant tempol prevents and partially reverses dexamethasone-induced hypertension in the rat. *American journal of hypertension*. 2004;17(3):260-5.
418. Safaeian L, Zabolian H. Antioxidant effects of bovine lactoferrin on dexamethasone-induced hypertension in rat. *ISRN pharmacology*. 2014;2014:943523.
419. Chaumais MC, Ranchoux B, Montani D, Dorfmueller P, Tu L, Lecerf F, et al. N-acetylcysteine improves established monocrotaline-induced pulmonary hypertension in rats. *Respiratory research*. 2014;15:65.
420. Hu L, Zhang Y, Lim PS, Miao Y, Tan C, McKenzie KU, et al. Apocynin but not L-arginine prevents and reverses dexamethasone-induced hypertension in the rat. *American journal of hypertension*. 2006;19(4):413-8.
421. Burke MA, Chang S, Wakimoto H, Gorham JM, Conner DA, Christodoulou DC, et al. Molecular profiling of dilated cardiomyopathy that progresses to heart failure. *JCI insight*. 2016;1(6).
422. Sangeetha KN, Lakshmi BS, Niranjali Devaraj S. Dexamethasone promotes hypertrophy of H9C2 cardiomyocytes through calcineurin B pathway, independent of NFAT activation. *Molecular and cellular biochemistry*. 2016;411(1-2):241-52.
423. Ren R, Oakley RH, Cruz-Topete D, Cidlowski JA. Dual role for glucocorticoids in cardiomyocyte hypertrophy and apoptosis. *Endocrinology*. 2012;153(11):5346-60.
424. Shibusawa N, Yamada M, Hashida T, Hashimoto K, Satoh T, Horiguchi J, et al. Dilated cardiomyopathy as a presenting feature of Cushing's syndrome. *Internal medicine*. 2013;52(10):1067-71.
425. Halliday HL. Update on Postnatal Steroids. *Neonatology*. 2017;111(4):415-22.
426. Ong Sharon L.H. ZY, . Whitworth Judith A. Mechanisms of Dexamethasone-Induced Hypertension. *Current Hypertension Reviews*. 2009;5(1):61-74.
427. Veit F, Pak O, Egemnazarov B, Roth M, Kosanovic D, Seimetz M, et al. Function of NADPH oxidase 1 in pulmonary arterial smooth muscle cells after monocrotaline-induced pulmonary vascular remodeling. *Antioxidants & redox signaling*. 2013;19(18):2213-31.
428. Barman SA, Chen F, Su Y, Dimitropoulou C, Wang Y, Catravas JD, et al. NADPH oxidase 4 is expressed in pulmonary artery adventitia and contributes to hypertensive vascular remodeling. *Arteriosclerosis, thrombosis, and vascular biology*. 2014;34(8):1704-15.

429. Semenza GL. Involvement of hypoxia-inducible factor 1 in pulmonary pathophysiology. *Chest*. 2005;128(6 Suppl):592S-4S.
430. Stenmark KR, Fagan KA, Frid MG. Hypoxia-induced pulmonary vascular remodeling: cellular and molecular mechanisms. *Circulation research*. 2006;99(7):675-91.
431. Lai YL, Law TC. Chronic hypoxia- and monocrotaline-induced elevation of hypoxia-inducible factor-1 alpha levels and pulmonary hypertension. *Journal of biomedical science*. 2004;11(3):315-21.
432. Price LC, Montani D, Tcherakian C, Dorfmueller P, Souza R, Gambaryan N, et al. Dexamethasone reverses monocrotaline-induced pulmonary arterial hypertension in rats. *The European respiratory journal*. 2011;37(4):813-22.
433. Kriemler S, Kohler M, Zehnder M, Bloch KE, Brunner-La Rocca H. Successful treatment of severe acute mountain sickness and excessive pulmonary hypertension with dexamethasone in a prepubertal girl. *High altitude medicine & biology*. 2006;7(3):256-61.
434. Hodivala-Dilke K. alphavbeta3 integrin and angiogenesis: a moody integrin in a changing environment. *Current opinion in cell biology*. 2008;20(5):514-9.
435. Gorlach A. Regulation of HIF-1alpha at the transcriptional level. *Current pharmaceutical design*. 2009;15(33):3844-52.
436. Laurent A, Nicco C, Chereau C, Goulvestre C, Alexandre J, Alves A, et al. Controlling tumor growth by modulating endogenous production of reactive oxygen species. *Cancer Res*. 2005;65(3):948-56.
437. Kopetz S, Hoff PM. Cytotoxic chemotherapy for advanced colorectal cancer. *Recent advances in management. Oncology (Williston Park)*. 2005;19(13 Suppl 6):11-7.
438. Biroccio A, Benassi B, Amodei S, Gabellini C, Del Bufalo D, Zupi G. c-Myc down-regulation increases susceptibility to cisplatin through reactive oxygen species-mediated apoptosis in M14 human melanoma cells. *Mol Pharmacol*. 2001;60(1):174-82.
439. Alcindor T, Beauger N. Oxaliplatin: a review in the era of molecularly targeted therapy. *Current oncology*. 2011;18(1):18-25.
440. Jiao L, Li DD, Yang CL, Peng RQ, Guo YQ, Zhang XS, et al. Reactive oxygen species mediate oxaliplatin-induced epithelial-mesenchymal transition and invasive potential in colon cancer. *Tumour biology : the journal of the International Society for Oncodevelopmental Biology and Medicine*. 2016;37(6):8413-23.
441. Shi Y, Tang B, Yu PW, Tang B, Hao YX, Lei X, et al. Autophagy protects against oxaliplatin-induced cell death via ER stress and ROS in Caco-2 cells. *PLoS one*. 2012;7(11):e51076.
442. Massicot F, Hache G, David L, Chen D, Leuxe C, Garnier-Legrand L, et al. P2X7 Cell Death Receptor Activation and Mitochondrial Impairment in Oxaliplatin-Induced Apoptosis and Neuronal Injury: Cellular Mechanisms and In Vivo Approach. *PLoS one*. 2013;8(6):e66830.
443. Lim SC, Choi JE, Kang HS, Han SI. Ursodeoxycholic acid switches oxaliplatin-induced necrosis to apoptosis by inhibiting reactive oxygen species production and activating p53-caspase 8 pathway in HepG2 hepatocellular carcinoma. *Int J Cancer*. 2010;126(7):1582-95.
444. Chocry M, Leloup L, Kovacic H. Reversion of resistance to oxaliplatin by inhibition of p38 MAPK in colorectal cancer cell lines: involvement of the calpain / Nox1 pathway. *Oncotarget*. 2017;8(61):103710-30.
445. Chang G, Chen L, Lin HM, Lin Y, Maranchie JK. Nox4 inhibition enhances the cytotoxicity of cisplatin in human renal cancer cells. *J Exp Ther Oncol*. 2012 10(1):9-18.
446. Kim HJ, Lee JH, Kim SJ, Oh GS, Moon HD, Kwon KB, et al. Roles of NADPH oxidases in cisplatin-induced reactive oxygen species generation and ototoxicity. *The Journal of neuroscience : the official journal of the Society for Neuroscience*. 2010 30(11):3933-46.

447. Ozdian T, Holub D, Maceckova Z, Varanasi L, Rylova G, Rehulka J, et al. Proteomic profiling reveals DNA damage, nucleolar and ribosomal stress are the main responses to oxaliplatin treatment in cancer cells. *Journal of proteomics*. 2017;162:73-85.
448. Ren G, Luo W, Sun W, Niu Y, Ma DL, Leung CH, et al. Psoralidin induced reactive oxygen species (ROS)-dependent DNA damage and protective autophagy mediated by NOX4 in breast cancer cells. *Phytomedicine : international journal of phytotherapy and phytopharmacology*. 2016;23(9):939-47.
449. Ditch S, Paull TT. The ATM protein kinase and cellular redox signaling: beyond the DNA damage response. *Trends Biochem Sci*. 2012;37(1):15-22.
450. Weyemi U, Redon CE, Aziz T, Choudhuri R, Maeda D, Parekh PR, et al. NADPH oxidase 4 is a critical mediator in Ataxia telangiectasia disease. *Proceedings of the National Academy of Sciences of the United States of America*. 2015;112(7):2121-6.
451. Kodama R, Kato M, Furuta S, Ueno S, Zhang Y, Matsuno K, et al. ROS-generating oxidases Nox1 and Nox4 contribute to oncogenic Ras-induced premature senescence. *Genes Cells*. 2013;18(1):32-41.
452. Weyemi U, Lagente-Chevallier O, Boufraquech M, Prenois F, Courtin F, Caillou B, et al. ROS-generating NADPH oxidase NOX4 is a critical mediator in oncogenic H-Ras-induced DNA damage and subsequent senescence. *Oncogene*. 2012;31(9):1117-29.
453. Eid AA, Ford BM, Block K, Kasinath BS, Gorin Y, Ghosh-Choudhury G, et al. AMP-activated protein kinase (AMPK) negatively regulates Nox4-dependent activation of p53 and epithelial cell apoptosis in diabetes. *The Journal of biological chemistry*. 2010;285(48):37503-12.
454. Salmeen A, Park BO, Meyer T. The NADPH oxidases NOX4 and DUOX2 regulate cell cycle entry via a p53-dependent pathway. *Oncogene*. 2010;29(31):4473-84.
455. Budanov AV, Karin M. p53 target genes sestrin1 and sestrin2 connect genotoxic stress and mTOR signaling. *Cell*. 2008;134(3):451-60.
456. Boudreau HE, Ma WF, Korzeniowska A, Park JJ, Bhagwat MA, Leto TL. Histone modifications affect differential regulation of TGFbeta- induced NADPH oxidase 4 (NOX4) by wild-type and mutant p53. *Oncotarget*. 2017;8(27):44379-97.
457. Mirmohammadsadegh A, Mota R, Gustrau A, Hassan M, Nambiar S, Marini A, et al. ERK1/2 is highly phosphorylated in melanoma metastases and protects melanoma cells from cisplatin-mediated apoptosis. *The Journal of investigative dermatology*. 2007;127(9):2207-15.
458. Toscano F, Fajoui ZE, Gay F, Lalaoui N, Parmentier B, Chayvialle JA, et al. P53-mediated upregulation of DcR1 impairs oxaliplatin/TRAIL-induced synergistic anti-tumour potential in colon cancer cells. *Oncogene*. 2008;27(30):4161-71.
459. Waldman T, Kinzler KW, Vogelstein B. p21 is necessary for the p53-mediated G1 arrest in human cancer cells. *Cancer Res*. 1995;55(22):5187-90.
460. Qu K, Xu X, Liu C, Wu Q, Wei J, Meng F, et al. Negative regulation of transcription factor FoxM1 by p53 enhances oxaliplatin-induced senescence in hepatocellular carcinoma. *Cancer letters*. 2013;331(1):105-14.
461. Wang R, Dashwood WM, Nian H, Lohr CV, Fischer KA, Tsuchiya N, et al. NADPH oxidase overexpression in human colon cancers and rat colon tumors induced by 2-amino-1-methyl-6-phenylimidazo[4,5-b]pyridine (PhIP). *Int J Cancer*. 2011;128(11):2581-90.
462. Chang G, Chen L, Lin HM, Lin Y, Maranchie JK. Nox4 inhibition enhances the cytotoxicity of cisplatin in human renal cancer cells. *J Exp Ther Oncol*. 2012;10(1):9-18.

10 Appendix



Damir Kračun
Experimental and Pediatric Cardiology
German Herat Center
Lazarettstr. 36
80636 Munich
Germany
damir.kracun@gmx.de

March 23, 2018

Dear Mr. Kračun:

The following permissions are for your doctoral thesis only.

Copyright permission is granted to use Figures 1-9, and the text of the article:

"The β 3-Integrin Binding Protein β 3-Endonexin Is a Novel Negative Regulator of Hypoxia-Inducible Factor-1" by Damir Kračun, Florian Rieß, Ivan Kanchev, Meinrad Gawaz, Agnes Görlach
Antioxidants & Redox Signaling, Vol. 20, No. 13: April 9, 2014, DOI: [10.1089/ars.2013.5286](https://doi.org/10.1089/ars.2013.5286)

Copyright permission is granted to use Figures 1-6 and Supplemental Figures, and the text of the article:

"Folic Acid Promotes Recycling of Tetrahydrobiopterin and Protects Against Hypoxia-Induced Pulmonary Hypertension by Recoupling Endothelial Nitric Oxide Synthase" by Karel Chalupsky*, Damir Kračun*, Ivan Kanchev, Katharina Bertram, Agnes Görlach
Antioxidants & Redox Signaling, Volume: 23 Issue 14: November 19, 2015, DOI: [10.1089/ars.2015.6329](https://doi.org/10.1089/ars.2015.6329)
(*-equal contribution)

Kind Regards,

A handwritten signature in black ink, appearing to read "Karen Ballen".

Karen Ballen
Manager, Copyright Permissions
Mary Ann Liebert, Inc., publishers
KBallen@liebertpub.com

11 Acknowledgements

I would like to thank to Prof. Dr. Agnes Görlach for the support in this long-lasting process, in which I did not just successfully completed my doctoral studies, but also developed scientific, independent and critical thinking. In this scientific journey guidance of Prof. Görlach was indispensable.

To Prof. Dr. Michael Groll I am thankful for accepting the role of my second supervisor, as well as, for the support and patience in this process.

I owe my gratitude to late Prof. Dr. Manfred Schmitt for accepting the role of the mentor in my thesis committee and his contributions that increased the quality of this manuscript.

In addition, I would like to thank my fellow colleagues who actively contributed to successful completion of these studies: Ivan Kanchev, Karel Chalupsky, Florian Rieß, Andreas Petry, Anna Knirsch, Mathieu Klop, Katharina Bertram and Cordula Wolf. In addition, I would like to thank to my friend Nataša Pavlov for the help with graphical design of the thesis.

12 Curriculum Vitae

First name: Damir

Family name: Kračun

Citizenship/Nationality: Serbian

Address: Funkerstr. 12/308

80636 Munich, Germany

Mobile phone: +49 151/ 675 260 87

e-mail address: damir.kracun@gmx.de

Date of birth: 27th November 1976

Place of birth: Bela Crkva, Serbia

Education:

July 2013 – present: PhD student at the Faculty of Medicine (Experimental biomedicine) at the Technical University of Munich and German Heart Center, The Department of Experimental and Molecular Pediatric Cardiology (Head Prof. Dr. med. Agnes Görlach).

January 2006 – June 2013: Researcher at German Heart Center, The Department of Experimental and Molecular Pediatric Cardiology (Head Prof. Dr. med. Agnes Görlach).

March 2005 - December 2005: Adolf-Butenandt Institute for Biological Chemistry (Head Prof. Dr. med. Dr. rer. nat. Walter Neupert) on project: Molecular basis of biogenesis of mitochondria, establishing in vitro model of mitochondrial fusion.

1995-2005: Master Studies of Molecular Biology and Physiology at The Faculty of Biology, University of Belgrade (Belgrade, Serbia). I have graduated with an average grade 9.06 (out of 10.0). MSc thesis title: „ Differential expression of c-Jun, JunD and JunB in rat cortex following brain trauma injury“

1991-1995: High school education.

1984-1991: Elementary school education.

Publications:

1. Chalupsky K*, Kračun D*, Kanchev I, Bertram K, Gorlach A. Folic Acid Promotes Recycling of Tetrahydrobiopterin and Protects Against Hypoxia-Induced Pulmonary Hypertension by Recoupling Endothelial Nitric Oxide Synthase. *Antioxidants & redox signaling*. 2015;23(14):1076-91.
2. Diebold I*, Kračun D*, Bonello S, Gorlach A. The 'PAI-1 paradox' in vascular remodeling. *Thrombosis and haemostasis*. 2008;100(6):984-91.
3. Egea J, Fabregat I, Frapart YM, Ghezzi P, Görlach A, Kietzmann T, Kubaichuk K, Knaus UG, Lopez MG, Olaso-Gonzalez G, Petry A, Schulz R, Vina J, Winyard P, Abbas K, Ademowo OS, Afonso CB, Andreadou I, Antelmann H, Antunes F, Aslan M, Bachschmid MM, Barbosa RM, Belousov V, Berndt C, Bernlohr D, Bertrán E, Bindoli A, Bottari SP, Brito PM, Carrara G, Casas AI, Chatzi A, Chondrogianni N, Conrad M, Cooke MS, Costa JG, Cuadrado A, My-Chan Dang P, De Smet B, Debelec-Butuner B, Dias IHK, Dunn JD, Edson AJ, El Assar M, El-Benna J, Ferdinandy P, Fernandes AS, Fladmark KE, Förstermann U, Giniatullin R, Giricz Z, Görbe A, Griffiths H, Hampl V, Hanf A, Herget J, Hernansanz-Agustín P, Hillion M, Huang J, Ilikay S, Jansen-Dürr P, Jaquet V, Joles JA, Kalyanaraman B, Kaminsky D, Karbaschi M, Kleanthous M, Klotz LO, Korac B, Korkmaz KS, Koziel R, Kračun D, Krause KH, Křen V, Krieg T, Laranjinha J, Lazou A, Li H, Martínez-Ruiz A, Matsui R, McBean GJ, Meredith SP, Messens J, Miguel V, Mikhed Y, Milisav I, Milković L, Miranda-Vizuete A, Mojović M, Monsalve M, Mouthuy PA, Mulvey J, Münzel T, Muzykantov V, Nguyen ITN, Oelze M, Oliveira NG, Palmeira CM, Papaevgeniou N, Pavićević A, Pedre B, Peyrot F, Phylactides M, Pircalabioru GG, Pitt AR, Poulsen HE, Prieto I, Rigobello MP, Robledinos-Antón N, Rodríguez-Mañas L, Rolo AP, Rousset F, Ruskovska T, Saraiva N, Sasson S, Schröder K, Semen K, Seredenina T, Shakirzyanova A, Smith GL, Soldati T, Sousa BC, Spickett CM, Stancic A, Stasia MJ, Steinbrenner H, Stepanić V, Steven S, Tokatlidis K, Tuncay E, Turan B, Ursini F, Vacek J, Vajnerova O, Valentová K, Van Breusegem F, Varisli L, Veal EA, Yalçın AS, Yelisseyeva O, Žarković N, Zatloukalová M, Zielonka J, Touyz RM, Papapetropoulos A, Grune T, Lamas S, Schmidt HHHW, Di Lisa F, Daiber A.. European contribution to the study of ROS: A summary of the findings and prospects for the future from the COST action BM1203 (EU-ROS). *Redox biology*. 2017;13:94-162.
4. Egea J, Fabregat I, Frapart YM, Ghezzi P, Görlach A, Kietzmann T, Kubaichuk K, Knaus UG, Lopez MG, Olaso-Gonzalez G, Petry A, Schulz R, Vina J, Winyard P, Abbas K, Ademowo OS, Afonso CB, Andreadou I, Antelmann H, Antunes F, Aslan M, Bachschmid MM, Barbosa RM, Belousov V, Berndt C, Bernlohr D, Bertrán E, Bindoli A, Bottari SP, Brito PM, Carrara G, Casas AI, Chatzi A, Chondrogianni N, Conrad M, Cooke MS, Costa JG, Cuadrado A, My-Chan Dang P, De Smet B, Debelec-Butuner B, Dias IHK, Dunn JD, Edson AJ, El Assar M, El-Benna J, Ferdinandy P, Fernandes AS, Fladmark KE, Förstermann U, Giniatullin R, Giricz Z, Görbe A, Griffiths H, Hampl V, Hanf A, Herget J, Hernansanz-Agustín P, Hillion M, Huang J, Ilikay S, Jansen-Dürr P, Jaquet V, Joles JA, Kalyanaraman B, Kaminsky D, Karbaschi M, Kleanthous M, Klotz LO, Korac B, Korkmaz KS, Koziel R, Kračun D, Krause KH, Křen V, Krieg T, Laranjinha J, Lazou A, Li H, Martínez-Ruiz A, Matsui R, McBean GJ, Meredith SP, Messens J, Miguel V, Mikhed Y, Milisav I, Milković L, Miranda-Vizuete A, Mojović M, Monsalve M, Mouthuy PA, Mulvey J, Münzel T, Muzykantov V, Nguyen ITN, Oelze M, Oliveira NG, Palmeira CM, Papaevgeniou N, Pavićević A, Pedre B, Peyrot F, Phylactides M, Pircalabioru GG, Pitt AR, Poulsen HE, Prieto I, Rigobello MP,

Robledinos-Antón N, Rodríguez-Mañas L, Rolo AP, Rousset F, Ruskovska T, Saraiva N, Sasson S, Schröder K, Semen K, Seredenina T, Shakirzyanova A, Smith GL, Soldati T, Sousa BC, Spickett CM, Stancic A, Stasia MJ, Steinbrenner H, Stepanić V, Steven S, Tokatlidis K, Tuncay E, Turan B, Ursini F, Vacek J, Vajnerova O, Valentová K, Van Breusegem F, Varisli L, Veal EA, Yalçın AS, Yelisseyeva O, Žarković N, Zatloukalová M, Zielonka J, Touyz RM, Papapetropoulos A, Grune T, Lamas S, Schmidt HHHW, Di Lisa F, Daiber A.. Corrigendum to "European contribution to the study of ROS: A summary of the findings and prospects for the future from the COST action BM1203 (EU-ROS)" [Redox Biol. 13 (2017) 94-162]. Redox biology. 2017.

5. Kračun D, Riess F, Kanchev I, Gawaz M, Gorlach A. The beta3-integrin binding protein beta3-endonexin is a novel negative regulator of hypoxia-inducible factor-1. *Antioxidants & redox signaling*. 2014;20(13):1964-76.

6. Rzymiski T, Petry A, Kračun D, Riess F, Pike L, Harris AL, et al. The unfolded protein response controls induction and activation of ADAM17/TACE by severe hypoxia and ER stress. *Oncogene*. 2012;31(31):3621-34.

7. Zhang Z*, Trautz B*, Kračun D*, Vogel F, Weitnauer M, Hochkogler K, et al. Stabilization of p22phox by Hypoxia Promotes Pulmonary Hypertension. *Antioxidants & redox signaling*. 2018.

* - equal first authorship